

**An *in vitro* investigation of microbial volatile analysis
for diagnosis of wound infection**

Elisabeth Alice Slade

A thesis submitted in partial fulfilment of the requirements of the University of
the West of England, Bristol for the degree of Doctor of Philosophy

Faculty of Health and Applied Sciences, University of the West of England, Bristol

May 2020

ABSTRACT

Infection is detrimental to wound healing and is the leading cause of mortality in wound patients. Currently, diagnosis of wound infection relies on clinical experience complimented by microbiological analysis and non-specific blood tests.

Point of care diagnostics have the potential to revolutionise treatment of wound infection. Early identification of the causative organism of infection, would facilitate appropriate prescribing, reducing overuse of antimicrobials and the emergence of resistance, while improving patient outcomes.

Analysis of bacterial culture headspace using Selected Ion Flow Tube Mass Spectrometry (SIFT-MS) was combined with multivariate analysis. Using this approach it is possible to discriminate between species of bacteria associated with wound infection in planktonic culture, including in simulated wound fluid.

It is also possible to detect volatile profiles from discarded clinical wound dressing material, irrespective of dressing type. Within this research it is not possible to link the volatile profiles detected to specific bacterial species identified from routine wound swab microbiology.

A collagen wound biofilm model has been developed that can be utilised for real-time analysis of volatile metabolites during biofilm formation and growth. The biofilm model incorporates a collagen gel growth matrix and continuous flow of simulated wound fluid to provide wound-like conditions for biofilm culture.

Discrimination between *Staphylococcus aureus*, *Pseudomonas aeruginosa* and *Streptococcus pyogenes* biofilms is possible using SIFT-MS in both full scan and selected ion modes when combined with multivariate statistical analysis. Comparison of headspace analysis of multi-species biofilms with that of single species biofilms reveals that the headspace is generally dominated by a volatile profile associated with one of the species within the biofilm community.

This research successfully demonstrates the feasibility of using volatile analysis to discriminate between important pathogens associated with causing clinically relevant wound infection and lays a scientific foundation for the development of rapid point of care diagnostics.

ACKNOWLEDGMENTS

Undertaking this PhD has been quite a journey, one which I may not have made it to the end of without the unwavering support and guidance of those around me. I am grateful to my supervisory team; Professor Darren Reynolds and Dr Robin Thorn for giving me the opportunity to undertake this research and for providing direction and encouragement throughout. I would also like to thank Dr Amber Young and everyone at the Children's Burns Research Centre for welcoming me to their research meetings and providing clinical insights. Thanks must also go to all the other members of the 'Team Reynolds' research group, which has grown considerable over the years. In particular Dr Beth Fox, who has always been happy to provide sound advice over a cuppa and collaborate on a lunchtime Zygolex.

I would like to thank the technical teams at UWE for all their help over the years, particularly Barbara Rees for keeping the Microbiology research labs running like clockwork. I would also like to thank Paul Bowdler for his help with GC-MS and Dave Corry and Dave Patton for their help with Confocal and Electron Microscopy. I must also acknowledge all the years of service and hard work of 'Lefty' the spiral plater (RIP).

I would like to thank my friends, new and old, and my family for all their love and emotional support. I have made some incredible friends during the last 4 years, Elle and Llama, it's been an honour to share this PhD journey with you both. I know we'll be drinking tea, baking and doing crosswords together for many years to come. I am so grateful to my husband Ell, for his constant encouragement and for believing I could make my aspirations a reality, especially when I've doubted myself. Thank you also for learning to cook, this undertaking would've been even harder surviving only on egg and beans on toast. Finally, I would like to thank my parents, for raising me to be strong, stubborn and independent, and always teaching me to believe in myself and follow my dreams. This thesis is dedicated to you. Thank you!

TABLE OF CONTENTS

Abstract	i
Acknowledgments	iii
List of Figures	ix
List of Tables	xi
Abbreviations	xiii
Chapter 1: Introduction	1
1.1 Overview	1
1.2 Skin Structure	4
1.3 Wounds	8
1.3.1 Wound Types	8
1.3.2 Wound Healing	9
1.3.3 Skin Microflora	12
1.3.4 Wound Infection	14
1.4 Biofilms	19
1.4.1 Biofilm Formation	20
1.4.2 Biofilms in Wounds	24
1.4.3 Biofilm Tolerance	25
1.5 Diagnosis of Wound Infection	27
1.5.1 Antimicrobial Resistance	29
1.5.2 Emerging Approaches to Wound Diagnostics	33
1.5.3 Microbial Volatiles	38
1.6 Biofilm models	45
1.6.1 Wound biofilm models	47
Chapter 2: Materials & Methods	51
2.1 Culture media	51
2.1.1 Simulated Wound Fluid (SWF)	52
2.2 Bacterial strains	53
2.3 Preparation of bacterial inoculum	55
2.4 Enumeration of bacteria	55
2.4.1 Spread Plate Method	55
2.4.2 Spiral Plating	56
2.5 Planktonic cultures for headspace analysis	57
2.5.1 Liquid Culture - TSB	57
2.5.2 Liquid Cultures - Simulated Wound Fluid	57
2.6 Collagen wound biofilm model	58

2.6.1	Collagen Coating of Glass Slide Coupons	58
2.6.2	Growth of Bacterial Biofilms within the Collagen Wound Biofilm Model	58
2.6.3	Enumeration of Bacterial Biofilms	61
2.7	Imaging of bacterial biofilms and collagen matrix	62
2.7.1	Scanning Electron Microscopy (SEM)	62
2.7.2	Confocal Scanning Laser Microscopy (CSLM)	62
2.8	Detection of bacterial volatile metabolites	64
2.8.1	Profile 3 SIFT-MS Instrument	64
2.8.2	Voice200 Ultra SIFT-MS instrument	67
2.8.3	Gas Chromatography – Mass Spectrometry	72
2.9	Antimicrobial Susceptibility	73
2.9.1	Minimum Inhibitory Concentration (MIC)	73
2.9.2	Antimicrobial Susceptibility of Biofilms	74
2.10	Data Analysis	75
2.10.1	Hierarchical Cluster Analysis	75
2.10.2	Principal Component Analysis (PCA)	76
Chapter 3:	<i>In vitro discrimination of wound-associated bacteria in planktonic culture</i>	79
3.1	Introduction	79
3.2	Methods Summary	81
3.2.1	Preparation of Bacterial Cultures	81
3.2.2	Selected Ion Flow Tube - Mass Spectrometry (SIFT-MS)	81
3.2.3	Data Analysis	82
3.3	Results	84
3.3.1	Headspace Analysis of Wound Associated Bacteria Cultured in Complex Growth Media (TSB).	84
3.3.2	Headspace Analysis of Wound Associated Bacteria Cultured in a Simulated Wound Fluid (SWF).	90
3.4	Discussion	100
Chapter 4:	<i>Analysis of volatile compounds from discarded patient wound dressings</i>	107
4.1	Introduction	107
4.2	Methods Summary	108
4.2.1	Dressing Collection	108
4.2.2	SIFT-MS Analysis	108
4.2.3	Wound Swab Microbiology and Clinical Information	109
4.2.4	Data Analysis	109
4.3	Results	111
4.4	Discussion	123

Chapter 5:	<i>An in vitro collagen perfusion wound biofilm model</i>	127
5.1	Introduction	127
5.2	Methods Summary	131
5.2.1	Biofilm Model	131
5.2.2	Enumeration of Bacterial Biofilms	131
5.2.3	Imaging of Bacterial Biofilms	132
5.2.4	Volatile Analysis	132
5.2.5	Antimicrobial Susceptibility	133
5.2.6	Data Analysis	134
5.3	Results	135
5.3.1	Characterisation of Biofilm Growth in the Collagen Wound Biofilm Model	135
5.3.2	Application of the Collagen Wound Biofilm Model for Studying Biofilm Volatile Metabolites	140
5.3.3	Application of the Collagen Wound Biofilm Model for Studying Antimicrobial Kinetics	144
5.4	Discussion	151
Chapter 6:	<i>In vitro discrimination of wound associated bacterial biofilms</i>	157
6.1	Introduction	157
6.2	Methods Summary	159
6.2.1	Biofilm Model	159
6.2.2	Volatile Analysis	160
6.2.3	Enumeration of Multispecies Biofilms	162
6.2.4	Data Analysis	162
6.3	Results	165
6.3.1	Single Species Biofilms	165
6.3.2	Multispecies Biofilms	185
6.4	Discussion	195
Chapter 7:	<i>Discussion & Future Work</i>	207
7.1	General Discussion	207
7.2	Summary and Conclusions	214
7.2.1	Chapter 3	214
7.2.2	Chapter 4	215
7.2.3	Chapter 5	217
7.2.4	Chapter 6	218
7.3	Future work	221
7.3.1	Volatile Analysis	221
7.3.2	Collagen Wound Biofilm Model	223
7.3.3	Statistical Analysis	224
7.3.4	Diagnostic Applications	226
References		229

<i>Appendix I: Published Material</i>	255
<i>Appendix II: Supplementary Material</i>	282

LIST OF FIGURES

Figure 1.1:	Structure of the skin	4
Figure 1.2:	Phases of wound healing	10
Figure 1.3:	The infection continuum	16
Figure 1.4:	Biofilm formation and maturation	22
Figure 1.5:	Schematic of the Profile 3 SIFT-MS instrument	43
Figure 2.1:	<i>In vitro</i> collagen wound biofilm model	60
Figure 3.1:	Dendrogram generated by hierarchical cluster analysis; FS in TSB	84
Figure 3.2:	Principal component analysis plot and loading plot; FS in TSB by SIFT-MS analysis of cultures incubated for 5 h in TSB	87
Figure 3.3:	PCA plot (PC 2 and 3); FS in TSB	88
Figure 3.4:	Dendrogram generated by hierarchical cluster analysis; FS in TSB, 24 hour	89
Figure 3.5:	Dendrogram generated by hierarchical cluster analysis; FS in SWF	91
Figure 3.6:	Dendrogram generated by hierarchical cluster analysis; FS in SWF	92
Figure 3.7:	Principal component analysis plot and loading plot; FS in SWF	95
Figure 3.8:	PCA plot (PC 2 and 3); FS in SWF	96
Figure 3.9:	Dendrogram generated by hierarchical cluster analysis; FS in SWF, 24 hour	97
Figure 4.1:	Dendrogram generated by hierarchical cluster analysis; discarded patient wound dressings	118
Figure 4.2:	Principal component analysis plot of dressing samples (<i>Pseudomonas</i> species)	120
Figure 4.3:	Principal component analysis plot of dressing samples (<i>S.</i> <i>aureus</i>)	121
Figure 4.4:	Principal component analysis plot of dressing samples (Streptococci)	122
Figure 5.1:	Enumeration of <i>Pseudomonas aeruginosa</i> , <i>Staphylococcus aureus</i> and <i>Streptococcus pyogenes</i> biofilm in the collagen wound biofilm model	137
Figure 5.2:	Scanning electron micrographs of collagen gel matrix, <i>P.</i> <i>aeruginosa</i> biofilm, <i>S. aureus</i> biofilm and <i>S. pyogenes</i> biofilm	139

Figure 5.3:	Detection of hydrogen cyanide over 72 hours	142
Figure 5.4:	Detection of ammonia over 72 hours	143
Figure 5.5:	Treatment of <i>P. aeruginosa</i> biofilms with ceftazidime	145
Figure 5.6:	Confocal scanning laser micrographs of <i>P. aeruginosa</i> biofilm	148
Figure 5.7:	Confocal scanning laser micrographs of biofilms treated with ceftazidime	150
Figure 6.1:	Dendrogram generated by hierarchical cluster analysis; FS Biofilms	166
Figure 6.2	: Principal component analysis plot and loading plot; FS Biofilms	167
Figure 6.3:	Dendrogram generated by hierarchical cluster analysis; SIM Biofilms	172
Figure 6.4:	Principal component analysis plot and loading plot; SIM Biofilms	173
Figure 6.5:	Dendrogram generated by hierarchical cluster analysis; FS Biofilms (MANOVA)	175
Figure 6.6:	Principal component analysis plot and loading plot; FS Biofilms (MANOVA)	177
Figure 6.7:	PCA plot (PC 2 and 3); FS Biofilms (MANOVA)	179
Figure 6.8:	Dendrogram generated by hierarchical cluster analysis; SIM Biofilms (MANOVA)	182
Figure 6.9:	Principal component analysis plot and loading plot; SIM Biofilms (MANOVA)	183
Figure 6.10:	PCA plot (PC 2 and 3); SIM Biofilms (MANOVA)	184
Figure 6.11:	Enumeration of single and multi-species biofilms at 48 hours	187
Figure 6.12:	Enumeration of multi-species biofilms at 48 hours	188
Figure 6.13:	Product ion array for single species and multi species biofilms	193
Figure 6.14:	Principal component analysis plot; single species and multispecies biofilms	194
Figure S1:	Principal component analysis plot 22 'core' headspace volatile product ion peaks	283
Figure S2:	PCA plot (PC 2 and 3); SIM Biofilms showing <i>S. aureus</i> and <i>S. pyogenes</i>	284

LIST OF TABLES

Table 1.1:	Signs and symptoms of infection	29
Table 1.2:	10 strategies to combat AMR	32
Table 2.1:	Bacterial isolates used in this research	54
Table 2.2:	Profile 3 SIFT-MS Validation Checks	65
Table 2.3:	Syft Voice200 Ultra SIFT-MS Automated Validation Procedure	68
Table 2.4:	Voice200 Ultra SIM Scan parameters	70
Table 3.1:	Presumptive compound identification	99
Table 3.2:	Product ion array for bacterial cultures grown in TBS and SWF	100
Table 4.1:	Clinical symptoms indicating infection	113
Table 4.2:	Clinical wound presentation	114
Table 4.3:	Microbiological wound surface swab results	115
Table 4.4:	Product ion array for discarded patient dressings	116
Table 6.1:	Table of compounds detected by HS-SPME-GC-MS	169
Table 6.2:	Product ion array for single species and multi species biofilms	192
Table 7.1:	Discriminatory volatile compound product ion peaks common to both the planktonic and biofilm headspace SIFT-MS analysis	210

ABBREVIATIONS

Abbreviation	Definition
AMR	Antimicrobial resistance
ATCC	American Type Culture Collection
CAR/PDMS	Carboxen/Polydimethylsiloxane
CC	Culture collection
CFC	<i>Pseudomonas</i> CFC selective agar (Cetrimide, Fucidin, Cephalosporin)
cfu	Colony forming units
COBA	Colistin-Oxolinic acid blood agar
cps	Counts per second
CSLM	Confocal scanning laser microscopy
Da	Daltons
EPS	Extracellular polymeric substances
FBS	Foetal bovine serum
FS	Full scan
GC	Gas chromatography
GC-MS	Gas chromatography mass spectrometry
LCWB	Lubbock chronic wound biofilm model
m/z	Mass to charge ratio
MANOVA	Multivariate analysis of variance
MHB	Mueller-Hinton Broth
MIC	Minimum inhibitory concentration
MIM	Multi ion monitoring
MRSA	Methicillin resistant <i>Staphylococcus aureus</i>
MSA	Mannitol salt agar
MW	Molecular weight
NBT	North Bristol NHS trust
NCIMB	National Collection of Industrial, Food and Marine Bacteria
NCTC	National Collection of Type Cultures
NIST	National Institute of Standards and Technology
OD	Optical density
PBS	Phosphate buffered saline
PCA	Principal component analysis
PEEK	Polyether ether ketone
PIA	Polysaccharide intercellular antigen
ppb	Parts per billion

PTFE	Polytetrafluoroethylene
QS	Quorum sensing
SD	Standard deviation
SEM	Scanning electron microscopy
SIFT-MS	Selected ion flow tube mass spectrometry
SIM	Selected ion mode
SPME	Solid phase micro extraction
SWF	Simulated wound fluid
TOFMS	Time of flight mass spectrometry
TSA	Tryptone soya agar
TSB	Tryptone soya broth
UHB	University hospitals Bristol
UWE	University of the West of England
VOCs	Volatile organic compounds
WASP	Whitley Automated Spiral Plater

Chapter 1: Introduction

1.1 OVERVIEW

Infection is detrimental to wound healing and is the leading cause of mortality in wound patients. Currently, diagnosis of wound infection relies on clinical experience complimented by microbiological analysis of the wound surface, which may not effectively inform treatment. Novel approaches to the diagnosis of wound infection are essential, not only to improve patient outcomes, but also to help combat the continuing emergence of antimicrobial resistance. Discrimination between bacterial species through the analysis of volatile metabolites may inform the development of new rapid techniques for diagnosis of wound infection.

The aim of this research was to investigate if bacterial species associated with causing wound infection produce species specific volatile profiles *in vitro* that can be used for discrimination between species. The specific aims addressed to achieve this were;

- (1) To investigate if planktonic cultures of wound associated bacteria produce species specific volatile profiles *in vitro*, enabling significant discrimination.
- (2) To investigate if the concept of species discrimination based on volatile compound detection could be applied to analysis of discarded wound dressings, as part of routine wound care.
- (3) To develop and characterise a suitable biofilm model for culture and headspace analysis of wound associated bacterial biofilms, that provides wound-like culture conditions.

- (4) To investigate the volatile profiles of biofilm cultures of wound associated bacteria *in vitro* that can be used for the discrimination between species.
- (5) To investigate the effect of multispecies biofilms on bacterial volatile profiles *in vitro*.

This thesis consists of seven chapters. This chapter (**Chapter 1**) comprises a general introduction, which includes wound healing and infection, biofilm formation and models of biofilm infection, and an overview of bacterial production of volatile metabolites. **Chapter 2** describes the experimental methods employed throughout this research and introduces the analytical instrumentation used for the detection of volatile metabolites. **Chapter 3** details a proof of concept study, to determine if bacterial species associated with wound infection produce species specific volatile profiles when cultured in complex media and simulated wound fluid. **Chapter 4** investigates the detection of volatile compounds from discarded wound dressing material, to determine if dressing materials capture volatile compounds from the patients wound and if these volatiles can be related to the bacteria present. **Chapter 5** describes the development of a collagen wound biofilm model, to facilitate the analysis of bacterial volatile metabolites under controlled conditions, that are more representative of the real wound environment. **Chapter 6** investigates the detection of species specific volatile profiles from biofilm cultures of wound associated bacteria for discrimination between species, and explores any effect of culturing multispecies biofilms on the headspace volatiles detected. **Chapter 7** presents a general

discussion, the main conclusions of this research and recommendations for future work.

1.2 SKIN STRUCTURE

The skin is comprised of distinct layers; the epidermis, where keratinocytes are the primary cell type, the dermis, primarily comprised of fibroblasts, and a subcutaneous fat layer (Figure 1.1). The epidermis is the outer layer, protecting the body from water loss and environmental threats, and is itself comprised of layers. These layers are characterised by the maturation of keratinocytes as they migrate towards the skin surface. The stratum basale is the deepest layer of the epidermis and comprises dividing basal cells (stem cells), some of which differentiate to form keratinocytes and begin migration (Baroni *et al.*, 2012; Losquadro, 2017). Keratinocytes mature as

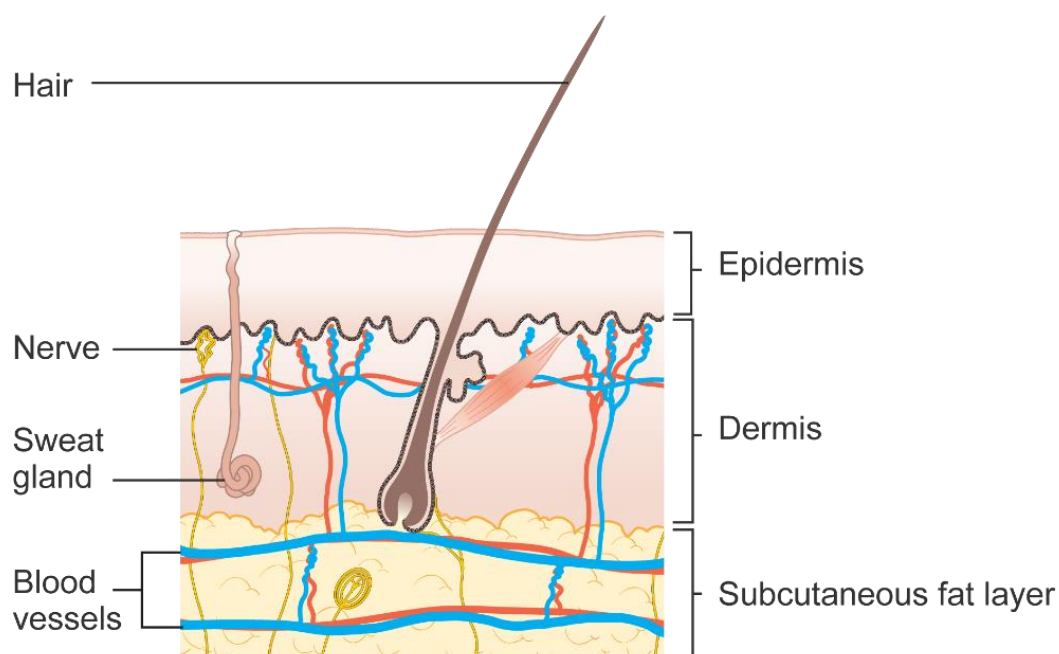


Figure 1.1: Structure of the skin, showing epidermis, dermis and subcutaneous layers, vascular network, nerve cells and hair follicle arrangement through the layers. Reproduced (modified) with permission from [Cancer Research UK/Wikimedia commons](https://www.cancerresearchuk.org/wikimedia-commons) [CC-BY-SA 4.0](https://creativecommons.org/licenses/by-sa/4.0/).

they progress through the subsequent epidermal layers; the stratum spinosum and the stratum granulosum, which are responsible for synthesis of structural proteins including keratin and lipids. When they reach the outermost layer, the stratum corneum, the keratinocytes undergo structural changes, lose their organelles and become compact, flat squamous cells known as corneocytes (Baroni *et al.*, 2012). Tight junction attachments form between keratinocytes, these combined with keratin filaments and the cross-linked proteins and covalently bound lipids of the cell envelope, provide a tough resistant barrier (Losquadro, 2017). Nutrients are supplied to the epidermis by diffusion, as there is no direct blood supply crossing the basement membrane known as the dermal-epidermal junction (Losquadro, 2017; Baroni *et al.*, 2012). This layer not only separates the two distinct sections of the skin barrier but also conveys overall structural integrity, limiting the passage of molecules between the two layers and regulating the transit of migrating cells (Losquadro, 2017).

The dermal-epidermal junction contains an array of structural proteins and anchoring filaments, including a lattice of type IV and VIII collagen fibres (Burgeson and Christiano, 1997; Losquadro, 2017). The dermis lies below the epidermis, between the dermal-epidermal junction and the subcutaneous fat layer, and is responsible for variations in local thickness of the skin.

The dermis is primarily composed of collagen, and the major cellular component are fibroblasts which produce collagen, elastin and other dermal proteins (Losquadro, 2017; Wang *et al.*, 2015). The dermis also contains blood vessels, nerves and sweat and sebaceous glands. The upper layer of the dermis, the papillary dermis, contains

loosely packed fibroblasts, collagen and blood vessels. The deep layer, the reticular dermis, is thicker and contains fewer cells, but a coarser denser network of collagen fibres (Losquadro, 2017; Nyström and Bruckner-Tuderman, 2019). The extracellular matrix of the dermis is primarily composed of two types of collagen fibres; type I which make up 80% of the dermis, and conveys tensile strength, and type III which makes up a further 15%, and gives the skin pliability (Meigel, Gay and Weber, 1977; Losquadro, 2017). Both collagen and elastin (another structural protein which gives the tissue its elasticity) are synthesised within fibroblast cells (Branchet *et al.*, 1991; Losquadro, 2017; Meigel, Gay and Weber, 1977; Nyström and Bruckner-Tuderman, 2019; Wang *et al.*, 2015). The blood supply to the dermis consists of a network of vessels throughout the reticular dermis with vascular loops supplying the papillary dermis (Losquadro, 2017). Structures that traverse the layers of the skin include the pilosebaceous units; comprising of a hair follicle, sebaceous gland, arrector pili muscle and nerve ending which cross the dermis and epidermis. Sweat glands are located in the reticular dermis and subcutaneous tissue, with ducts that traverse the epidermis; of these, the eccrine glands empty on to the skin surface and the apocrine glands to the hair shaft (Mellott, Zamierowski and Andrews, 2016; Losquadro, 2017).

In addition to providing a physical barrier against potential pathogens, the skin also exhibits a variety of biochemical and immunological functions; these include chemical barriers in the form of lipids, sweat and sebum, and secretion of antimicrobial peptides, complement proteins, cytokines and chemokines (Baroni *et al.*, 2012; Di Meglio, Perera and Nestle, 2011). Keratinocytes employ surface receptors to detect and recognise the presence of microbes, including detection of

lipopolysaccharide (LPS), peptidoglycan and flagellin, which allows the keratinocytes to distinguish commensals from potentially harmful pathogens, facilitating activation of the skins immune response (Nestle *et al.*, 2009). This results in recruitment and activation of immune cells, including neutrophils macrophages and natural killer cells (Di Meglio, Perera and Nestle, 2011). In addition, the presence of commensal flora provide competition for nutrients and physical space (Nestle *et al.*, 2009).

1.3 WOUNDS

In the UK, wound management is predominantly led by nurses and mainly includes patients treated in the community (66%), at secondary care facilities or those in long term care (Guest *et al.*, 2015). Annually, the management of wounds by the NHS is estimated to require 18.6 million practice nurse visits, 10.9 million community nurse visits, 7.7 million GP appointments and 3.4 million hospital outpatient appointments, at a total estimated cost of between £4.5 billion and £5.1 billion (Guest *et al.*, 2015). A recent study identified 11% of wounds managed by the NHS as unhealed surgical wounds, of these 68% were infected or considered at risk of infection at the commencement of management within the community (Guest, Fuller and Vowden, 2018). The study revealed that over a 12 month follow-up period, 18% of patients received antimicrobial dressings, 66% were prescribed systemic antimicrobials and 28% of patients were prescribed topical antimicrobials for a duration of 6 months or more. On average, patients whose wounds were not afflicted by infection healed in 1.9 months at an estimated cost of £2000 per wound, while the cost of managing unhealed surgical wounds with infection ranged from £5000 to £11200 per wound (Guest, Fuller and Vowden, 2018).

1.3.1 *Wound Types*

Wounds result from loss of integrity of the skin barrier due to injury, such as burns, or illnesses which result in the development of chronic skin ulcers (Singer and Clark, 1999). Wounds that result from injury are initially classified as acute wounds

regardless of aetiology, and may be caused by accident or traumatic injury, burn injury or surgery (Whitney, 2005). Acute wounds that fail to progress through the expected stages of healing, and therefore do not heal in a timely manner, are classified as chronic wounds.

Chronic wounds are defined as those which exhibit a delay in the normal wound healing trajectory (Metcalf, Bowler and Hurlow, 2014; Percival, 2017). Over ninety percent of chronic wounds are accounted for by venous ulcers, diabetic ulcers and pressure sores (Mustoe, O'Shaughnessy and Kloeters, 2006). These chronic wounds are associated with the pathophysiology of the patients concomitant underlying medical conditions. Venous ulcers occur in the legs, as a result of poorly functioning valves. Diabetic ulcers develop from minor cuts and abrasions due to poor circulation and compromised immune function, and pressure ulcers occur in patients who are bedridden or those who have very limited mobility (Kathawala *et al.*, 2019). All chronic wounds are characterised by their failure to heal and chronic inflammation of the wound bed (Demidova-Rice, Hamblin and Herman, 2012). In addition to underlying pathophysiology, infection of the wound bed plays a significant role in the transition of an acute wound to a chronic wound state (Edwards and Harding, 2004).

1.3.2 *Wound Healing*

Wound healing is a continuous process classified in to four distinct yet overlapping phases; haemostasis, inflammation, proliferation and remodelling (Figure 1.2) (Mellott, Zamierowski and Andrews, 2016). During haemostasis a fibrin clot is formed

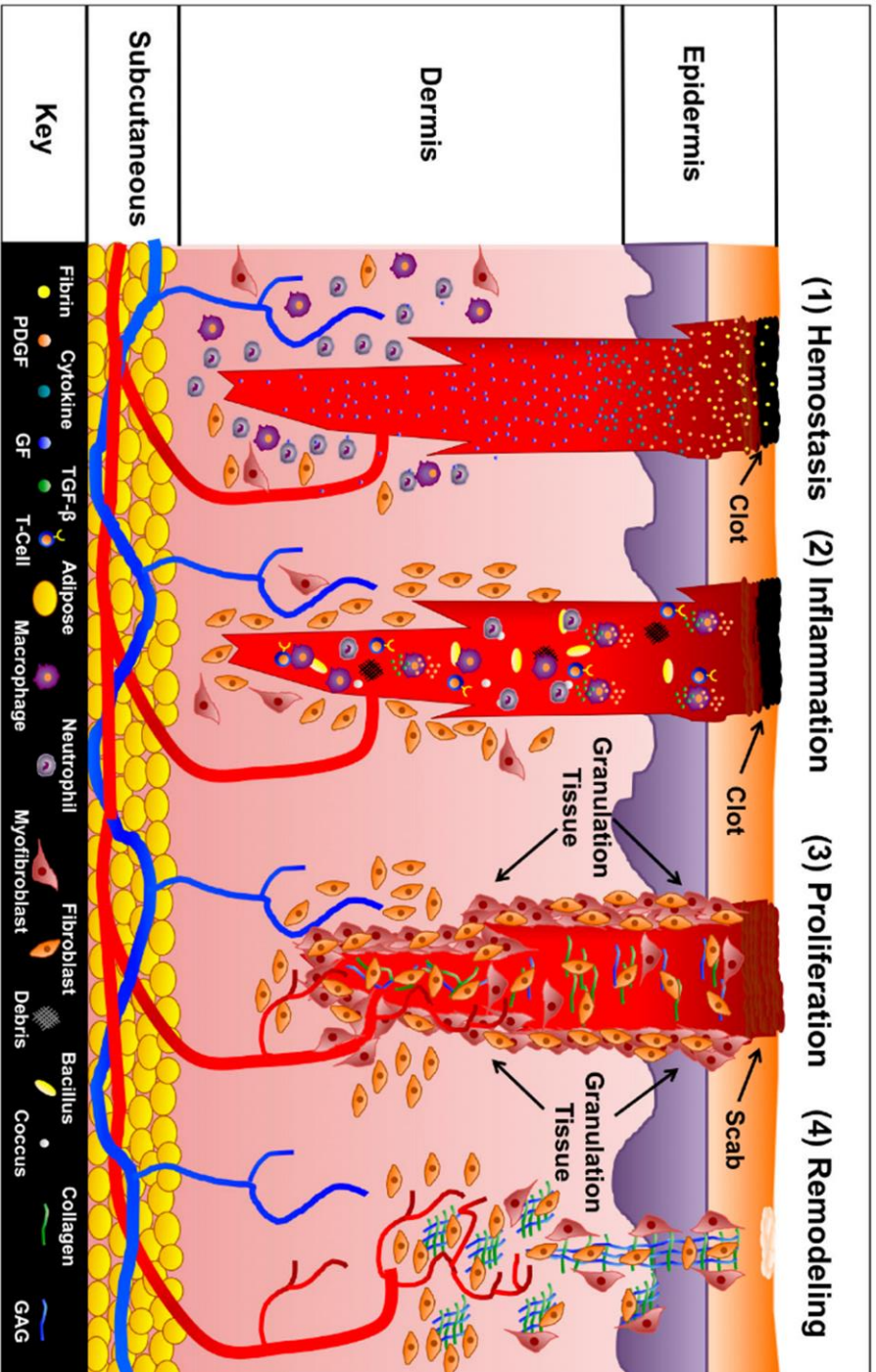


Figure 1.2: Illustration showing the 4 phases of wound healing; haemostasis, inflammation, proliferation and remodelling. Reproduced from Mellott, Zamierowski and Andrews, (2016) [CC BY 4.0].

and aggregation of platelets occurs, this controls bleeding from the site of injury. Chemokines are released from activated platelets to attract cells involved in the inflammatory phase; namely neutrophils, macrophages and lymphocytes. These inflammatory cells then release pro-inflammatory cytokines and growth factors, ingest foreign material, increase vascular permeability and stimulate fibroblast activity (Gosain and DiPietro, 2004; Guo and DiPietro, 2010; Mellott, Zamierowski and Andrews, 2016).

The proliferation phase is characterised by angiogenesis and granulation tissue formation, filling the wound site with new tissue. Fibroblast proliferation and collagen synthesis then result in re-epithelialisation by keratinocytes, which migrate to the surface from the basal layer (stratum basale) of the epidermis (Gosain and DiPietro, 2004; Guo and DiPietro, 2010; Mellott, Zamierowski and Andrews, 2016).

The process of remodelling occurs gradually over time whereby synthesis, cross-linking and proper alignment of collagen conveys strength to the new tissue. As this process progresses the proportion of mature type I collagen to type III collagen increases. However, scar tissue will retain a higher proportion of type III collagen long term compared to healthy skin, and will not regain the full strength of normal skin (Robins *et al.*, 2003; Singh, Young and McNaught, 2017). Progression of wound healing is dependent on a variety of factors, such as wound size, depth and location on the body, the age of the patient and the presence of underlying disease (Morton and Phillips, 2016).

Acute wounds; those resulting from burns or traumatic injury, surgical wounds and minor injuries, usually progress through the normal phases of healing in a timely manner. However, failure to manage healing of these wounds properly can result in complications, infection and delayed healing. Chronic wounds fail to progress, and in general wounds failing to heal within 3 months are considered chronic (Morton and Phillips, 2016). The expected healing trajectory of a wound of any size can be estimated based on the expected rate in reduction of wound size over time (Whitney, 2005).

Chronic wounds are often associated with underlying medical conditions including diabetes mellitus and vascular disease, or infection. Several factors characterise chronic wounds, including poor oxygenation, high levels of inflammatory cytokines, proteases and reactive oxygen species, senescent fibroblasts, and high levels of bacterial colonisation (Nicks *et al.*, 2010; Siddiqui and Bernstein, 2010; Morton and Phillips, 2016).

1.3.3 *Skin Microflora*

The surface of the skin, as well as its hair follicles, sweat and sebaceous glands, are covered with approximately 10^6 bacteria per square centimetre (Belkaid and Segre, 2014). However, skin sampling technique influences the estimated bacterial load, whereby one study has shown that 1×10^4 organisms per square centimetre was detected by swabbing, 5×10^4 per square centimetre by scraping and 1×10^6 per square centimetre from the analysis of punch biopsy specimens taken from skin at

the inner elbow of healthy human volunteers, detected by qPCR sequencing of 16S rRNA (Grice *et al.*, 2008). Samples from this skin site were found to be dominated by *Proteobacteria*, particularly *Pseudomonas* species and *Janthinobacterium* species (Grice *et al.*, 2008).

Species diversity of the skin microflora occurs between individuals, as well as across the varied range of microenvironments represented by different body sites, and includes a high diversity of viral and fungal commensals (Oh *et al.*, 2014). Studies comparing bacterial microflora detected across body sites have been conducted using sequencing of 16S rRNA collected from twenty skin sites representing diverse microenvironments, including sebaceous, dry and moist sites (Grice *et al.*, 2009) and comparing those collected from skin and other body sites (Costello *et al.*, 2009). Both studies concluded that the composition of the microbial community varies with the type of sampling site, and that variation between individuals is greater than the variation over time in each individual subject sampled. *Propionibacteria* species and *Staphylococci* were found to dominate sebaceous skin sites, while *Corynebacteria* species predominated at moist sites, although *staphylococci* were also present. Dry skin sites were found to harbour mixed communities without notable dominant species (Grice *et al.*, 2009). These sequencing based studies identified 19 microbial phyla across 20 skin sites (Grice *et al.*, 2009), and 22 microbial phyla from 27 skin and other body sites (Costello *et al.*, 2009). However, both studies concluded that the vast majority of sequences identified were attributed to four phyla, *Actinobacteria*, *Firmicutes*, *Proteobacteria* and *Bacteroidetes* (Grice *et al.*, 2009; Costello *et al.*, 2009).

Historically, studies of the skin microflora have relied on culture based methods to identify resident organisms and it is now apparent that the diversity of the skin microflora was hugely underestimated (Fredricks, 2001). Early studies of the skin microflora identified organisms such as species of *Staphylococci*, *Micrococci*, *Corynebacterium* and *Propionibacterium*, but concluded that gram negative rods were uncommon inhabitants of human skin (Roth and James, 1989; Evans *et al.*, 1950), in direct contrast to the contemporary studies discussed above which identified *Proteobacteria* as the third most common phyla using sequencing based approaches.

1.3.4 *Wound Infection*

Bacterial infection delays wound healing and plays a significant role in the failure of a wound to move through the four phases of healing (haemostasis, inflammation, proliferation and remodelling) in a timely manner (Barajas-Nava *et al.*, 2013; Bowler, Duerden and Armstrong, 2001; Edwards and Harding, 2004; Morton and Phillips, 2016). However, the mere presence of bacteria within a wound site does not necessarily result in a clinically significant effect on the patient. The ‘wound infection continuum’ (Figure 1.3) describes the progression of infection in a wound by breaking down this continuous process in to a number of phases (Haesler and Ousey, 2018). The first phase, contamination, is characterised by the presence of low numbers of microbes within the wound bed that are not actively undergoing replication, and do not elicit a host response (Macgregor *et al.*, 2008; Landis, 2008; International Wound Infection Institute, 2016). During the second phase, known as colonisation, microbes

begin to replicate within the wound bed and increase in number, although there is no tissue damage or host response seen, and this microbial proliferation has no clinical impact on the wound (Macgregor *et al.*, 2008; Landis, 2008; International Wound Infection Institute, 2016).

Local infection occurs when multiplying organisms begin to have a detrimental effect on wound healing, causing damage to tissue within the wound bed. Microbes move deeper in to the wound tissues and proliferate at a faster rate, resulting from failure of the host immune system to control bacterial proliferation and invasion (Macgregor *et al.*, 2008; Landis, 2008; International Wound Infection Institute, 2016) The term local infection has previously been used interchangeably with ‘critical colonisation’, with some debate surrounding use of the latter to define clinical observation of infection in the absence of microbiological analysis. The most recent international consensus document advises against use of ‘critical colonisation’ to avoid ambiguity (International Wound Infection Institute, 2016). Without intervention, local infection may spread to adjacent tissue beyond the wound border (spreading infection), where infection may involve deep tissues, muscles and organs or body cavities. Eventually infection may progress to affect the body as a whole (systemic infection), with microbes spreading through the systemic circulatory and lymphatic system, resulting in sepsis, organ failure and death (Macgregor *et al.*, 2008; International Wound Infection Institute, 2016). Wound contamination will likely be poly-microbial, with bacteria originating from the surrounding skin flora and other endogenous sources, primarily from the oral cavity, gastrointestinal and genitourinary tracts (Bowler, Duerden and Armstrong, 2001).

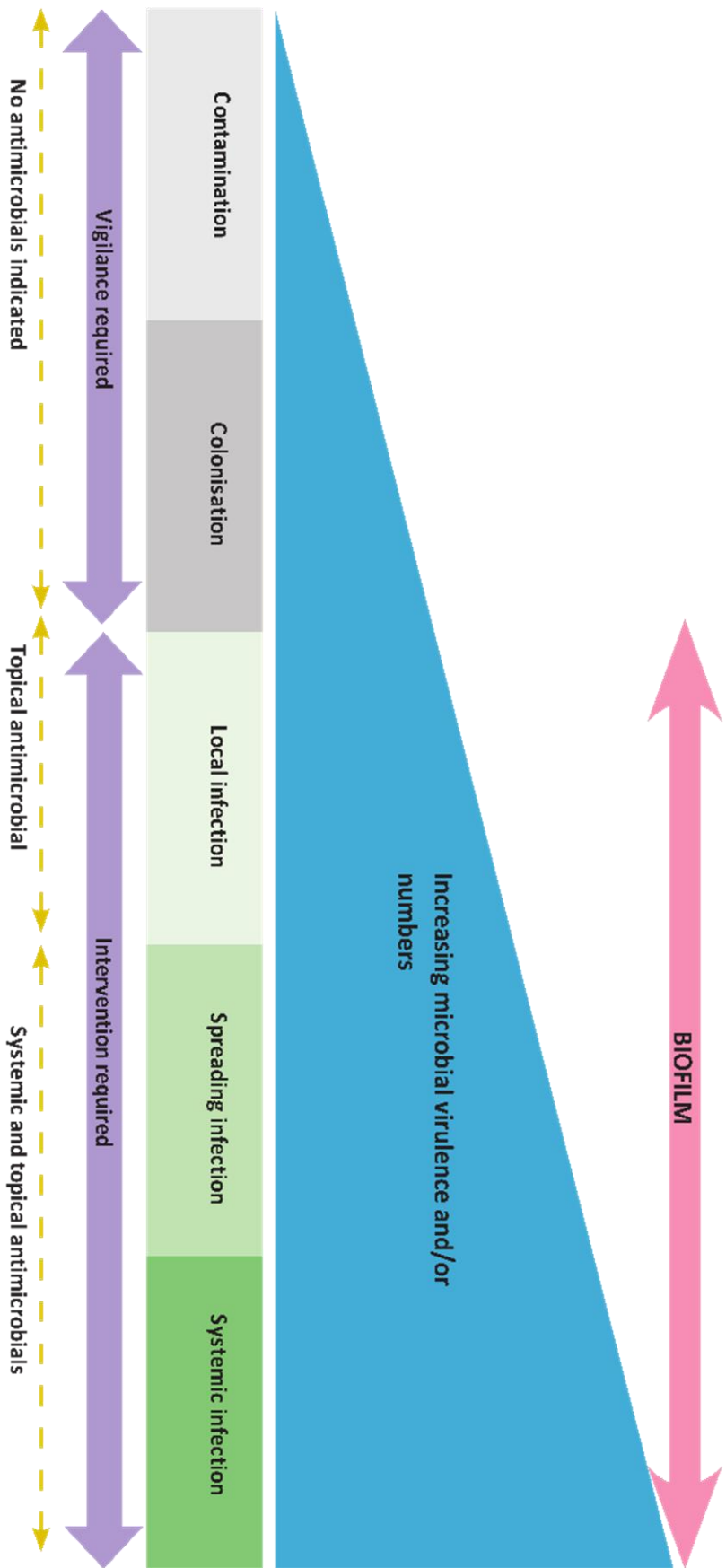


Figure 1.3: The wound infection continuum describes the progression of wound infection through five phases from contamination to systemic infection. Reproduced with permission from [International Wound Infection Institute \(IWII\)](#), (2016).

In chronic wounds, coagulase negative staphylococci and *Staphylococcus aureus* generally dominate at the early stage of infection, subsequently infection of the wound bed frequently involves endogenous gram negative rods including *Escherichia coli*, *Klebsiella pneumoniae* and *Enterobacter* species, as well as *Pseudomonas* species and *Acinetobacter* species from environmental sources (Bowler, Duerden and Armstrong, 2001; Daeschlein, 2013). Changes in the wound microenvironment allow anaerobes to become established as the infection matures. Anaerobes may originate from the gastrointestinal tract and oral cavity, where a high proportion of such organisms make up the normal microflora, and may include *Bacteroides*, *Prevotella*, *Porphyromonas* and *Peptostreptococcus* species (Bowler, 2002; Bowler, Duerden and Armstrong, 2001; Daeschlein, 2013).

The presence of bacterial infection and bacterial toxins (e.g. LPS) in the wound bed results in an excessive inflammation leading to tissue damage (Demidova-Rice, Hamblin and Herman, 2012; Crompton *et al.*, 2016); inflammatory cells produce proteases which breakdown collagen and other extracellular matrix proteins and growth factors within the wound bed (Demidova-Rice, Hamblin and Herman, 2012). *S. aureus*, *Pseudomonas aeruginosa* and beta-haemolytic streptococci, as well as anaerobes, are primarily implicated in delayed healing in both acute and chronic wounds (Bowler, Duerden and Armstrong, 2001; Alrawi, Crowley and Pape, 2014; DiMuzio *et al.*, 2014). The causative organisms of wound infection are now widely thought to exist as biofilms; aggregates of microorganisms encased in a self-produced extracellular matrix (James *et al.*, 2008; Kennedy, Brammah and Wills, 2010; Bertesteanu *et al.*, 2014). If the microbial burden of wounds is not adequately

managed, then there is a significant risk of the development of sepsis. This is serious complication in patients with chronic wounds and severe burns, and is the leading cause of mortality. Early management of clinically relevant wound infection is essential to minimise the risk of sepsis (Ma, Tian and Liang, 2016; Patil *et al.*, 2017; White *et al.*, 2015).

1.4 BIOFILMS

It is now widely accepted that bacteria commonly exist in sessile communities known as biofilms, rather than as individual free swimming cells. Biofilms are complex communities of microorganisms attached to surfaces or formed from aggregates of cells, encased in self-produced extracellular polymeric substances (EPS) (Hall and Mah, 2017; Roy *et al.*, 2018) comprised of polysaccharides, proteins, lipids and extracellular DNA (Vyas and Wong, 2016). Biofilms in environmental water systems were identified as early as 1936 when the tendency for marine organisms to adhere to solid surfaces was first observed (Zobell and Anderson, 1936). However, the potential importance of biofilm formation in a clinical setting didn't become apparent for several decades. The first clinically relevant biofilms were identified when bacterial aggregates were recognised in the formation of dental plaques, within sputum from the lungs of cystic fibrosis patients and adhered to indwelling catheters (Costerton, Geesey and Cheng, 1978; Lam *et al.*, 1980; Gibbons *et al.*, 1966; Høiby, 2009; Høiby and Axelsen, 2009; Marrie and Costerton, 1984). It is now understood that biofilm formation plays a role in the establishment and persistence of a vast array of infections and diseases (Costerton, Stewart and Greenberg, 1999; Dufour, Leung and Lévesque, 2010). Once established, biofilms are known to be highly resistant to antimicrobials and the host immune response, being responsible for various clinically relevant infections, including lung infection in cystic fibrosis, endocarditis, osteomyelitis, acute burn infection and chronic wound infections (Cooper, Bjarnsholt and Alhede, 2014; Høiby *et al.*, 2015; Furukawa, Kuchma and O'Toole, 2006).

1.4.1 *Biofilm Formation*

The formation and development of biofilm can be described as occurring in 5 stages (Figure 1.4); Initial attachment to the surface, whether inanimate or a tissue, followed by irreversible attachment where cells become more firmly adhered and EPS production begins. The first stage of maturation includes early development of biofilm architecture, followed by a further second phase of maturation where this architecture develops complexity, and finally the dispersal phase characterised by the release of cells from the biofilm (Stoodley *et al.*, 2002). Quorum sensing (QS); population density dependent cell to cell signalling systems, mediate co-ordinated behaviour in bacteria when certain threshold cell densities are established, and are considered fundamental regulators of biofilm formation and virulence (Passos da Silva *et al.*, 2017; Saxena *et al.*, 2019). However, the importance of QS regulation of biofilm formation is influenced by the local environmental conditions, and hence the contribution of QS to biofilm infection varies depending on the site of infection (Passos da Silva *et al.*, 2017).

The intra cellular signalling molecule cyclic di-GMP (c-di-GMP) is thought to be responsible for co-ordinating the transition from planktonic to the biofilm mode of growth, with high levels of this signalling molecule associated with biofilm formation and low levels of c-di-GMP present in motile cells (Valentini and Filloux, 2016). The mechanism of surface attachment varies between bacterial species. Initial attachment of *P. aeruginosa* (a widely studied model organism) during biofilm formation is mediated by flagellar swimming motility and usually occurs at the cell poles (Sauer *et al.*, 2002; Ha and O'Toole, 2015). Movement across a surface by these

reversibly attached cells is facilitated by type IV pili mediated 'twitching motility or swarming motility powered by flagella (O'Toole and Kolter, 1998b; Ha and O'Toole, 2015).

Irreversible' attachment is facilitated by suppression of these motility functions (Ha and O'Toole, 2015). In *S. aureus* there are several modes of surface attachment, either involving a polysaccharide antigen named polysaccharide intercellular antigen (PIA) or by PIA independent mechanisms involving alternative strain dependant attachment proteins (Archer *et al.*, 2011). Production of EPS stabilises and reinforces attachment and facilitates the development of three-dimensional biofilm structures. The composition of the EPS varies depending on the species present within the biofilm and influences the formation of structural architecture (O'Toole and Wong, 2016; Borlee *et al.*, 2010), with EPS production thought to be regulated by quorum sensing (Frederick *et al.*, 2011).

Maturation occurs as cells within the biofilm divide and multiply, and as a result of EPS production; the overall structure of the biofilm architecture is dependent on the nature of the components of the EPS. This process can result in the formation of cone shaped or mushroom shaped microcolonies interspersed with water channels. Gradients of pH, oxygen and nutrients within the biofilm provides a diverse range of microenvironments, allowing fastidious organisms with a variety of specific environmental requirements to co-exist within multispecies biofilms (Costerton *et al.*, 1995; Kuchma, Connolly and O'Toole, 2005; Frederick *et al.*, 2011; Flemming and Wingender, 2010).

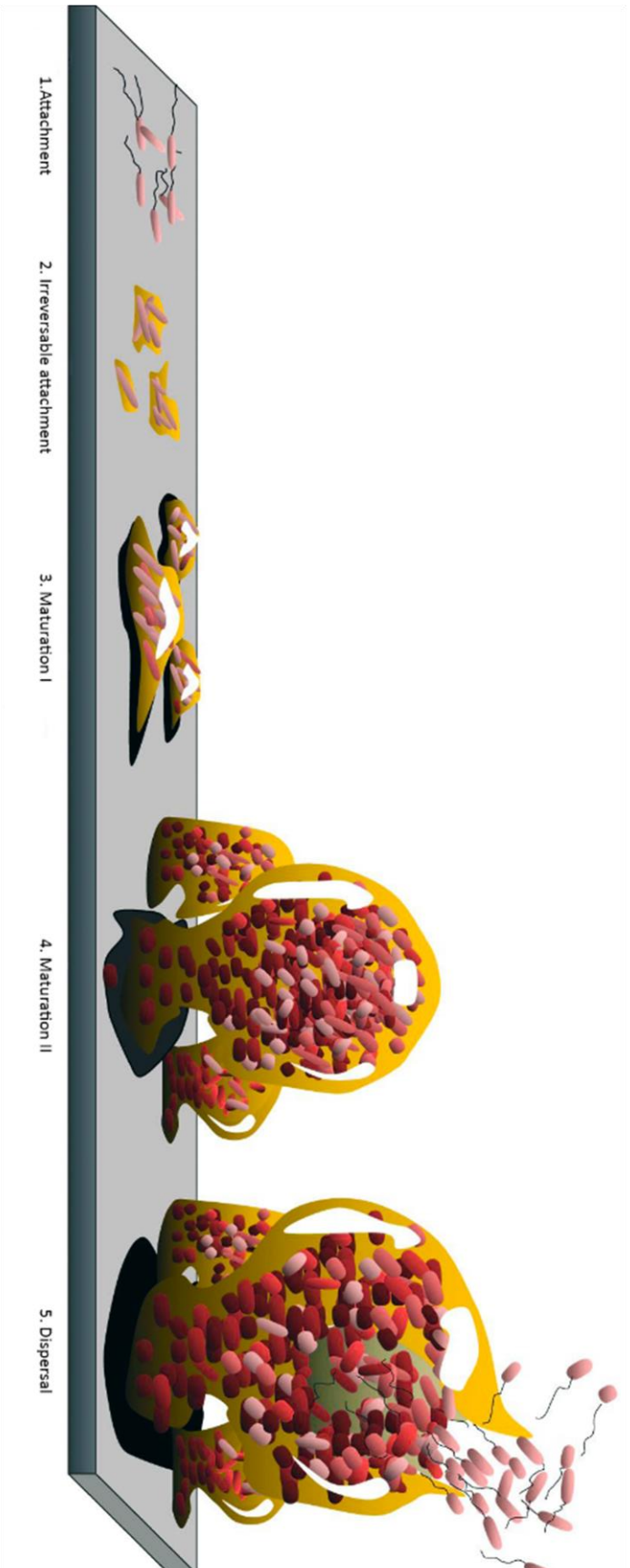


Figure 1.4: Five stages of biofilm formation and maturation, showing initial attachment, irreversible attachment, stages of maturation and dispersal Adapted from Monroe (2007) CC BY 2.5.

Maturation occurs as cells within the biofilm divide and multiply, and as a result of EPS production; the overall structure of the biofilm architecture is dependent on the nature of the components of the EPS. This process can result in the formation of cone shaped or mushroom shaped microcolonies interspersed with water channels. Gradients of pH, oxygen and nutrients within the biofilm provides a diverse range of microenvironments, allowing fastidious organisms with a variety of specific environmental requirements to co-exist within multispecies biofilms (Costerton *et al.*, 1995; Kuchma, Connolly and O’Toole, 2005; Frederick *et al.*, 2011; Flemming and Wingender, 2010).

The final phase of the biofilm life-cycle, dispersal, involves detachment of cells from the biofilm and their release in to the environment; a process essential for dissemination to a new location and enabling disease transmission (Kaplan, 2010; Petrova and Sauer, 2016). There are several processes by which cells can leave a biofilm, which include both active and passive mechanisms of dispersal. Passive mechanisms include abrasion, erosion and sloughing which are driven by the actions of external forces on the biofilm. Active dispersal is mediated from within the biofilm, usually in response to changes in conditions in the local biofilm environment (Fleming and Rumbaugh, 2017), driven by many species dependent cues and signalling systems involved in the active dispersal of cells from within the biofilm. These ultimately lead to degradation of areas of the EPS to facilitate mobilisation of cells from within the biofilm which are then released as planktonic cells able to disperse to a new location (McDougald *et al.*, 2012).

1.4.2 *Biofilms in Wounds*

The formation of biofilms in the wound bed has been implicated in the transition from an acute to chronic wound state, due to resultant persistent inflammation, delayed granulation and epithelial migration, and impaired migration and proliferation of keratinocytes (Rajpaul, 2015). Microscopic evaluation of the presence of biofilm in both chronic and acute wounds resulted in identification of large aggregates, classified as biofilm by the authors, in 60% of chronic wounds and 6% of acute wounds (James *et al.*, 2008). In addition, the authors noted that small micro colonies were often present in the acute wounds examined in this clinical study. Furthermore, a systematic review and meta-analysis on studies conducted between 2008 and 2015 reported evidence for the presence of biofilms in 78.2% of human chronic wounds (Malone *et al.*, 2017). The studies included diabetic foot ulcers, venous leg ulcers, pressure ulcers and non-healing surgical wounds. A recent study assessed the presence of biofilm in acute epidermal wounds, blisters that were formed on the buttocks of healthy human volunteers (Bay *et al.*, 2018). This study demonstrated the formation of aggregates of coagulase negative staphylococci in 78% of wounds. These were generally localised at the wound edges and were significantly more common within the wounded tissue than on the adjacent healthy skin (Bay *et al.*, 2018).

Animal studies have been performed to assess the effect of biofilm formation on wound healing under controlled conditions. For example, in a rabbit model of wound infection (Gurjala *et al.*, 2011), *S. aureus* was found to form a mature biofilm within 24 hours of inoculation and generate a sustained low grade host response localised

within the wound bed. The study also demonstrated that the presence of biofilm contributed to the impairment of wound healing processes. A mouse model of chronic wound infection has been used to compare the effect of biofilm formation in diabetic and healthy animals (Nguyen *et al.*, 2013). Biofilm formation delayed healing in both groups but the effect was exaggerated in the diabetic animals, demonstrating the importance of this underlying pathophysiology for predisposing the development of chronic wounds. These studies clearly demonstrate the presence of biofilm in a variety of wound types, providing evidence for the involvement of biofilm formation in the development of wound infection.

1.4.3 *Biofilm Tolerance*

Reduced susceptibility to antimicrobials is intrinsic to the biofilm mode of growth, but is usually considered tolerance rather than true resistance, and can be lost when biofilm bacteria are released in to the environment and revert to a planktonic state (Bridier *et al.*, 2011). Contributing mechanisms include, interaction with the extracellular matrix slowing penetration of antimicrobial agents, slow growth rate resulting in reduced susceptibility, heterogeneous metabolism due to distinct sub-populations and the presence of persisters (Olsen, 2015). The concentration of antibiotics required to treat biofilms are thought to be 100 to 1000-fold higher than the planktonic minimum inhibitory concentration (MIC) (Hall and Mah, 2017; Del Pozo, 2018). As a result biofilm infections are likely to persist long-term despite

antibiotic treatment, and are prone to relapse after treatment is completed (Hall and Mah, 2017; Del Pozo, 2018).

Mature biofilms are characterised by the production of EPS which can interact with and inhibit the diffusion of antimicrobial agents. Positively charged antimicrobials in particular, may become bound to negatively charged polymers present within the biofilm EPS, preventing transit into the biofilm structure and interaction with drug targets (Jolivet-Gougeon and Bonnaure-Mallet, 2014). Nutrient and oxygen concentration vary between the surface and centre of biofilm formations, resulting in variability in the growth rate of bacterial cells within the biofilm (Stewart, 2015; Høiby *et al.*, 2010). This impacts susceptibility to antimicrobials which are only effective against actively growing cells, for example the β -lactams which inhibit bacterial cell wall synthesis (Stewart, 2015; Høiby *et al.*, 2010). In addition, dormant persister cells are thought to exist as a small sub-population, able to repopulate a biofilm when cell numbers are depleted by an antimicrobial, possibly resulting in the resurgence of infection after treatment (Lewis, 2010; Fisher, Gollan and Helaine, 2017). Furthermore, a high mutation rate among biofilm bacteria compared to their planktonic counterparts, as well as high cell density facilitating increased horizontal gene transfer, results in an elevated occurrence of multi-drug resistance mechanisms among bacterial cells within a biofilm (Jolivet-Gougeon and Bonnaure-Mallet, 2014). In addition, expression of β -lactamase enzymes, induced in response to exposure to β -lactam antibiotics can accumulate in the biofilm EPS (Giwercman *et al.*, 1990; Bagge *et al.*, 2004), affording protection not only to the enzyme producing cells themselves but also adjacent cells within the biofilm.

1.5 DIAGNOSIS OF WOUND INFECTION

There is no universally adopted consensus for the diagnosis of wound infection (Hughes, 2016), which usually relies on the ability of clinicians to identify the clinical signs of infection. Diagnosis of wound infection is therefore somewhat subjective, relying on the specific experience of the clinician and their interpretation of clinical symptoms and non-specific test results (Haalboom *et al*, 2019). Indicators of infection include increased pain, an excessive or increased volume of exudate, localised heat and swelling, malodour and erythema (Hughes, 2016; Macgregor *et al.*, 2008). However, in chronic wounds these classic clinical signs of infection are often minimal or absent (Siddiqui and Bernstein, 2010). Conversely, the systemic response to burn injury results in the release of high levels of inflammatory mediators (Greenhalgh *et al.*, 2007; Jeschke and Herndon, 2014). As a result the standard indicators are difficult to apply to both these wound types.

Visual observation is often important during preliminary wound assessment, whereby the appearance of the wound is categorised and documented. Photography and digital tracing may be employed to facilitate recording of wound appearance parameters and can subsequently be employed to monitor progression (Li *et al*, 2020). There is no definitive testing available to identify wound infection, but microbiological wound cultures are often employed to supplement clinical diagnosis and inform treatment (Blokhus-Arkes *et al.*, 2015; Greenhalgh *et al.*, 2007). However, it should be noted that bacterial load or type detected cannot provide a diagnosis in itself and microbiological analysis should only be used to complement

clinical diagnosis; to confirm the presence of pathogenic strains within the wound bed and establish antibiotic sensitivities (Sibbald *et al.*, 2003; International Wound Infection Institute (IWII), 2016; Macgregor *et al.*, 2008; Edwards and Harding, 2004; Landis, 2008).

A bacterial load in excess of 10^5 cfu per gram of tissue within the wound bed, as measured by wound biopsy, has been correlated with an increased risk of the development of sepsis. However, although wound biopsy is considered the gold standard method for the identification of bacteria in the wound bed, this is rarely used in routine clinical practice because it is an invasive and painful procedure (Sjöberg *et al.*, 2003; Uppal *et al.*, 2007; Haalboom *et al.*, 2019). The signs and symptoms that clinicians use as indicators of wound infection vary as the wound infection continuum progresses (see section 1.3.4) and are outlined in Table 1.1 below.

Table 1.1: Signs and symptoms indicative of infection as the phases of the wound infection continuum progress (International Wound Infection Institute (IWII), 2016).

Local Infection		Spreading infection	Systemic infection
Subtle	Classic		
Hypergranulation	Erythema	Lymphangitis	Severe sepsis
Bleeding, friable granulation	Local warmth	Crepitus	Septic shock
Epithelial bridging and pocketing in granulation tissue	Swelling	Wound breakdown/dehiscence	Organ failure
	Purulent discharge		Death
Delayed healing	Delayed healing	Malaise/Lethargy	
	Wound breakdown and enlargement	Loss of appetite	
	New or increasing pain	Inflammation, swelling of lymph glands	
	Increasing malodour		
New or increasing pain			
Increasing malodour			

1.5.1 *Antimicrobial Resistance*

The relationship between antibiotic use and resistance was documented in the 1940s, before penicillin was widely available for clinical use; when the first bacterial penicillinase enzymes were isolated from *Escherichia coli* (Greenwood, 2008). At this early stage in the development of β -lactam antibiotics, it was also demonstrated that resistance to penicillin could be induced in Staphylococci, by repeatedly sub-culturing

in the presence of the antibiotic (Greenwood, 2008; Kong, Schneper and Mathee, 2010).

Bacteria employ a variety of mechanisms to convey resistance to antibiotics, including deactivation of the antibiotic, modification of the target site, antibiotic sequestering and efflux. In addition, bacteria exhibit high levels of genetic plasticity, allowing adaptation to new antibiotic treatments. This manifests as genetic mutation to avoid the mechanism of action of the antibiotic, or uptake of DNA by horizontal gene transfer resulting in acquisition of established resistance mechanisms (Munita and Arias, 2016; Peterson and Kaur, 2018). For example, there are three primary mechanisms of resistance to the β -lactam antibiotics: Firstly, deactivation of the antibiotic through hydrolysis by β -lactamase enzymes; a mechanism of resistance found among both gram-positive and gram-negative organisms (Wilke, Lovering and Strynadka, 2005; Babic, Hujer and Bonomo, 2006; Peterson and Kaur, 2018). Secondly, alteration of the target site, through modification or acquisition of resistant penicillin binding proteins (PBPs), found in several important gram-positive pathogens, including species of Staphylococci and Streptococci (Wilke, Lovering and Strynadka, 2005; Peterson and Kaur, 2018). Finally, prevention of access of the antibiotic to the target site through alterations to membrane permeability, and upregulation of efflux pumps which actively remove antimicrobial compounds from the bacterial cell, as identified in *Pseudomonas* species and other gram-negatives (Wilke, Lovering and Strynadka, 2005; Babic, Hujer and Bonomo, 2006; Peterson and Kaur, 2018).

1.5.1.1 Strategies to Combat AMR

It is now widely accepted that we are facing a public health crisis as antimicrobial resistance (AMR) continues to emerge globally, resulting in ever increasing numbers of multi-drug resistant organisms. It is estimated that without intervention, annual deaths attributed to antimicrobial resistance will reach 10 million by 2050 with a global economic cost of 100 trillion USD (O'Neill, 2014, 2016). Both the World Health Organisation and the UK Government have committed to addressing this crisis through the development of 'The global action plan on antimicrobial resistance' and 'The review on antimicrobial resistance' (World Health Organization, 2016; O'Neill, 2016). The final report of 'The Review on Antimicrobial Resistance' (O'Neill, 2016) highlights 10 fundamental recommendations or 'commandments' for tackling the AMR crisis. These are summarised in Table 1.2 and firstly, includes suggested strategies to reduce the current demand by altering the ways antibiotics are consumed and prescribed (1-7). Secondly, the need to increase the number of available antimicrobials to treat infections that have developed resistance to those currently available (8-9) and finally, the need for global cooperation in these actions (10). However, a review of achievement of these recommendations two years after publication of the final report, suggests progress has so far has been slow and that more investment and government commitment are required to achieve these goals (Collier and O'Neill, 2018).

Table 1.2: Summary of the 10 strategies to combat AMR recommended by the review on antimicrobial resistance (O’Neill, 2016), including the aims of each recommendation.

Strategy	Aims
1 A massive global public awareness campaign	Raise awareness to reduce demand by patients and farmers and hence prescribing by clinicians and veterinarians when antibiotics are not needed
2 Improve hygiene and prevent the spread of infection	Reducing the risk of infection to decrease the demand for treatment and the emergence of resistance. Improvements needed worldwide regardless of current levels of hygiene and sanitation.
3 Reduce unnecessary use of antimicrobials in agriculture and their dissemination into the environment	Halt use of antibiotics to prevent infection and as growth promoters with a particular focus on those critical for treatment of human disease. Improve transparency of antimicrobial use by food producers.
4 Improve global surveillance of drug resistance and antimicrobial consumption in humans and animals	Collection and sharing of data on antimicrobial use and emergence of resistance including biological mechanisms.
5 Promote new, rapid diagnostics to cut unnecessary use of antibiotics	Development of diagnostic tests that inform prescription of antibiotics to reduce unnecessary use, working towards a system where it is mandatory for prescribing to be informed by data and testing technology.
6 Promote development and use of vaccines and alternatives	Promote use of existing vaccines and early stage research, and sustain vaccine preventing infection hence the need for treatment.
7 Improve the numbers, pay and recognition of people working in infectious disease	Improved funding and career paths will attract more professionals to AMR related disciplines which are currently deemed less prestigious and financially rewarding than other sectors.
8 Establish a Global Innovation Fund for early-stage and non-commercial research	Link and expand currently established initiatives, and encourage further investment to boost innovative research and crucial but neglected areas within AMR research.
9 Better incentives to promote investment for new drugs and improving existing ones	Stimulate investment in antibiotic drug development by guaranteeing commercial returns as well as aiming to lower drug development cost by streamlining regulation and clinical trials networks.
10 Build a global coalition for real action – via the G20 and the UN	The AMR crisis can’t be solved by countries or regions alone, a cooperative global effort is required to achieve a meaningful outcome.

The research detailed within this thesis has relevance to strategy number 5 ‘Promote new, rapid diagnostics to cut unnecessary use of antibiotics’. Infection is the greatest cause of mortality in wound patients and is of particular concern in those with burn wounds (Lachiewicz *et al.*, 2017; Mir, Khurram and Khan, 2017). As a result, and due to the difficulty associated with definitively diagnosing wound infection and reliably identifying the causative organism, antibiotic treatment is commonly prescribed empirically (Shortt and Thoma, 2008; Lachiewicz *et al.*, 2017; Mir, Khurram and Khan, 2017). Treatment strategies vary widely, with choice of antibiotic usually determined by the perceived risk of infection, and the most likely contaminating organism based on wound location and knowledge of local epidemiology (Shortt and Thoma, 2008; Mir, Khurram and Khan, 2017; Nicks *et al.*, 2010). The common practice of empirical prescribing of antimicrobials is a major concern leading to huge over-use of antibiotics and further perpetuates the rise in antimicrobial resistance. The development of new rapid approaches to the diagnosis of wound infection would allow clinicians to confidently identify infection at an early stage and aid identification of the causative organisms. This would facilitate early use of appropriate antibiotics and eliminate the need for empiric therapy, thus eliminating use of antibiotics when they are not required, while promoting targeted therapy.

1.5.2 *Emerging Approaches to Wound Diagnostics*

Considering the difficulties associated with wound management it is unsurprising that there is increasing interest in the use of novel technologies for wound

monitoring and infection diagnosis. The use of three-dimensional imaging to monitor wound healing progress has been explored (Savage and Jeffery, 2013). The authors found that the technology could be successfully implemented for the measurement of wound size, volume and depth, and that it provided a useful record of the visual status of the wound. However, it was concluded that the high cost compared to traditional photography and the time consuming set up required made the technology unsuitable for routine clinical management without further technological advancements (Savage and Jeffery, 2013).

Several studies have investigated the use of small sensors to monitor a variety of wound parameters. For example, a sensing system combining temperature, moisture and pressure sensors with a wireless telemetry system connected to a portable receiver has been trialled in healthy volunteers (Mehmood *et al.*, 2015). This study successfully demonstrated the potential to continuously monitor these wound parameters in real-time, without disturbing the wound, and suggested that changes in both temperature and moisture level could provide early indication of infection.

Sensing of uric acid as an indicator of wound severity has been explored by a number of studies, which have integrated uric acid sensors into wound dressings, so called 'smart dressings' (Sharp and Davis, 2008; Phair *et al.*, 2014; Kassal *et al.*, 2015). The application of uric acid sensing is two-fold; uric acid concentration is expected to rise as wound healing progresses normally (Sharp and Davis, 2008), but a rapid and sustained decrease in uric acid concentration could indicate increased metabolism by invasive bacterial species (capable of uric acid metabolism, such as *P. aeruginosa*)

and hence provide an early indication of infection (Phair *et al.*, 2014; Kassal *et al.*, 2015).

Another sensing approach to chronic wound management is the use of pH detection for monitoring healing progression (Rahimi *et al.*, 2016). Development of a flexible pH sensor array based on a polymer coated paper substrate allows pH mapping of the wound bed, in contrast to traditional probe devices which allow only single point pH measurement. This study successfully demonstrates the linear range of the sensor array between pH 4 and 10, and suggests the response rate, stability and biocompatibility of the device will make it suitable for integration in to a wound dressing for regular monitoring of chronic wounds (Rahimi *et al.*, 2016). A further study investigating the use of pH monitoring for wound management reports the development of a dual electrochemical sensor array, combining a pH sensor with a bacterial attachment sensor (Sheybani and Shukla, 2017). The aim of combining the two sensing elements was to increase selectivity over the use of pH sensors alone, to improve accuracy of the detection of bacterial infection in the wound bed. The authors used a polymer coating to stabilise the sensor array and promote bacterial attachment while preventing non-specific protein fouling. The study reports successful detection of bacterial growth within 30 minutes of inoculation at 10^2 cfu mL⁻¹, a pH range of 1 to 13 and 14 day stability of the sensor array, which was tested in the presence of a simulated wound fluid (Sheybani and Shukla, 2017).

Another 'smart dressing' technology has been developed that integrates lipid vesicles containing a fluorescent dye within a wound dressing to provide an early detection system for pathogenic bacterial biofilms (Thet *et al.*, 2016). In this study the authors

successfully demonstrated the efficacy of the dressing using an *ex vivo* porcine skin model of wound infection, whereby contact with bacterial biofilms of *P. aeruginosa*, *S. aureus* and *Enterococcus faecalis* resulted in release of the self-quenching dye from its vesicles, activating the fluorescence.

A recent study investigated the use of a multi-electrode sensor array for long term monitoring of wound healing (Kekonen *et al.*, 2019). The sensor was integrated in to a primary wound dressing and used to monitor the electrical impedance of both intact and wounded skin. The study reported a significant reduction in electrical impedance measured when the sensor was in contact with wounded skin compared to intact skin and suggested the sensor may be suitable for long term monitoring of wound healing processes. In addition, the study demonstrated concurrent stimulation of the wound with low intensity direct current, resulting in production of hydrogen peroxide at clinically relevant concentrations. Hydrogen peroxide is a known antimicrobial and production at the wound site may aid healing by preventing development of infection (Kekonen *et al.*, 2019)

An investigation in to the use of Field Asymmetric Ion Mobility Spectroscopy (FAIMS), a technique used to analysed gas phase ions based on their mobility in a carrier gas, demonstrated the potential application of this technology to the diagnosis of wound infection (Sun *et al.*, 2019). The authors combined the FAIMS technology with machine learning analysis to demonstrate the ability to successfully recognise 96.15% of samples from wounds infected with *E. coli* compared and uninfected controls. The study included samples from excised tissue, wound secretions and drain fluid that were culture positive for *E. coli* either alone or in combination with

other organisms. If further development of this study demonstrates that FAIMS technology can be utilised to recognise uninfected controls from a range of clinical relevant organisms this technology has the potential to provide useful diagnostic insight.

Use of the imaging mass spectrometry (IMS) technique MALDI IMS has been explored for the assessment of treatment of pressure ulcers (Taverna *et al*, 2015). This technique permits direct analysis of intact tissue without preliminary protein purification and was utilised within this study to identify protein signatures from three distinct niches; wound bed, hypertrophic epidermis and adjacent dermis, within chronic, intermediate and healing pressure ulcers. The authors found characteristic localisation of proteins within the different wound niches and suggest this technique could be implemented to facilitate monitoring response to treatment in pressure ulcers (Taverna *et al.*, 2015).

Development of low cost sensors for direct non-invasive detection of wound infection could revolutionise diagnostics. A recent study (Salinas Alvarez *et al*, 2019) begins to explore the use of a combination of low cost gas sensors for the detection of volatile compounds emitted from *P. aeruginosa* and 6 other microorganisms found on the skin. In this study four gas sensors for the detection of ammonia and amines, carbon dioxide, alcohol and acetone were investigated. The authors found that there were clear differences in the sensor response between this microbial species analysed, indicating the potential of this approach for the development of non-invasive diagnosis of infection.

Electronic nose technology aims to simulate the ability of the human olfactory system, through the use of multiple gas sensors, to detect characteristic signatures of odorous volatile compounds (Sun *et al.*, 2017). One study describes the optimisation of an array of 34 electrochemical and metal oxide sensors for the detection of bacterial infection of wounds. The optimal combination of 20 of these sensors, determined within this study, achieved a recognition rate of 96.15% of samples of *E. coli*, *S. aureus*, *P. aeruginosa* and bacterial culture media, effectively demonstrating the feasibility of this technology for identifying wound infections (Sun *et al.*, 2017).

Further development of these and additional novel approaches to wound management, and in particular the diagnosis of wound infection, is essential to improve patient care while reducing over-use of antibiotics in light of the ongoing AMR crisis.

1.5.3 *Microbial Volatiles*

Bacteria produce volatile compounds; metabolites with a low molecular weight and high vapour pressure that readily evaporate, and are released in to the surrounding environment. Bacterial production of over 1000 volatile compounds has been described, with a single species capable of producing up to 80 different compounds (Audrain *et al.*, 2015; Schulz and Dickschat, 2007). Primary fermentation of carbohydrates gives rise to short chain fatty acids (including lactate, acetate and propionate) and ethanol, while secondary fermentation produces butyrate,

propionate, propanol, butanol, and hexanol (Thorn and Greenman, 2012). Degradation of fatty acids through the β -oxidation pathway provides precursors for a range of classes of volatile compounds produced by bacteria (Schulz and Dickschat, 2007; Audrain *et al.*, 2015). Decarboxylation of these fatty acid derivatives then results in the production of alkanes, alkenes and methyl ketones (Schulz and Dickschat, 2007). Acetoin and 2,3-butanedione arise from fermentation of pyruvate (Audrain *et al.*, 2015), and modification of branched amino acids results in production of branched alcohols and branched aldehydes (Schulz and Dickschat, 2007; Audrain *et al.*, 2015). Organic sulphur compounds such as dimethyl sulphide and methanethiol are derived from the amino acid methionine, while hydrogen sulphide production results from the breakdown of cysteine, another sulphur containing amino acid (Audrain *et al.*, 2015). Nitrogen containing compounds, such as ammonia and amines are produced by metabolism of amino acids (Halász *et al.*, 1994; Audrain *et al.*, 2015) and trimethylamine is generated by catabolism of choline by anaerobic bacteria and through reduction of trimethylamine oxide under both aerobic and anaerobic conditions (Craciun and Balskus, 2012; Audrain *et al.*, 2015). Bacterial metabolism of the aromatic amino acids gives rise to phenolic and indolic compounds. For example, phenol, 4-ethylphenol and 4-methylphenol from tyrosine, phenylpropanoate and phenylacetate from phenylalanine, and indole and skatole from tryptophan (Windey, De Preter and Verbeke, 2012). Metabolism of carbon energy sources differs between bacterial species due to the availability of different metabolic pathways and hence result in the production of species specific volatile profiles (Thorn and Greenman, 2012). These differences can be detected by

implementing a variety of analytical techniques. In recent years there has been increasing interest in monitoring microbial volatile metabolites as a non-invasive approach to the diagnosis of infection.

Gas chromatography (GC) is considered the gold standard technology for the analysis of volatile compounds, and has been implemented in several studies investigating the potential of using detection of bacterial volatile metabolites in the diagnosis of infection. Analysis of breath samples to identify markers of lung infections have been the focus of a number of studies, including breath sampled from ventilated patients using thermal desorption tube GC-MS, coupled with microbiological analysis of lavage fluid samples to determine if volatile analysis could identify infection in these patients (Fowler *et al.*, 2015). The authors of this study found that the volatile profiles of the breath of ventilated patients showed clear separation between infected and non-infected patients.

Volatile compound profiling using solid phase microextraction (SPME) and two dimensional GC with time of flight mass spectrometry (GCxGC TOFMS) has been employed for *in vitro* discrimination of 6 bacterial species associated with infection of the lungs of cystic fibrosis patients (Nizio *et al.*, 2016). Similarly, GCxGC TOFMS has been employed in the analysis of respiratory epithelial cells infected with *P. aeruginosa*, respiratory syncytial virus or both, in a human bronchial epithelial cell line to determine if infection could be identified using volatile analysis (Purcaro *et al.*, 2018). It was found that detection of volatile metabolites could be utilised to discriminate between cells that were and were not infected with *P. aeruginosa*. GC-MS has been used within *in vitro* studies for the analysis of the headspace of pure

planktonic bacterial cultures, to characterise and compare VOCs released or consumed by *S. aureus* and *P. aeruginosa* cultures (Filipiak *et al.*, 2012b) and to characterise and quantify VOCs in the headspace of *E. coli* and *P. aeruginosa* cultures using needle-trap GC-MS (Zscheppank *et al.*, 2014). Both of these studies concluded that the volatile compounds produced varied between species under the specific culture conditions investigated.

The potential application of volatile analysis to the diagnosis of wound infection using GC-MS has also been explored, through the analysis of the headspace of bacterial biofilms cultured in a model of wound infection utilising human skin explants (Ashrafi *et al.*, 2018). This study successfully demonstrated the detection of volatile compound profiles from bacterial biofilms in these models. GC-MS analysis of breath or bacterial culture headspace usually requires immobilisation and pre-concentration of headspace volatiles onto sorbent material, which can be performed using desorption tubes, SPME fibres or using a needle trap system, as in the studies mentioned above. In addition to the pre-concentration step, the length of GC-MS run times makes this technique time consuming. So, although considered the gold standard technique, highly sensitive for the identification of volatile compounds, particularly in complex mixtures, GC-MS is not well suited to real-time analysis.

Rapid mass spectrometry techniques that lack a chromatographic separation phase have been developed that facilitate real-time analysis of volatile compounds in gaseous samples. These included Proton Transfer Reaction Mass Spectrometry (PTR-MS) and Selected Ion Flow Tube Mass Spectrometry (SIFT-MS), techniques which rely on selective soft ionisation with little fragmentation of compounds (Thalavitiya

Acharige, Koshy and Koo, 2018). Application of technologies to detect and quantify bacterial volatile compounds in real-time has the potential to inform development of non-invasive point of care diagnostics. SIFT-MS is used for real-time analysis of the gaseous headspace of bacterial culture within this research.

SIFT-MS facilitates real-time detection and quantification of volatile compounds in humid air samples; reagent ions (H_3O^+ , NO^+ , O_2^+) generated in a gas ion discharge source and selected by a quadrupole mass filter are injected in to a fast flowing helium carrier gas in the reaction flow tube. Figure 2.2 shows a schematic of the Profile 3 SIFT-MS instrument. The sample gas is introduced to the flow tube via a heated sample inlet (120°C), where chemical ionisation occurs resulting in the production of characteristic product ions. Downstream reagent and product ions are separated and counted by a further quadrupole mass spectrometer and electron multiplier detector system. Absolute concentrations of trace gases can be quantified based on the ratios of ion count rates and the previously determined reaction rate constants contained within the integrated SIFT-MS kinetics library (Smith and Španěl, 2011, 2015; Španěl, Dryahina and Smith, 2006) when running the instrument to monitor for specific product ions.

SIFT-MS has been applied to a number of studies investigating detection of microbial volatiles. SIFT-MS has been used to directly measure hydrogen cyanide (HCN) levels in the breath of cystic fibrosis patients chronically infected with *P. aeruginosa* and in uninfected controls (Gilchrist *et al.*, 2013). This study determined that measurement of HCN may provide a non-invasive approach to the diagnosis of *P. aeruginosa* lung infection.

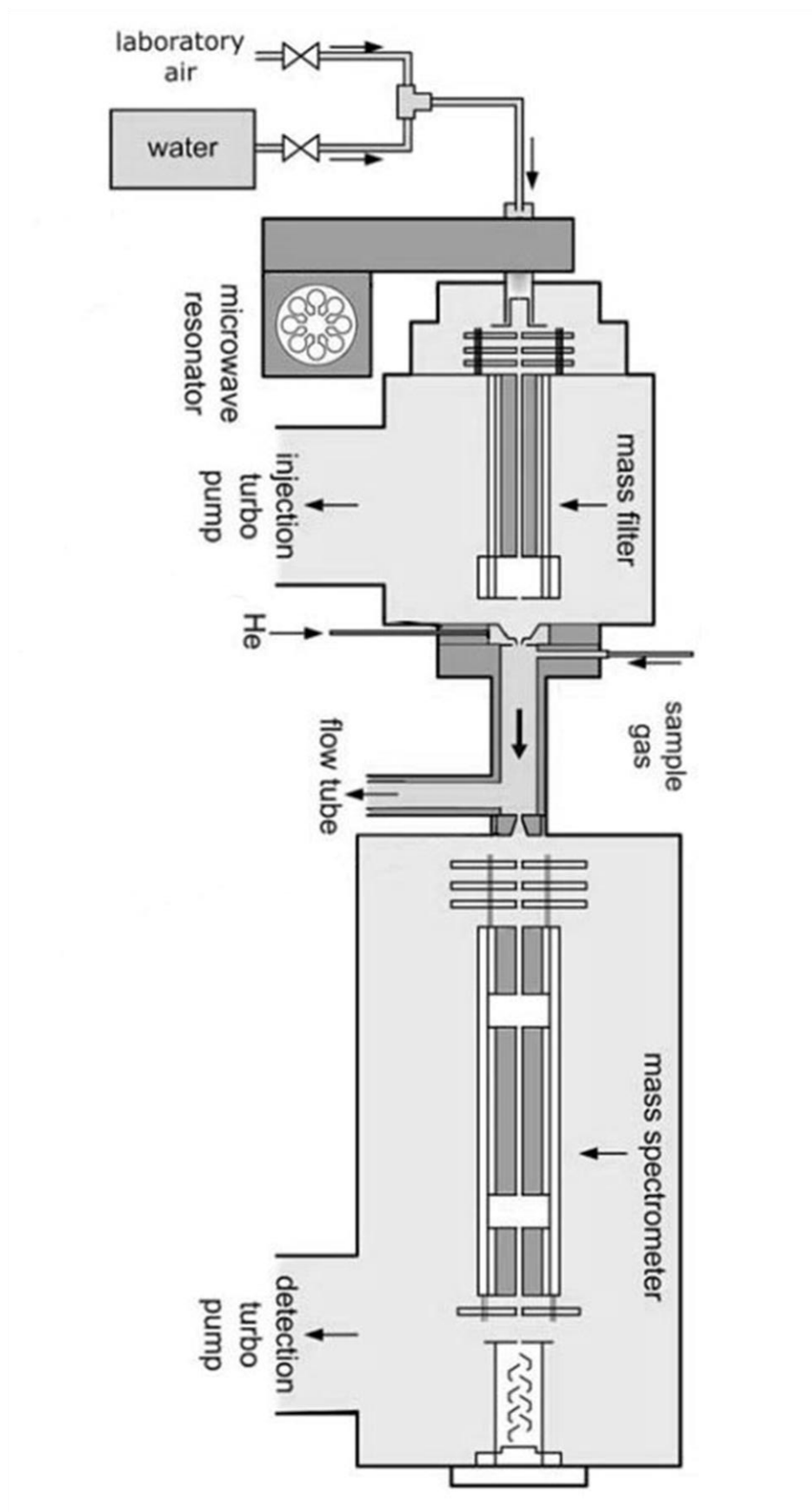


Figure 1.5: Schematic of the Profile 3 SIFT-MS instrument; Adapted from Smith and Španěl (2011) with permission of [The Royal Society of Chemistry](#).

In addition, SIFT-MS has been utilised to determine the potential application for the identification of organisms responsible for causing urinary tract infections, through analysis of the headspace of sterile urine samples inoculated with 8 species of interest (Storer *et al.*, 2011). This study was able to successfully demonstrate discrimination of 5 of the 8 species investigated, through analysis of a panel of 21 volatile compounds. Coupled with multivariate statistical data analysis techniques, SIFT-MS has been employed for the differentiation of pathogenic bacterial species in planktonic culture in complex culture media (Thorn, Reynolds and Greenman, 2011; Dryahina *et al.*, 2016).

SIFT-MS has also been used to identify the presence of pathogenic bacteria in inoculated blood samples and this approach compared to an established blood culture system (Scotter *et al.*, 2006). The study found that in general the time to positive result was faster when determined by SIFT-MS than by the BacT/ALERT automated system. These studies demonstrate the potential of SIFT-MS for the detection and quantification of microbial volatile metabolites originating from organisms growing in a range of sample types; human breath, biological matrices and complex culture media.

1.6 BIOFILM MODELS

In vitro studies of biofilms usually employ one of two general approaches; a closed multi-well plate based model, or an open flow system with continuous perfusion of nutrients in to and waste products out of the system (Coenye and Nelis, 2010). Both these approaches involve the development of biofilm on a solid surface. The simplest and most commonly used biofilm model system utilises multi-well plates to analyse the ability of organisms to form biofilm on plastic surfaces; the bottom and sides of the culture plate wells, or on the surface of small coupons placed in the wells. The biofilm forming ability of different strains and species can be compared using crystal violet to stain adhered cells (Fletcher, 1977; Djordjevic, Wiedmann and McLandsborough, 2002; O'Toole and Kolter, 1998a).

A development of this approach is the Calgary biofilm device, which involves use of a specialised lid which fits in to a standard 96-well plate; the lid contains pegs that protrude in to the well of the plate (Ceri *et al.*, 1999). Formation of biofilm on these pegs negates the potential problem of sedimentation of non-adherent bacterial cells which may occur in the bottom of culture plate wells. After biofilm has been cultured on the device, pegs can be individually removed or the entire lid moved to a new 96-well plate for further experiments such as antimicrobial susceptibility testing (Olson *et al.*, 2002). Both these multi-well plate based methods for biofilm culture are batch culture type models, which will result in the nutrient supply becoming exhausted and build-up of waste products unless the nutrient media is manually replaced.

A variety of devices have been developed that facilitate the culture of biofilms under continuous flow conditions. For example, the modified Robins device consists of an acrylic block containing multiple ports which house disks, constructed from the material of interest, attached to sampling plugs. Nutrient media is continuously pumped through the device and the disks on which the biofilm is formed can be removed and replaced during experimentation, by removing the attached sampling plug, to allow for sampling of the biofilm (Nickel *et al.*, 1985; Kharazmi, Giwercman and Høiby, 1999). Flow cell devices allow for biofilm formation in a small channel machined into a plastic block or constructed from microscope slides and coverslips (Berg and Block, 1984; Caldwell and Lawrence, 1988; Mittelman, Kohring and White, 1992). The small and precise construction of these devices allow for controlled flow of media through the device and precise control of the internal pressure and shear forces, and also facilitates direct microscopy of the developing biofilm (Tolker-nielsen and Sternberg, 2014).

Flow displacement reactors include the rotating disk reactor (Vinogradov *et al.*, 2004), annular biofilm reactor (Caylet *et al.*, 2011) and CDC biofilm reactor (Fernández-Rivero *et al.*, 2017) all of which involve the formation of biofilm on solid coupons housed on rods or disks submerged in nutrient media within a glass reaction vessel, facilitating simultaneous formation of a number of identical biofilms. Shear forces are generated either by rotation of the coupon holders or by a magnetic stirring baffle. A constant supply of nutrients is provided by an influx of fresh media into the reaction vessel which results in displacement of waste media out through the effluent port (Coenye and Nelis, 2010).

The drip flow biofilm reactor consists of multiple parallel reaction channels each designed to house a microscope slide coupon, the reaction vessel is orientated at a 10° angle to allow nutrients dripping in at the top of the reaction chamber to drip on to and flow over the surface of the coupon. This allows biofilm formation close to the air-liquid interface under low shear conditions (Goeres *et al.*, 2009).

1.6.1 *Wound biofilm models*

A variety of models have been described for the investigation of biofilms of bacterial species associated with wound infection. The Lubbock chronic wound biofilm (LCWB) model (Sun *et al.*, 2008) uses media comprised of Bolton broth with 50% plasma and 5% horse red blood cells to provide nutrients similar to those available within the wound bed. The model uses the ejected pipette tip, used for inoculation, as a solid surface for biofilm growth. The Lubbock chronic wound biofilm model was subsequently adapted to facilitate efficacy testing of topical antimicrobial treatments soaked in to gauze dressings (Kucera *et al.*, 2014). Following initial formation of the biofilm on a solid surface in the LCWB model, the biofilm was transferred to an artificial wound bed comprised of two layers of media consisting of Bolton broth set with gelatine and agar. Although the Lubbock model aims to provide nutrients akin to those found within a real wound bed it relies on the formation of biofilm on a solid surface. However, wound infection *in vivo* will consist of biofilm growth on the surface of, or suspended within the semi-solid matrix of the tissue (James *et al.*, 2008).

Collagen based gel matrices have been used as a substratum for culturing biofilms *in vitro*, in an attempt to more closely simulate the semi-solid nature of a wound, allowing biofilms to develop within, as well as on, the surface of the growth matrix (Werthén *et al*, 2010). This model is the first to implement the use of collagen gel matrices to provide a growth medium for biofilm formation more reflective of the environment found in a real wound bed. Collagen gels produced to include a simulated wound fluid are cast in to wells of a micro titre plate or 8 well culture slides and polymerised. The collagen surface is then inoculated and biofilms allowed to form. The author's demonstrated growth of *P. aeruginosa* and *S. aureus* biofilms in this model system.

This model has been further developed to allow for efficacy testing of antimicrobial dressings (Hakonen *et al.*, 2014). The use of collagen gel matrices has also been implemented to develop a model of infection of diabetic foot ulcers (Price *et al.*, 2016). Whereby collagen gels are cast into 6 well plates with tissue culture inserts, resulting in formation of a gel with a central void which is filled with simulated wound fluid, to generate a 'closed high-exudate' model, for testing topical antimicrobial treatment against *S. aureus* and *P. aeruginosa*.

Finally, collagen gels have also been used in combination with keratinocytes and fibroblasts; harvested and cultured from surplus human skin from plastic surgery patients, for development of 'human skin equivalents' (Haisma *et al.*, 2013). These 'human skin equivalents' have been wounded and used to produce a biofilm model of thermal wound infection.

Human skin samples have also been utilised within a wound biofilm model system (Ashrafi *et al.*, 2018). *Ex vivo* cutaneous human skin with incisional or excisional wounds were housed within wells of a 24-well plate and bathed in nutrient media (Mueller Hinton broth). This was used as a substrate for biofilm formation, to form a human skin wound infection model, mimicking both surgical and open wounds. Although these models provide a realistic matrix for culture of wound associated biofilms, replication of the models using human skin would require access to healthy human skin samples which is likely to be prohibitive to many researchers.

The models described above are all closed systems, which do not include the addition of nutrients to the biofilm during formation and growth, to simulate the replacement of nutrients and moisture that occurs within the wound bed, as described previously. The Duckworth biofilm model was designed to provide a continuous flow of nutrients to the growing biofilm, supplied from beneath, to simulate the production of exudate within a wound. This model utilised a 3D printed device, containing rows of wells which house agar plugs, each supporting a cellulose membrane on which the biofilms were cultured (Duckworth *et al.*, 2018). Although the authors used nutrient broth for the characterisation of this model, they also suggested that a simulated wound fluid could be used, to provide a nutrient supply that better represents the wound environment.

The drip flow biofilm reactor has been utilised to develop wound biofilm models that incorporate a continuous flow of nutrient media. Biofilms have been grown on a polycarbonate membrane, inspired by the colony biofilm model (Anderl, Franklin and Stewart, 2000), placed on top of a moistened absorbent pad fixed to a microscope

slide housed in the channels of the drip flow reactor (Lipp *et al.*, 2010; Agostinho *et al.*, 2011). The purpose of the absorbent pad used in these studies was to provide nutrients to the growing biofilm from beneath. However, although the mode of delivery was designed to simulate that of a real wound, the choice of a complex culture media (tryptone soya broth) does not closely simulate the nutrients available.

The drip flow reactor system has also been used to develop a multispecies model of chronic wound infection (Woods *et al.*, 2012). Firstly, the authors cultured biofilms from homogenised chronic wound tissue samples, after 7 days biofilms were disrupted and plated on to various agars for anaerobic incubation in order to demonstrate the successful culture of anaerobic species within the multispecies biofilm. Secondly, they used the drip flow reactor set up with absorbent pad and cellulose membrane, as described in the studies mentioned above, to culture 3 species biofilms containing *S. aureus*, *P. aeruginosa* and the obligate anaerobe *Clostridium perfringens*.

These studies utilising the drip flow reactor, provide a constant flow of nutrients to simulate the production of exudate within the wound bed. However, they lack the provision of a semi-solid matrix and simulated wound fluid used to provide wound-like conditions in the collagen based wound biofilm models described previously. Combining both of these approaches would allow development of a continuous flow biofilm model, with a collagen matrix perfused with a simulated wound fluid. This would utilise important elements from both types of model, and provide *in vitro* wound-like conditions without the logistical and ethical issues associated with the use of human tissue or animal models.

Chapter 2: Materials & Methods

2.1 CULTURE MEDIA

All components of bacterial culture media were obtained from Oxoid Ltd. (Basingstoke, UK), unless otherwise stated. Dehydrated culture media were reconstituted according to manufacturer's instructions and sterilised by autoclaving at 121°C for 15 minutes. Tryptone Soya Agar; CM0131 (TSA) and Blood Agar (blood agar base No. 2; CM0271 with 5% defibrinated horse blood) were used as general purpose non-selective solid media throughout this study.

The following selective media were used during the multispecies biofilm experiments described in chapter 6;

- Mannitol Salt Agar; CM0085 (MSA) for selective isolation of *Staphylococcus aureus*.
- Pseudomonas C.F.C. Selective Agar (CFC), comprised of Pseudomonas Agar base; CM0559 and C.F.C supplement; SR0103 with glycerol (Fisher, UK) (5mL per 500mL), for selective isolation of *Pseudomonas aeruginosa*.
- Colistin-Oxolinic Acid Blood Agar (COBA), comprised of Blood Agar base No. 2 with 5% defibrinated horse blood and streptococcus selective supplement; SR0126, for selective isolation of *Streptococcus pyogenes*.

Initially, headspace analysis of wound associated bacteria cultured in liquid media, as described in chapter 3, were carried out using Tryptone Soya Broth; CM0129 (TSB). Antimicrobial susceptibility testing, as described in chapter 5 was carried out using

Mueller-Hinton Broth; CM0405 (MHB). Phosphate buffered saline; BR0014 (PBS), reconstituted according to manufacturer's instructions and sterilised by autoclaving at 121°C for 15 minutes was used as a diluent throughout this research.

2.1.1 *Simulated Wound Fluid (SWF)*

The second phase of experiments described in Chapter 3, culturing planktonic bacteria under 'wound-like' conditions utilised a simulated wound fluid (SWF) consisting of equal volumes of foetal bovine serum (FBS; Gibco, UK) and a solution of 0.1% bacteriological peptone (Oxoid, UK) and 0.85% NaCl (Fisher, UK) (Bowler *et al.*, 2004; Werthén *et al.*, 2010; Said *et al.*, 2014; Price *et al.*, 2016). The peptone/NaCl solution was sterilised by autoclaving at 121°C for 15 minutes and allowed to cool prior to the addition of sterile FBS. Simulated wound fluid was also used for the culture of bacterial biofilms in the collagen wound biofilm model, as described in Chapters 5 and 6.

2.2 BACTERIAL STRAINS

Bacterial isolates were obtained from the University of the West of England, Bristol (UWE) culture collection (CC). Strains used for this study (Table 2.1) include isolates originally obtained from the National Collection of Type Cultures, UK (NCTC), the American Type Culture Collection, USA (ATCC), the National Collection of Industrial, Food and Marine Bacteria, UK (NCIMB) and clinical isolates held within the UWE culture collection.

Bacterial cultures were maintained on cryopreservation beads (Microbank, Pro Lab Diagnostics, Canada) at -80°C, resuscitated as required on TSA or blood agar (i.e. *S. pyogenes*) and incubated aerobically at 37°C. Working cultures were maintained on sealed plates at 4°C for up to 4 weeks.

Table 2.1: Bacterial isolates used within this study, indicating bacterial species and strain reference number.

Species	Strain reference	Strain information
Staphylococcus aureus	NCIMB 6571	Original strain reference 'Heatley Oxford'
Staphylococcus aureus	ATCC 6538	Isolated from a human lesion
Staphylococcus aureus	CC 437 (MRSA-Llewelyn)	Clinical strain
Staphylococcus aureus	CC 174	Clinical strain
Streptococcus pyogenes	NCTC 10871	Isolated from human skin lesions
Streptococcus pyogenes	NCTC 10874	Isolated from human case of pyoderma and nephritis
Streptococcus pyogenes	NCTC 10881	Isolated from human skin lesions
Pseudomonas aeruginosa	NCIMB 10548	Isolated from an Infected wound
Pseudomonas aeruginosa	ATCC 15442	Isolated from animal room water bottle, strain used in BS EN standard methods
Pseudomonas aeruginosa	NCIMB 8295	Type strain
Pseudomonas aeruginosa	CC 197	Clinical strain
Escherichia coli	NCTC 10418	Strain used for antibiotic assays and sensitivity testing
Escherichia coli	ATCC 10536	Strain used in BS EN standard methods
Escherichia coli	NCTC 12900	Reference strain for testing culture media
Escherichia coli	CC 443 (SMH6099)	Clinical strain
Proteus mirabilis	NCIMB 701880	Isolated from human source
Proteus mirabilis	CC 324 (NP1)	Clinical strain
Proteus mirabilis	CC 325 (NP4)	Clinical strain
Proteus mirabilis	CC 326 (NP6)	Clinical strain
Staphylococcus epidermidis	NCIMB 12721	Type strain, isolated from a nose
Staphylococcus epidermidis	NCTC 11536	Type strain, isolated from throat

2.3 PREPARATION OF BACTERIAL INOCULUM

TSA or blood agar plates were inoculated by streak plating a single colony from bacterial working cultures and incubated overnight at 37°C. These were used to prepare suspensions of the test organism in 10 mL of liquid culture media, adjusted to an OD_{620nm} of 0.2 (equalling a cell density of $1.4 - 2.1 \times 10^8$ cfu mL⁻¹).

To prepare a mixed inoculum containing *S. aureus* and *S. pyogenes*, inoculum suspensions of each organism were prepared in 10mL SWF adjusted to an OD_{620nm} of 0.4. Five mL each of these suspensions was then mixed together, resulting in an inoculum suspension containing both organisms at a concentration equivalent to an OD_{620nm} of 0.2 of each organism.

2.4 ENUMERATION OF BACTERIA

Bacterial numbers were determined by enumeration using either the spread plate method or using the Whitley Automated Spiral Plater (WASP; Don Whitley Scientific Limited, UK) following serial dilution of the bacterial inoculum in PBS.

2.4.1 *Spread Plate Method*

One hundred microlitres of a diluted bacterial suspension was pipetted on to the surface of an agar plate and spread evenly across the surface with a sterile plastic L-shaped spreader, appropriate dilutions were plated in duplicate. Plates were allowed to dry and inverted before incubation overnight at 37°C. Colonies were counted and

the average (mean) calculated for the duplicate plates. The total number of colony forming units (cfu) were calculated as follows;

$$cfu = \text{average number of colonies} \times \left(\frac{1}{\text{dilution factor}}\right) \times \left(\frac{1}{\text{volume(mL)}}\right)$$

2.4.2 *Spiral Plating*

The 50 μ L Log function of the spiral plater was used to dispense 50 μ L of bacterial suspension on to the surface of agar plates, appropriate dilutions were plated in duplicate. Plates were allowed to dry and inverted before incubation overnight at 37°C. The total number of colony forming units was calculated using a counting grid and tables provided by the instrument manufacturer.

2.5 PLANKTONIC CULTURES FOR HEADSPACE ANALYSIS

2.5.1 *Liquid Culture - TSB*

One mL of the bacterial inoculum suspension (prepared in TSB as described in Section 2.3) was used to inoculate 9 mL of sterile TSB aseptically dispensed into sterile 40 mL glass vials with a PTFE screw cap containing a silicone septum (Supelco, UK), resulting in a final starting OD_{620nm} of 0.02. Vials were incubated aerobically at 37°C and 200 rev min⁻¹ (Stuart S150 Orbital Incubator; Bibby Scientific, UK) for 5 h or 24h.

2.5.2 *Liquid Cultures - Simulated Wound Fluid*

One mL of the bacterial inoculum suspension (prepared in peptone/NaCl diluent as described in section 2.1) was used to inoculate 40 mL glass vials (as specified above), containing 5 mL FBS (Sigma Aldrich) and 4 mL peptone/NaCl resulting in a SWF (see Section 2.3) at a final starting OD_{620nm} of 0.02 in each test vial. Vials were incubated aerobically at 37°C and 200 rev min⁻¹ (Stuart S150 Orbital Incubator; Bibby Scientific, UK) for 5 h or 24 h.

2.6 COLLAGEN WOUND BIOFILM MODEL

2.6.1 *Collagen Coating of Glass Slide Coupons*

The collagen gel matrix was prepared based on the method described by Werthén *et al.* (2010) by preparing a collagen solution (2.0 mg mL^{-1}) in SWF (see Section 2.1.1). High concentration collagen (type I) from rat tail supplied in 0.02 M acetic acid (Corning Incorporated, Wiesbaden, Germany) was neutralised to pH 7 with 1 M sodium hydroxide according to manufacturer instructions and diluted to the desired concentration with SWF. For example, to prepare 10 mL of 2.0 mg mL^{-1} collagen solution in SWF from a collagen stock solution supplied by the manufacturer at a concentration of 9.59 mg mL^{-1} ; 48 μL of ice cold NaOH was added to 7.866 mL of ice cold SWF and mixed. On ice, 2.086 mL of ice cold collagen stock solution was then added and the solution mixed gently. Sterile glass microscope slides measuring 76 mm x 26 mm were coated with 1.5 mL of neutralised collagen solution (2.0 mg mL^{-1}), resulting in a depth of 760 μm . Collagen coated slides were incubated at 37°C for 1 hour to allow polymerisation of the three-dimensional collagen matrix.

2.6.2 *Growth of Bacterial Biofilms within the Collagen Wound Biofilm Model*

The collagen wound biofilm model apparatus is shown in figure 2.1. One millilitre of inoculum suspension (section 2.3) in SWF was used to inoculate each collagen coated microscope slide (individually housed in sterile petri dishes) and incubated at 33°C for 2 hours to allow initial adherence of bacterial cells. An incubation temperature of 33°C was chosen to simulate average wound bed temperature (Dini *et al.*, 2015).

Following incubation, the inoculated slides were rinsed gently three times with 1 mL of sterile SWF to remove planktonic cells, and carefully transferred to individual channels within a commercially available drip flow reactor (Biosurface Technologies Corporation, Bozeman, MT, USA). Sterile silicone tubing (3mm ID) was used to connect a 500 mL Duran bottle containing the sterile SWF medium to the miniert valve lid inlets via a 23 Gauge 11/4" sterile needle. Waste was collected in 250 mL Duran bottles connected to the waste outlet ports using lengths of sterile silicone tubing (8mm ID). The reactor was incubated at 33°C for 48-72 hours at an angle of 10° to allow SWF to flow through the individual chambers of the model system (Figure 2.1). The collagen wound biofilm model was continuously perfused with SWF at a flow rate of 2 mL hr⁻¹ for the duration of incubation to simulate the flow of a moderately exuding wound (Thomas *et al.*, 1996).

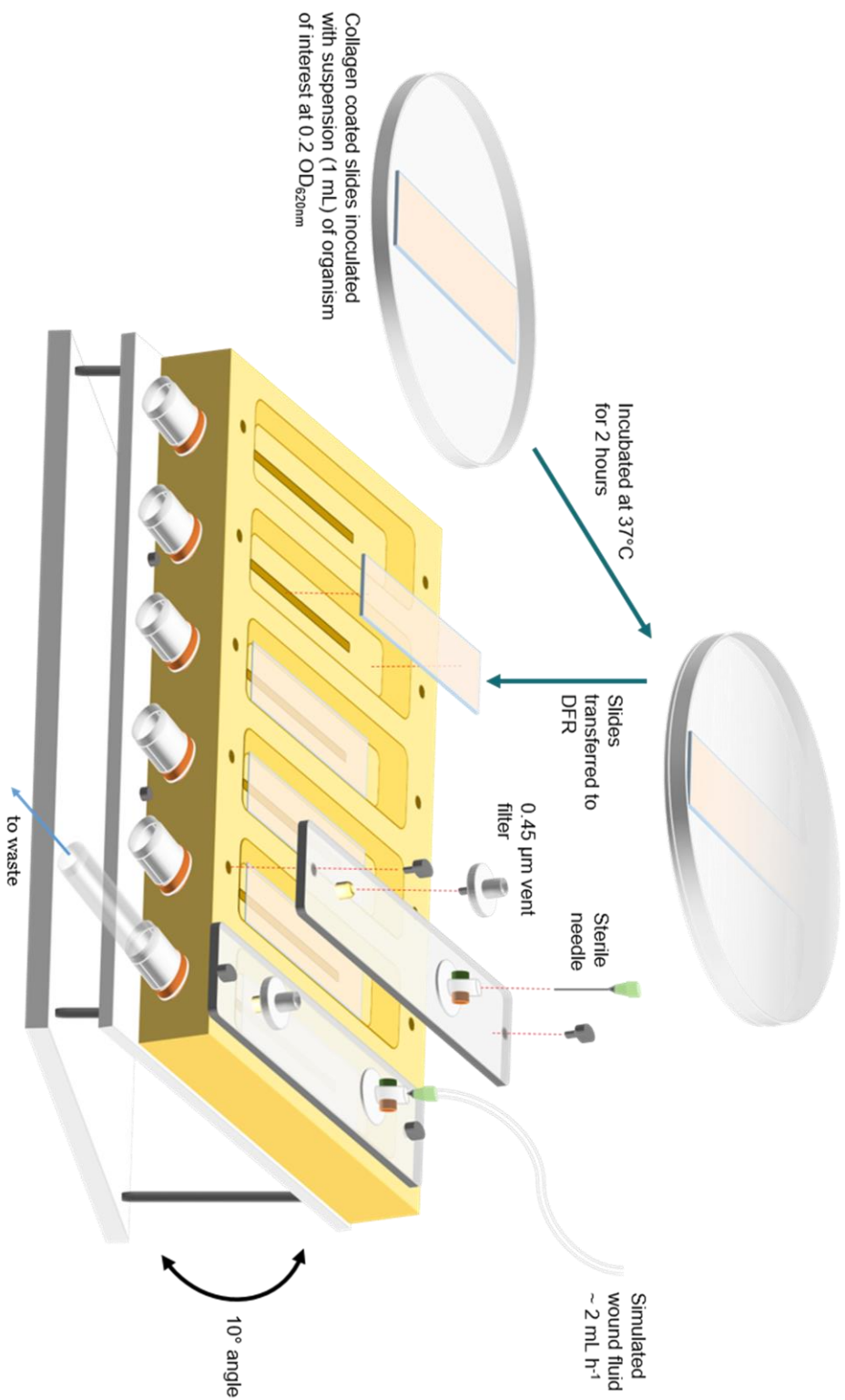


Figure 2.1: In vitro collagen wound biofilm model, comprising a drip flow reactor (DFR) set-up incorporating collagen coated slide coupons, showing assembly with tubing connected to simulated wound fluid reservoir (perfused at a rate of 2 mL h⁻¹) and waste collection.

2.6.3 *Enumeration of Bacterial Biofilms*

Bacterial biofilms were sampled at 0, 3 and 6 hours, then every 6 hours until 48 hours and finally at 72 hours. At each time point a coated slide was aseptically removed from the reactor and the entire collagen layer containing the bacterial biofilm scraped into a 50 mL falcon tube using a sterile L-shaped scraper, while rinsing with 3 x 1 mL phosphate buffered saline (PBS). Two millilitres of 500 µg mL⁻¹ collagenase solution (Life Technologies Limited, Paisley, UK) was added to the tube and mixed, incubated at 37°C for 20 minutes, and then subsequently vortex mixed and incubated for a further 20 minutes. The resulting suspension was disrupted by sonication in a water bath (Fisherbrand FB11078, Fisher Scientific Limited, Loughborough, UK) at 35 kHz for 5 minutes. Collagenase solution was washed from the bacterial cells; whereby the suspension was centrifuged at 4000 x g (Beckman Coulter Allegra X-30R), the supernatant discarded and pellet re-suspended in 10 mL PBS, this process was repeated a total of two times. Bacterial density (cfu slide⁻¹) was determined by serially diluting in PBS and spiral plating on to TSA as described in section 2.4.2 and colonies counted after 24 hours incubation at 37°C.

The effect of collagenase solution on the viability of *S. aureus*, *P. aeruginosa* and *S. pyogenes* was tested. Whereby, a suspension of each of the organisms was prepared in SWF and treated with either collagenase solution or PBS. Following incubation the bacterial suspensions were spiral plated on to TSA for enumeration. The recovery of organisms from the collagenase treated and PBS control solutions were compared using t-tests. No statistically significant difference between the collagenase treated and PBS controls ($p > 0.05$) was found for *S. aureus*, *P. aeruginosa* or *S. pyogenes*.

2.7 IMAGING OF BACTERIAL BIOFILMS AND COLLAGEN MATRIX

During preparation of collagen gel matrices for imaging experiments, a #1 glass cover slip measuring 18mm x 18mm was included between the microscope slide and collagen gel layer. The inclusion of a coverslip facilitated the sampling of a suitable sized section of the biofilm for microscopy. This was removed by cutting the collagen around the cover slip with a bespoke square stainless steel cutter and lifting away the coverslip supporting the biofilm sample with the aid of a scalpel blade.

2.7.1 *Scanning Electron Microscopy (SEM)*

Biofilm samples and an un-inoculated collagen gel control were fixed in 4% glutaraldehyde (Sigma-Aldrich Company Limited, Gillingham, UK) in a 0.1 M phosphate buffer for 1 hour at room temperature. This was rinsed in PBS and dehydrated with increasing concentrations of ethanol and hexamethyldisilazane (Acros Organics, Geel, Belgium), air dried in a fume hood, mounted and gold sputter coated. A FEI Quanta 650 FEG scanning electron microscope operating at 10 kV was used to examine the samples.

2.7.2 *Confocal Scanning Laser Microscopy (CSLM)*

Biofilm samples were stained using the FilmTracer LIVE/DEAD Biofilm Viability Kit (Fisher Scientific UK Limited, Loughborough, UK) according to manufacturer's instructions: 3 µL each of Component A (SYTO 9 green fluorescent nucleic acid stain 3.34 mM in DMSO) and Component B (Propidium iodide 20 mM in DMSO) were

added to 1 mL of sterile filtered deionised water to prepare a working solution. Three hundred microliters of the prepared staining solution was gently added to the biofilm surface. Samples were incubated at room temperature for 30 minutes in the dark. Following incubation samples were rinsed gently with sterile filtered deionised water to remove excess stain and imaged using the x40 oil objective of the Leica DMI8 Inverted microscope with confocal scanner (Leica Microsystems (UK) Limited, Milton Keynes, UK). Confocal Z-stack scans were exported to Fiji (Schindelin *et al.*, 2012) for processing and producing figures.

2.8 DETECTION OF BACTERIAL VOLATILE METABOLITES

During this research volatile compounds were detected from the gaseous headspace of bacterial cultures *in vitro*, cultured both in liquid media and in a collagen wound biofilm model. Two selected ion flow tube mass spectrometers were used during this work; the Profile 3 (Instrument Science Limited, UK) and the Voice200 Ultra (Syft technologies, New Zealand). A brief description of the selected ion flow tube mass spectrometry (SIFT-MS) validation procedures and operational parameters for both instruments is included in this section.

2.8.1 *Profile 3 SIFT-MS Instrument*

The Profile 3 SIFT-MS instrument contains a reaction flow tube 5 cm in length and uses helium as a carrier gas (Smith and Španěl, 2011) and has a limit of detection of <10 ppb for quantification of volatile compounds (Instrument Science, 2006). Daily validation checks were carried out every day that the instrument was used during this research and are outlined in Table 2.2.

Table 2.2: Table of daily validation checks carried out to confirm performance of the Profile 3 SIFT-MS instrument.

Validation Step	Procedure
Instrument Source Tuning	H ₃ O ⁺ Full Mass Scan 10 -100 m/z, 10 seconds, x3. Confirm reagent ion peak generation at 19 m/z and water cluster peaks at 37 m/z, 55m/z and 73 m/z.
Quadrupole Performance	H ₃ O ⁺ Full Mass Scan 10 -100 m/z, 10 seconds, x3. Confirm peak alignment at 19 m/z and 73 m/.
Sample Flow Rate	Multi Ion Mode, Scan for Water. Make 5 exhalation in to the sample inlet and confirm water vapour content equals 5.5% - 6.0%.
Reagent Ion Intensity	Multi Ion Mode, Scan for Water. Confirm total count rate $\geq 1 \times 10^6$ cps.

2.8.1.1 Headspace analysis of liquid bacterial cultures using the Profile 3 SIFT-MS.

Following incubation for 5 or 24 hours, samples were analysed by SIFT-MS (Profile 3; Instrument Science Limited, UK) in Full Mass Scan (FS) mode using the H₃O⁺ reagent ion. Samples were introduced to the instrument by piercing the silicone septum of the sample vial with a sterile needle attached to the heated SIFT-MS direct sampling inlet, samples were vented with a second sterile needle attached to a 0.2 μ M syringe filter (Ministat; Sartorius Stedim Biotech, Germany) to allow the free flow of headspace gases. Each sample was analysed three times using repeat scans of 100

seconds, over a spectrum range of 10–200 m/z, to generate a total of nine scans per bacterial strain from three independent samples.

2.8.1.2 Headspace analysis of dressing samples using the Profile 3 SIFT-MS.

Following incubation, the gaseous headspace of the dressing samples were analysed by SIFT-MS (Profile 3, Instrument Science Limited, UK) in ‘Full Mass Scan’ mode using the H_3O^+ precursor ion; each sample was analysed using 3 repeat scans of 100 seconds, over a spectrum range of 10–200 m/z. Headspace samples were introduced to the instrument by piercing the silicone septum of the sample bag with a sterile needle attached to the SIFT-MS direct sampling inlet.

2.8.2 *Voice200 Ultra SIFT-MS instrument*

The Voice200 Ultra SIFT-MS instrument can use either a nitrogen or helium carrier gas, and was run using helium for the duration of this research. The instrument has a limit of detection of 50 ppt for quantification (Syft Technologies Ltd, 2012) and can perform full mass scans over a spectrum range of 10 – 250 m/z.

The flow tube pressure was checked daily to ensure the inlet flow is within the correct range of 80 – 120 mTorr with the inlet cap removed, the flow tube pressure with the inlet cap in place should be less than 20 mTorr. The Voice200 ultra incorporates an automated daily instrument validation procedure, which was carried out on every day the instrument was used during this research. Before the validation procedure was initiated the calibration gas cylinder was turned on and the flow pressure matched to that of the flow tube pressure. The validation procedure consists of 9 steps outlined in Table 2.3.

The 'Syft standard validation' results in application of an internal correction factor for compound quantification, based on the analysis of the Syft standard calibration gas which contains toluene, isobutene, tetrafluorobenzene, hexafluorobenzene, ethylbenzene, ethylene, benzene and octafluorotoluene at 2ppm. This step may result in adjustment of the instrument calibration function (ICF) if necessary, which facilitates reliable quantification of compounds with known reaction rates that are stored in the Labsyft compound library and ensures day to day repeatability of the instruments performance.

Table 2.3: Steps in the Syft Voice200Ultra automated daily validation procedure

Validation Step	Description
Reset quadrupoles	Sets quadrupoles to the correct modes for validation.
Carrier gas	Ensures carrier gas is switched on and checks flow rate.
Downstream pressure validation	Measures downstream chamber pressure with and without carrier gas flow to detect leaks in downstream vacuum chamber.
Upstream quad scanline validation	Checks the reagent ion peak alignment.
Downstream quad scanline validation	Checks alignment of product ion masses using Syft standard.
Detector verification	Adjusts detector voltage to maintain maximum count rate of each reagent ion.
Detector linearity validation	Ensures the detector provides a linear response to a range of reagent /product ion ratios.
Syft Standard Validation	Compares measured and expected values for Syft standard mixture and adjusts ICF if required.
Background	Full Scan with inlets closed to detect instrument contamination.

Within this research the Voice200 ultra was used to analyse biofilm samples cultured in the collagen wound biofilm model, two analysis methods were created for this research using the following parameters:

(1) Full scan (FS) mode, H_3O^+ 10 – 200 m/z, NO^+ 10 – 200 m/z, O_2^+ 10 – 200 m/z, using 3 repeat scans.

(2) Selected Ion Mode (SIM), selected compounds, scanned masses and their branching ratios listed in Table 2.4, scan duration of 60 seconds.

Table 2.4: Voice200 Ultra SIFT-MS Selected Ion Mode scan parameters, including selected compounds, and scanned masses used for quantification and corresponding branching ratios.

	H_3O^+		NO^+		O_2^+	
	Mass	Branching ratio (%)	Mass	Branching ratio (%)	Mass	Branching ratio (%)
Ethanol	47	100	45	100		
1-butanol	57	95	57	5	56	80
Isobutyl alcohol	57	100	73	95	42	25
2-methyl-2-propanol	57	100	57	100	59	100
3-methyl-1-butanol	71	100	87	85	59	85
Acetaldehyde	45	100	43	100		
2-methylpropanal			71	100	72	70
2-methylbutanal	87	94	85	98	58	72
3-methylbutanal	69	30	85	100		
	87	70				
Acetoin	89	100	118	100	88	20
Acetone	59	100	88	100		
Butanone			102	100	72	35
2,3-butanedione	87	100	86	75	86	35
3-methylbutanoic acid	103	95	85	30		
			132	70		
Butane					43	65
					58	20
					42	10
Dimethyl sulfide	63	100	62	100	62	60
Dimethyl disulfide	95	100	94	100	61	10
					94	80
Hydrogen cyanide	28	100				
Ammonia	18	100			17	100

2.8.2.1 Headspace analysis of bacterial biofilms using the Voice200 ultra in full scan mode.

Following 48 hours of continuous culture in the collagen wound biofilm model, biofilm headspace gases were sampled by connecting the heated direct sample inlet of the SIFT-MS instrument (Voice200Ultra, Syft technologies, NZ) to the reactor channel via a length of PEEK tubing (Supelco, UK) of O.D. 1/16 in. × I.D. 0.030 in. The SIFT-MS instrument was operated in Full Scan Mode (FS) using method parameters described above in section 2.8.4; 3 independent biofilms of each strain were analysed.

2.8.2.2 Headspace analysis of biofilms – Selected Ion mode

The channels of the drip flow reactor were connected to the SIFT-MS instrument as described above. The SIFT-MS instrument was operated in selected ion mode (SIM) using the H_3O^+ , NO^+ and O_2^+ reagent ions to quantify the concentration of selected compounds in the bacterial biofilm headspace. The method parameters of the SIM scan are detailed above in section 2.8.4. Scanning each biofilm for 60 seconds, resulted in a total of 12 replicate measurements of each of the 19 compounds (shown in table 2.2), 3 independent biofilms of each strain were analysed.

2.8.3 *Gas Chromatography – Mass Spectrometry*

2.8.3.1 *HS-SPME-GC-MS analysis of bacterial biofilms*

To ensure correct operation of the GC-MS instrument, auto-tune calibration of the mass spectrometer was undertaken monthly and daily blanks samples were analysed to rule out contamination of the GC column. Volatile compounds were sampled from the headspace of drip flow reactor channels by solid phase microextraction (SPME) using a 75 µm Carboxen/Polydimethylsiloxane (CAR/PDMS) fibre assembly (Supelco, UK) for 30 minutes at 33°C. After sampling, the fibre was retracted and transported in a sealed container to the GC-MS instrument and immediately inserted into the heated inlet. The GC (6890N, Agilent Technologies) was programmed with the following method, adapted from the method described by Shestivska *et al.* (2012): splitless injection, inlet temperature held at 305°C, Helium carrier gas flow rate 1 mL min⁻¹, oven temperature programme set to 35°C for 3 minutes, then 4°C per minute ramp up to 100°C followed by 8 °C per minute ramp up to 300°C with a 5 minute hold at the final temperature. A 25 m, 5%-Phenyl-methylpolysiloxane column (HP-5ms, Agilent technologies) was used. The mass selective detector (5973 MSD, Agilent Technologies) was used in 'Full Scan Mode' to detect ions over a spectrum range of 15-400 m/z. Analysis software (Agilent MassHunter Workstation software) was used for compound identification using chromatogram deconvolution algorithms and comparison with the NIST2.0 library with a minimum match score of 80%.

2.9 ANTIMICROBIAL SUSCEPTIBILITY

A ceftazidime stock solution was prepared by dissolving ≥ 100 mg of powder in saturated sodium bicarbonate solution in a 100 mL volumetric flask, the minimum volume required to dissolve the powder was used. The volume was then made up to 100 mL with filter sterilised deionised water. The final concentration of the stock solution was calculated as follows;

$$\text{concentration (mg L}^{-1}\text{)} = \left(\frac{\text{weight (mg)}}{\text{total volume (L)}} \right) * \text{potency}$$

2.9.1 *Minimum Inhibitory Concentration (MIC)*

The antimicrobial susceptibility of *P. aeruginosa* NCIMB 10548 to ceftazidime was tested based on the broth microdilution method described by BS EN ISO 20776-1:2006 (British Standards Institution, 2006). Ceftazidime was prepared in Mueller-Hinton Broth (MHB) at concentrations ranging from 256 mg L⁻¹ to 0.25 mg L⁻¹. Fifty microliters of each antibiotic concentration and a control (0 mg L⁻¹) were dispensed in triplicate into wells of a 96 well multi-well plate. Overnight plate cultures were used to prepare a suspension of *P. aeruginosa* NCIMB 10548 in 10 mL MHB; colonies were picked from the overnight plate cultures and emulsified in 10 mL PBS and adjusted to an OD₆₂₅ of 0.08 – 0.13. The suspension was then diluted by adding 100 μ L to 9.9 mL of MHB, to produce an inoculum suspension of approximately 1×10^6 cfu/mL. Fifty microliters of the inoculum suspension was added to each of the wells of the multi-well plate containing 50 μ L of MHB or MHB with antibiotic. The resulting

final inoculum was approximately 5×10^5 cfu mL⁻¹ and final antibiotic concentrations ranged from 128 mg L⁻¹ to 0.125 mg L⁻¹, plus antibiotic free controls. Additionally, three wells were prepared containing 100 µL of MHB only as un-inoculated negative controls. The multi-well plate was then incubated at 37°C for 18 hours. The inoculum suspension was serially diluted and 100 µL spread plated (see Section 2.4.1) on to TSA and incubated at 37°C overnight to confirm appropriate inoculum preparation. Following incubation each test well of the plate was visually inspected to identify turbidity, (indicating growth of the test organism) and compared to the control wells. The MIC was recorded as the lowest concentration of ceftazidime that completely inhibited visible growth of *P. aeruginosa*. Agar plates were counted after 18-24 hours to confirm inoculum density was within the required range.

2.9.2 *Antimicrobial Susceptibility of Biofilms*

Biofilm cultures were grown on collagen coated slides in the drip flow reactor system (see Section 2.6.2). Antibiotic treatment was started after either 6 hours, when cultures are at an early stage of biofilm development, or 30 hours of continuous culture, when biofilms are established and maturing. Residual SWF was drained via the tubing and the media reservoir refilled with fresh SWF containing antibiotic. Biofilms were sampled periodically as described in Section 2.6.3, to determine the effect of antibiotic treatment on biofilm density over time.

2.10 DATA ANALYSIS

The use of selected ion flow tube mass spectrometry results in the generation of large complex data sets containing many variables; either mass spectral product ion intensities or volatile compound concentrations. Univariate methods and descriptive statistics can be utilised to identify and visualise between group differences for individual variables. However, multivariate methods of analysis allow multiple variables to be interpreted simultaneously and facilitate modelling of the relationships among these multiple variables. (Saccenti *et al.*, 2014). In addition, the multivariate statistical methods utilised are capable of dealing with data sets such as those presented within this research, where the number of variables greatly exceeds the number of samples/observations and where a significant amount of collinearity between variables is likely (Worley and Powers, 2013).

This section describes the statistical analysis employed throughout this research. Data processing prior to multivariate statistical analysis is described in detail in each chapter. Analysis of both full scan and selected ion mode data was performed using hierarchical cluster analysis and principal component analysis using IBM SPSS Statistics versions 20 - 25 (IBM Corporation, Armonk, NY).

2.10.1 *Hierarchical Cluster Analysis*

Hierarchical cluster analysis is a data mining technique which aims to identify groups within the data set. An algorithm is used to score the dissimilarity between samples in the data set and construct a matrix; the matrix being made up of scores of pairwise

comparisons between each sample based on the entire data set of original variables. The dissimilarity matrix is visualised through the production of a dendrogram, in which the branching of the clusters groups the cases (samples) with the least dissimilarity. Ward's method, as used within this research, is an agglomerative method of clustering, whereby each case is initially placed in an individual cluster, the two closest (least dissimilar) clusters are merged to form a larger cluster. This process continues until a single cluster containing all samples is formed (Wijetunge *et al.*, 2013). In hierarchical cluster analysis there is no restriction on the number of clusters formed, hence the resulting dendrogram can indicate the data structure and relationships between each individual sample (Ren *et al.*, 2015). The distance between the nodes indicates the relationship between the clusters. The distances between clusters within the dendrogram are expressed in squared Euclidean distance, a mathematical measure of the straight line distance between two points.

2.10.2 *Principal Component Analysis (PCA)*

Principal component analysis (PCA) is considered an important tool for the analysis of multivariate data and is widely used in metabolomics studies (Saccenti *et al.*, 2014). PCA aims to reduce the number of variables that make up a complex data set, to facilitate simpler visualisation of the data, while retaining as much information as possible. PCA generates new variables (principal components) from the data set that represent linear uncorrelated combinations of the original variables, with much of the variation from the original data set accounted for in the first few new variables

(principal components). The first component describes the largest variation within the data set, the second component the second largest variation etc. This allows only the first two or three variables to be utilised for visualisation of the data set, reducing the dimensions while retaining the majority of the information contained within the original data set. Two sets of scores are generated by PCA; firstly the scores of the observations/samples against each principal component and secondly the loading of each original variable against the principal components (Grace and Hudson, 2016). These data sets can be visualised by generating scatter plots of these scores for the first two principal components. Plotting the scores of the samples for the first two principal components can provide a clear summary of the data set and reveal if there are differences between groups of samples as well as highlight any outliers. In addition, plotting the loading scores of the original variables against the first two principal components will indicate the influence of these variables within the model. The direction of the principal component scores of the samples and the variable loadings are equivalent, hence comparison of the two plots can indicate the variables that are most important for separating groups of samples (Grace and Hudson, 2016).

Chapter 3: *In vitro* discrimination of wound-associated bacteria in planktonic culture

3.1 INTRODUCTION

Characteristic volatile metabolites of certain microorganisms have long been recognised by microbiologists, for example the distinctive odour of indole from *E. coli* (Li and Young, 2013). Previous work has shown that using selected ion flow tube mass spectrometry (SIFT-MS) analysis, it is possible to detect and quantify the different types and concentrations of volatile compounds produced by a range of bacterial species *in vitro* (Allardyce *et al.*, 2006; Scotter *et al.*, 2006; Storer *et al.*, 2011; Shestivska *et al.*, 2012; Chippendale *et al.*, 2014) and that by employing appropriate statistical techniques the characteristic profiles can be used to discriminate between bacterial species (Thorn, Reynolds and Greenman, 2011). SIFT-MS analysis has been used to investigate bacterial volatiles emanating from a variety of sample types including; blood culture samples (Allardyce *et al.*, 2006; Allardyce, Hill and Murdoch, 2006; Scotter *et al.*, 2006), serum (Spooner *et al.*, 2009), urine (Storer *et al.*, 2011) and breath (Dummer *et al.*, 2013; Gilchrist *et al.*, 2013), as well as microorganisms prepared in liquid culture medium (Thorn, Reynolds and Greenman, 2011; Shestivska *et al.*, 2015).

This chapter addresses the first main research aim;

- To investigate if planktonic cultures of wound associated bacteria produce species specific volatile profiles *in vitro*, enabling significant discrimination.

Bacterial species were cultured in complex media; (Tryptone Soya Broth [TSB]) and in simulated wound fluid (SWF) to simulate wound similar conditions (Bowler *et al.*, 2004; Werthén *et al.*, 2010; Said *et al.*, 2014; Price *et al.*, 2016), thus providing the bacterial cultures with substrates for metabolism similar to those available to organisms colonising the wound bed *in vivo*. This approach was developed to determine whether the main bacterial species associated with wound infection produce characteristic volatile profiles, which could be used for speciation and have the potential to be used in the development of diagnostics based on detection of volatile metabolites.

A subset of the data presented in this chapter has been published in a peer reviewed journal (Slade *et al.*, 2017), which is included in Appendix I.

3.2 METHODS SUMMARY

Isolates of six bacterial species were used during this study; *Escherichia coli* NCTC 10418, ATCC 10536 and NCTC 12900, *Pseudomonas aeruginosa* NCIMB 10548, ATCC 15442, NCIMB 8295 and CC197, *Proteus mirabilis* NP1, NP4 and NP6, *Staphylococcus aureus* NCIMB 6571, NCTC 6538, MRSA Llewelyn and CC174, *Staphylococcus epidermidis* NCIMB 12721 and NCTC 11536, and *Streptococcus pyogenes* NCTC 10871 and NCTC 10874 (see section 2.2).

3.2.1 *Preparation of Bacterial Cultures*

Headspace vials containing either TSB or SWF were inoculated with a suspension of the test organism as described in sections 2.5.1 and 2.5.2. Vials were incubated at 37°C and 200 rev min⁻¹ for 5 or 24 hours. A total of three independent samples were prepared for each bacterial strain in each of the liquid culture media used. Where bacterial strains were incubated for 5 hours and 24 hours, three independent samples were prepared for each incubation time.

3.2.2 *Selected Ion Flow Tube - Mass Spectrometry (SIFT-MS)*

Following incubation, the sample head space gases were analysed using the SIFT-MS Profile 3 instrument in Full Scan mode using the H₃O⁺ reagent ion as described in Section 2.8.1.1. The headspace of each vial was analysed by three repeat scans over a spectrum range of 10 – 200 m/z.

3.2.3 *Data Analysis*

Mean count rates were calculated as follows: Where a product ion was detected in both the headspace of a bacterial culture and the un-inoculated control, t-tests were performed to compare the count rate detected. Only product ions detected at significant levels ($p < 0.05$) from the bacterial cultures compared to background control levels were included for further analysis. The mean product ion count rate of background volatiles from the un-inoculated culture media were then subtracted from those detected in bacterial culture head-space, to determine the total count rate attributed to production of volatile compounds in the bacterial culture. Any corrected negative values were disregarded (indicating a reduction significantly below the background levels), as were reagent ion peaks.

A threshold detection signal of 10 counts per second (cps) was applied to negate instrument signal noise and identify discriminant volatile compound product ion data. Further selection was required to identify discriminate product ions for the SWF data: A minimum signal of 10 cps was required in at least two of the strains analysed for each species in order for each product ion to be included for further analysis.

Hierarchical cluster analysis (see Section 2.10.1) was applied to the resultant data set, enabling construction of a dendrogram which indicates relationship between each of the samples based on the product ion peaks detected in the sample headspace. The data was subsequently transformed using Principal Component Analysis (PCA), described in Section 2.10.2, visualised by constructing plots of the principal components scores for each data set, and generating loading plots to

indicate the impact of each of the measured variables on the principal component scores. All data was analysed using Microsoft Excel 2013 (Microsoft Corporation, Redmond, Washington, USA) and IBM SPSS Statistics version 20.0 (IBM Corporation, Armonk, NY, USA).

3.3 RESULTS

3.3.1 *Headspace Analysis of Wound Associated Bacteria Cultured in Complex Growth Media (TSB).*

Multivariate analysis of the headspace count rates (\log^{10}) of 51 selected mass spectral product ions using Ward's method of hierarchical clustering analysis is visualised by the dendrogram in Figure 3.1. This shows successful discrimination between *P. mirabilis*, *E. coli* and the staphylococci based on the profile of selected

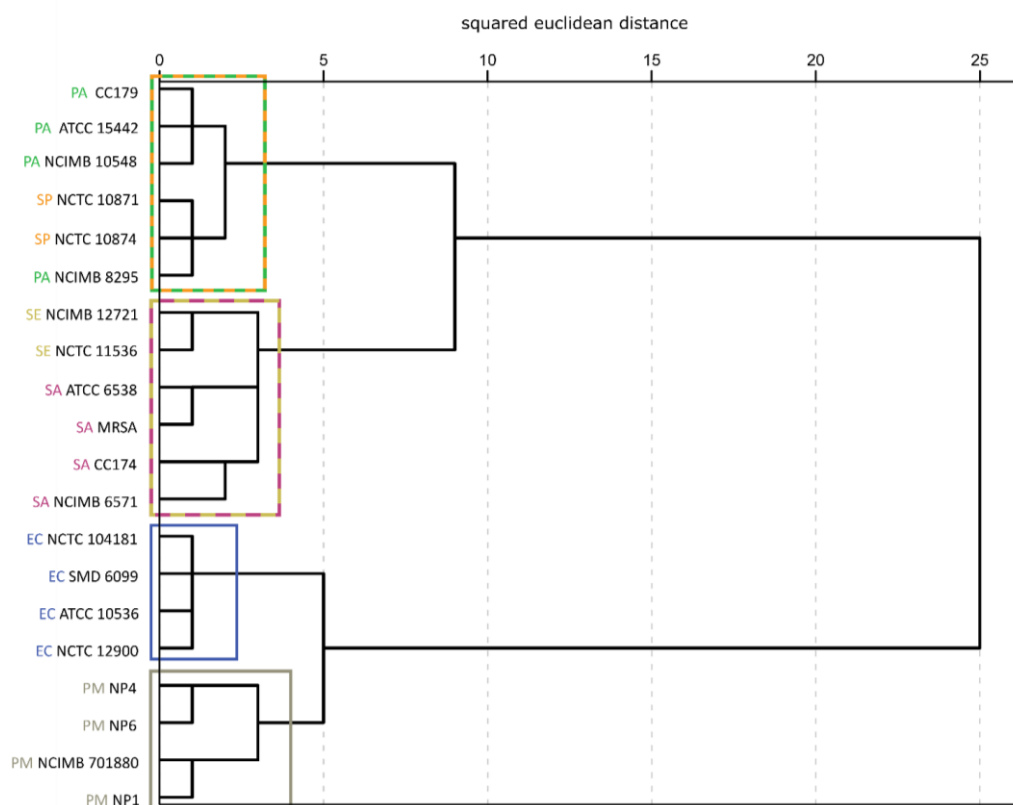


Figure 3.1: Dendrogram generated by hierarchical cluster analysis using 51 selected headspace volatile compound product ion peaks, detected by SIFT-MS following 5 hours incubation ($n = 3$ per strain) in TSB. EC; *Escherichia coli*, PM; *Proteus mirabilis*, SE; *Staphylococcus epidermidis*, PA; *Pseudomonas aeruginosa*, SP; *Streptococcus pyogenes*, SA; *Staphylococcus aureus*.

volatile compound product ions detected. The data was transformed using principal component analysis to reduce the selected variables to principal components. The first two principal components account for 36.3% and 21.7% of the variability within the data respectively (Figure 3.2a). Plotting the scores generated by PCA enables the complex data set to be represented in 2-dimensional space and clearly visualises the association of each bacterial strain with the derived principal components. This shows that the strains of *P. mirabilis* and *E. coli*, occupy discrete regions of the 2-dimensional plot. Figure 3.2b shows the loading of the 51 selected product ions constituting the original variables for the principal component analysis shown in Figure 3.2a. This plot shows the contribution of each of the original variables; product ion count rates, to the derived first two principal components and indicates the influence of these variables in determining the position of each test strain. It is important to note that both the absence and presence of product ions dictates the spatial location of the given bacterial strain within the principal component plot. For example, when considering *P. aeruginosa* and *S. pyogenes* within the principal component plot, the absence of the majority of detected product ions and the presence of product ions m/z 18 and 28 dictate the plotted location of these species. Figure 3.2a shows *P. aeruginosa* and *S. pyogenes* are located very close together on the two-dimensional plot, with some overlap between the two species, and are not well discriminated based on the profile of selected volatile compound product ions detected following 5 hour incubation in TSB. This was predominantly due to the absence of product ions detected in the culture headspace, as indicated by Figure 3.2b, rather than the presence of numerous similar volatile product ions. *S. aureus*

and *S. epidermidis* appear to occupy overlapping regions on the plot shown in Figure 3.2a. However, when the third principal component is employed (accounting for 10.1% of the total variance) to construct a 3-dimensional plot, these two species separate along this theoretical z-axis.

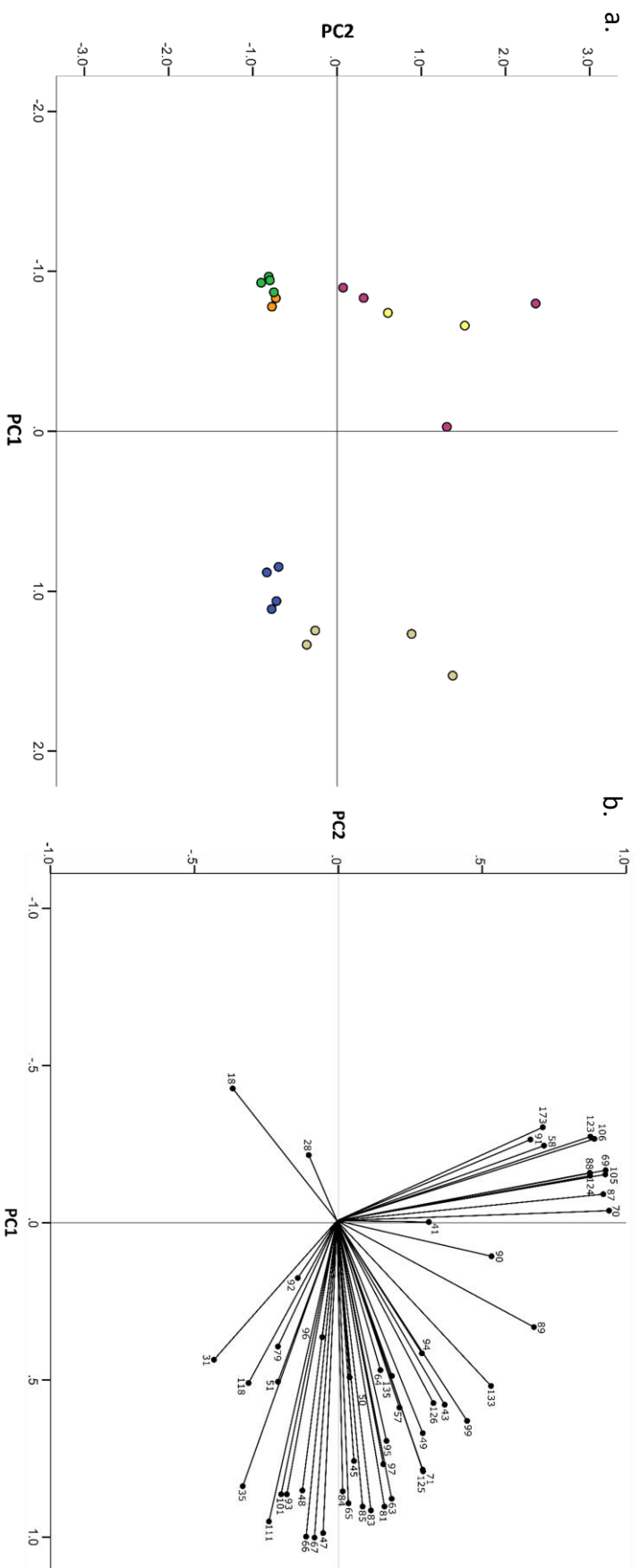


Figure 3.2: (a) Plot of the scores of the first two principal components generated by principle component analysis of selected SIFT-MS product ion peaks detected from the headspace of bacterial cultures incubated for 5 h in TSB (n = 3). Principal component 1 (horizontal axis) accounts for 36.3% of the total variation in the original data set and principal component 2 (vertical axis) accounts for 21.7%. *Escherichia coli* (blue), *Pseudomonas aeruginosa* (Green), *Proteus mirabilis* (Grey), *Staphylococcus epidermidis* (Yellow), *Staphylococcus aureus* (Pink), *Streptococcus pyogenes* (Orange). (b) Principal component analysis loading plot of selected m/z peaks detected by SIFT-MS analysis of cultures incubated for 5 h in TSB. Data points indicate the loading of each m/z peak (variable) on the first two principal components generated from the principal component analysis.

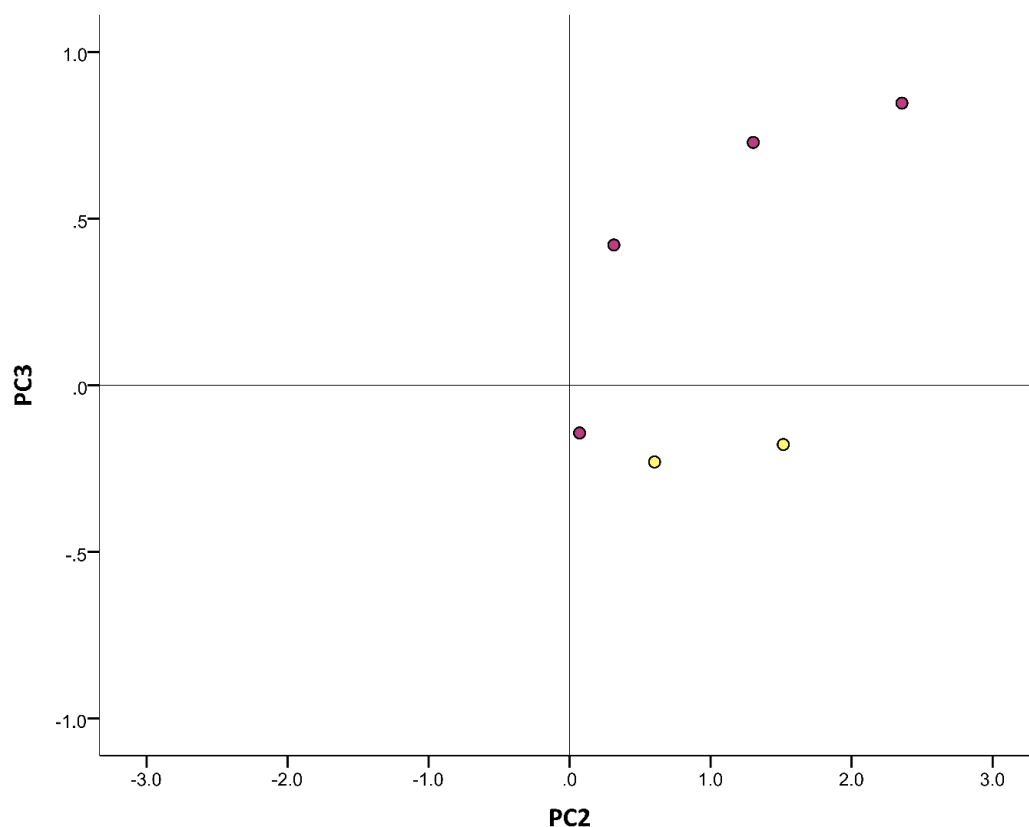


Figure 3.3: Plot of the scores of the second and third principal components generated by principle component analysis of selected SIFT-MS product ion peaks from bacterial cultures incubated for 5 h in TSB (n = 3). Principal component 2 (horizontal axis) accounts for 21.7% and principal component 3 (vertical axis) accounts for 10.1% of the variation within the original data set. Showing separation of *Staphylococcus aureus* (Pink) and *Staphylococcus epidermidis* (Yellow).

Although it is not possible to display the 3-dimensional plot within this thesis, the data can be visualised by plotting the second and third principal components against each other in a 2-dimensional plot, as shown in Figure 3.3.

To further investigate whether *P. aeruginosa* and *S. pyogenes* could be differentiated based on volatile analysis when cultured in TSB, independent samples were cultured

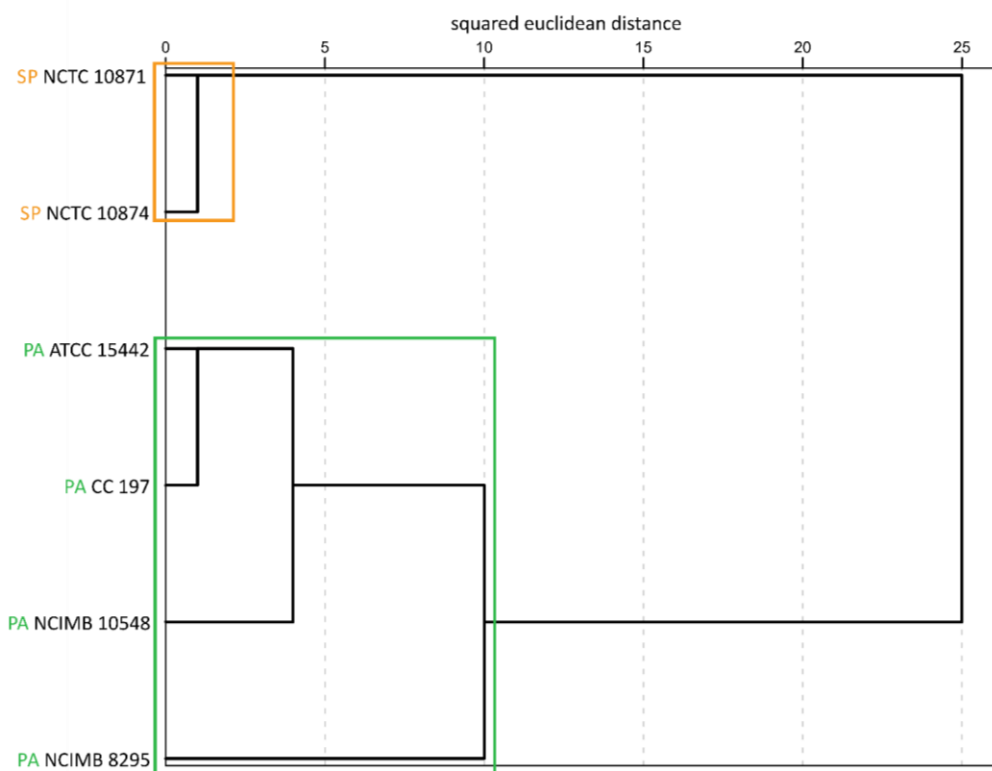


Figure 3.4: Dendrogram generated by hierarchical cluster analysis using selected headspace volatile product ion peaks, detected by SIFT-MS following 24 h of incubation in TSB (n = 3 per strain). PA; *Pseudomonas aeruginosa*, SP; *Streptococcus pyogenes*.

for 24 hours and headspace gases analysed by SIFT-MS, with the resultant data processed as previously described. Following product ion selection, hierarchical cluster analysis resulted in the production of the dendrogram shown in Figure 3.4. This shows that through analysis of the headspace gases of *P. aeruginosa* and *S. pyogenes* cultured in TSB for 24 hours, the two species can be separated into discrete clusters. Therefore indicating differences between headspace volatile compound product ions of *P. aeruginosa* and *S. pyogenes* detected following 24 hour incubation that were not present after 5 hours incubation.

3.3.2 *Headspace Analysis of Wound Associated Bacteria Cultured in a Simulated Wound Fluid (SWF).*

Analysis of the data generated through SIFT-MS analysis of bacterial cultures grown in SWF following the same processing procedure as that used for the samples cultured in TSB, indicated that the threshold detection level of 10 cps was not sufficient to identify discriminatory product ions within the data set. Applying this threshold to the SWF headspace m/z data resulted in the identification of 55 potentially discriminatory product ion peaks.

Analysis of these selected product ion peaks using hierarchical cluster analysis resulted in construction of the dendrogram shown in Figure 3.5. This dendrogram shows no species specific clustering based on the detection of the 55 selected SIFT-MS product ions in the headspace of bacterial cultures in SWF following 5 hours incubation. However, the dendrogram shown in Figure 3.5 does indicate that the staphylococci can be discriminated from all other species based on analysis of these 55 selected product ions.

In order to identify discriminatory product ion peaks an additional level of thresholding was applied to the data set, product ions were only included in the analysis if the 10 cps threshold was met by at least two strains of any of the species included in the study. This resulted in the selection of 26 potentially discriminatory product ions. Hierarchical clustering analysis of these selected product ions, enabled discrimination of *P. mirabilis*, *E. coli*, *S. pyogenes* and *P. aeruginosa* at the species

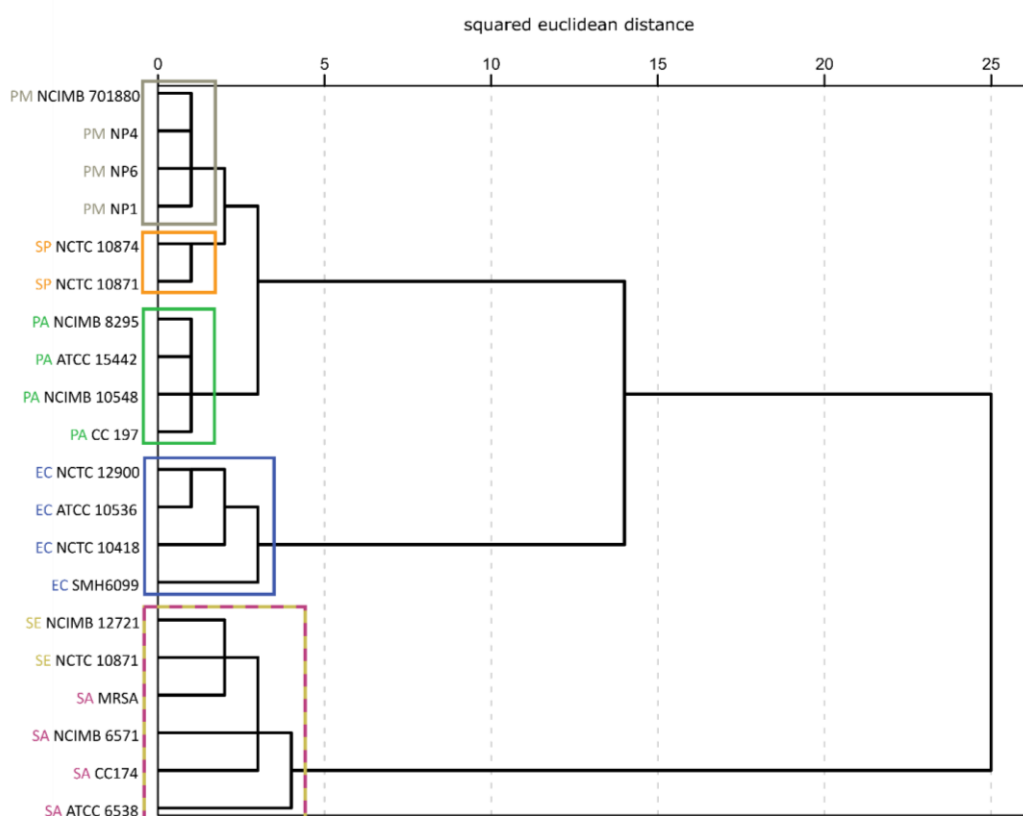


Figure 3.6: Dendrogram generated by hierarchical cluster analysis using 26 selected headspace volatile product ion peaks, detected by SIFT-MS following 5 h of incubation in SWF ($n = 3$ per strain). EC; *Escherichia coli*, PM; *Proteus mirabilis*, SE; *Staphylococcus epidermidis*, PA; *Pseudomonas aeruginosa*, SP; *Streptococcus pyogenes*, SA; *Staphylococcus aureus*.

Principal component analysis was utilised to transform this data set; the first two principal components account for 34.3% and 19.7% of the total variance (Figure 3.7a). Figure 3.7a shows that strains of *E. coli* and staphylococci each occupy specific discrete regions of the 2-dimensional plot, but that there is overlap between *S. pyogenes*, *P. mirabilis* and *P. aeruginosa*. Figure 3.7b shows the loading plot of the 26 original variables (product ions) detected by SIFT-MS headspace analysis on the first two principal components, generated by the principal component analysis represented in figure 3.7a. In Figure 3.7a, strains of *P. mirabilis*, *P. aeruginosa* and *S. pyogenes* appear to occupy overlapping regions. An additional plot was constructed using the third principal component, which accounts for 9.5% of the total variation within the original data set (Figure 3.8). This shows that the *P. aeruginosa* and *P. mirabilis* are separated along the horizontal axis (third principal component). The strains of *S. pyogenes* do not occupy a discrete area of this plot, one strain is more closely associated with the *P. mirabilis* strains than with the other strain of *S. pyogenes* (Figure 3.8).

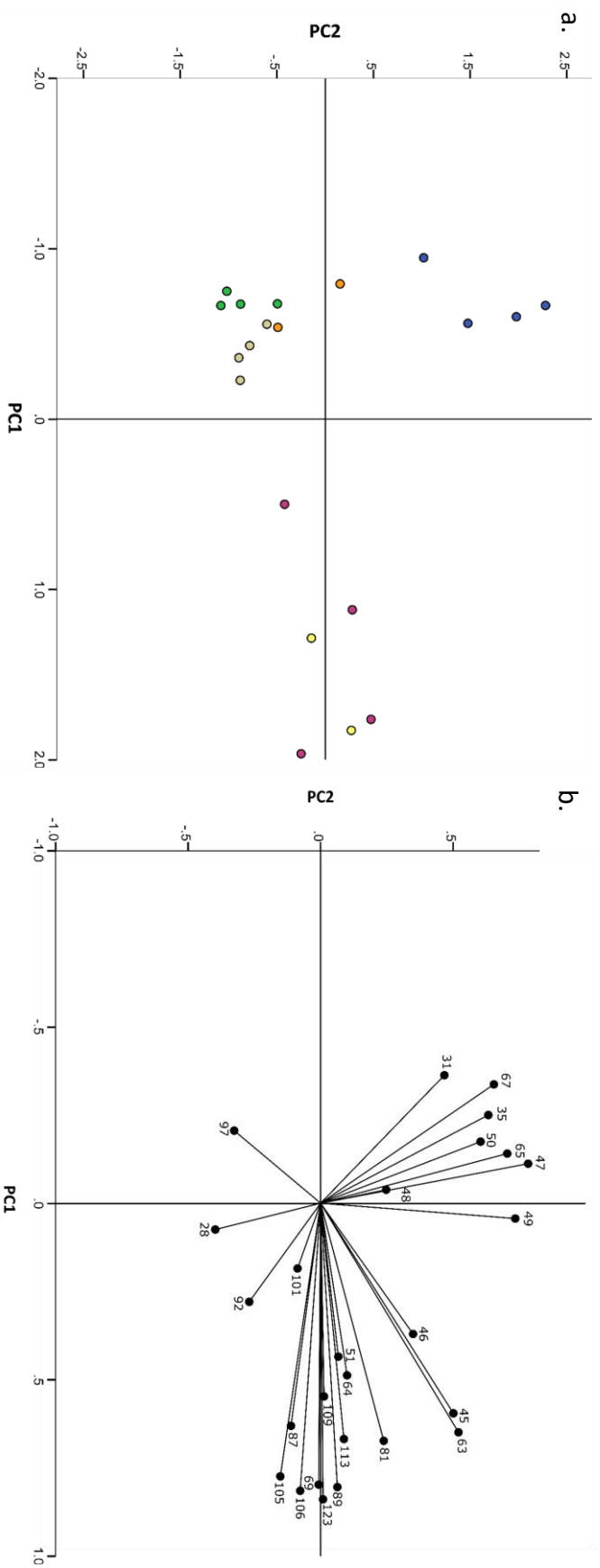


Figure 3.7: (a) Plot of the scores of the first two principal components generated by principle component analysis of selected SIFT-MS production peaks from bacterial cultures incubated for 5 h in SWF (n = 3). Principal component 1 (horizontal axis) accounts for 34.3% of the total variation in the original data set and principal component 2 (vertical axis) accounts for 19.7%. *Escherichia coli* (blue), *Pseudomonas aeruginosa* (Green), *Proteus mirabilis* (Grey), *Staphylococcus epidermidis* (Yellow), *Staphylococcus aureus* (Pink), *Streptococcus pyogenes* (Orange). (b) Principal component analysis loading plot—selected m/z peaks detected by SIFT-MS analysis of cultures incubated for 5 h in SWF. Data points indicate the loading of each m/z peak (variable) on the first two principal components generated from the principal component analysis.

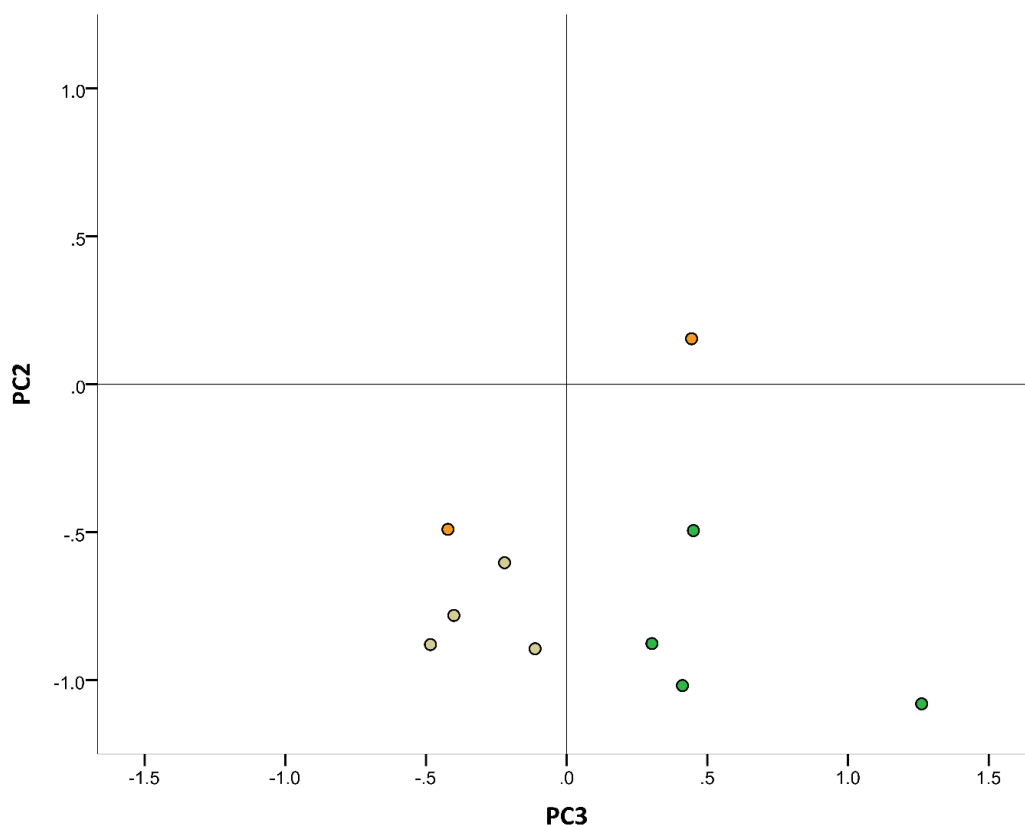


Figure 3.8: Plot of the scores of the second and third principal components generated by principle component analysis of selected SIFT-MS product ion peaks from bacterial cultures ($n = 3$) incubated for 5 h in SWF. Principal component 2 (vertical axis) accounts for 19.7% and principal component 3 (horizontal axis) accounts for 9.5% of the variation within the original data set. Showing separation of *Proteus mirabilis* (Grey), *Pseudomonas aeruginosa* (Green) and *Streptococcus pyogenes* (Orange).

The strains of *S. aureus* and *S. epidermidis* did not form separate clusters in the dendrogram shown in figure 3.6 or occupy discrete regions of the PCA plot shown in Figure 3.7. Additional independent samples of *S. aureus* and *S. epidermidis* were inoculated and incubated for 24 hours, to investigate whether strains of these species could be differentiated based on the headspace volatiles produced during culture in SWF with an extended incubation period. Following background

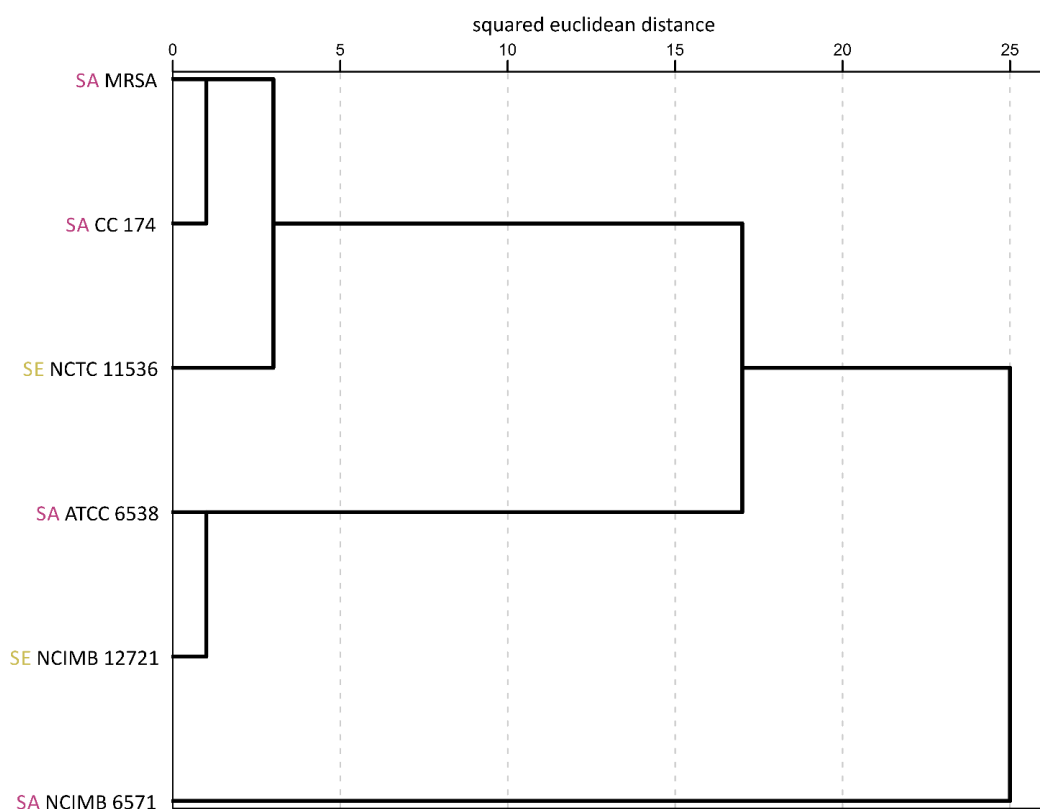


Figure 3.9: Dendrogram generated by hierarchical cluster analysis using selected headspace volatile product ion peaks, detected using SIFT-MS following 24 h incubation of *Staphylococcus aureus* and *Staphylococcus epidermidis* (n=3 per strain) in SWF. SA; *S. aureus*, SE; *S. epidermidis*.

subtraction and product ion selection as described previously, hierarchical cluster analysis was used to generate the dendrogram show in Figure 3.9. This dendrogram does not show any species specific clustering of *S. aureus* and *S. epidermidis*, indicating that these species cannot be discriminated using detection of headspace volatiles when cultured in simulated wound fluid for 24 hours.

The SIFT-MS Profile 3 instrument has an associated kinetics library, usually employed when operating the instrument in multi ion mode for the quantification of known compounds. Searching this library for the selected m/z product ion peaks detected in the bacterial culture headspace allows for a preliminary identification of the neutral analyte compounds that may have given rise to the detected product ion peaks. Table 3.1 shows presumptive identification for the 26 selected product ion peaks used for the analysis of the headspace of bacterial cultures in SWF following 5 hours incubation. Some of these product ions peaks, such as 48, 64 and 106 m/z did not correspond with any entry in the kinetics library, while others match with multiple entries. Table 3.1 indicates each of the product ions detected, the library entries (compounds) associated with each product ion where applicable, the compound molecular formula and molecular weight (MW), and the reaction with the H₃O⁺ reagent ion that that would give rise to the detected product ion from the suggested analyte compound. For example, a product ion at 81 m/z could be generated from acetaldehyde, which has a MW of 44, ionised by the addition of H₃O⁺. H₂O or dimethyl disulphide which has a MW of 62, ionised by the addition of H₃O⁺.

Table 3.2 shows the product ions detected from each bacterial strain and their intensity, when cultured in both TSB and SWF for 5 hours. Comparing these tables shows clear differences between the volatile compound product ions detected when these organisms are cultured in these two different liquid media. Table 3.2 shows that in general, the product ion peaks detected from the bacterial species included in this study, are greater in number and often at higher intensities in the TSB data set compared to the SWF data set.

Table 3.1: Presumptive identification of compounds corresponding to SIFT-MS product ions detected in the headspace of bacterial cultures in SWF. Including detected product ion peak, the possible corresponding compound(s) with the formula, molecular weight and the reaction with the H₃O⁺ reagent ion that would give rise to the detected product ion from the suggested analyte compound, for example H⁺ indicates protonation reaction.

m/z ion	Compound	Molecular formula	Molecular Weight	H ₃ O ⁺ reagent ion reaction
28	Hydrogen Cyanide	HCN	27	H ⁺
31	Formaldehyde	CH ₂ O	30	H ⁺
35	Hydrogen sulphide	H ₂ S	34	H ⁺
45	Acetaldehyde	C ₂ H ₄ O	44	H ⁺
46	-	-	-	-
47	Ethanol	C ₂ H ₆ O	46	H ⁺
48	-	-	-	-
49	methylmercaptan/methanthiol	CH ₄ S	48	H ⁺
50	-	-	-	-
51	Methanol	CH ₃ OH	32	H ₃ O ⁺
63	Acetaldehyde, Dimethylsulphide/ethanthiol	C ₂ H ₄ O, C ₂ H ₆ S	44, 62	H ₃ O ⁺ , H ⁺
64	-	-	-	-
65	Ethanol	C ₂ H ₆ O	46	H ₃ O ⁺
67	methylmercaptan/methanthiol	CH ₄ S	48	H ₃ O ⁺
69	Methanol, Isoprene	CH ₄ O, C ₅ H ₈	32, 68	H ₃ O ⁺ , H ₂ O, H ⁺
81	Acetaldehyde, Dimethylsulphide	C ₂ H ₄ O, C ₂ H ₆ S	44, 62	H ₃ O ⁺ , H ₂ O, H ₃ O ⁺
87	-	-	-	-
89	Pentanol, Butyric acid, Putresceine	C ₅ H ₁₂ O, C ₃ H ₇ COOH, C ₄ H ₁₂ N ₂	88, 88, 88	H ⁺
92	-	-	-	-
97	Propanol, Acetic acid,	C ₃ H ₈ O, CH ₃ COOH,	60, 60	H ₃ O ⁺ , H ₂ O
101	Hexanal, Hexan-2-one	C ₆ H ₁₂ O, C ₆ H ₁₂ O	100, 100	H ⁺
105	2-phenylethanol, Pentan-2-one,	C ₈ H ₁₀ O, C ₅ H ₁₀ O	86	H ₃ O ⁺
106	-	-	-	-
109	Methylphenol,	C ₇ H ₈ O	108	H ⁺
113	-	-	-	-
123	Ethylphenol	C ₈ H ₁₀ O	122	H ⁺

3.4 DISCUSSION

The main aim of this chapter was;

- To investigate if planktonic cultures of wound associated bacteria produce species specific volatile profiles *in vitro*, enabling significant discrimination.

The mass spectral profile of volatile compound product ions derived from the tested wound-associated bacterial species varies between species. This also extends, to some strains from a single species, as reported in previous studies (Thorn, Reynolds and Greenman, 2011; Shestivska *et al.*, 2015). This work has demonstrated that the culture conditions; namely composition of culture media and duration of incubation, influence the range of product ions and count rates of the resultant volatile compound mass spectra. The variability in the range and relative concentrations of bacterial volatiles detected under different physicochemical conditions has been previously observed in other research studies (Dolch *et al.*, 2012a, 2012b; O'Hara and Mayhew, 2009; Chippendale, Španěl and Smith, 2011). The range and count rates of product ions detected are greater in TSB, a complex nutrient rich commercially available culture media, compared to a simulated wound fluid containing Peptone, NaCl and Fetal Bovine Serum (Table 3.2). The differing nutrient sources in the culture media almost certainly results in the upregulation of altered bacterial metabolic pathways, resulting in the production of different volatile metabolites (Audrain *et al.*, 2015).

The results from this work demonstrate that, it is possible to discriminate selected wound associated bacterial species based on the detected volatile compound

product ion profiles, whether cultures are grown within complex medium (TSB) or under wound similar conditions (in SWF). After 5 hours incubation it was possible to discriminate several species based on the volatile compound product ion profiles using hierarchical clustering analysis; however, it was not possible to discriminate between strains of *P. aeruginosa* and *S. pyogenes*. Similarly, when the transformed data set was plotted as principal components, *P. aeruginosa* and *S. pyogenes* occupy closely adjacent regions on the two-dimensional plot. This is the result of the absence of product ions detected in the headspace of either species under these conditions, visualised by comparing the two plots in Figure 3.2.

Increasing the incubation period to 24 hours resulted in an increase in the number and count rates of SIFT-MS product ions detected from *P. aeruginosa*. This included high count rates for the 18 m/z product ion in all strains and the 28 m/z product ion in two of the four strains analysed. Hierarchical clustering analysis of the data obtained after 24 hours of incubation resulted in successful discrimination between the strains of these two species, based on the clustering shown in the resulting dendrogram (Figure 3.4).

It is possible to make a preliminary identification of the volatile compounds which correspond with the detected SIFT-MS product ions, using predetermined reaction rate constants. When using the H_3O^+ reagent ion, 18 and 28 m/z product ions indicate the presence of protonated ammonia and hydrogen cyanide respectively (Turner, Španěl and Smith, 2006; Španěl, Wang and Smith, 2004). It has been previously demonstrated that both ammonia and hydrogen cyanide production are characteristic of *P. aeruginosa* (Nawaz *et al.*, 1991; Gilchrist *et al.*, 2011). A study

which investigated the production of these volatiles over time in a number of *P. aeruginosa* strains determined that both compounds began to rise above detectable levels only in older cultures, as they began to enter stationary phase (Neerincx *et al.*, 2015). This would explain the presumptive detection of these discriminant volatiles only after 24 hours of culture within this study. It is highly likely that these volatiles will be important for identification of *P. aeruginosa in vivo*, where growth conditions likely result in a slow growing biofilm state. Indeed, elevated hydrogen cyanide concentrations in nose-exhaled breath have been identified using SIFT-MS as a potential biomarker of *P. aeruginosa* infection in adult Cystic fibrosis patients (Gilchrist *et al.*, 2013).

The results of this study successfully demonstrated that it is possible to discriminate wound-associated bacterial species based on a profile of selected SIFT-MS product ions when cultured under wound similar conditions. Using hierarchical cluster analysis to determine strain relatedness, four of the six bacterial species were successfully discriminated, based on the clustering shown in the resulting dendrogram (Figure 3.6). Using PCA and constructing plots using the scores of the first 3 principal components resulted in incomplete discrimination of the bacterial species investigated, suggesting some essential information for discrimination may have been lost to the other smaller components not included in the plots. The two species of staphylococci could not be discriminated from each other based on the analysis of headspace volatile compound product ions following 5 hours of incubation. Further analysis of the headspace of both species of staphylococci

following 24 hours of incubation in SWF, also failed to successfully discriminate these species, in contrast to staphylococci cultured in complex culture media (TSB).

The discrimination of these wound associated microorganisms based on the analysis of headspace gases using SIFT-MS resulted from careful selection of appropriate discriminatory product ions through the application of signal thresholds. As noted earlier, analysis of different discriminatory product ions was required for successful species specific clustering under the two different culture conditions testing during this work. The majority of studies of bacterial volatile metabolites to date rely on detection or quantification of specific compounds, which requires pre selection of appropriate compounds previously identified in the bacterial culture headspace. The approach used here facilitates discrimination of bacterial species based on all the volatile compound product ion peaks detected across a spectrum range. One advantage of this approach is that unknown compounds that have not been previously identified and may be important for species discrimination can contribute to the analysis, but conversely many non-discriminatory product ions peaks will be detected and so selection of discriminatory product ion peaks forms an important phase of the data analysis. Further investigation of alternative methods for selection of potentially discriminatory volatile compound product ion peaks would be an advantage for future work.

Using the predetermined reaction rate constants, presumptive identification of the neutral analyte compounds which correspond to the detected SIFT-MS product ions is possible. However, it is important to be aware that the reaction of a single selected precursor ion with similar volatile compounds or compound fragments can result in

the production of the same product ions (Table 3.1). For example, utilising the H_3O^+ precursor ion as used within this study, the production of 89 m/z product ion can result from the protonation of a number of different analytes with a molecular weight of 88 Da, including pentanol ($\text{C}_5\text{H}_{12}\text{O}$), butyric acid ($\text{C}_3\text{H}_7\text{COOH}$) and putrescine ($\text{C}_4\text{H}_{12}\text{N}_2$). Furthermore, if a mixture known to contain more than one of these compounds were analysed using only the H_3O^+ precursor ion in MIM mode, it would only be possible to determine the total partial pressure of all compounds resulting in the common product ion (Wang, Španěl and Smith, 2004). In some cases it may be possible to rule out the presence of certain compounds based on the nature of the sample being analysed. However, pentanol ($\text{C}_5\text{H}_{12}\text{O}$), butyric acid ($\text{C}_3\text{H}_7\text{COOH}$) and putrescine ($\text{C}_4\text{H}_{12}\text{N}_2$) could all be produced as a result of bacterial metabolism, as products of fermentation and decarboxylation reactions (Schulz and Dickschat, 2007; Audrain *et al.*, 2015; Thorn and Greenman, 2012). Ambiguity in the identification of neutral analyte compounds can potentially be overcome by the analysis of the sample using multiple precursor ions, usually H_3O^+ and NO^+ , as the reaction of compounds with different precursor ions can result in the production of different product ions. The compounds may then be identified and quantified using the appropriate precursor ion reaction (Wang, Španěl and Smith, 2004).

This study has demonstrated that using SIFT-MS and multivariate statistical analysis, it is possible to discriminate wound-associated bacterial species based on the profile of selected SIFT-MS product ions when these species are grown in complex culture media (TSB) and under wound similar conditions in SWF. Discrimination of bacterial species associated with wound infection cultured in SWF to simulate the nutrients

supplied in wound like conditions begins to demonstrate the possibility of using detection of volatile metabolites for the identification of the causative organism of wound infection. This provides the first important step in this research, towards the application of volatile analysis for point of care identification of the cause of clinically relevant wound infection.

Further work will assess whether it is possible to discriminate between bacterial species based on volatile headspace analysis when grown as biofilm rather than in liquid culture. A biofilm model will simulate more closely the real wound environment (James *et al.*, 2008) and the altered growth conditions will likely affect the metabolic profile of the organisms and result in a change in the volatile metabolites produced, and hence the discriminatory products required for the resulting analysis. This approach required the development of a wound biofilm model based on a continuously perfused semi-solid matrix which is the focus of Chapter 5. Enabling volatile profiles of the wound associated organisms to be investigated under conditions that more closely simulate wound infection, will further facilitate the development of this approach to clinically useful wound diagnostics.

Chapter 4: Analysis of volatile compounds from discarded patient wound dressings

4.1 INTRODUCTION

The results presented in chapter three demonstrate that bacterial species associated with wound infection produce characteristic volatile profiles *in vitro*, and that differences between volatile profiles can be exploited to facilitate discrimination between bacterial species. Regular wound dressing changes are carried out during routine patient care and this material is usually discarded. Dressing material that has been in contact with an infected wound will absorb exudate (Spear, 2012) and may also capture volatile compounds emitted by the infecting bacteria. Hence, it may be possible to identify species specific volatile profiles derived from the organism causing an infection, using selected ion flow tube mass spectrometry (SIFT-MS) for analysis of discarded dressing material. In addition, wound dressing removal is associated with increased pain, which can cause considerable patient distress, and can contribute to delayed wound healing (Price et al. 2008; Upton et al. 2012). The ability to assess a wound for infection by direct assessment of discarded dressing material would be of significant clinical significance, since this would minimize additional interference with the wound.

The main aim of this chapter was to address the second main research aim:

- To investigate if the concept of species discrimination based on volatile compound detection could be applied to analysis of discarded wound dressings, as part of routine wound care.

4.2 METHODS SUMMARY

4.2.1 *Dressing Collection*

Burn wound dressings were collected from patients with scald, contact and flame burn injuries, presenting to the adult and children's burn services at Bristol Royal Hospital for Children and Southmead Hospital, Bristol between April 2016 and September 2017. Dressings were collected from patients with suspected burn wound infection, once removed were stored refrigerated in a sealed container or bag for up to 72 hours. Dressings were then transported to UWE for analysis (UWE FREC number: HAS.15.08.005, NHS REC reference: 15/YH/0304, Human Tissue Register Reference: HTSC-31A) and analysed within 7 days. The clinical indicators of infection used as inclusion criteria for this study were high temperature, rash, vomiting, diarrhoea, decrease appetite, lethargy, wound odour, increased pain and wound appearance. In addition, a description of the wound presentation was recorded in line with the following criteria; Normal healing, red/inflammation, swelling, hot to touch, exudate, biofilm, pus, necrosis/tissue death, strong odour.

4.2.2 *SIFT-MS Analysis*

Dressing samples were transferred aseptically to a 1 L gas sampling bag (Tedlar®, Supelco, UK) which was sealed, filled with synthetic air (20% oxygen, 80% nitrogen) and incubated for 1 hour at 37°C to allow the equilibration of headspace gases.

Following incubation, the gaseous headspace of the dressing samples were analysed by SIFT-MS (Profile 3, Instrument Science Limited, UK) in 'Full Mass Scan' mode using

the H_3O^+ precursor ion; each sample was analysed using 3 repeat scans of 100 seconds, over a spectrum range of 10-200 m/z. Headspace samples were introduced to the instrument by piercing the silicone septum of the sample bag with a sterile needle attached to the SIFT-MS direct sampling inlet. After sampling was complete, the samples were destroyed by autoclaving (in line with the ethical approval requirements).

In addition, sterile dressing sample controls (n=3) for each dressing type included in the study were analysed by SIFT-MS using the same experimental conditions and parameters as detailed above.

4.2.3 Wound Swab Microbiology and Clinical Information

The results of routine clinical wound swabbing microbiology, carried out at the time of dressing change, and anonymised patient clinical symptoms and wound presentation information, were provided by Bristol Royal Hospital for Children and Southmead Hospital (UWE FREC number: HAS.15.08.005, NHS REC reference: 15/YH/0304, Human Tissue Register Reference: HTSC-31A).

4.2.4 Data Analysis

To allow comparison between samples, where different dressing types were used, corresponding sterile dressing samples were analysed and background subtraction performed. This allowed identification of the detected volatile compound product ion peaks that could be attributed to the patient sample, irrespective of dressing

type. Where a product ion peak was detected from both the patient dressing sample and the sterile control dressing, t-tests were performed to compare the count rate detected. Only product ions detected at significant levels ($p < 0.05$) from the patient dressing sample when compared to sterile control dressings were included for further analysis. The mean product ion count rate of background volatiles from the sterile control dressings, were subtracted from those detected in patient dressing samples, to determine the total count rate attributed to volatile compounds detected from the patient dressing sample. Reagent ion peaks and corrected negative values (indicating a reduction below the background levels) were disregarded.

4.3 RESULTS

Table 4.1 details the clinical signs and symptoms indicative of infection for each patient included in the study, Tables 4.2 details the clinical wound presentation recorded, and Table 4.3 details the results of routine clinical microbiological analysis of wound surface swabs. The patient ID indicates the origin of the patient dressing sample. The DRV2 samples were collected from paediatric patients at the Bristol Royal Hospital for Children, whilst NBT samples were collected from adult patients at Southmead Hospital. High temperature and vomiting were the most common clinical indicators of infection among children, recorded in 94% and 47% of these patients respectively. Wound appearance (100%), odour (76%) and increased pain (57%) were the most common clinical indicators of infection among the adult patients. *Staphylococcus aureus* was the most commonly isolated organism from all the wound surface swabs (54%).

Patient dressing samples were analysed by SIFT-MS in full scan mode, using 3 repeat scans employing the H₃O⁺ reagent ion, over a spectrum range of 10 – 200 m/z. Following analysis, t-tests and background subtraction of data obtained from scans of sterile controls of the same dressing type as the sample were carried out. Table 4.4 shows the resulting data set, including only the product ion peaks with corrected values that were detected at levels significantly ($p < 0.05$) in excess of the control dressing levels. Conditional formatting has been used on this table to ease interpretation, with colour increasing in intensity from white (not detected) to deep red with increased product ion intensity. Of the 55 dressing samples analysed by SIFT-

MS there were 7 samples in which no volatile compounds product ion peaks were detected at an intensity significantly above that of the sterile control dressing. These were DRV2010, DRV2021, NBT009, NBT010, NBT012, NBT013 and NBT015.

Table 4.1: Clinical indicators of infection corresponding to each of the discarded patient dressing samples included in this study.

Sample ID	Clinical indicators of Infection
DRV2005	High temperature
DRV2007	High temperature, rash, vomiting, wound appearance
DRV2008	High temperature, rash, vomiting
DRV2009	High temperature, rash, vomiting, lethargy
DRV2010	Wound appearance, odour
DRV2011	High temperature, vomiting
DRV2012	High temperature
DRV2013	High temperature
DRV2014	High temperature, rash, wound appearance
DRV2015	High temperature, rash, vomiting
DRV2016	High temperature, vomiting, decreased appetite
DRV2017	High temperature, decreased appetite, lethargy
DRV2018	High temperature, vomiting, lethargy
DRV2019	High temperature, rash, vomiting
DRV2020	High temperature, decreased appetite, lethargy
DRV2021	High temperature, vomiting, lethargy, tachycardia, low leukocytes
DRV2022	High temperature, rash, decreased appetite, lethargy
NBT002	High temperature, lethargy, wound appearance , odour, increased pain
NBT003	Wound appearance
NBT004	Wound appearance , odour, increased pain
NBT005	Wound appearance , odour
NBT006	High temperature, wound appearance, odour, raised CRP
NBT007	Wound appearance , odour, increased pain
NBT008	Wound appearance, odour, tracking cellulitis
NBT009	Wound appearance , odour, increased pain
NBT010	Wound appearance , odour, increased pain
NBT011	Wound appearance , odour, increased pain
NBT012	Rash, wound appearance , odour, increased pain
NBT013	Rash, wound appearance
NBT014	Wound appearance
NBT015	Wound appearance
NBT016	Wound appearance, odour
NBT017	Wound appearance , odour, increased pain
NBT018	Wound appearance , odour, increased pain
NBT019	Wound appearance , odour
NBT021	Wound appearance , odour, increased pain
NBT022	Wound appearance , odour, increased pain
NBT023	Wound appearance , odour, increased pain
NBT024	High temperature, lethargy, wound appearance , odour, increased pain
NBT025	High temperature, lethargy, wound appearance , odour, increased pain, shivers
NBT026	Wound appearance
NBT027	Lethargy, wound appearance , odour
NBT028	Wound appearance , odour, increased pain
NBT029	Wound appearance, increased pain, erythema around wound
NBT030	Wound appearance , odour
NBT031	Vomiting, decreased appetite, lethargy, wound appearance , increased pain
NBT032	High temperature, wound appearance , odour, increased pain
NBT033	Wound appearance , odour, increased pain
NBT034	Rash, wound appearance, odour
NBT036	Wound appearance , odour, increased pain
NBT037	Wound appearance , odour, increased pain
NBT038	Wound appearance , odour
NBT039	Wound appearance
NBT040	Wound appearance , increased pain

Table 4.2: The clinical wound presentation corresponding to each of the discarded patient dressing samples included in this study.

Sample ID	Wound presentation
DRV2005	Red inflamed, necrosis, strong odour
DRV2007	Biofilm
DRV2008	Normal healing, exudate, biofilm, rash
DRV2009	Normal healing
DRV2010	Red inflamed, swelling, pus, abscess
DRV2011	Normal healing, exudate
DRV2012	Exudate, deep burn
DRV2013	Exudate
DRV2014	Red inflamed, biofilm, rash with pustules
DRV2015	Exudate, biofilm, rash
DRV2016	Normal healing, exudate, deep burn
DRV2017	Exudate
DRV2018	Normal healing
DRV2019	Red inflamed, exudate
DRV2020	Exudate, deep burn
DRV2021	Deep burn
DRV2022	Normal healing, exudate, deep burn
NBT002	Red inflamed, exudate
NBT003	Red inflamed, hot to touch, exudate
NBT004	Normal healing, Red inflamed, exudate, eschar
NBT005	Red inflamed, exudate, biofilm
NBT006	Red inflamed, exudate, biofilm, odour
NBT007	Red inflamed, swelling, hot to touch, exudate, odour
NBT008	Red inflamed, exudate
NBT009	Normal healing, tattooing
NBT010	Red inflamed, biofilm
NBT011	Red inflamed, hot to touch, exudate
NBT012	Red inflamed, hot to touch, exudate
NBT013	Red inflamed, exudate, odour
NBT014	Red inflamed, exudate, biofilm, odour
NBT015	Red inflamed, hot to touch
NBT016	Red inflamed, exudate, pus, odour
NBT017	Red inflamed, hot to touch, exudate, odour
NBT018	Red inflamed, hot to touch, exudate, biofilm, pus, odour
NBT019	Red inflamed, exudate, biofilm, odour
NBT021	Exudate, biofilm, odour
NBT022	Red inflamed, biofilm, odour
NBT023	Red inflamed, swelling, hot to touch, exudate
NBT024	Red inflamed, swelling, hot to touch, exudate, odour
NBT025	Red inflamed, biofilm
NBT026	Red inflamed, exudate, odour
NBT027	Red inflamed, hot to touch, exudate, odour
NBT028	Red inflamed, hot to touch, biofilm, odour
NBT029	Red inflamed, hot to touch, exudate,
NBT030	Red inflamed, exudate, odour
NBT031	Red inflamed, swelling, hot to touch, exudate
NBT032	Red inflamed, hot to touch, exudate
NBT033	Red inflamed, swelling, hot to touch, exudate, pus
NBT034	Red inflamed, swelling, exudate
NBT036	Red inflamed, hot to touch, exudate, odour
NBT037	Red inflamed, swelling, hot to touch, exudate, odour
NBT038	Red inflamed, hot to touch, exudate, odour
NBT039	Red inflamed, hot to touch, exudate
NBT040	Red inflamed, hot to touch, exudate

Table 4.3: Microbiological results from analysis of wound surface swabs corresponding to each of the discarded patient dressing samples included in this study.

Sample ID	Microbiological Swab Result
DRV2005	Staphylococcus aureus
DRV2007	-
DRV2008	Staphylococcus aureus and scanty Acinetobacter ursingii.
DRV2009	Mixed growth including <i>Staphylococcus aureus</i>
DRV2010	MRSA and Staphylococcus aureus
DRV2011	-
DRV2012	Staphylococcus aureus
DRV2013	Staphylococcus aureus, Moraxella catarrhalis, Streptococcus pneumoniae
DRV2014	Pseudomonas species, Staphylococcus aureus
DRV2015	Diphtheroids, Staphylococcus aureus, CoN Staphylococcus, Acinetobacter lwoffii
DRV2016	Staphylococcus aureus, Diphtheroids
DRV2017	Staphylococcus aureus
DRV2018	<i>Streptococcus</i> (Alpha Haemolytic)
DRV2019	Staphylococcus aureus, CoN Staphylococcus
DRV2020	Staphylococcus aureus
DRV2021	No growth
DRV2022	No growth
NBT002	Group A Streptococcus, Staphylococcus sp., Coliforms
NBT003	Staphylococcus aureus, Coliforms
NBT004	Coliforms, <i>Enterococcus</i> sp
NBT005	-
NBT006	Staphylococcus aureus
NBT007	Staphylococcus aureus, Group G Streptococcus, Diphtheroids
NBT008	CoN Staphylococcus, Staphylococcus aureus, Group G Streptococcus
NBT009	No growth
NBT010	CoN Staphylococcus
NBT011	Enterobacter cloacae, Alpha haemolytic Streptococcus, Diphtheroids
NBT012	Staphylococcus aureus
NBT013	-
NBT014	CoN <i>Staphylococcus</i> , Coliforms
NBT015	Staphylococcus aureus
NBT016	Enterococcus sp, Pseudomonas sp, CoN Staphylococcus
NBT017	Enterococcus sp, Staphylococcus aureus, Alpha haemolytic Streptococcus
NBT018	-
NBT019	Staphylococcus aureus
NBT021	Staphylococcus aureus
NBT022	Staphylococcus aureus
NBT023	Staphylococcus aureus
NBT024	Staphylococcus aureus
NBT025	Group A Streptococcus
NBT026	Group G & Group C <i>Streptococcus</i> , MRSA
NBT027	Staphylococcus aureus, CoN Staphylococcus, Coliforms
NBT028	Staphylococcus haemolyticus, Enterococcus faecalis, Diphtheroids
NBT029	CoN Staphylococcus
NBT030	Staphylococcus aureus, Klebsiella pneumoniae, Enterococcus sp, Diphtheroids
NBT031	Staphylococcus aureus and Coliforms
NBT032	Pseudomonas aeruginosa
NBT033	Staphylococcus aureus
NBT034	Staphylococcus aureus, CoN Staphylococcus
NBT036	CoN <i>Staphylococcus</i> , Diphtheroids
NBT037	CoN Staphylococcus, Alpha haemolytic Streptococcus
NBT038	-
NBT039	No growth
NBT040	MRSA

Hierarchical cluster analysis of the data shown in Table 4.4 resulted in construction of the dendrogram shown in Figure 4.1. The dendrogram contains four main clusters, which are highlighted by the addition of the coloured boxes within the figure. The first cluster (green) contains 22 patient dressing samples, and includes those with few product ions that do not share common features with the other three clusters. The second cluster (blue) contains 19 patient dressing samples, common features among these samples are a product ion peak at 77 m/z, 59 m/z and/or 36 m/z. The 6 patient dressing samples in the third cluster (yellow) are characterised by product ion peaks at 43 m/z, 44 m/z, 59 m/z, 61 m/z and 70 m/z. Finally, the bottom cluster (orange) contains 8 patient dressing samples which share common product ion peaks detected at 43 m/z, 45 m/z, 47 m/z, 65 m/z, 77 m/z and 83 m/z.

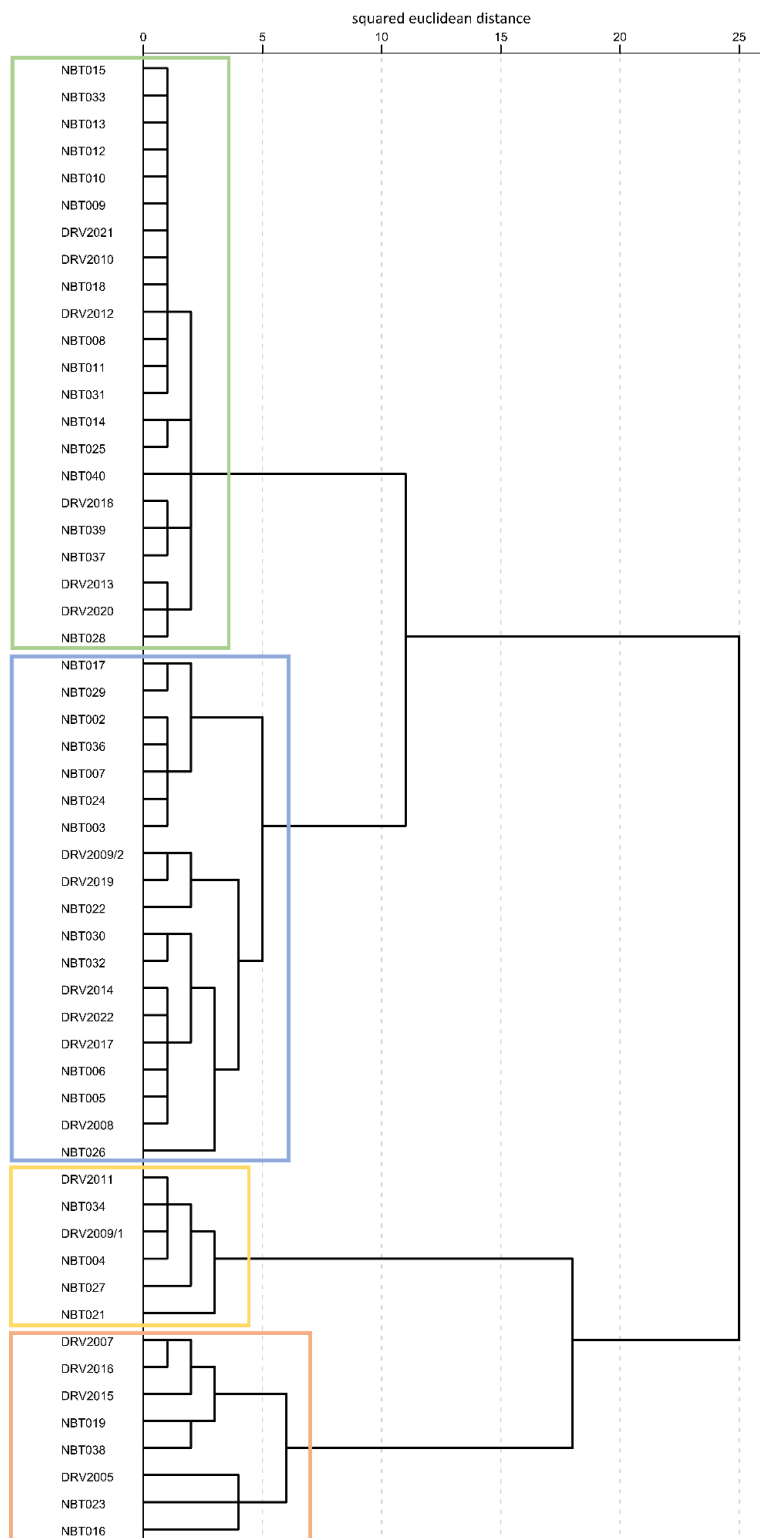
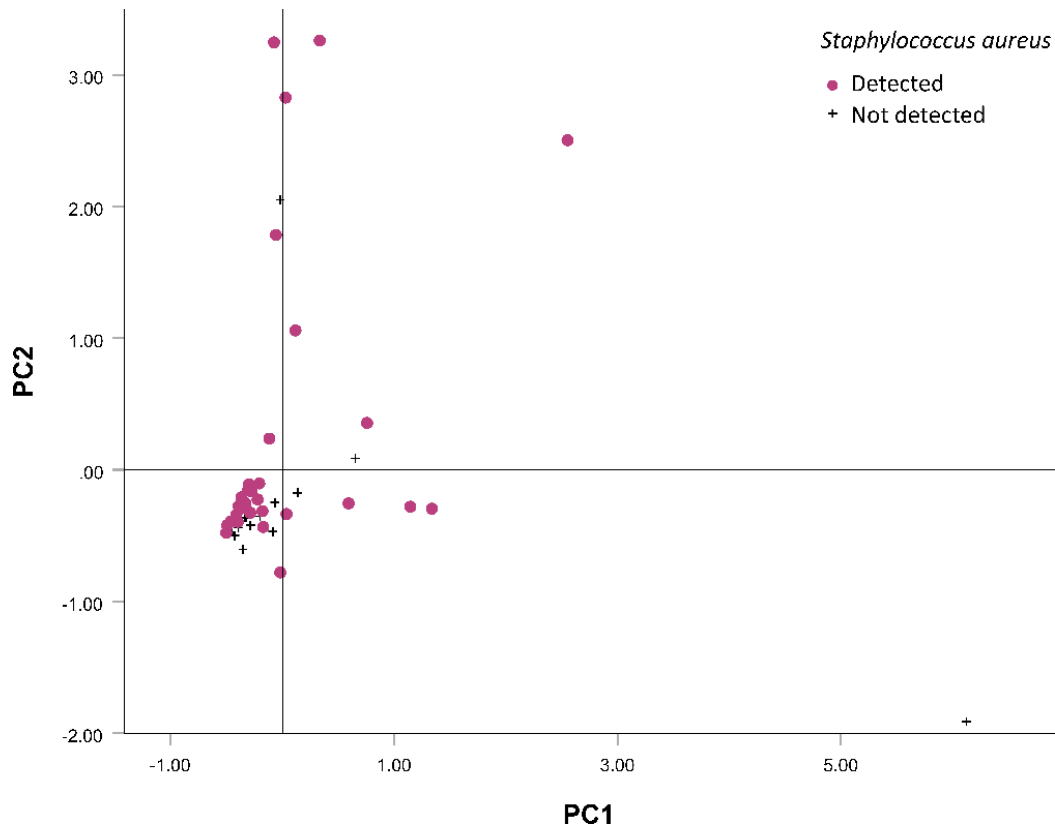


Figure 4.1: Dendrogram generated by hierarchical cluster analysis of SIFT-MS data from the analysis of discarded patient wound dressings (n=3 scans per dressing) following background subtraction of sterile control dressings. Coloured boxes highlight the four main cluster groupings.

Principal component analysis was used to transform the dressing sample data set to principal components. Figure 4.2 to 4.4 show scatter plots of the first two principal components, accounting for 22.0% and 14.0% of the variation within the original data set respectively. These scatter plots have been labelled to show the location of dressing samples within the two dimensional plot that had three of the key species that cause wound infections, isolated from the associated routine clinical wound swab. These plots show that there are no clear groupings of samples within the PCA plot, with the majority of samples grouping together, irrespective of microbiological swab result, and several scattered outside the main cluster of dressing samples.

Figure 4.2, shows the dressing samples with corresponding routine clinical wound swabs that detected the presence of *S. aureus*. This shows that *S. aureus* was isolated from many of the routine wound surface swabs but that these samples did not all group together on the PCA plot based on the volatile compound product ion peaks detected from the dressing sample headspace.

Figure 4.3 shows the same PCA plot, but labelled to show the location of samples that has *Pseudomonas* species detected from the microbiological analysis of wound surface swabs. Only three routine clinical wound swabs detected the presence of *Pseudomonas* species from the wound surface, two of these are located in the main cluster of samples on the PCA plot and one is located separately, scoring high against PC1 and negatively against PC2. The location of dressing samples with corresponding routine clinical wound swabs that detected Streptococci are show in Figure 4.4, all of these dressing samples are located in the main cluster of this plot, which also contains samples where *Pseudomonas* species and *S. aureus* were detected.



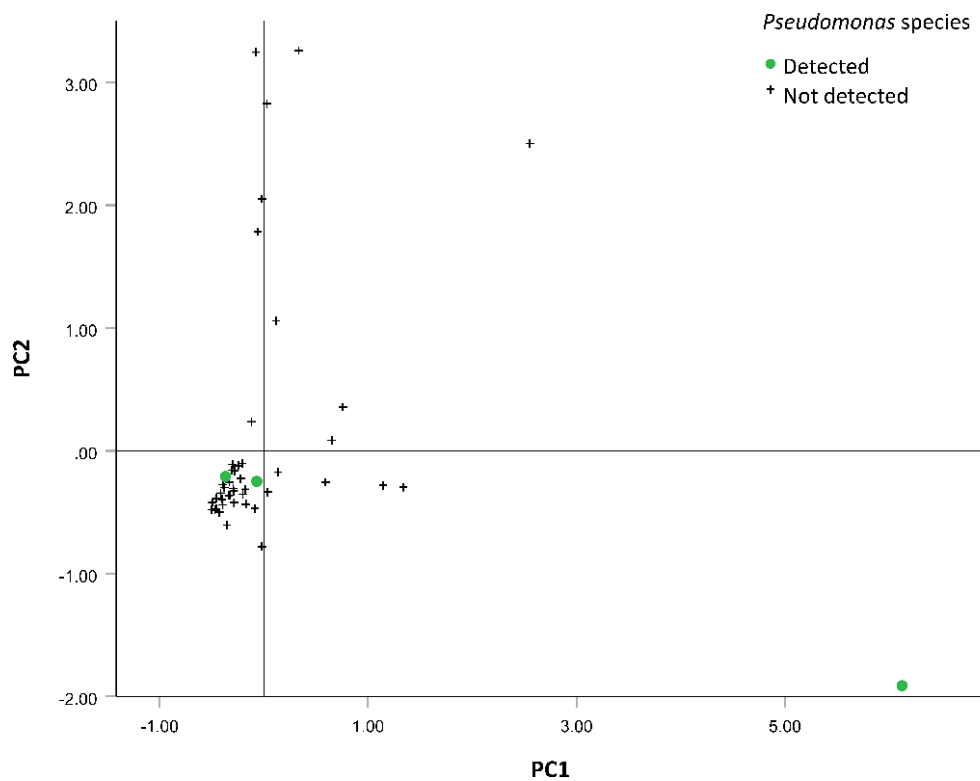


Figure 4.3: Plot of the scores of the first two principal components generated by principle component analysis of SIFT-MS full scan data of headspace volatiles product ion peaks of discarded patient dressing samples (n = 3 scans per sample). Principal component 1 (horizontal axis) accounts for 22.0% of the total variation in the original data set and principal component 2 (vertical axis) accounts for 14.0% of the total variation. Labelling highlights the location of dressings with a corresponding wound surface swab that detected the presence of *Pseudomonas* species.

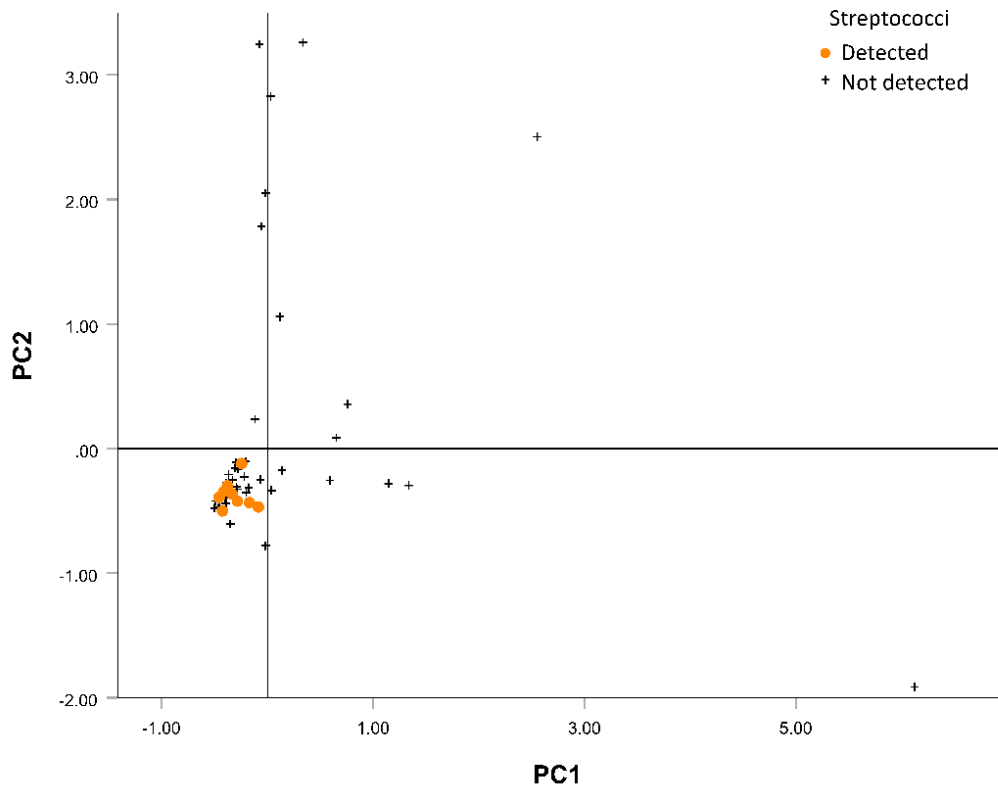


Figure 4.4: Plot of the scores of the first two principal components generated by principle component analysis of SIFT-MS full scan data of headspace volatiles product ion peaks of discarded patient dressing samples (n = 3 scans per sample). Principal component 1 (horizontal axis) accounts for 22.0% of the total variation in the original data set and principal component 2 (vertical axis) accounts for 14.0% of the total variation. Labelling highlights the location of dressings with a corresponding wound surface swab that detected the presence of Streptococci.

4.4 DISCUSSION

The main aim of this chapter was;

- To investigate if the concept of species discrimination based on volatile compound detection could be applied to analysis of discarded wound dressings, as part of routine wound care.

A range of volatile compound product ions from across the full mass spectral range analysed were detected from 87% of the dressing samples analysed, after background subtraction of the volatile profile detected from the corresponding sterile dressing control sample. Volatile profiles detected from the samples analysed by SIFT-MS, differed between patient dressings irrespective of the dressing type.

Hierarchical cluster analysis was used to group the dressing samples based on the profiles of volatile compound product ions detected from each sample. This analysis resulted in the generation of a dendrogram consisting of four main clusters (Figure 4.1). Comparison of these cluster groupings with the microbiological data obtained from routine wound surface swabbing does not reveal the identification of specific bacterial species within each of these groupings. *S. aureus* was cultured from all of the wound surface swabs corresponding to the samples within the bottom cluster (highlighted in orange), but was also cultured from swabs corresponding to some of the samples in each of the other cluster groupings. Therefore, it is possible that *S. aureus* was the infecting organism in the orange group of samples, but was not responsible for infection when detected within the other groups. However, the data collected here is inconclusive.

These observations are reinforced by the PCA plots shown in Figures 4.2, 4.3 and 4.4 where there is only one main cluster of dressing samples based on SIFT-MS analysis of volatile product ions from the discarded dressing headspace. These plots show that when comparing microbiological analysis of routine wound surface swabs with the distribution of samples based on this headspace analysis, the samples do not form discreet groupings associated with the bacterial species isolated from the corresponding wound surface swabs.

The use of swabbing for the identification of the causative organism of wound infection has an important limitation; the technique only samples organisms that are present on the surface of the wound (Cooper and Lawrence, 1996; Halstead *et al.*, 2018). Quantitative biopsy of the wound bed is a superior method for the identification of bacteria in a wound, but this technique is not routinely used within clinical practice because specialist training is required and it is invasive and painful (Sjöberg *et al.*, 2003; Uppal *et al.*, 2007; Haalboom *et al.*, 2019). In addition, the results obtained from the microbiological analysis of the wound surface swabs are qualitative only, and give no indication of the relative abundance of each of the organisms detected or the overall bioburden of the wound. It is likely that in addition to volatile compounds derived from bacteria present within the wound, the dressing material may have also captured volatile compounds emanating from the host and surrounding skin flora.

A recent study used SPME-GC-MS to capture and analyse volatile compounds from the enclosed headspace of healthy skin on the forearm of seven participants (Duffy *et al.*, 2017). The study identified 37 volatile compounds, 14 of which were common

to all seven participants, clearly demonstrating the diversity of volatiles detected from healthy human skin. Furthermore, the study found that damaging the integrity of the skin barrier, by repeated tape stripping of the stratum corneum, affected the volatile profiles detected (Duffy *et al.*, 2017). Hence, it is possible that the differences seen in the volatile profiles detected from patients discarded wound dressings reported in this chapter, could be the result of natural patient variability coupled with differences in wound health. Due to the difficulties associated with the identification of infection, it is possible that some patients' wounds were uninfected, despite infection being suspected at the time of recruitment to the study.

In future, a comparison of volatile compounds detected from clinically infected versus clinically uninfected wounds, may facilitate identification of volatile compounds that indicate the infection status of the wound. In addition, parallel analysis of wounded and healthy skin on a larger cohort of patients may be valuable, to gain a clearer understanding of the effect of different wound types, as well as infection status on the profile of volatiles emitted from the skin.

During this study, the sample dressing material was removed from the patient during routine care and would otherwise have been discarded. This approach facilitated relative ease of obtaining such samples and enabled an entirely non-invasive process of collecting samples for this proof-of-concept study. In future studies, it would be advantageous to identify and validate a reliable method for the collection and analysis of volatile compounds directly from wounded skin, as use of dressing material, which is not optimised for the capture of volatile compounds, is likely to have resulted in the loss of information within this study. A previous study has

identified volatile compounds from healthy human skin, using SIFT-MS connected to Nalophan tubing placed over the entire arm to collect skin volatiles directly from volunteers (Turner *et al.*, 2008). Such an approach may also provide a suitable method for direct collection of volatiles from skin wounds. However, it may not be practical to transport and locate a SIFT-MS instrument within a clinical environment, so use of a purpose designed material to trap and transport wound volatile compounds for off-site analysis may provide a more suitable approach.

The results of this proof-of-concept study demonstrate that it is possible to detect volatile compounds from discarded wound dressings. This suggests in future, it may be appropriate to implement volatile analysis in the clinic through the assessment of dressing material during routine wound care. It may also prove possible to routinely monitor wound infection with the dressing *in situ*.

However, the data collected within this study, does not provide any specific insight in to the links between detected volatile profiles in the wound dressing and the bacteria present on the wound surface. This study does serve to highlight the potential challenges of validating a novel approach to wound diagnostics, due to the current difficulty in definitively diagnosing wound infection and identifying the causative organism(s). Before further patient studies are undertaken it will be essential to further characterise the volatile profiles of wound associated bacterial species cultured under controlled conditions more representative of the real wound environment, this is the focus of Chapters 5 and 6.

Chapter 5: An *in vitro* collagen perfusion wound biofilm model

5.1 INTRODUCTION

In vitro studies of biofilms employ one of two approaches; a closed multi-well plate based model, or an open flow system with the continuous perfusion of nutrient into the model and waste products continuously exiting the system (Coenye and Nelis, 2010). Both of these approaches often involve the development of biofilms on solid surfaces, usually plastic or glass. Microbial infection *in vivo* consists of biofilm growth on the surface of, or suspended within, the semi-solid matrix of the tissue, unless adhered to an implanted medical device or catheter (James *et al.*, 2008). Collagen based gel matrices have been used as a substratum for culturing biofilms within closed systems *in vitro*, in an attempt to closely simulate the semi-solid nature of the wound (Werthén *et al.*, 2010; Brackman *et al.*, 2011; Hakonen *et al.*, 2014; Price *et al.*, 2016; Pompilio *et al.*, 2017). However, a limitation of these closed systems, is that they do not simulate the replacement of nutrients and moisture that occur within the wound bed due to the production of exudate, which provides the continuous flux of nutrients available to the biofilm during formation and growth (Thorn and Greenman, 2009; Rhoads, Wolcott and Percival, 2008).

To further assess the application of volatile analysis for the discrimination of wound associated bacteria, a wound biofilm model was required that combines the dynamic environment of a continuous flow biofilm model system with a semi-solid 'wound-like' growth substrate, thereby simulating more closely the wound environment. This

chapter details the development of an *in vitro* method for culturing wound associated microorganisms within a collagen wound biofilm model, combining a drip flow reactor system (Biosurface technologies, MZ, USA) with a three-dimensional type I collagen gel growth matrix and continuous perfusion of a simulated wound fluid (SWF) is described within this chapter. *Staphylococcus aureus*, *Pseudomonas aeruginosa* and beta-haemolytic streptococci are the main aerobic bacterial species thought to be responsible for delayed wound healing (Bowler, Duerden and Armstrong, 2001; Alrawi, Crowley and Pape, 2014; DiMuzio *et al.*, 2014). As such, characterisation of the collagen wound biofilm model focuses on cultivation of *P. aeruginosa*, *S. aureus* and *S. pyogenes* biofilms. The main aim of this chapter is to elucidate the growth characteristics of these three pathogenic bacterial species in the collagen wound biofilm model.

To demonstrate the application of this method, it has been utilized to study the antimicrobial kinetics of ceftazidime, when used to treat *P. aeruginosa* biofilms during early or late stage development. *P. aeruginosa* is among the most commonly isolated pathogens from both chronic and acute burn wound infections (Alrawi, Crowley and Pape, 2014; Branski *et al.*, 2009) and biofilms have been shown to rapidly result in systemic infection in a mouse model of acute burn infection (Schaber *et al.*, 2007). Ceftazidime is considered a first choice antipseudomonal antibiotic (Alou *et al.*, 2005; Aubert *et al.*, 2010) for treatment when there is a high risk of systemic infection developing from an infected wound.

To further demonstrate the potential of this novel model, a preliminary investigation of microbial metabolomics in relation to microbial biofilm development was

undertaken using selected ion flow tube mass spectrometry (SIFT-MS). Ammonia and hydrogen cyanide have previously been reported as important potential diagnostic metabolites detected in the headspace of *P. aeruginosa* liquid cultures *in vitro* (Neerinx *et al.*, 2015), and in *P. aeruginosa* infections *in vivo* (Gilchrist *et al.*, 2013; Smith *et al.*, 2013), through analysis of the exhaled breath of cystic fibrosis patients. Hydrogen cyanide was also identified from the Profile 3 SIFT-MS library as a possible compound responsible for the product ion at 28 m/z from the data presented in Chapter 3. Hydrogen cyanide is generated through decarboxylation of the amino acid glycine by the membrane bound hydrogen cyanide synthase enzyme (Blumer and Haas, 2000), ammonia is produced by the metabolism of nitrogen containing compounds including hydrogen cyanide (Neerinx *et al.*, 2015).

Real-time monitoring of bacterial volatile metabolites, has gained momentum in recent years as a potential rapid diagnostic tool (Spooner *et al.*, 2009; Storer *et al.*, 2011; Dummer *et al.*, 2013; Gilchrist *et al.*, 2013; Slade *et al.*, 2017; Lewis *et al.*, 2017; Greenman *et al.*, 2013; Ashrafi *et al.*, 2018). The novel collagen wound biofilm model reported here, allows the development of this diagnostic approach in the context of wound infection. For example by the detection of volatile metabolite profiles emitted by biofilm cultures, produced under conditions which closely simulate the wound environment. This chapter therefore addresses the third main research aim;

- To develop and characterise a suitable biofilm model for culture and headspace analysis of wound associated bacterial biofilms, that provides wound-like culture conditions.

A subset of the data presented in this chapter has been published in a peer reviewed journal (Slade *et al*, 2019), which is included in Appendix I.

5.2 METHODS SUMMARY

P. aeruginosa NCIMB 10548, *S. aureus* NCIMB 6571 and *Streptococcus pyogenes* NCTC 10881 were used for characterisation of the collagen wound biofilm model detailed in this chapter (see Section 2.2 for bacterial strain information).

5.2.1 *Biofilm Model*

Isolates of *P. aeruginosa*, *S. aureus* and *S. pyogenes* were used to prepare inoculum suspensions in SWF as described in Section 2.3. Bacterial suspensions (1mL) were used to inoculate collagen coated microscope slides, which were then incubated at 33°C for 2 hours to allow adherence of bacterial cells to the collagen growth matrix. Following the initial incubation, the inoculated slides were transferred to the biofilm reactor connected to the media reservoir and waste containers. The reactor was incubated for up to 72 hours at 33°C. A detailed description of the collagen wound biofilm model set-up can be found in Section 2.6.

5.2.2 *Enumeration of Bacterial Biofilms*

Bacterial biofilms were sampled at 0, 3 and 6 hours, then every 6 hours until 48 hours and finally at 72 hours. At each time point a slide was aseptically removed from the reactor and the entire collagen layer containing the bacterial biofilm scraped in to a 50 mL centrifuge tube. The collagen gel was digested using a collagenase solution. The resulting suspension was then disrupted by sonication in a water bath and washed two times in PBS to remove the collagenase solution as described in Section

2.6.3. The bacterial density of each biofilm was determined by spiral plating on to TSA plates as described in Section 2.4.2.

5.2.3 *Imaging of Bacterial Biofilms*

A coverslip was used to facilitate removal of a section of collagen gel for imaging experiments (see Section 2.7).

5.2.3.1 *Scanning Electron Microscopy (SEM)*

Biofilm samples were fixed, mounted and gold coated as described in Section 2.7.1 before being examined and imaged using a FEI Quanta 650 FEG scanning electron microscope operating at 10 kV.

5.2.3.2 *Confocal Scanning Laser Microscopy*

Biofilm samples were stained with the FilmTracer LIVE/DEAD Biofilm Viability Kit as described in Section 2.7.2 and imaged using a Leica DMI8 Inverted microscope with confocal scanner.

5.2.4 *Volatile Analysis*

Custom made (Biosurface Technologies Corporation, Bozeman, MT, USA) reactor channel lids, containing an additional sampling port were used to facilitate sampling of the volatile headspace of biofilm samples.

5.2.4.1 Selected Ion flow tube mass spectrometry

Throughout the 72 hour incubation, the headspace of biofilms cultured in the collagen wound biofilm model were analysed using SIFT-MS. The heated direct sample inlet of the Syft Voice200 Ultra instrument was connected to a sampling port in the lid of the sealed reactor channel via a length of PEEK tubing (45 cm x 1.59 mm x 0.762 mm; L x OD x ID). Biofilm sample headspace was analysed in SIM scan mode as described in Section 2.8.2.2, to quantify the headspace concentration of hydrogen cyanide and ammonia over 72 hours, with mean hourly concentration reported.

5.2.5 *Antimicrobial Susceptibility*

5.2.5.1 Broth microdilution

The antimicrobial susceptibility of *P. aeruginosa* NCIMB 10548 to ceftazidime was tested based on the broth microdilution method described by BS EN ISO 20776-1:2006 58 and detailed in Section 2.9.1.

5.2.5.2 Biofilms

Biofilm cultures of *P. aeruginosa* NCIMB 10548 were grown on collagen coated slides in the drip flow reactor system as described in section 2.6 and treated with ceftazidime. Treatment was started after either 6 hours or 30 hours of continuous culture as detailed in section 2.9.2.

5.2.6 *Data Analysis*

Biofilm enumeration data are presented as mean \pm standard deviation, n=3 independent biofilms per species per time point. Antibiotic susceptibility data was analysed by performing t-tests comparing specific time points of interest using Graphpad Prism 7 (GraphPad Software Inc., California, USA).

5.3 RESULTS

5.3.1 *Characterisation of Biofilm Growth in the Collagen Wound Biofilm Model*

The collagen wound biofilm model supports growth of reproducible *P. aeruginosa*, *S. aureus* and *S. pyogenes* biofilms. Figure 5.1 shows growth of biofilms over 72 hours at 33°C in the collagen wound biofilm model. A maximum biofilm density of 8×10^{10} cfu slide⁻¹ (dictated by the experimental conditions) was achieved by 30 hours of continuous culture for *P. aeruginosa*, and maintained at an approximately steady-state of $6 - 8 \times 10^{10}$ cfu slide⁻¹, from 30 hours until the end of experimentation (72 hours).

S. aureus is the only one of the three species that showed a lag phase when cultured in the collagen wound biofilm model, the biofilm density remaining stable at $5 - 6 \times 10^8$ cfu slide⁻¹ for the first 12 hours of continuous culture. The biofilm density then increased between 12 and 36 hours to an approximately steady state between 9×10^9 and 1×10^{10} cfu slide⁻¹ for the remaining duration of the experiment.

The density of *S. pyogenes* increased for the first 18 hours to reach a lower maximum density than the other two species at 3×10^9 cfu slide⁻¹, although it should be noted that the mean density at the start of continuous culture was also lower in *S. pyogenes* at 4×10^7 cfu slide⁻¹ compared to 3×10^8 and 4×10^8 cfu slide⁻¹ respectively for *P. aeruginosa* and *S. aureus*. However, the observed differences between the three species at the start of continuous culture, following 2 hours incubation to allow adherence of bacterial cells to the collagen growth matrix, were not statistically significant ($p > 0.05$). There are significant differences ($p < 0.01$) between the final

mean maximum biofilm density (i.e. at 72 hours) achieved for each species grown under these specific culture conditions.

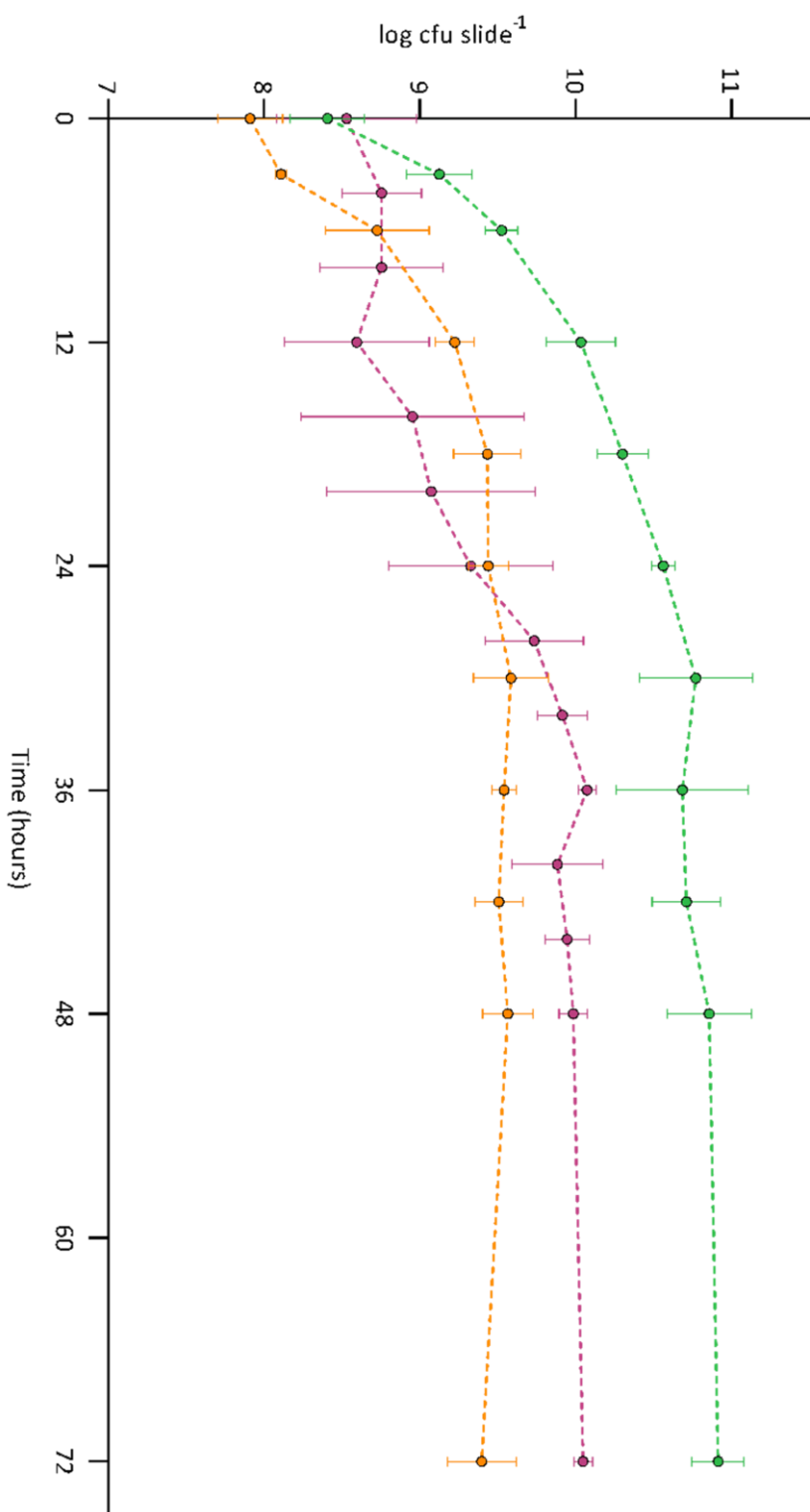


Figure 5.1: *Pseudomonas aeruginosa* (green), *Staphylococcus aureus* (pink) and *Streptococcus pyogenes* (orange) biofilm density when grown in the collagen wound biofilm model system over 72 hours at 33°C (n=3 per time point; mean ± SD).

5.3.1.1 Imaging of Collagen Gel Matrix and Bacterial Biofilms

The un-inoculated collagen growth matrix, which polymerizes at 37°C to form a hydrated three-dimensional semi-solid gel layer on the surface of the microscope slide coupons, was imaged using scanning electron microscopy. The fixation and dehydration process required for preparation of samples for SEM results in collapse of the three-dimensional structure, although the mesh-like network of long collagen fibres remains clearly visible as shown in Figure 5.2a.

Figure 5.2b shows SEM imaging of a *P. aeruginosa* biofilm cultured on the collagen gel growth matrix, which forms a dense layer of microbial cells masking the collagen fibres below. Multiple layers of *P. aeruginosa* are visible, as is the dehydrated biofilm extracellular polymeric substances (EPS) which can be seen connecting adjacent bacterial cells. Figure 5.2c shows that the *S. aureus* biofilm appears to form large three-dimensional aggregates of cells, with areas of un-colonised collagen fibres visible between the aggregates. Figure 5.2d show that *S. pyogenes* forms long chains of bacterial cells which have become tangled together and intertwined with the collagen fibres of the growth matrix.

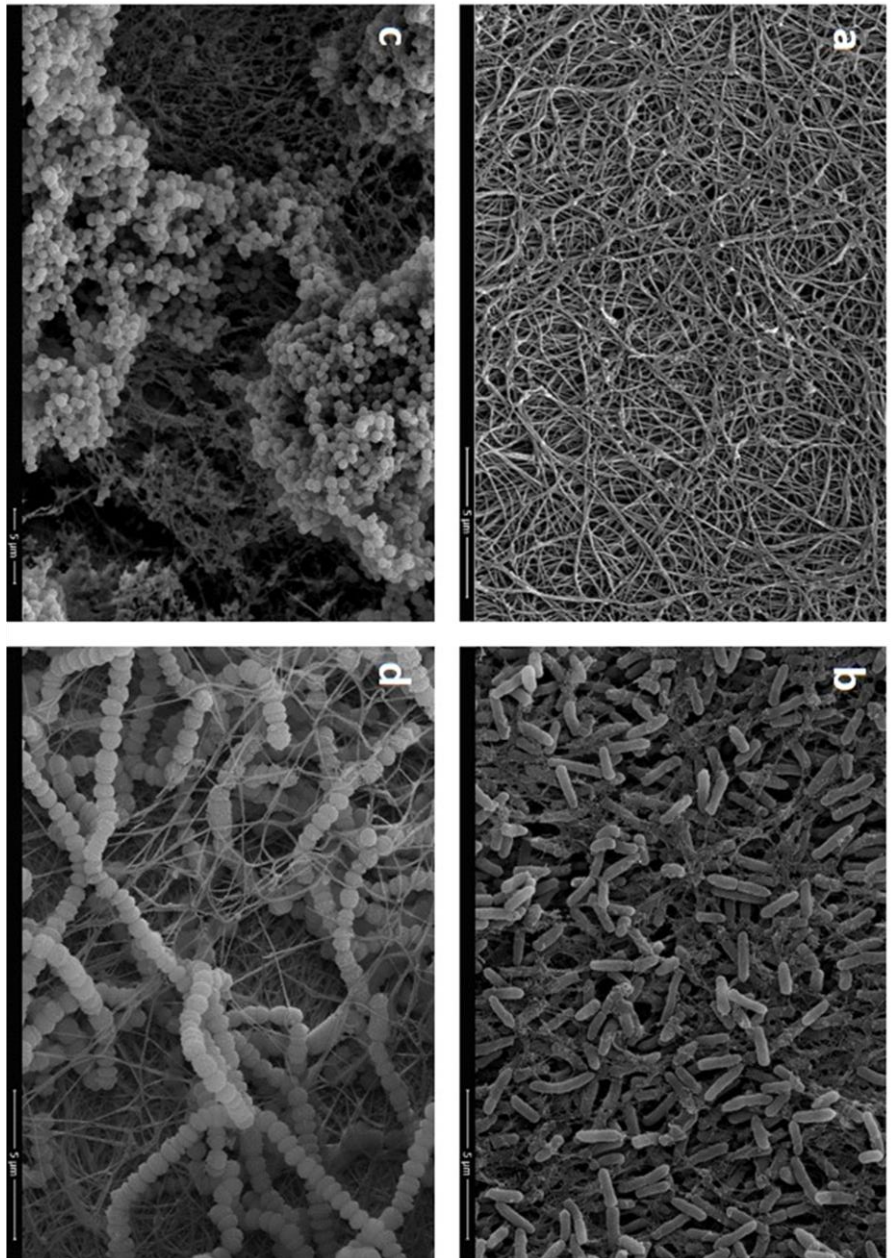


Figure 5.2: Scanning electron micrographs of a – collagen gel matrix, b – *Pseudomonas aeruginosa* biofilm, c – *Staphylococcus aureus* biofilm and d – *Streptococcus pyogenes* biofilms cultured within the collagen wound biofilm model. Imaged following fixation, dehydration and gold sputter coating with a FEI Quanta 650 FEG scanning electron microscope operating at 10 kV.

5.3.2 *Application of the Collagen Wound Biofilm Model for Studying Biofilm Volatile Metabolites*

Selected ion flow tube mass spectrometry (SIFT-MS) was used to quantify headspace concentration of hydrogen cyanide and ammonia in real-time, to demonstrate the capability of analysing volatile metabolites produced by developing biofilms in the collagen wound biofilm model. Biofilm headspace was repeatedly sampled and analysed using the SIFT-MS instrument throughout the 72 hour duration of biofilm growth and development.

Figures 5.3 and 5.4 show the concentration of hydrogen cyanide and ammonia detected in the headspace of *P. aeruginosa*, *S. aureus* and *S. pyogenes* biofilm cultures. The concentration of hydrogen cyanide (ppb) detected in the headspace of *P. aeruginosa* biofilms increased from zero to an initial peak with a mean concentration of 138 ppb at 12 hours and then then dropped to a mean concentration of 81 ppb at 18 hours before again increasing gradually to a peak of 191 ppb.

The concentration of ammonia also peaked with a mean concentration of 2273 ppb at 12 hours in the headspace of *P. aeruginosa* biofilms. For both *S. aureus* and *S. pyogenes* biofilms, the concentration of hydrogen cyanide remained at less than 10 ppb throughout the 72 hour duration of sampling. The concentration of ammonia remained at relatively low levels in the headspace of both *S. aureus* and *S. pyogenes* biofilms throughout the 72 hour sampling period, compared to *P. aeruginosa*, with maximum mean concentrations recorded of 458 ppb and 343 ppb respectively. From

6 hours onwards the concentration of hydrogen cyanide detected in the headspace of *P. aeruginosa* biofilms was significantly higher ($p < 0.05$) than in the headspace of both *S. aureus* and *S. pyogenes* biofilms. However, the concentration of ammonia in the headspace of *P. aeruginosa* biofilms was only significantly higher ($p < 0.05$) than *S. aureus* and *S. pyogenes* biofilms between 9 and 34 hours, with the exception of 4 time points (17, 20, 21 and 24 hours) where greater variability resulted in no significant difference between the headspace concentration of the three species.

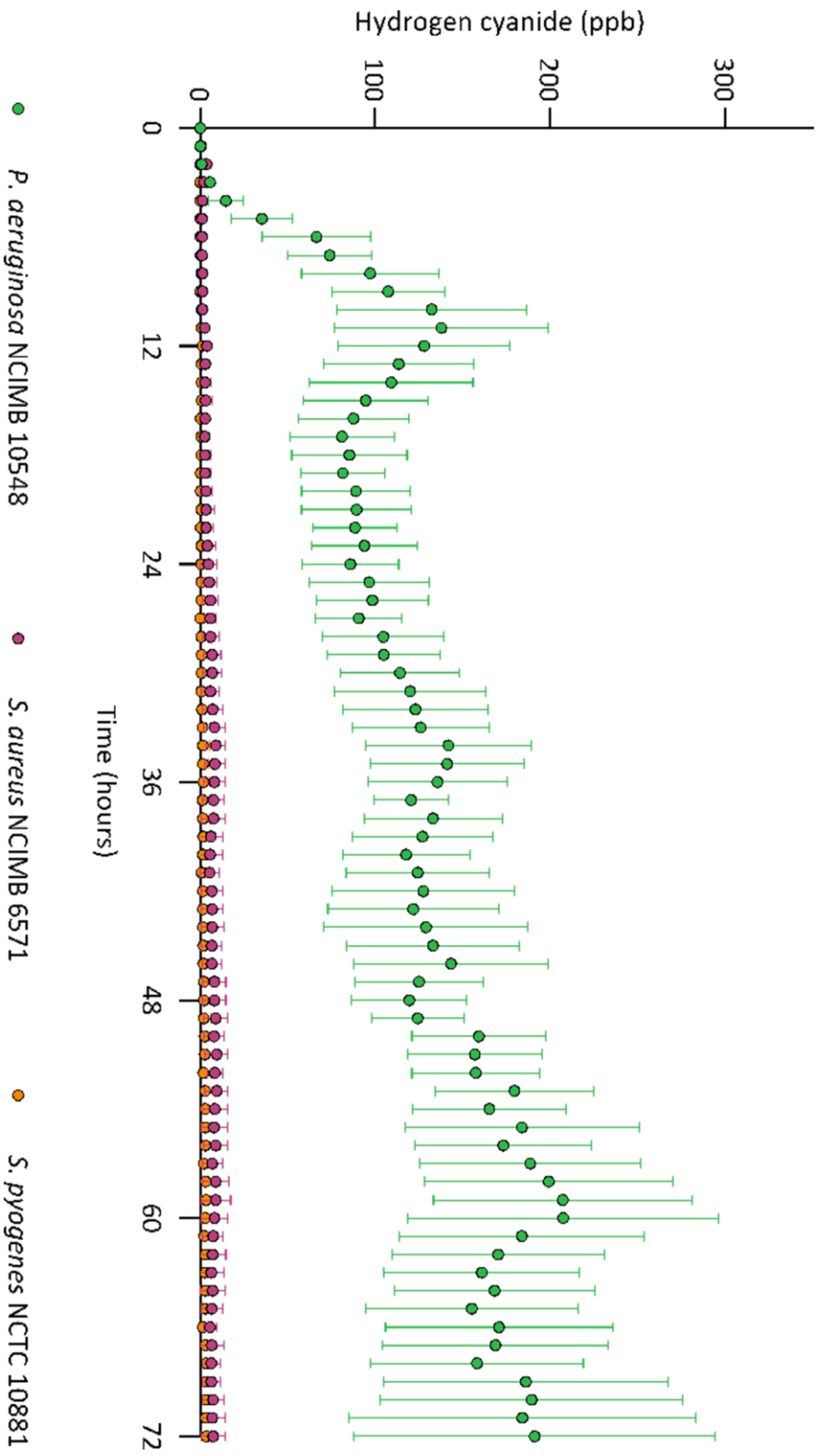


Figure 5.3: Detection of hydrogen cyanide during growth and development of *Pseudomonas aeruginosa* (Green), *Staphylococcus aureus* (Pink) and *Streptococcus pyogenes* (Orange) biofilms cultured in the collagen wound biofilm model. (n=4; mean \pm SD).

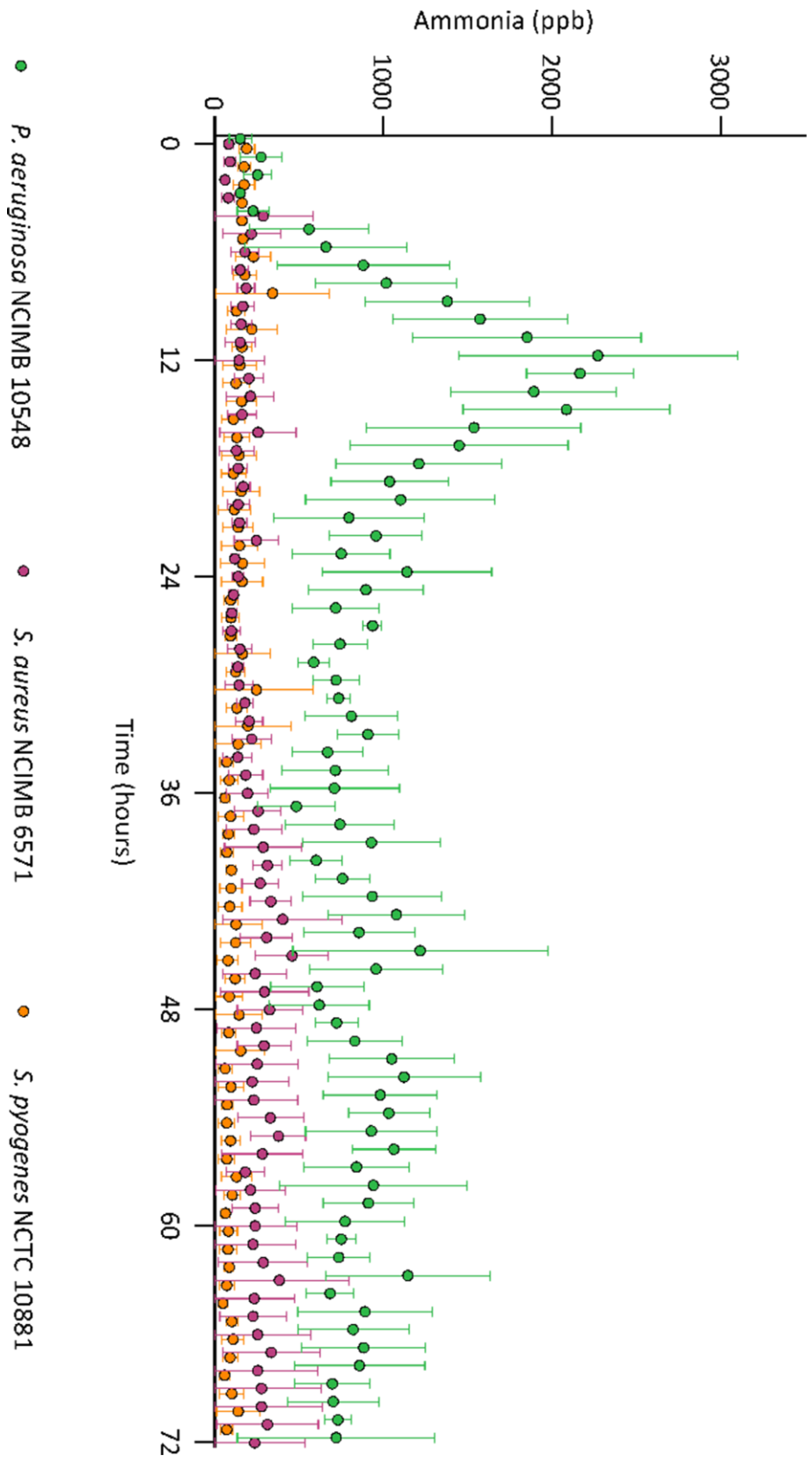


Figure 5.4: Detection of ammonia during growth and development of *Pseudomonas aeruginosa* (Green), *Staphylococcus aureus* (Pink) and *Streptococcus pyogenes* (Orange) biofilms cultured in the collagen wound biofilm model (n=4; mean \pm SD).

5.3.3 *Application of the Collagen Wound Biofilm Model for Studying Antimicrobial Kinetics*

To demonstrate the application of this model, the collagen wound biofilm model was used to investigate the antimicrobial activity of antibiotic therapy against biofilms at a clinically relevant dose. To confirm susceptibility of *P. aeruginosa* NCIMB 10548 to ceftazidime, planktonic minimum inhibitory concentration (MIC) values were determined (n=3) using a standard microdilution multi-well plate assay; the MIC was determined to be 2.0 mg L⁻¹. The clinical breakpoint for ceftazidime against *P. aeruginosa* according to the European Committee on Antimicrobial Susceptibility testing is 8 mg L⁻¹ (The European Committee on Antimicrobial Susceptibility Testing, 2018). Hence, the MIC of 2.0 mg L⁻¹, indicates that this strain is considered sensitive to ceftazidime.

Once susceptibility of the strain was confirmed the efficacy of ceftazidime against *P. aeruginosa* biofilms was investigated using the collagen wound biofilm model. A target serum concentration of 40 mg L⁻¹ for continuous infusion of ceftazidime is recommended for effective treatment of *P. aeruginosa* infections *in vivo* (Alou *et al*, 2005; Aubert *et al*, 2010; Buijk *et al*, 2002), hence this drug concentration was selected to challenge the *P. aeruginosa* biofilms in the collagen wound biofilm model.

Figure 5.5 shows the change in biofilm density resulting from ceftazidime treatment at 40 mg L⁻¹, compared to normal growth conditions. Treatment was started after either 6 hours or 30 hours of continuous culture, to enable comparison of treatment efficacy on the early stage of biofilm formation and on established steady state

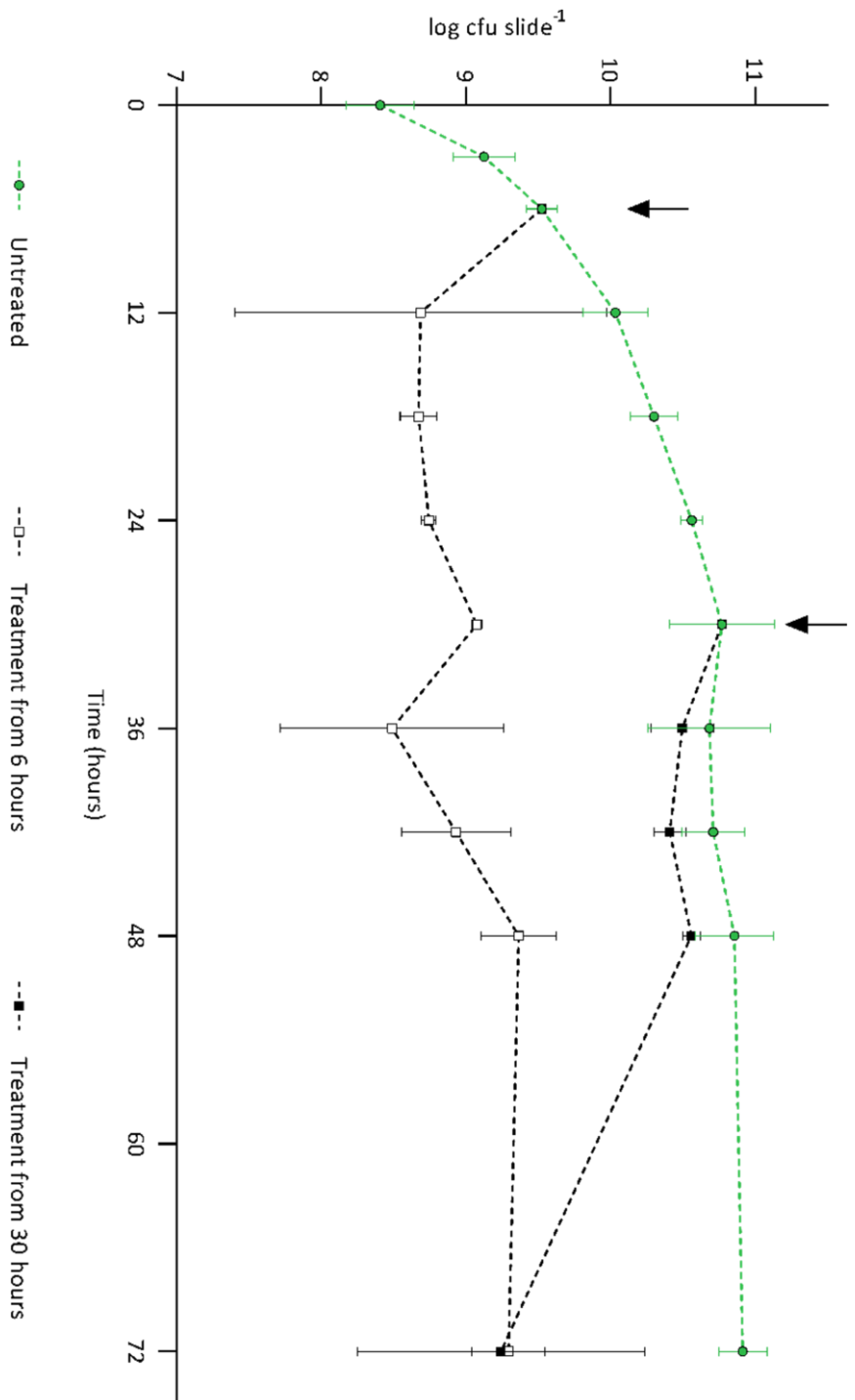


Figure 5.5: Treatment of *Pseudomonas aeruginosa* biofilms with ceftazidime at 40mg L⁻¹, showing antimicrobial kinetics when used against established maturing biofilms (Black Square, 30 hours) and early stage biofilms (White Square, 6 hours) cultured within the collagen wound biofilm model, compared to untreated controls (Green). (n=3 per time point per condition; mean ± SD). Arrows indicate treatment start times.

maturing *P. aeruginosa* biofilms.

When treatment was initiated at the early stage of biofilm formation, the total biofilm density decreased for the first 12 hours of treatment to approximately 5×10^8 cfu slide⁻¹ (1.63 log reduction compared to untreated controls; $p < 0.01$). The biofilm density remained stable at the subsequent sampling time, but increased over the following 24 hours to reach a density of 2×10^9 cfu slide⁻¹. This density was maintained until the final sampling time (72 hours of continuous culture) resulting in a significant 1.6 log reduction compared to untreated controls ($p < 0.05$) at the end of experimentation.

During treatment of established maturing biofilms, the biofilm density gradually decreased ultimately resulting in a mean biofilm density of 5.5×10^9 cfu slide⁻¹ at 72 hours (a significant 1.2 log reduction compared to the untreated control; $p < 0.05$). When comparing the antimicrobial efficacy of treatment initiated at the early stage of biofilm development or on established maturing biofilms, there was no significant difference in biofilm density between these treatment groups after 72 hours of continuous culture. In order to determine the effect of ceftazidime treatment on biofilm structure, both untreated and treated biofilms were sampled for confocal microscopy.

Figure 5.6 shows untreated *P. aeruginosa* biofilms sampled after 6, 12, 24 and 48 hours of continuous culture. The biofilm sampled at 6 hours consisted of sparsely arranged *P. aeruginosa* cells with some small aggregates (Figure 5.6a), whereas at 12 hours the cell density had increased and some larger aggregates were visible (Figure

5.6b). At 24 hours the density of the bacterial cells had again increased, in line with the enumeration data (Figure 5.1), whereby more complex structural formations and the development of surface protrusions and channels can be seen (Figure 5.6c). At 48 hours, the biofilm architecture within the maturing biofilm shows evidence of increased variability in surface topography, as described within other biofilm studies (Luján *et al.*, 2011; Klausen *et al.*, 2003; Ghafoor, Hay and Rehm, 2011).

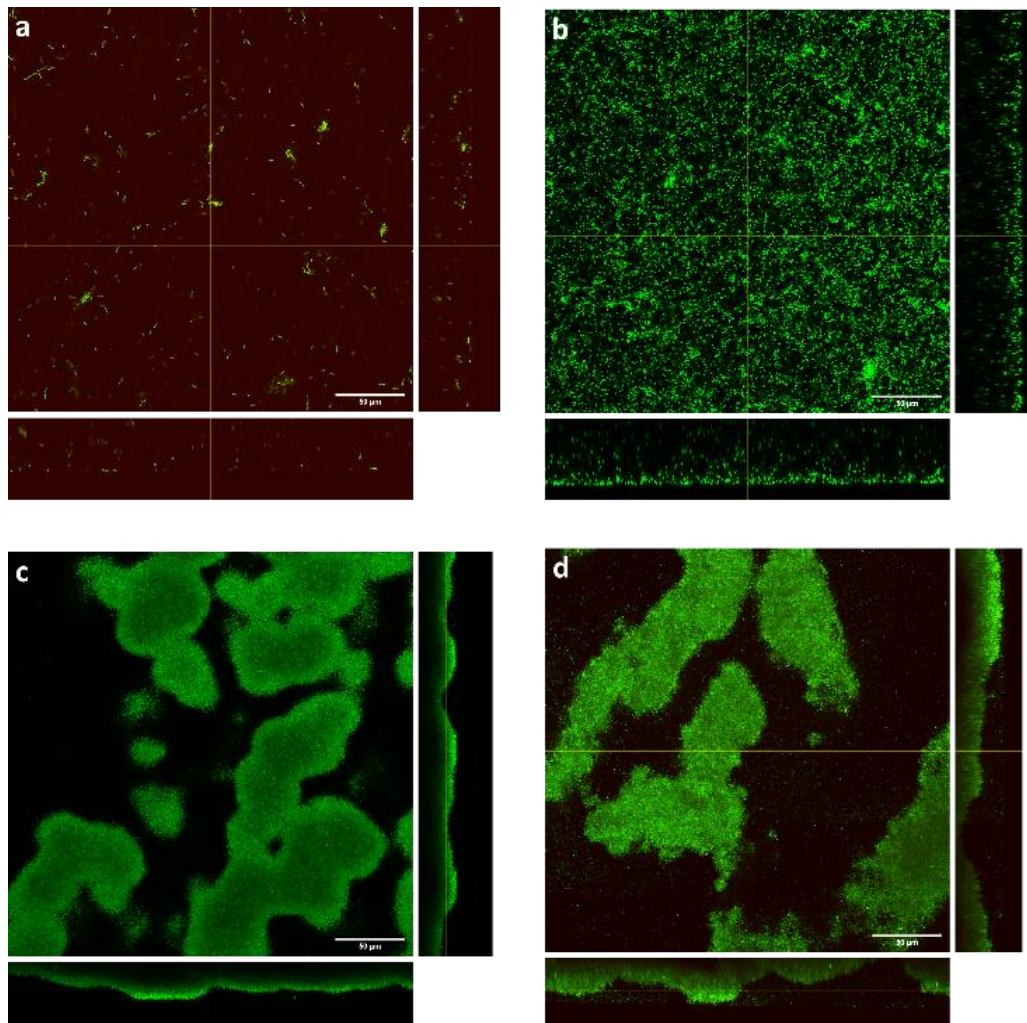


Figure 5.6: Confocal scanning laser micrographs of *Pseudomonas aeruginosa* biofilms grown in the collagen wound biofilm model. Sampled after (a) 6 hours, (b) 12 hours, (c) 24 hours and (d) 48 hours of continuous culture. Main panels show XY plane, right panels show YZ slice and bottom panels show XZ slice. Green Syto 9 staining indicates live bacterial cells and red propidium iodide staining indicates dead bacterial cells.

Figure 5.7 shows confocal scanning laser micrographs of *P. aeruginosa* biofilms treated with 40mg L⁻¹ ceftazidime. Samples for both treatment regimens were imaged after both 18 hours and 42 hours of exposure to the ceftazidime; this corresponds to a total culture time of 24 hours and 48 hours for the samples where antibiotic treatment was started at the early stage of biofilm formation, and 48 hours and 72 hours total culture time for the samples where treatment was started on established biofilms.

Samples imaged following 18 hour of exposure to ceftazidime at 40 mg L⁻¹ (Figure 5.7; a1 & b1) both show some elongation of *P. aeruginosa* cells. Within the confocal z-stack, it was observed that this was most pronounced in the bacterial cells nearest to the surface of the biofilms, whereas cells deeper within the biofilm were morphologically more similar to the untreated samples (Figure 5.6). After 42 hours of antibiotic exposure, it was observed that there was a high proportion of elongated bacterial cells (Figure 5.7; a2 & b2). The biofilm appears less densely packed with clear spaces between the tangles of filamentous cells, compared to untreated biofilms shown in Figure 5.6.

By comparing untreated (Figure 5.6c) and treatment of early stage biofilms (Figure 5.7; a1 and a2) it is clear that the ceftazidime treatment prevents the development of complex biofilm architecture. In addition, when comparing untreated (Figure 5.6d) and the treatment of established biofilms (Figure 5.7; b1), it is evident that ceftazidime treatment has resulted in the collapse of the characteristic three-dimensional biofilm structure. This demonstrates the effect of ceftazidime on the complex biofilm structure, as well as the morphology of individual bacterial cells.

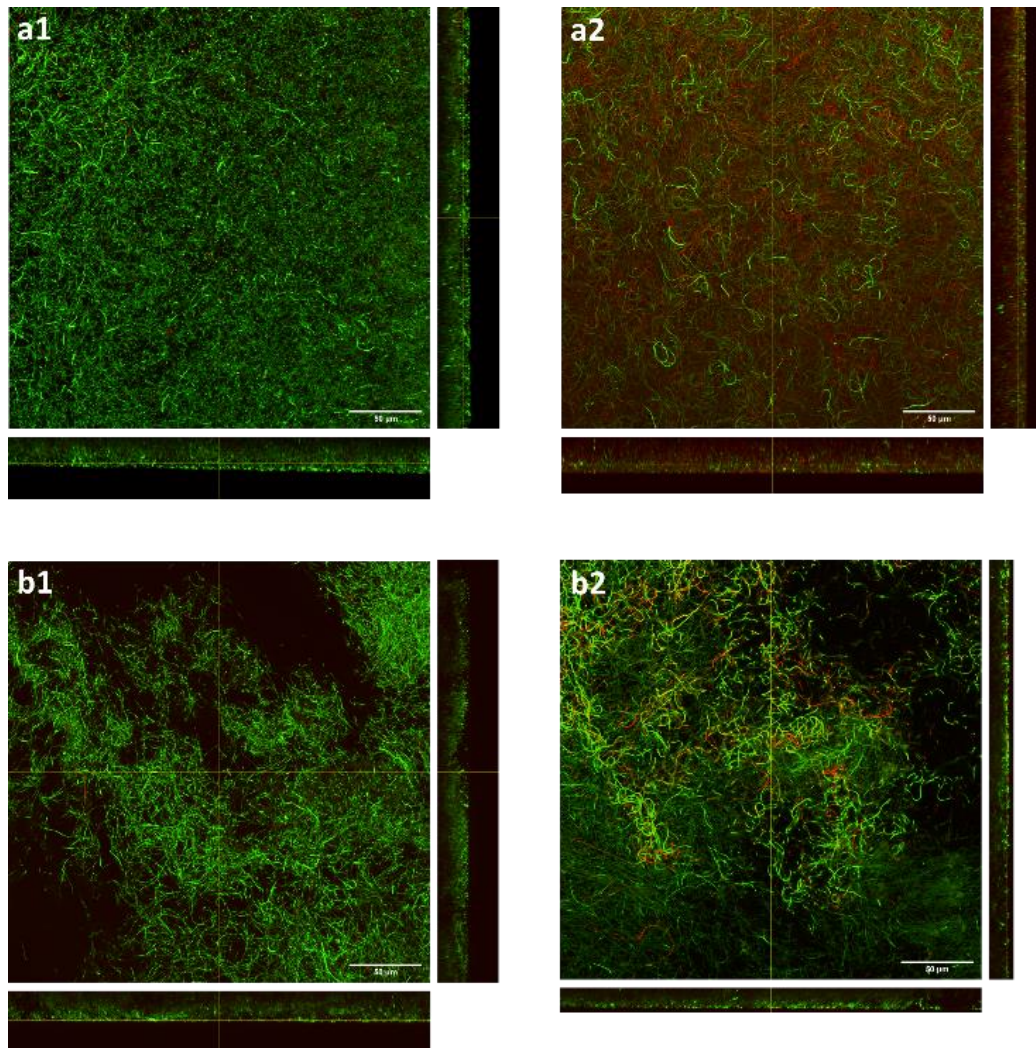


Figure 5.7: Confocal scanning laser micrographs of *Pseudomonas aeruginosa* biofilms treated with ceftazidime at 40 mg L^{-1} . Top panels, treatment initiated at 6 hours (early stage of biofilm formation); (a1) sample imaged following 18 hours exposure to treatment and (a2) 42 hours exposure to treatment. Bottom panels, treatment initiated at 30 hours (maturing biofilm); (b1) biofilm sampled following 18 hours exposure to treatment (48 hours) and (b2) 42 hours exposure to treatment. Main panels show XY plane, right panels show YZ slice and bottom panels show XZ slice. Green Syto 9 staining indicates live bacterial cells and red propidium iodide staining indicates dead bacterial cells.

5.4 DISCUSSION

The main aim of this chapter was;

- To develop and characterise a suitable biofilm model for culture and headspace analysis of wound associated bacterial biofilms, that provides wound-like culture conditions.

The dermis of human skin is primarily composed of the protein collagen (Church *et al*, 2006). Type I collagen is the most abundant type found in human skin and is distributed throughout all layers of the dermis (Meigel, Gay and Weber, 1977). This chapter demonstrated the successful development of a dynamic collagen wound biofilm model utilising a three-dimensional collagen gel growth matrix comprised of a mesh of polymerized type I collagen fibres (Figure 5.2a), to simulate the semi-solid wound environment found *in vivo*.

Continuous perfusion with SWF provides replacement of moisture and nutrients, and removal of waste products, that would be provided by the flow of exudate within infected wounds (Vuolo, 2004). The simulated wound fluid provides a similar range of nutrients as exudate, a high protein fluid that leaks from the blood vessels in response to inflammation associated with wound healing processes (Cutting and White, 2002). Biochemical analysis of wound fluid has shown that a similar range of constituents are present when compared to serum, with concentrations in wound fluid at lower levels than in serum for the majority of components (Trengove, Langton and Stacey, 1996). This suggests use of a simulated wound fluid comprised

of 50 % serum will provide a suitable range of nutrients, many of which will be at biologically relevant concentrations.

The growth of *P. aeruginosa*, *S. aureus* and *Streptococcus pyogenes* biofilms has been validated within this biofilm model system producing reproducible steady state biofilms at a density greater than that considered to be the critical threshold of clinically relevant wound infection. A density of 10^5 cfu g⁻¹ tissue is considered the critical threshold indicative of clinically relevant wound infection (Bowler, Duerden and Armstrong, 2001; Sjöberg *et al*, 2003; Uppal *et al.*, 2007), with a bioburden of between 10^9 and 10^{11} cfu g⁻¹ tissue identified from infected wounds with the heaviest bacterial loads (Levine *et al.*, 1976; Sjöberg *et al.*, 2003). Hence, the density achieved within the collagen wound biofilm model represents an appropriate bacterial load, reflective of a challenging clinical situation for assessing antimicrobial efficacy. The final biofilm density varied between the species utilised for characterisation of this model. However, differences in biofilm forming ability, not only between bacterial species but also between strains of the same species have been reported previously (Hou *et al.*, 2012; Lajhar, Brownlie and Barlow, 2018).

Within the collagen wound biofilm model, the biofilm density after 72 hours of continuous culture was greatest in *P. aeruginosa* biofilms (8×10^{10} cfu slide⁻¹). *S. aureus* biofilms achieved a final density (1×10^{10} cfu slide⁻¹) less than that of *P. aeruginosa* but greater than *S. pyogenes*, which had the lowest final biofilm density (3×10^9 cfu slide⁻¹) of these three species cultured within the collagen wound biofilm model.

The collagen wound biofilm model enabled investigation of microbial volatile metabolites produced by bacterial species associated with causing clinically relevant wound infection. SIFT-MS was used for real-time detection of hydrogen cyanide and ammonia in the collagen wound biofilm model. Monitoring of volatile compounds during biofilm growth and development from a perfusion biofilm model has not been reported previously. In the collagen wound biofilm model, the concentration of hydrogen cyanide increased for approximately the first 12 hours in the headspace of *P. aeruginosa* biofilms, corresponding to the most rapid increase in biofilm density. The concentration then decreased over the subsequent 6 to 12 hours. Investigations of real-time production of hydrogen cyanide from reference strains and clinical isolates of *P. aeruginosa* in liquid culture indicated a peak in hydrogen cyanide concentration at the transition to stationary phase only (Neerincx *et al.*, 2015). Interestingly the drop in concentration of this volatile compound between 12 and 24 hours corresponds with distinct changes in the arrangement of bacterial cells and development of biofilm structures observed by confocal microscopy (Figure 5.5), as well as a decrease in the rate at which the biofilm density was increasing. When the *P. aeruginosa* biofilm density had stabilized within the collagen wound biofilm model (≥ 30 hours) the concentration of hydrogen cyanide continued to increase gradually throughout the remaining analysis time. Again, this is in contrast to that reportedly seen in planktonic culture (Neerincx *et al.*, 2015), whereby production of HCN was maintained for only 1 to 4 hours after the initial peak. These differences may result from changes in the metabolic activity associated with the biofilm mode of growth, coupled with the continuous supply of substrates for metabolism and removal of

waste products within the model, which is more representative of the *in vivo* environment.

In contrast to the headspace of *P. aeruginosa* biofilms, the headspace concentration of hydrogen cyanide from *S. aureus* and *S. pyogenes* cultures remained below 10 ppb for the entire 72 hour sampling period. Monitoring hydrogen cyanide production within this model system demonstrates the feasibility of sampling the headspace of developing biofilms and shows that differences between species can be detected from an early stage of biofilm development (6 hours) and throughout growth and maturation. However, the concentration of ammonia was only significantly higher in the headspace of *P. aeruginosa* biofilms than that of *S. aureus* and *P. aeruginosa* for a portion of the 72 hour analysis, indicating that this compound may be less useful than hydrogen cyanide for discrimination between these species.

MIC assays are routinely used clinically to determine the susceptibility of bacterial isolates to the antibiotic treatments available. However, as demonstrated within this study, this is unlikely to predict the effectiveness of antimicrobials against biofilms and hence their therapeutic effectiveness against biofilm infections. To demonstrate the application of this model system for evaluating the efficacy and kill kinetics of antimicrobial agents, both developing and established *P. aeruginosa* biofilms were challenged with the cephalosporin antibiotic ceftazidime.

There was no significant difference ($p > 0.05$) in the final biofilm density after 72 hours of continuous culture, when comparing the two treatment start times. Both treatment strategies resulted in a significant reduction of total biofilm density at 72

hours compared to the untreated biofilm. Although a statistically significant reduction in viable *P. aeruginosa* biofilm density was demonstrated, the remaining mean biofilm density of 2.2×10^9 and 5.5×10^9 cfu slide⁻¹ for the two treatment regimens equates to 1.5×10^9 and 3.6×10^9 cfu g⁻¹ of collagen 'tissue' respectively. This density remains vastly in excess of the 10^5 cfu g⁻¹ of 'tissue', used as the critical threshold indicative of invasive infection and risk of sepsis in studies of quantitative microbiological analysis of wound biopsy samples (Sjöberg *et al*, 2003; Uppal *et al*, 2007).

It has previously been reported that there are differences between the planktonic MIC and the concentration of ceftazidime (and a range of other antimicrobials) required to eradicate biofilms, with concentrations 1000-fold greater than the MIC unable to eradicate *P. aeruginosa* biofilms within a static model (Ceri *et al.*, 1999). Using the collagen wound biofilm model, the time course of the development of such tolerance has been demonstrated for the first time under wound like conditions *in vitro*, and the effect of drug treatment on the biofilm structure visualized.

Ceftazidime treatment resulted in distinct morphological changes in the general biofilm architecture as well as the discrete bacterial cells. This elongation response by *P. aeruginosa* to β -lactam antibiotics, including ceftazidime, has been described previously and was observed to result in cell lysis and a reduction in viable cells in planktonic culture (Elliott and Greenwood, 1984). It has been determined that inhibition of penicillin binding protein 3 (PBP3) by β -lactam antibiotics is responsible for causing filamentation in *P. aeruginosa*. This has been demonstrated by deletion of the gene required for PBP3 expression and comparison of the resulting

morphological changes to those seen when *P. aeruginosa* was exposed to sub-lethal concentrations of β -lactam antibiotics (Chen, Zhang and Davies, 2017). This phenomena has also been observed in response to β -lactam exposure in *Escherichia coli* (Yao, Kahne and Kishony, 2012), where cell elongation is reported to be the first of a four step process leading to eventual cell lysis.

In conclusion, the collagen wound biofilm model has been successfully developed and evaluated for the growth of steady-state biofilms under wound like conditions. The potential of the collagen wound biofilm model for use in studies of volatile metabolites has been demonstrated, by characterising hydrogen cyanide and ammonia production from *P. aeruginosa*, a clinically relevant pathogen associated with wound infection, while demonstrating absence of production of these metabolites from other pathogenic species. Furthermore, the collagen wound biofilm model demonstrates the failure of biofilm eradication using a clinically relevant ceftazidime concentration, and also allows the evaluation of antimicrobial kinetics, clearly demonstrating the development of tolerance in the *P. aeruginosa* biofilm cultures during treatment of biofilms at both early and late stage development.

Application of the collagen wound biofilm model for the study of volatile metabolites produced by these wound associated bacterial species facilitated further progression of the work described in Chapter 3, by allowing investigation of volatile profiles from these species when cultured under wound like biofilm growth conditions, which is the focus of Chapter 6.

Chapter 6: *In vitro* discrimination of wound associated bacterial biofilms

6.1 INTRODUCTION

The use of volatile metabolite detection employing a range of analytical techniques to discriminate between species of planktonic bacteria *in vitro*, has been demonstrated in the literature (Scotter *et al.*, 2006; Storer *et al.*, 2011; Thorn, Reynolds and Greenman, 2011; Dolch *et al.*, 2012a; Nizio *et al.*, 2016). The data presented in Chapter 3 clearly demonstrates that discrimination of pathogenic species associated with wound infection is achievable through the detection of volatile metabolites produced when these organisms are cultured in liquid media. However, wound infection *in vivo* consists of biofilm growth on the surface of, or suspended within the wound tissue rather than as free swimming planktonic cells (James *et al.*, 2008).

The work described in this Chapter focuses on applying SIFT-MS coupled with multivariate data analysis for the detection and discrimination of bacterial biofilms cultured in the collagen wound biofilm model developed and described in chapter 5. This study uses both SIFT-MS modes, full scans (FS) to generate a full spectrum of volatile compound product ion peaks, as well as selected ion mode (SIM) to quantify specific bacterial volatile compounds following identification using GC-MS. Multiple approaches to statistical analysis of the resultant data sets are explored to determine an effective process for identification of discriminant product ions or compounds.

This chapter addresses the final two main research aims;

- To investigate the volatile profiles of biofilm cultures of wound associated bacteria *in vitro* that can be used for the discrimination between species.
- To investigate the effect of multispecies biofilms on bacterial volatile profiles *in vitro*.

6.2 METHODS SUMMARY

The following bacterial strains were used during this study; *Pseudomonas aeruginosa* NCIMB 10548, NCIMB 8295 and ATCC 15442, *Staphylococcus aureus* NCIMB 6571, ATCC 6538 and a clinical strain of methicillin resistant *S. aureus* obtained from the UAE culture collection, and *Streptococcus pyogenes* NCTC 10881, NCTC 10874 and NCTC 10871 (see Section 2.2 for bacterial strain information).

6.2.1 *Biofilm Model*

Isolates of *P. aeruginosa*, *S. aureus* and *S. pyogenes* were used to prepare inoculum suspensions in SWF as described in Section 2.3. These suspensions were used to inoculate collagen coated microscope slides, which were then incubated at 33°C for 2 hours to allow adherence of bacterial cells to the collagen growth matrix. Following the initial incubation, the inoculated slides were transferred to the biofilm reactor. Tubing to the media reservoir and waste containers was connected to the reactor, and the reactor incubated for 48 hours at 33°C. A detailed description of the collagen wound biofilm model can be found in Section 2.6.

6.2.1.1 Multispecies biofilms

When inoculating the collagen wound biofilm model for the culture of multispecies biofilms, initial inoculum suspensions containing *S. aureus* NCIMB 6571, *S. pyogenes* NCTC 10881 or a mixture of both organisms was prepared as described in Section 2.3. One mL of the inoculum suspension was used to inoculate collagen coated

microscope slides, which were then incubated at 33°C for 2 hours. Following incubation, the slides were transferred to the reactor channels and the reactor set up with continuous perfusion of simulated wound fluid, as previously described in Section 2.6.

For the culture of multispecies biofilms containing *P. aeruginosa*; after 18 hours of incubation at 33°C, the flow of nutrient media was halted and the reactor moved from a 10° angle to a flat surface. Inoculum suspensions of *P. aeruginosa* NCIMB 10548 were prepared in SWF as described in Section 2.3. The developing biofilms were then inoculated with one millilitre of *P. aeruginosa* inoculum suspension. The reactor was incubated in a flat position at 33°C for 1 hour, before perfusion of SWF at a 10° angle was resumed. As the flow of media was resumed, the reactor channels were briefly purged with SWF at the maximum pump speed (8.5 mL min⁻¹) to remove any planktonic cells, before normal perfusion rates were resumed for a further 29 hours, incubated at 33°C (48 hours in total).

6.2.2 *Volatile Analysis*

To facilitate sampling of the volatile headspace of the cultured biofilms, modified lids custom made (Biosurface Technologies Corporation, Bozeman, MT, USA) to contain an additional sampling port were used during the experiments described in this chapter.

6.2.2.1 Selected Ion Flow Tube – Mass Spectrometry (SIFT-MS)

Following incubation for a total of 48 hours, the headspace of biofilms cultured in the collagen wound biofilm model were analysed using SIFT-MS. The heated direct sample inlet of the Syft Voice200 Ultra instrument was connected to a sampling port in the lid of the sealed reactor channel via a length of PEEK tubing (45 cm x 1.59 mm x 0.762 mm; L x OD x ID).

Biofilm sample headspace was analysed in FS mode as described in section 2.8.2.1, to generate a profile of volatile compound product ion peaks. The headspace of each independent biofilm was analysed with three replicate scans across a spectrum range of 10 – 200 m/z. In addition, following gas chromatography mass spectrometry (GC-MS) to identify volatile compounds within the biofilm headspace (described in 6.2.2.2), biofilm sample headspace was analysed using the Syft Voice200 Ultra SIFT-MS instrument SIM scans to quantify the headspace concentration of 19 volatile compounds. The headspace of each independent biofilm was analysed for 60 seconds in SIM mode, resulting in 12 replicate measurements for each volatile compound (see Section 2.8.2.2).

6.2.2.2 Gas Chromatography – Mass Spectrometry

Following 48 hours of culture in the collagen wound biofilm model, the headspace of single species biofilm cultures were sampled on to solid phase micro extraction (SPME) fibres and analysed using an Agilent technologies GC-MS instrument (see Section 2.8.3). The biofilm headspace was sampled for 30 minutes, by inserting the

SPME fibre assembly through the sampling port in the lid of the sealed biofilm reactor channel. A detailed description of the procedure and instrument parameters can be found in Section 2.8.3.

6.2.3 *Enumeration of Multispecies Biofilms*

Following volatile analysis by SIFT-MS multispecies biofilms were aseptically removed from the biofilm reactor, the entire collagen layer scraped in to a falcon tube and then collagen gel digested using a collagenase solution. The resulting suspension was disrupted by sonication in a water bath and washed two times in PBS to remove the collagenase solution as described in Section 2.6.3. The bacterial density of each species within the resulting suspension was determined by spiral plating on to agar plates for selective enumeration as described in Section 2.4.2. The selective culture media used are detailed in Section 2.1.

6.2.4 *Data Analysis*

6.2.4.1 Comparing Mean Values

In the first instance, data processing was based on the procedure used for the analysis of planktonic culture headspace data (section 3.2.1). The mean count rates ($n=3$) of the full scan data were calculated for each mass-to-charge (m/z) product ion across the spectrum range (10-200 m/z) for each bacterial strain. T-tests were performed to compare the count rate detected from the biofilm headspace with uninoculated controls. Only product ions detected at a significant level ($p>0.05$) in

the biofilm headspace compared to the background level detected from uninoculated controls (n=9) were selected for further analysis. The mean count rate from the uninoculated controls was then subtracted from the count rate from the bacterial biofilm headspace samples for each corresponding product ion, to determine the volatile compound product ion count rate attributed to production of volatile compounds by the biofilm culture alone. Reagent ion peaks and any negative values, indicating a reduction in count rate below that of the uninoculated controls, were disregarded.

A threshold was applied to facilitate the identification of discriminant volatile compound product ions, as discussed in Section 3.2.3, whereby a minimum signal of 10 cps was required in at least two of the three strains analysed for each species in order for each product ion to be included for further analysis.

A similar process was followed for the analysis of selected ion mode (SIM) data whereby the mean concentration (ppb) for each bacterial strain (n=3) was calculated for each volatile compound quantified by SIFT-MS. The mean concentration detected in the headspace of uninoculated controls (n=9) was then subtracted, to calculate the mean compound concentration produced by each bacterial strain analysed.

6.2.4.2 Multivariate Analysis of Variance (MANOVA)

As an alternative to processing the data sets as described above, the mean product ion intensity or compound concentration was calculated for each independent biofilm from multiple replicate scans; for FS the mean was calculated from 3 replicate

scans across the spectrum range of 10-200 m/z and for SIM scans from 12 replicate measurements for each volatile compound.

Multivariate analysis of variance (MANOVA) was utilised to compare product ion intensity (cps) or compound concentration (ppb) between species. Product ions or volatile compounds that were identified by MANOVA as having a high level of statistically significant difference in intensity or concentration between bacterial species ($p < 0.01$) were selected as potentially discriminant variables. These variables were then carried forward for further analysis by hierarchical cluster analysis and principal component analysis as described below in Section 6.2.4.3.

6.2.4.3 *Multivariate Statistical Analysis*

Following selection of potential discriminatory product ions or compounds, hierarchical cluster analysis was applied to the selected data set, whereby a statistical algorithm creates a matrix of measures (squared Euclidean distance) of dissimilarity between each of the cases (bacterial strains). The dissimilarity matrix is then used to produce a dendrogram, the branching of which indicates the distance and therefore the dissimilarity between the clusters.

Both the FS and SIM scan data sets were also transformed using Principal Components Analysis (PCA), visualised by plotting the resulting scores in a scatter plot. The PCA loading scores for each of the original variables (m/z or volatile compound) were plotted on an additional scatter plot to indicate their influence over the positioning of each of the cases against the generated principal components.

6.3 RESULTS

6.3.1 *Single Species Biofilms*

6.3.1.1 Full Scan SIFT-MS Analysis of Bacterial Biofilms; Comparing Mean Values

The data presented in this section was analysed as described in section 6.2.3.1. Analysis of mean (\log_{10}) headspace count rates of selected mass spectral product ions from biofilm cultures of *P. aeruginosa*, *S. aureus* and *S. pyogenes*, using hierarchical cluster analysis, resulted in the production of the dendrogram in Figure 6.1. This shows successful discrimination of the three species analysed based on the profile of 46 selected volatile compound product ions detected.

The FS data set was also transformed using principal component analysis to reduce the selected variables to principal components. Figure 6.2a shows the scatter plot resulting from plotting the scores of the first two principal components. Principal components 1 and 2 account for 40.4% and 21.2% of the variability within the original data set respectively. Plotting the PCA scores in this way allows the complex data set to be represented in 2-dimensions and visualises the association of each bacterial strain with the derived principal components. Figure 6.2a shows that the strains of *S. aureus*, *P. aeruginosa* and *S. pyogenes* each occupy a discrete region of the 2-dimensional plot. Figure 6.2b shows the loading plot for the 46 selected product ions constituting the original variables for the principal component analysis shown in Figure 6.2a. This plot shows the contribution of each of the original variables; i.e. product ion count rates, to the derived first two principal components and indicates the influence of these variables in determining the position of each bacterial strain.

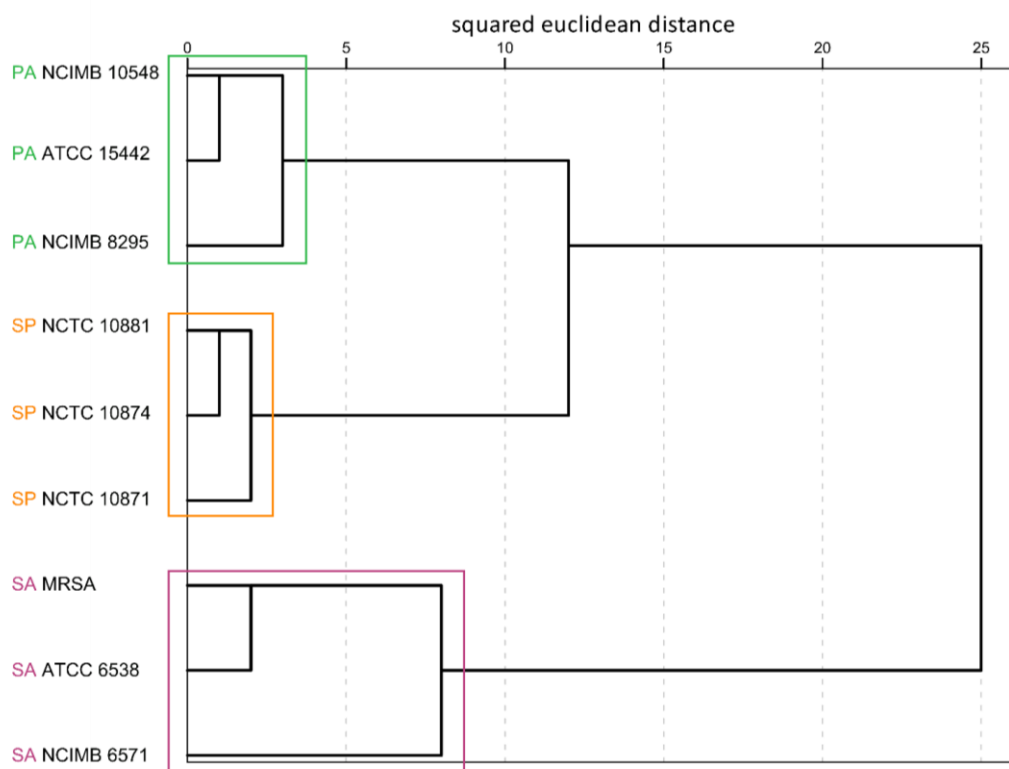


Figure 6.1: Dendrogram generated by hierarchical cluster analysis using 46 selected headspace volatile product ion peaks, detected by SIFT-MS following 48h of continuous culture in the collagen wound biofilm model. PA; *Pseudomonas aeruginosa*, SP; *Streptococcus pyogenes*, SA; *Staphylococcus aureus* (n=3 biofilms per strain). Coloured boxes indicate species specific clustering.

There are 7 product ions in the sector of the loading plot (Figure 6.2b) associated with the position occupied by *S. pyogenes* in the PCA plot (Figure 6.2a), 59, 60, 61, 77, 80, 114 and 117 m/z. Four product ions are associated with the positioning of *P. aeruginosa*, 29, 68, 76 and 155 m/z, whereas there are up to 35 product ions that are associated with the position of *S. aureus* on the PCA plot.

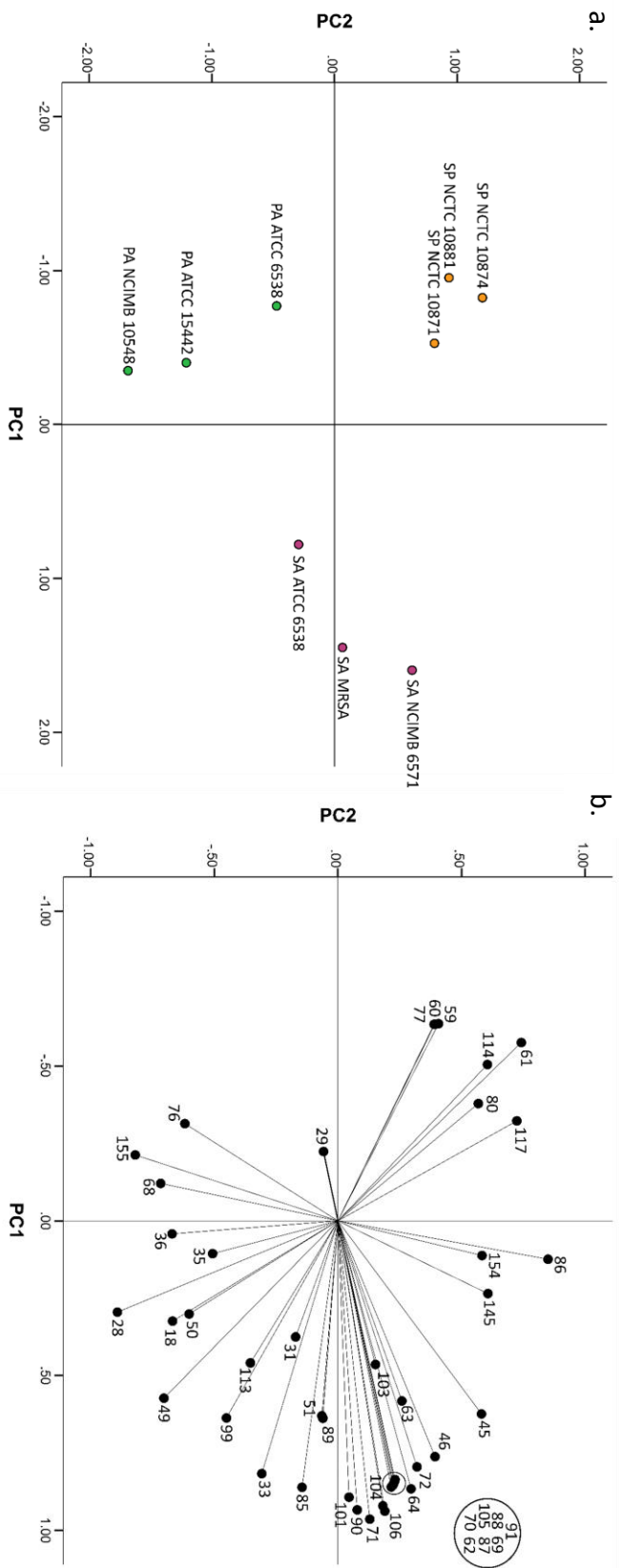


Figure 6.2: (a) Plot of the scores of the first two principal components generated by principle component analysis of headspace volatile compound product ion intensity, detected by SIFT-MS following 48h of continuous culture in the collagen wound biofilm model (n = 3 biofilms per bacterial strain, 3 scans per biofilm). Principal component 1 (horizontal axis) accounts for 40.4% of the total variation in the original data set and principal component 2 (vertical axis) accounts for 21.2%. *Pseudomonas aeruginosa* (Green), *Staphylococcus aureus* (Pink), *Streptococcus pyogenes* (Orange). (b) Principal component analysis loading plot of selected headspace volatile m/z peaks detected by SIFT-MS. Data points indicate the loading of each m/z peak (variable) on the first two principal components generated from the principal component analysis.

6.3.1.2 Headspace Solid Phase Micro Extraction Gas Chromatography Mass Spectrometry (SPME-GC-MS) Analysis of Bacterial Biofilms

Volatile compounds were sampled from the headspace of bacterial biofilms cultured for 48 hours in the collagen wound biofilm model, by solid phase micro extraction (SPME) for 30 minutes at 33°C. Compounds adsorbed to the fibre were then desorbed on to and analysed using GC-MS over a spectrum range of 15-400 m/z, as described in section 2.8.3. Chromatogram deconvolution and comparison with the NIST2.0 library was carried out using the Agilent Mass hunter software to identify compounds present (see Section 2.8.3).

Table 6.1 lists the compounds identified in the headspace of bacterial biofilm samples. Three biofilm samples each of *S. aureus* NCIMB 6571, *P. aeruginosa* NCIMB 10548 and *S. pyogenes* NCTC 10881 were analysed by HS-SPME-GC-MS. In addition uninoculated controls (n=4) were also analysed to identify compounds from the environment and emitted by culture media. Alongside the general compound information, the SIFT-MS product ions used for subsequent quantification of each of the compounds by SIFT-MS are listed, as well as the species of bacterial biofilm headspace the compound was detected from.

Table 6.1: Table of compounds detected by HS-SPME-GC-MS from bacterial biofilms cultured in the collagen wound biofilm model for 48 hours. Includes corresponding product ions for quantification using SIFT-MS and from which bacterial species each compound was detected.

Compound	Molecular formula	Molecular weight	Functional group	Species				SIFT-MS product ions		
				SP	PA	SA	SA	H3O+	NO+	O2+
Ethanol	C ₂ H ₆ O	46.08	alcohol	✓	✓	✓	✓	47	45	
1-butanol	C ₄ H ₁₀ O	74.14	alcohol	✓				57	73	56
Isobutyl alcohol	C ₄ H ₁₀ O	74.14	alcohol	✓		✓		57	73	42
2-methyl-2-propanol	C ₄ H ₁₀ O	74.14	alcohol	✓				57	57	59
3-methyl-1-butanol	C ₅ H ₁₂ O	88.17	alcohol			✓		71	87	59
Acetaldehyde	C ₂ H ₄ O	44.06	aldehyde	✓				45	43	
2-methylpropanal	C ₄ H ₈ O	72.12	aldehyde			✓			71	72
2-methylbutanal	C ₅ H ₁₀ O	86.15	aldehyde			✓		87	85	58
3-methylbutanal	C ₅ H ₁₀ O	86.15	aldehyde			✓		87	85	
Acetoin	C ₄ H ₈ O ₂	88.11	ketone			✓		89	118	88
Acetone	C ₃ H ₆ O	58.09	ketone	✓	✓	✓		59	88	
Butanone	C ₄ H ₈ O	72.12	ketone	✓		✓			102	72
2,3-butanedione	C ₄ H ₆ O ₂	86.09	ketone	✓		✓		87	86	86
3-methylbutanoic acid	C ₅ H ₁₀ O ₂	102.15	carboxylic acid	✓				103	132	
Butane	C ₄ H ₁₀	58.15	alkane	✓						43
Dimethyl sulfide	C ₂ H ₆ S	62.15	sulphur compound	✓				63	62	62
Dimethyl disulfide	C ₂ H ₆ S ₂	94.21	sulphur compound	✓				95	94	94

6.3.1.3 Selected Ion Mode (SIM) SIFT-MS Analysis of Bacterial Biofilms; Comparing Means.

All 17 compounds listed in Table 6.1 were used in the analysis, following background subtraction of volatile compound concentrations obtained from uninoculated controls as described in Section 6.2.4.1. In addition to the compounds identified using GC-MS, hydrogen cyanide and ammonia have been included due to consistent reporting in the literature of their importance as potential biomarkers of *P. aeruginosa* (Gilchrist *et al.*, 2013; Smith *et al.*, 2013; Neerincx *et al.*, 2016). The 28 m/z product ion, which could arise from the presence of hydrogen cyanide was also selected as a discriminatory product ion within SWF planktonic culture data in Chapter 3.

Analysis of mean headspace volatile compound concentrations (ppb) from biofilm cultures of *P. aeruginosa*, *S. aureus* and *S. pyogenes*, using hierarchical cluster analysis, resulted in the production of the dendrogram in Figure 6.3. Figure 6.3 shows successful discrimination of the three species analysed, with the exception of *S. aureus* NCIMB 6571, which shows a high level of dissimilarity from the other strains of *S. aureus* and the other two species analysed based on this statistical approach.

Principal component analysis was then utilised to transform this data set, the first two principal components accounting for 51.1% and 20.0% of the variation within the original data set respectively. Plotting the principal component scores, as shown in Figure 6.4a, results in each of the three species analysed occupying a separate area of the 2-dimensional plot. Figure 6.4b shows the loading plot of the 19 original volatile compounds quantified by SIFT-MS on the first two principal components,

indicating how these compounds influence the positioning of each of the bacterial strains in Figure 6.4a. Dimethyl sulphide, dimethyl disulphide, ethanol, hydrogen cyanide and ammonia appear to most strongly influence the position of *P. aeruginosa* on the PCA plot. Acetone is the only compound that is associated with the position of *S. pyogenes* on the PCA plot and the remaining 13 compounds all appear to be involved in the positioning of *S. aureus*.

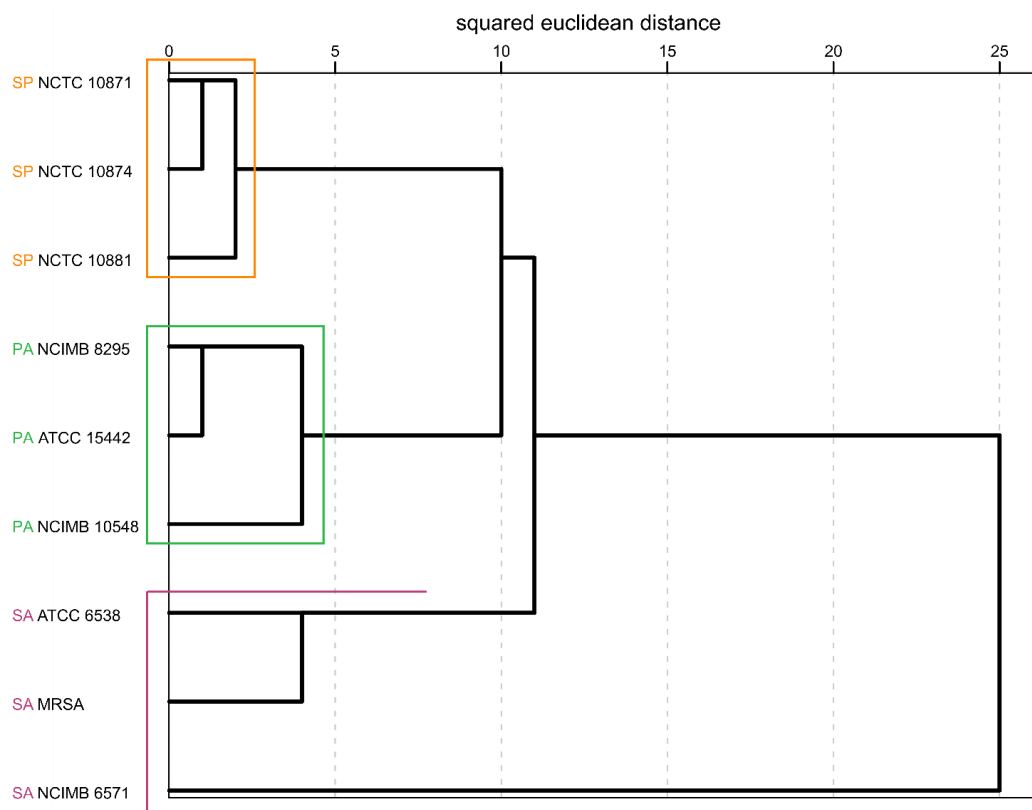


Figure 6.3: Dendrogram generated by hierarchical cluster analysis using 19 headspace volatile compound concentration (ppb), quantified by SIFT-MS following 48h of continuous culture in the collagen wound biofilm model. PA; *Pseudomonas aeruginosa*, SP; *Streptococcus pyogenes*, SA; *Staphylococcus aureus* (n=3 biofilms per strain). Coloured boxes indicate species specific clustering.

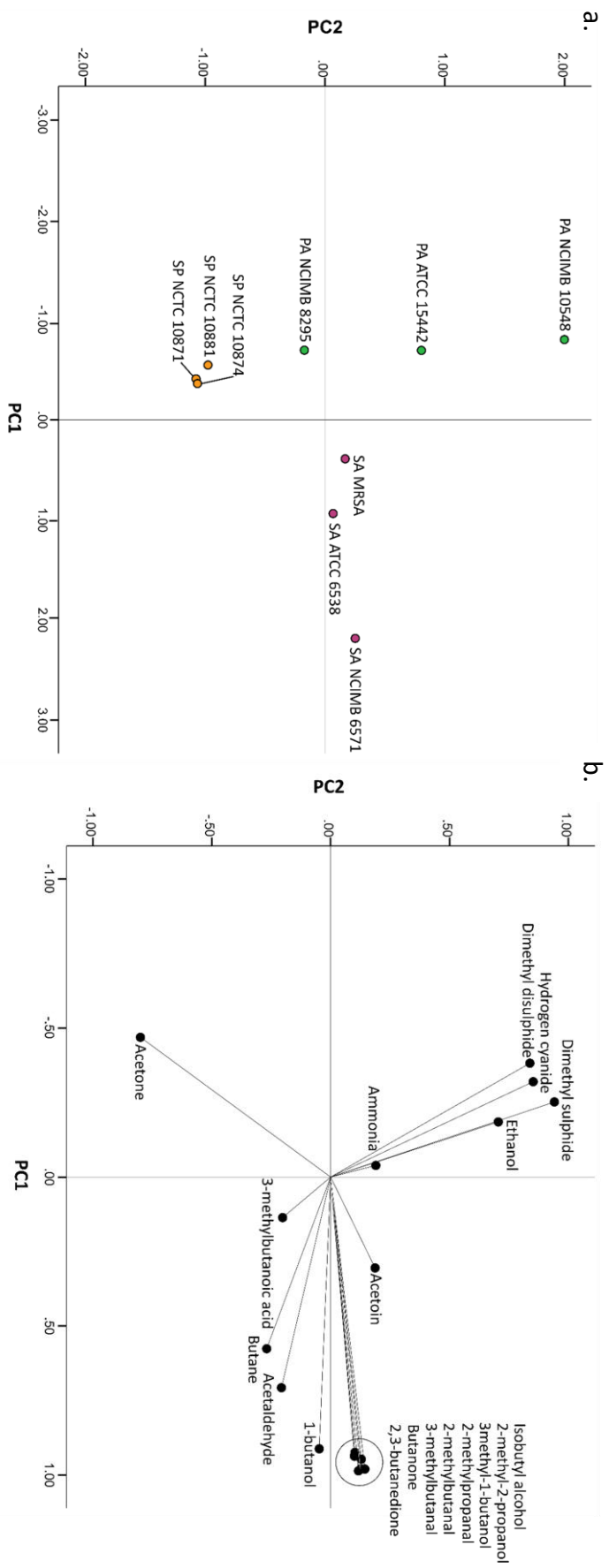


Figure 6.4: (a) Plot of the scores of the first two principal components generated by principle component analysis of 19 headspace volatile compound concentration (ppb), detected by SIFT-MS following 48h of continuous culture in the collagen wound biofilm model (n = 3 biofilms per bacterial strain, 12 scans per biofilm). Principal component 1 (horizontal axis) accounts for 51.1% of the total variation in the original data set and principal component 2 (vertical axis) accounts for 20.0%. *Pseudomonas aeruginosa* (Green), *Staphylococcus aureus* (Pink), *Streptococcus pyogenes* (Orange). (b) Principal component analysis loading plot of selected headspace volatile m/z peaks detected by SIFT-MS. Data points indicate the loading of each m/z peak (variable) on the first two principal components generated from the principal component analysis.

6.3.1.4 Full scan SIFT-MS analysis of bacterial biofilms; comparing independent biofilms with MANOVA

This section presents the same data set as Section 6.3.1.1 using an alternative process of statistical analysis. Background subtraction of uninoculated controls was not undertaken, to allow direct comparison between bacterial biofilm headspace and controls consisting of sterile collagen gel matrices perfused with SWF.

Multivariate analysis of variance (MANOVA), as described in Section 6.2.3.4, was used to select potentially discriminant product ion peaks. A total of 59 product ion peaks were identified by MANOVA and utilised for further analysis. Figure 6.5 shows the dendrogram generated to visualise the result of subsequent hierarchical cluster analysis, where each case shown represents headspace analysis of a single independent biofilm (3 biofilms per strain and 3 strains of each species). The dendrogram shows clear discrimination between *S. aureus*, *S. pyogenes* and *P. aeruginosa* biofilms based on the profile of selected headspace volatile compound product ion peaks detected in the sample headspace after 48 hours of continuous culture in the collagen wound biofilm model.

Principal component analysis was used to transform the data set (59 selected product ions), which included control data for the 59 selected product ions from uninoculated controls to enable direct comparison. Figure 6.6a shows a scatter plot of the scores for each of the independent biofilms against the first two principal components, while Figure 6.6b shows the loading of each of the original variables (m/z product ion peaks) on these components.

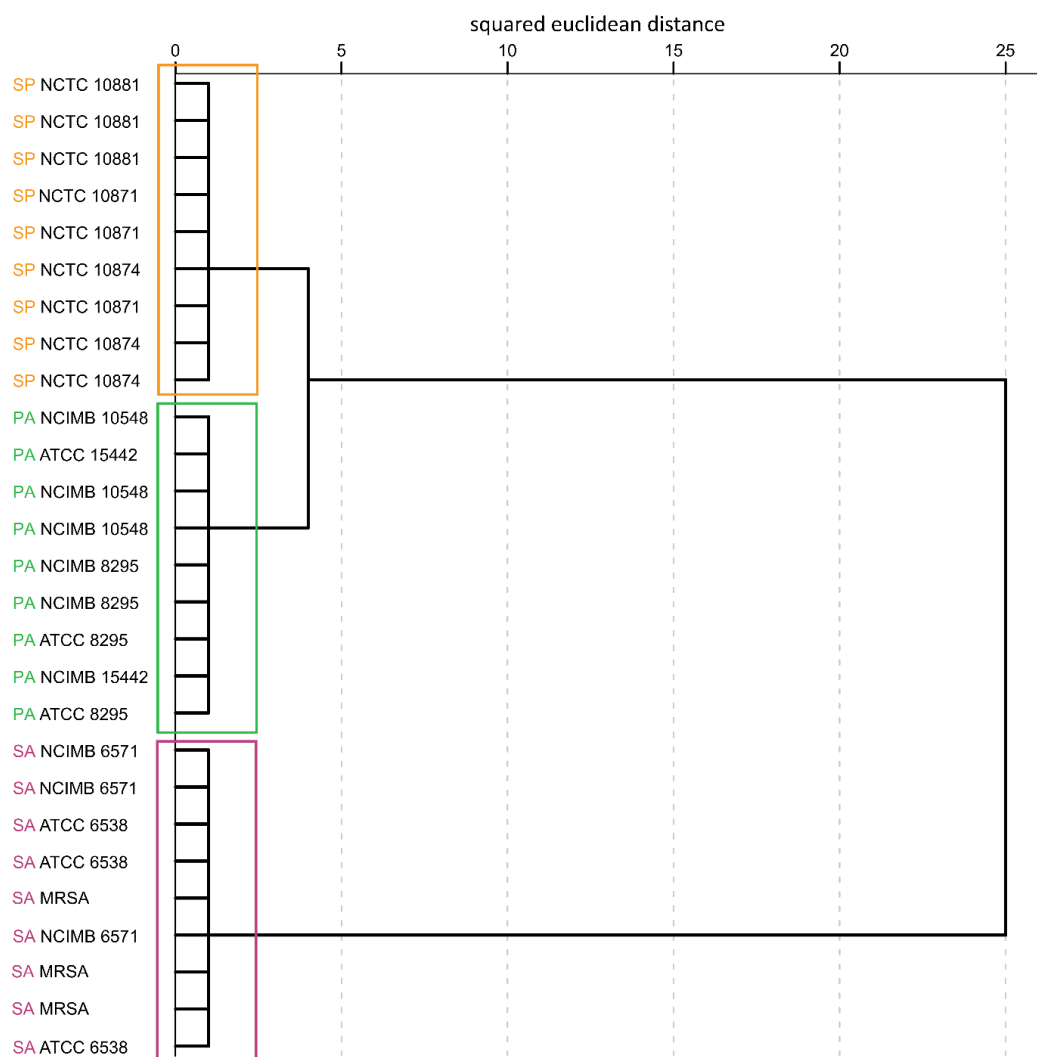


Figure 6.5: Dendrogram generated by hierarchical cluster analysis using 59 selected headspace volatile product ion peaks (Vcps), detected by SIFT-MS following 48h of continuous culture in the collagen wound biofilm model (n=3 biofilms per strain, with 3 replicate scans per biofilm). Coloured boxes indicate species specific clustering. PA; *Pseudomonas aeruginosa*, SP; *Streptococcus pyogenes*, SA; *Staphylococcus aureus*.

The first two principal components account for 57.7% and 22.6% of the total variation in the original data. Clear discrimination between the three bacterial species *S. aureus*, *S. pyogenes* and *P. aeruginosa* biofilms is demonstrated in Figure 6.6a, with each bacterial species occupying a discrete region of the plot. However, the inclusion of data from uninoculated controls indicates substantial overlap between *S. pyogenes* biofilms and the uninoculated collagen coated slides continuously perfused with simulated wound fluid within the collagen wound biofilm model. This is likely as a result of a lack of detection of product ions from either sample type. This is indicated on Figure 6.6b, which shows the loading of each of the selected product ion peaks on the first two principal components and indicates the influence these original variables have on the positioning of each biofilm sample in Figure 6.6a. Only 3 product ions are located within the region of the plot associated with the position of *S. pyogenes* and the uninoculated controls (60, 67 and 196 m/z). Eight product ions (28, 29, 50, 95, 96, 97, 98 and 115 m/z) appear to influence the position of *P. aeruginosa* on the PCA plot, while up to 41 product ions are involved in determining the position of the *S. aureus* biofilms.

order to further assess the relationship between *S. pyogenes* and the control samples an additional scatter plot including the third principal component was constructed (Figure 6.7a), component 3 accounted for 3.67% of the variation within the original data set. This showed clear separation of *S. pyogenes* and the control samples on the third principal component. Figure 6.7b shows the loading plot of the 59 selected product ions on the second and third principal components and indicates 12 main product ions potentially responsible for the separation of the *S. pyogenes* samples and the uninoculated controls on the third principal component. Of these 12, seven are primarily involved in the positioning of *S. pyogenes* (26, 30, 60, 144, 161, 175 and 196 m/z) and a further 5 (43, 65, 66, 67 and 93 m/z) drive the positioning of the uninoculated control samples.

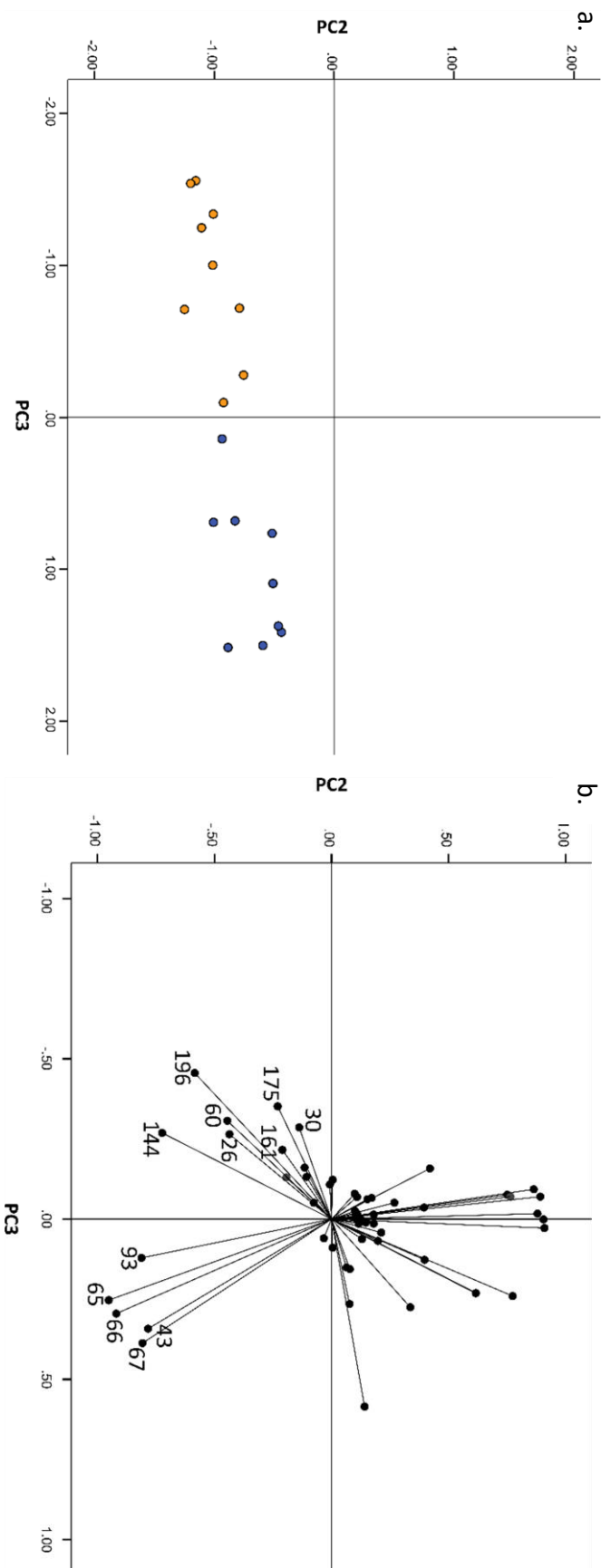


Figure 6.7: Plot of the scores of the second and third principal components generated by principle component analysis of SIFT-MS full scan data of selected headspace volatiles product ion peaks of bacterial biofilms and uninoculated controls, showing *Streptococcus pyogenes* (Orange) and control (Blue) only. The second principal component accounts for 22.6% and the third components accounts for 3.67% of the total variation of the original data set. (b) Principal component analysis loading plot of selected m/z peaks Data points indicate the loading of each m/z peak (variable) on the second and third principal components generated from the principal component analysis.

6.3.1.5 SIM Scan SIFT-MS Analysis of Bacterial Biofilms; Comparing Independent Biofilms with MANOVA.

This section presents the same data set as Section 6.3.1.3 but with individual biofilms analysed separately, using MANOVA to identify potentially discriminant volatile compounds and includes comparison of bacterial biofilm headspace volatiles to the background levels detected from uninoculated controls. Multivariate analysis of variance (MANOVA), as described in Section 6.2.4.2, was used to select potentially discriminant volatile compounds. Of the 19 compounds quantified using SIFT-MS in selected ion mode, 8 were found to be statistically highly significantly different ($p < 0.01$) between bacterial species. These potentially discriminant volatile compounds were hydrogen cyanide, dimethyl sulphide, acetaldehyde, 3-methyl-1-butanol, 2,3-butanedione, 2-methyl-2-propanol, 2-methylbutanal and 3-methylbutanal.

Hierarchical cluster analysis was applied to the data set, resulting in production of the dendrogram shown in Figure 6.8. The dendrogram shows clear discrimination between *S. aureus*, *S. pyogenes* and *P. aeruginosa* biofilms based on SIFT-MS quantification of selected headspace volatile compounds detected in the sample headspace after 48 hours of continuous culture in the collagen wound biofilm model.

Again, principal component analysis was used to transform the data set (8 selected volatile compound concentrations) to principal components, with the inclusion of data from SIFT-MS headspace analysis of uninoculated controls. Figure 6.9a shows the scatter plot of the scores of each bacterial biofilm and the uninoculated controls against the first two principal components. Principal components 1 and 2 account for

63.6% and 26.1% of the variability within the original data set of 8 selected volatile compounds. Figure 6.9a shows that all *P. aeruginosa* biofilms occupy a discrete region of the 2-dimensional plot, but that there is an overlap of one *S. pyogenes* biofilm sample in to the area of the plot otherwise occupied by *S. aureus*. As with the analysis of the FS data set presented in 6.3.1.4 there is also substantial overlap between *S. pyogenes* biofilms and the 'background' volatile compounds detected from uninoculated collagen coated slides continuously perfused with simulated wound fluid within the collagen wound biofilm model. Figure 6.9b shows the loading of the 8 quantified volatile compounds on the first two principal component and indicates the influence the production of these compounds has on the position of the biofilm samples on the scatter plot shown in Figure 6.9a. Dimethyl sulphide and hydrogen cyanide appear to influence the position of the *P. aeruginosa* samples on the PCA plot, while 3-methyl -1-butanol, 2,3-butanedione, 2-methyl-2-propanol, 2-methylbutanal, 3-methylbutanal and acetaldehyde appear to influence the positioning of *S. aureus* biofilm samples. The absence of these compounds from the headspace of the *S. pyogenes* samples as well as the uninoculated controls is likely driving the positioning of the samples on the PCA plot in Figure 6.9a.

Figure 6.10 shows an additional scatter plot which visualises the scores of the *S. pyogenes* biofilms and uninoculated controls against the second and third principal components, with principal component 3 accounting for 5.45% of the variation within the data set. Figure 6.10 show that there is substantial overlap between *S. pyogenes* and the controls on the third principal component and confirms that

discrimination between these two groups is not possible within this analysis, using only 8 selected volatile compounds.

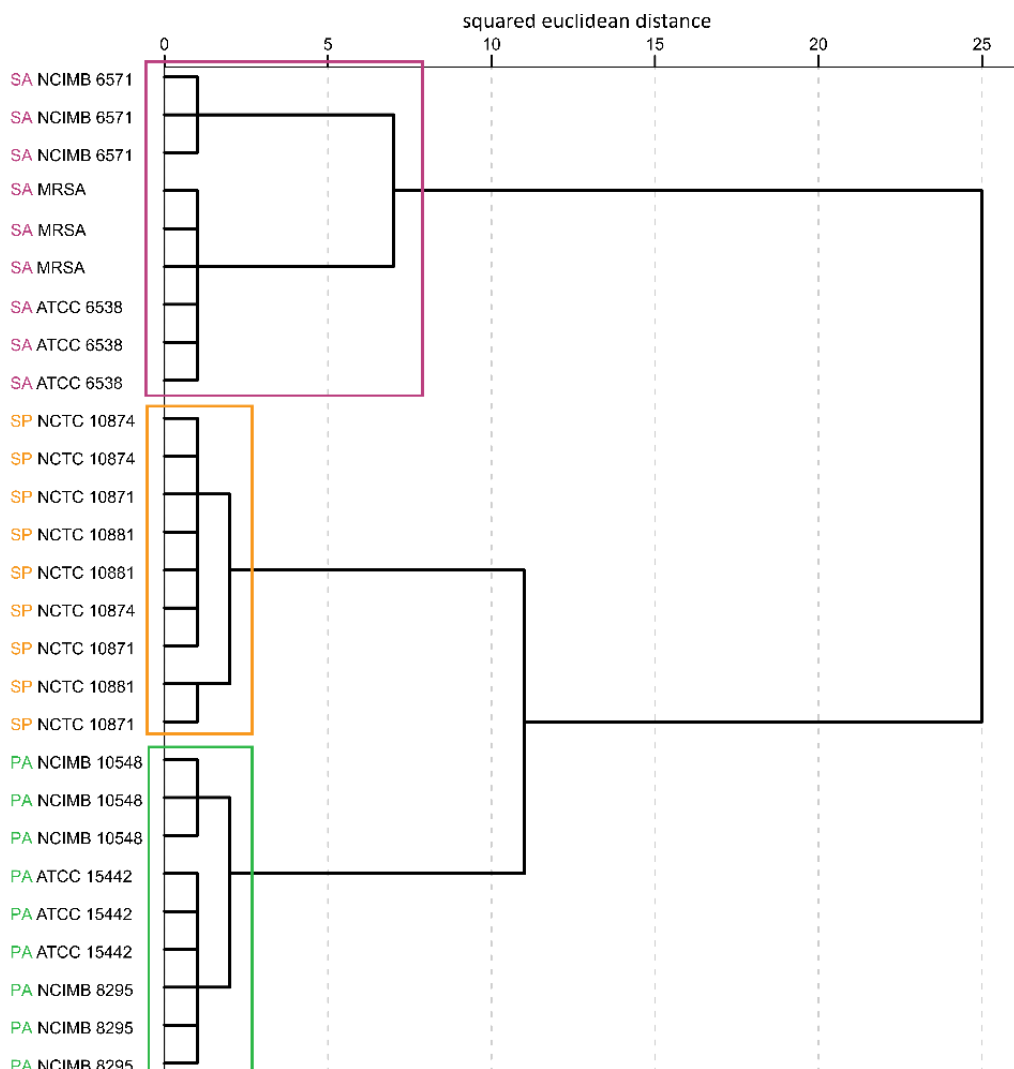


Figure 6.8: Dendrogram generated by hierarchical cluster using 8 selected headspace volatile compound concentrations (ppb), detected by SIFT-MS following 48h of continuous culture in the collagen wound biofilm model (n=3 biofilms per strain, with 12 replicate scans per biofilm). Coloured boxes indicate species specific clustering. PA; *Pseudomonas aeruginosa*, SP; *Streptococcus pyogenes*, SA; *Staphylococcus aureus*.

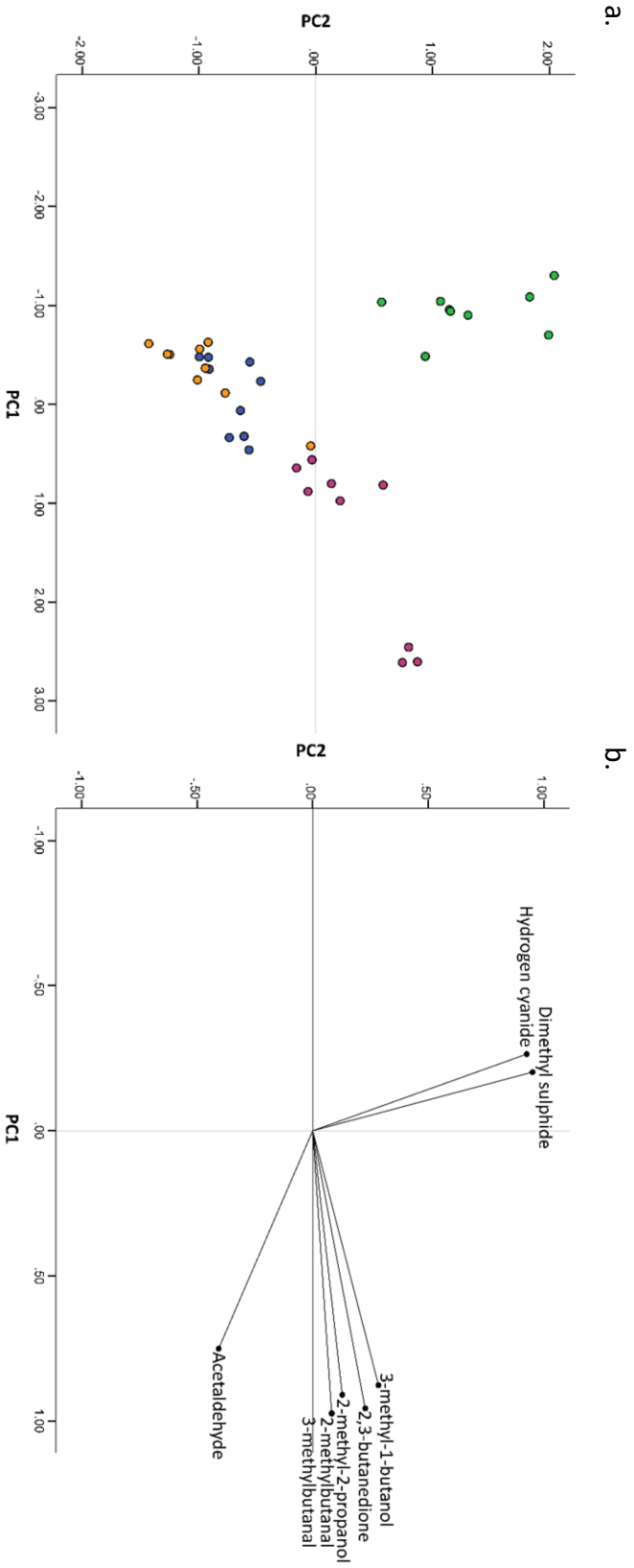


Figure 6.9: (a) Plot of the scores of the first two principal components generated by principle component analysis of SIFT-MS SIM scan data of selected headspace volatile compound concentrations (ppb) of bacterial biofilms and uninoculated controls (n = 3 scans per sample). Principal component 1 (horizontal axis) accounts for 63.6% of the total variation in the original data set and principal component 2 (vertical axis) accounts for 26.1% of the total variation. *Pseudomonas aeruginosa* (Green), *Staphylococcus aureus* (Pink), *Streptococcus pyogenes* (Orange), control (Blue). (b) Principal component analysis loading plot of selected m/z peaks. Data points indicate the loading of each m/z peak (variable) on the first two principal components generated from the principal component analysis.

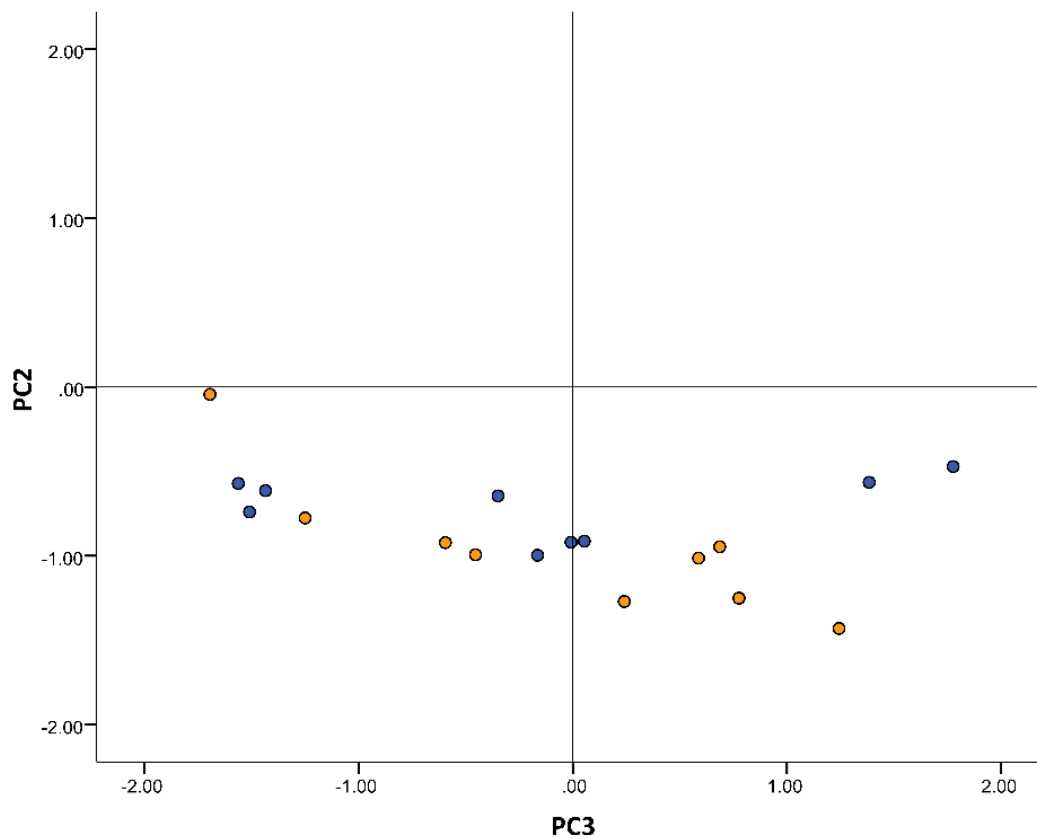


Figure 6.10: Plot of the scores of the second and third principal components generated by principle component analysis of SIFT-MS SIM data of selected headspace volatile compound concentrations (ppb) of bacterial biofilms and uninoculated controls, showing *S. pyogenes* (Orange) and control (Blue) only. Principal component 2 accounts for 26.1 % of the variation within the original data set, while the third components accounts for 5.45 % of the variation.

6.3.2 *Multispecies Biofilms*

6.3.2.1 Enumeration of Multispecies Biofilms

Previous studies have reported that when culturing multispecies biofilms containing *P. aeruginosa*, this organism readily dominates the bacterial population, allowing little or no recovery of other organisms present in the starting inoculum (Dalton *et al.*, 2011; Woods *et al.*, 2012). In order to allow growth of *S. aureus* and *S. pyogenes* in the multispecies biofilms containing *P. aeruginosa*, they were inoculated first and allowed to establish for 18 hours prior to inoculation with *P. aeruginosa*. As a result, the culture time of *P. aeruginosa* was limited to only 29 hours within the multispecies biofilms. However, comparison of *P. aeruginosa* biofilms at 30 and 48 hours (t-test), from the data presented in Chapter 5, which shows the development of single species biofilms over 72 hours, reveals that there is no statistically significant difference ($p > 0.05$) in *P. aeruginosa* biofilm density at 30 and 48 hours.

Figure 6.11 shows the density (cfu slide⁻¹) of each bacterial species when cultured as a single species biofilm, for 48 hours, and in multispecies biofilms with one or both of the other two species included in this study. Analysis of variance (ANOVA) was used to compare density of each species cultured as a single species biofilm, to the density achieved when that species was included in each multispecies biofilm combination. The density of *S. aureus* is significantly less ($p < 0.05$) in multispecies biofilms containing *P. aeruginosa* compared to single species biofilms. Similarly, the density of *P. aeruginosa* was significantly less ($p < 0.05$) in all multispecies biofilms compared to single species biofilms. Although there is some variability, there is no statistically significant differences in the density of *S. pyogenes* when cultured as a

single species biofilm or in any of the multispecies biofilms ($p > 0.05$) with one or both of the other species.

Figure 6.12 also show the enumeration of each bacterial species within multispecies biofilms, but indicates the total density (cfu slide⁻¹) of each multispecies biofilm combination (one per panel) and the density of each individual species included in the multi species community. In addition the percentage contribution to the multispecies biofilm of each species is indicated above the bars. Where *P. aeruginosa* is present within the multispecies biofilm this species makes up the majority of the multispecies community, this is consistent with the higher achievable density of this species seen in single species biofilms, under the specific culture conditions employed within the collagen wound biofilm model.

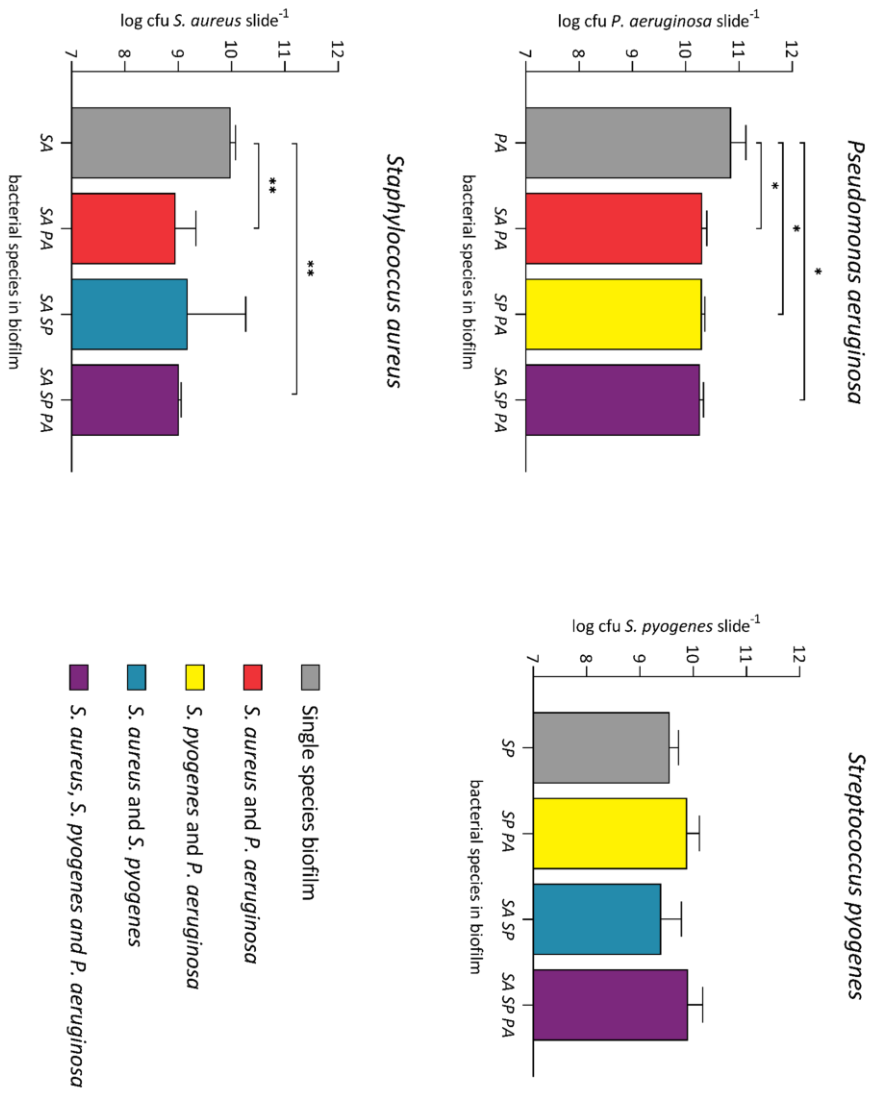


Figure 6.11: Enumeration of *Staphylococcus aureus*, *Streptococcus pyogenes* and *Pseudomonas aeruginosa* in single and multispecies biofilms following 48 hours total culture time (n=3 ±SD) within the collagen wound biofilm model, (Dunnett's test; * p<0.05, ** p<0.01).

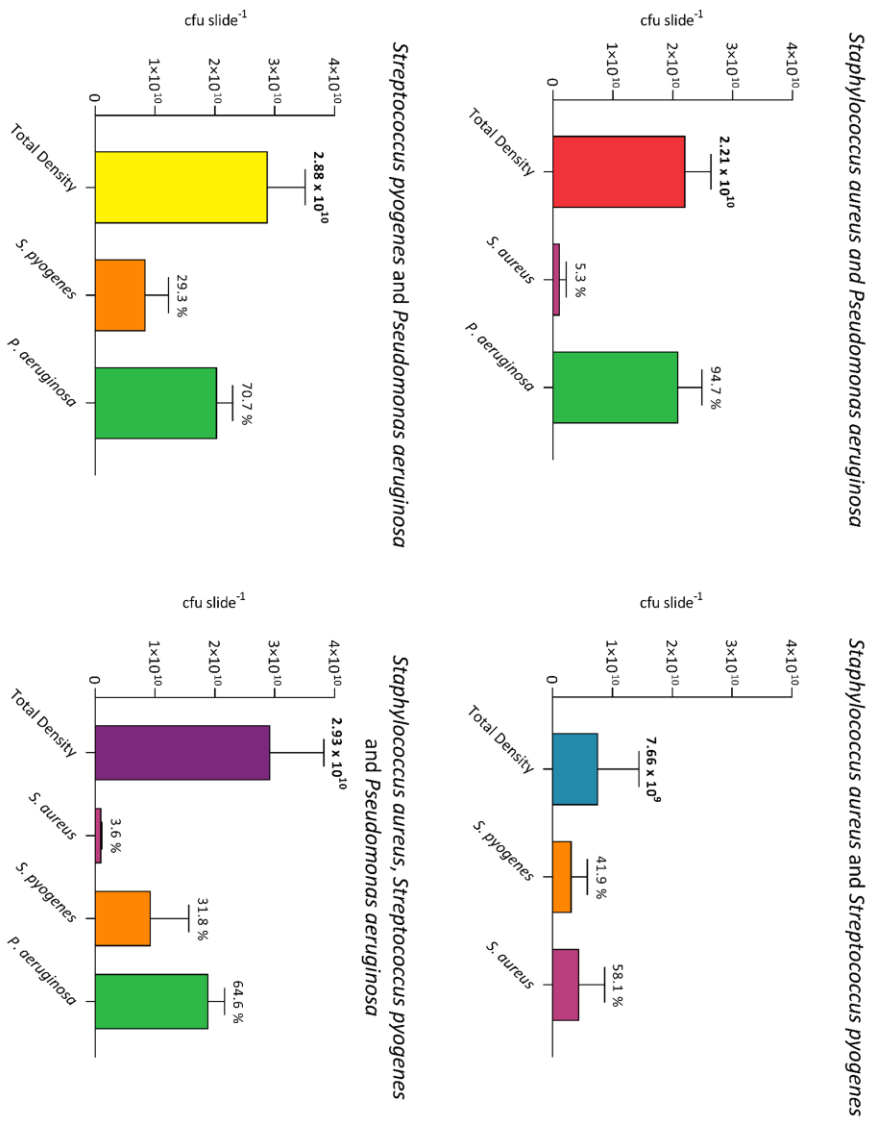


Figure 6.12: Enumeration of multispecies biofilms following 48 hours total culture time (n=3 \pm SD) within the collagen wound biofilm model. Panels show the total biofilm density of each multispecies biofilm combination with the density and percentage contribution of each individual species to the biofilm community.

6.3.2.2 SIFT-MS Analysis of Multispecies Biofilms

The headspace of multispecies biofilms cultured in the collagen wound biofilm model were analysed using SIFT-MS following a total of 48 hours continuous culture. SIM scans were performed to quantify the concentration of 19 volatile compounds in the biofilm headspace (see Section 6.3.1.3). This data was corrected by background subtraction of the concentrations quantified in the headspace of uninoculated controls, to determine the volatile compound production attributed to the bacterial biofilms only. Table 6.3 shows the compound concentration (ppb) detected in the headspace of multi species biofilms (n=3 per multi species combination) compared to the concentration of the same compounds detected in the headspace of single species biofilms of each of the three species included in this research.

Many of the compounds detected in the headspace of *S. aureus* biofilms are not present in the headspace of the *S. aureus* and *P. aeruginosa* biofilms, instead the compounds and concentrations detected are more similar to those detected in the headspace of *P. aeruginosa* biofilms. Eighteen of the 19 compounds quantified were detected in the headspace of *S. aureus* and *S. pyogenes* multispecies biofilms, the exception is ammonia. Ammonia is detected in the headspace of both species alone, but is absent from the headspace of the multispecies biofilms following background subtraction of controls. In general the composition of the headspace of the *S. aureus* and *S. pyogenes* multispecies biofilms appears more similar to that of *S. aureus* as a single species biofilm than that of *S. pyogenes*.

The headspace of multispecies biofilms containing *S. pyogenes* and *P. aeruginosa*, compared to single species biofilms of both these species indicates that the

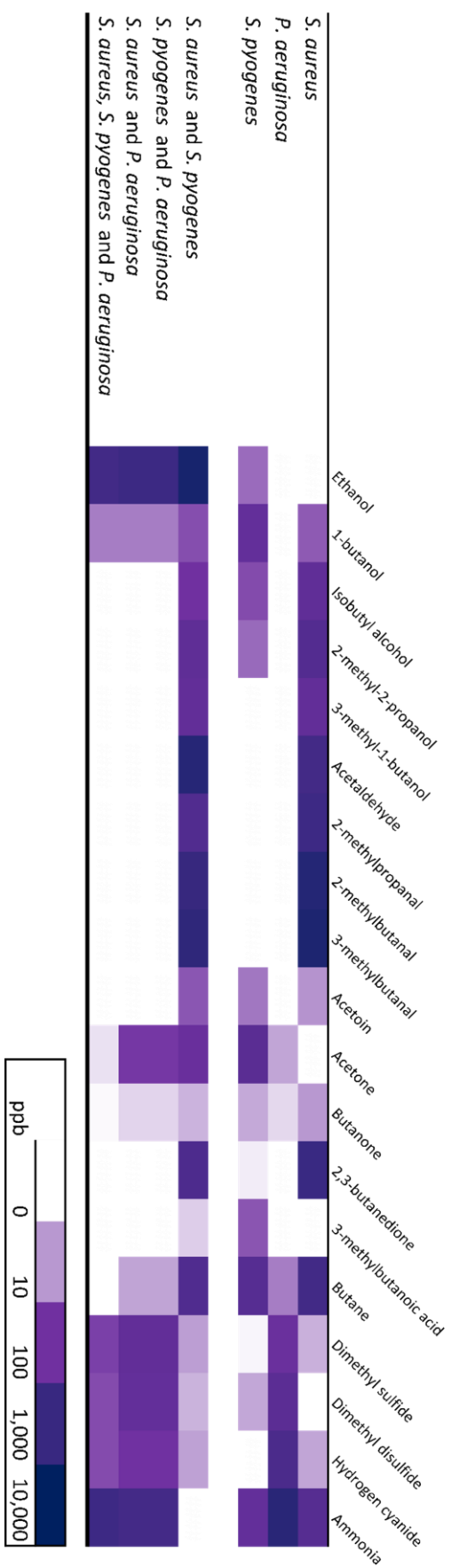
multispecies biofilms produce all compounds found in the headspace of *P. aeruginosa* biofilms, but lack several produced by *S. pyogenes* biofilms. These include acetoin and 2-methyl-2-propanol. Similarly, the headspace of multispecies biofilms containing *S. aureus*, *S. pyogenes* and *P. aeruginosa*, appear to be dominated by compounds detected in the headspace of *P. aeruginosa* single species, with many of the compounds detected in the headspace of *S. aureus* absent from the headspace of the multispecies biofilm. The compounds absent from the multispecies biofilm containing *P. aeruginosa* and *S. pyogenes*, that are produced by *S. pyogenes* single species biofilms, are also absent from the biofilm containing all three bacterial species.

In order to further compare multispecies and single species biofilms, the SIM scan data sets (without background subtraction) were combined (i.e. data from section 6.3.1.5 and 6.3.2.2). Hierarchical cluster analysis was applied to the combined data set, resulting in the dendrogram shown in Figure 6.13. The largest cluster grouping is formed by the single species *P. aeruginosa* biofilms with all the multi species biofilms containing *P. aeruginosa*, suggesting this species is dominant in determining the composition of headspace volatiles when cultured with either *S. aureus* or *S. pyogenes*. A second cluster contains the single species *S. aureus* biofilms and the multispecies biofilms containing *S. aureus* and *S. pyogenes*, and the final smallest cluster contains only the *S. pyogenes* single species biofilms.

The data sets, including all strains of single species biofilms as well as the multispecies biofilms, were then transformed using principal component analysis to reduce the complex data sets to a smaller number of principal components. Figure 6.14 shows

the scatter plots of the scores of all single and multispecies biofilms against the first two principal components from the analysis of SIM scan data, including the same 8 volatile compounds identified using MANOVA in Section 6.3.1.5. Component 1 accounts for 68.1 % and component 2 23.0 % of the variation within this data set. Figure 6.14 indicates that all three combinations of multispecies biofilm containing *P. aeruginosa* cluster with the *P. aeruginosa* single species biofilms in the 2-dimensional plot. This again suggests the headspace volatile compounds produced by multispecies biofilms containing *P. aeruginosa* are dominated by the production of volatiles associated with this species. The multispecies biofilms containing *S. aureus* and *S. pyogenes* locate with the *S. aureus* single species biofilms on the 2-dimensional PCA plot, showing that in this multi species biofilm volatile compounds produced by *S. aureus* dominate.

Table 6.2: Array of product ions detected using SIFT-MS analysis of the headspace of single species and multi species biofilms, showing the product ions detected from each biofilm type when cultured in the collagen wound biofilm model (n=3). Includes background subtraction of product ion intensities detected from uninoculated controls. The colour intensity indicates the compound concentration.



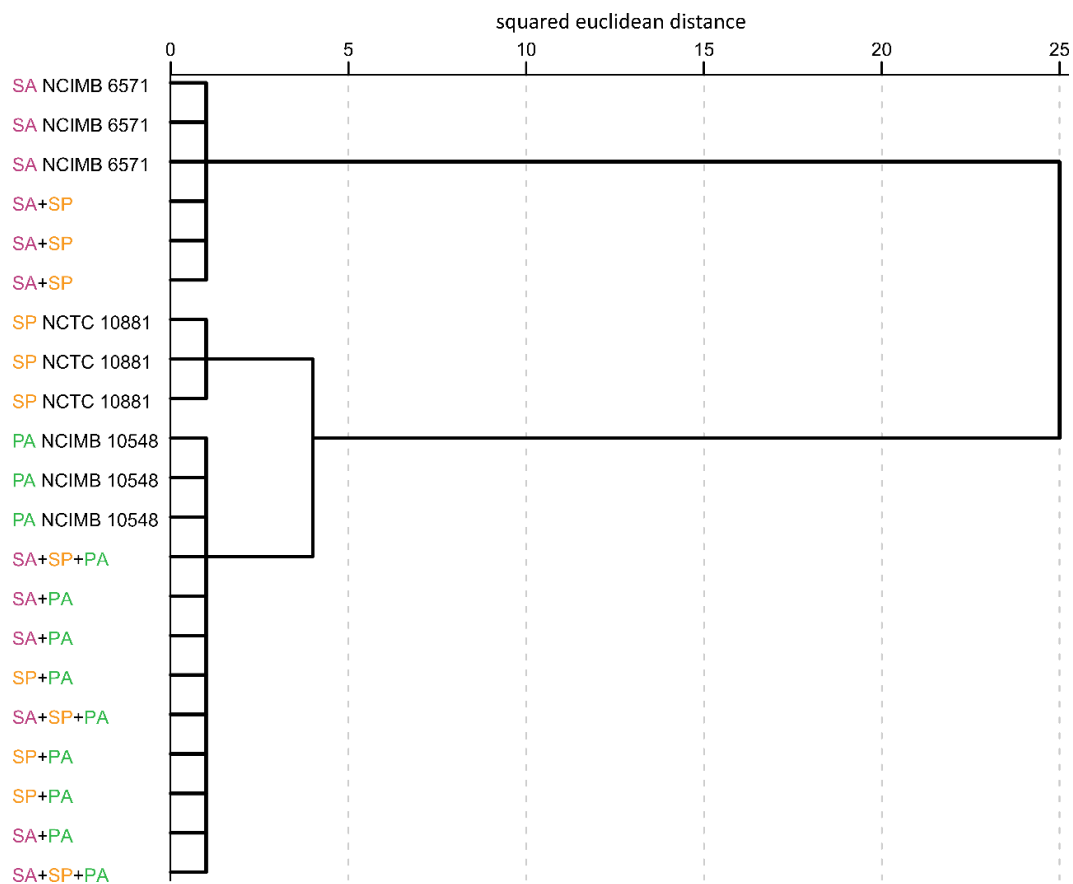


Figure 6.13: Dendrogram generated by hierarchical cluster using 8 selected headspace volatile compound concentrations (ppb), detected by SIFT-MS following 48h of continuous culture in the collagen wound biofilm model (n=3 biofilms per strain/multispecies combination, with 12 replicate scans per biofilm). PA; *Pseudomonas aeruginosa*, SP; *Streptococcus pyogenes*, SA; *Staphylococcus aureus*.

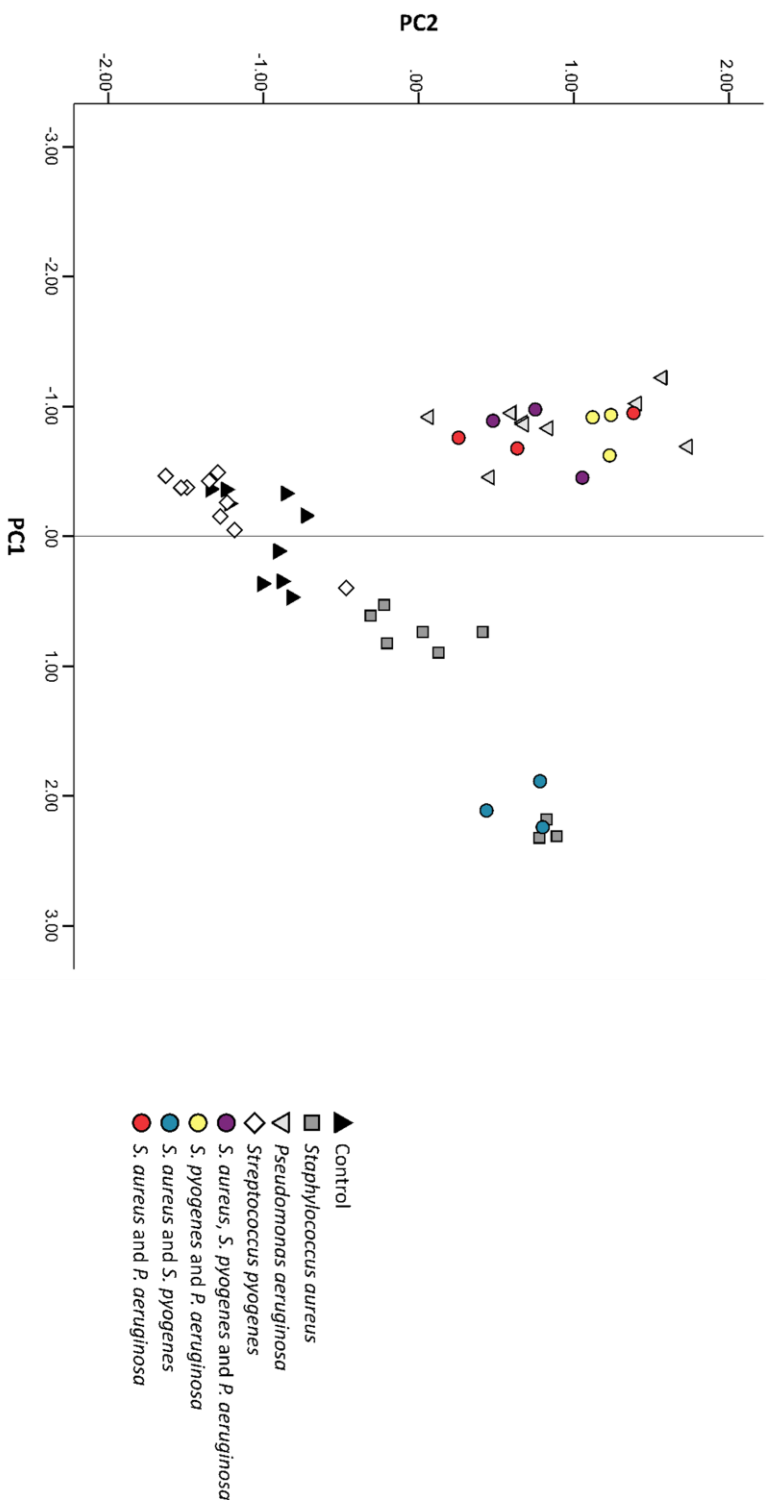


Figure 6.14: (a) Plot of the scores of the first two principal components generated by principle component analysis of headspace concentration (ppb) of 8 selected volatile compounds, detected by SIFT-MS following 48h of continuous culture in the collagen wound biofilm model (n = 3 biofilms per bacterial strain/multispecies combination, 12 scans per biofilm). Principal component 1 (horizontal axis) accounts for 68.1% of the total variation in the original data set and principal component 2 (vertical axis) accounts for 23.0%. Includes multispecies biofilms and all strains of single species biofilms.

6.4 DISCUSSION

The main aim of this chapter was to determine if three important bacterial pathogens associated with clinically relevant wound infection, *S. aureus*, *P. aeruginosa* and *S. pyogenes*, could be successfully discriminated based on their production of volatile metabolites when grown in a collagen wound biofilm model. The results of this chapter demonstrate that by using both SIFT-MS FS and SIM scans (following compound identification using GC-MS), to detect characteristic volatile profiles combined with the use of multivariate statistical analysis all three species could be successfully differentiated. Therefore, this work has shown that *S. aureus*, *P. aeruginosa* and *S. pyogenes* biofilms produce headspace gases that vary between species. These differences can be detected as volatile compound product ion profiles when employing SIFT-MS in full scan mode and through the quantification of specific volatile compounds when the SIFT-MS instrument is operated in selected ion mode. Two different methods for the selection of potentially discriminatory product ions were used for the analysis of the full scan data set. Initially the same process that was previously employed for the selection of discriminatory product ions for the analysis of volatile compound product ion peaks from the headspace of planktonic cultures (Chapter 3) was utilised. This process required comparison of bacterial sample headspace analysis to that of the uninoculated controls using t-tests, followed by background subtraction of the mean control product ion intensity from the mean test value for each bacterial strain. A threshold was then applied to this data set as

detailed in section 6.4.2.1. This method resulted in the identification of 46 product ions that were produced by at least one of the bacterial species, for further analysis.

A second method of analysis was carried out to test the application of a statistical test (MANOVA) for the selection of potentially discriminant product ions. This omitted the background subtraction to allow direct comparison of individual independent biofilms, rather than generating a corrected mean value for each strain analysed. This method of analysis resulted in selection of 59 product ion peaks ($p < 0.01$).

Comparison of these two methods highlights 22 product ion peaks common to both processes of selection. For both methods of analysis, the location of the product ion peaks on the PCA loading plots can be used to determine their likely influence on the discrimination of the three bacterial species on the corresponding plots of their PCA scores. Of these 22 product ion peaks 16 are located, in the direction that indicates involvement in positively determining the position of *S. aureus* on both loading plots (62, 63, 64, 69, 70, 71, 72, 87, 88, 90, 99, 101, 104, 105, 106 and 145 m/z), 1 product ion peak appears in the direction associated with *S. pyogenes* positioning (60 m/z) and a further 4 associated with *P. aeruginosa* (28, 29, 68 and 155 m/z). The product ion peak at 50 m/z is not positioned consistently within the two different analysis method PCA plots. Plotting PCA scores generated from transformation of the data sets including only these 22 'core' product ion peaks (appendix II, Figure S1) results in similar discrimination of the bacterial species as seen in Figures 6.2a and 6.6a, suggesting identification of the product ions most essential for species discrimination can be achieved by employing and comparing multiple methods of analysis.

The approach using background subtraction and a 10 cps threshold focuses on selection of product ion that are produced at high intensities by at least one of the bacterial species analysed but does eliminate product ions produced by several or all species. However, use of MANOVA selects only product ions produced at significantly different intensities between species. It is likely that product ions selected by the first method but not by MANOVA will be those produced at high levels in all species, which are therefore not useful for discrimination between species. Conversely, product ions selected by MANOVA, without thresholding, are likely to have significantly different intensities between species but may only be produced at relatively low intensities. Overall, if only one method of selection is to be used, MANOVA is likely to be most effective at identifying discriminatory product ions or volatile compounds.

HS-SPME-GC-MS was used to identify compounds in the bacterial biofilm headspace that may be responsible for the product ion peaks detected using SIFT-MS in full scan mode. Seventeen compounds were identified from the headspace of the three species included in this work. The 17 compounds identified by GC-MS included 5 alcohols; ethanol, 1-butanol, isobutyl alcohol, 2-methyl-2-propanol and 3-methyl-1-butanol. Ethanol and 1-butanol are produced by fermentation of carbohydrates (Thorn and Greenman, 2012) and the branched alcohols are thought to arise from the catabolism of branched amino acids (Audrain *et al.*, 2015). Four aldehydes; acetaldehyde, 2-methylpropanal, 2-methylbutanal and 3-methylbutanal, and 4 ketones; acetone, acetoin, butanone and 2,3-butanedione were identified by GC-MS.

3-methylbutanal arises from the catabolism of the amino acid leucine, as does the alcohol 3-methyl-1-butanol (Filipiak *et al.*, 2012). Catabolism of pyruvate produces acetaldehyde, acetone and acetoin (Filipiak *et al.*, 2012), and oxidation of acetoin results in 2,3-butanedione production (Audrain *et al.*, 2015). 3-methylbutanoic acid, the carboxylic acid identified by GC-MS, is also produced during catabolism of pyruvate, either from oxidation of 3-methylbutanal or using an alternative pathway via the intermediate isovaleryl-CoA (Filipiak *et al.*, 2012). It is suggested that bacterial production of butane may involve cysteine, but the role of this and other amino acids in volatile hydrocarbon synthesis remains unknown (Ladygina, Dedyukhina and Vainshtein, 2006). The sulphur compounds detected, dimethyl sulphide and dimethyl disulphide result from oxidation of methanethiol, which is itself produced from bacterial catabolism of methionine (Filipiak *et al.*, 2012; Audrain *et al.*, 2015).

In addition to the compounds identified by GC-MS, ammonia and hydrogen cyanide were included for further analysis of bacterial biofilm headspace using SIFT-MS SIM scans. These compounds have both previously been detected from the headspace of *P. aeruginosa*, both in liquid cultures and *in vivo* (Neerincx *et al.*, 2015; Gilchrist *et al.*, 2013; Smith *et al.*, 2013b), with the suggestion that they may be important markers of *P. aeruginosa* infection.

Hydrogen cyanide is generated through decarboxylation of glycine by the membrane bound HCN synthase enzyme in *P. aeruginosa* (Blumer and Haas, 2000), and ammonia is produced by the metabolism of nitrogen containing compounds, including hydrogen cyanide and amino acids (Neerincx *et al.*, 2015). It has been previously reported that interaction and competition between compounds in

complex mixtures can result in inconsistent results using SPME and that displacement of low molecular weight compounds by those of higher molecular weights can result in under detection of low molecular weight compounds (Murray, 2001). This may explain why ammonia (17 Da) and hydrogen cyanide (28 Da) were not detected during GC-MS analysis of *P. aeruginosa* biofilms, but were detected using SIFT-MS. Of the 17 compounds detected by GC-MS in this research acetaldehyde has the lowest molecular weight at 44 Da, giving rise to a SIFT-MS product ion peak of 45 m/z when using the H_3O^+ reagent ion. However, the 59 FS SIFT-MS product ions selected using MANOVA included 7 product ion peaks between 26 m/z and 44 m/z suggesting additional discriminant compounds of lower molecular weight may be present within the biofilm headspace. One of these product ions, 28 m/z may result from the production of hydrogen cyanide and is seen at high intensities (cps) in the headspace analysis of all 3 strains of *P. aeruginosa* when observing the raw data (not shown).

SIM mode was used to quantify the headspace concentration of 17 compounds previously detected using GC-MS and ammonia and hydrogen cyanide, for a scan duration of 60 seconds, resulting in the acquisition of 12 replicate measurements of each compound. Initial analysis of the SIM scan data set using the same background subtraction method as described for the FS data utilised all 19 compounds quantified by SIFT-MS and resulted in insufficient grouping of the three species by hierarchical cluster analysis. *S. pyogenes* and *P. aeruginosa* strains formed species specific clusters, but for *S. aureus*, only two of the strains analysed clustered together with the third strain forming its own distant cluster.

Scrutiny of the SIM scan data shows that strain NCIMB 6571 of *S. aureus* produced several compounds at much greater concentrations than the other strains of this species. For example, 2-methylbutanal, which has been previously reported in the headspace of *S. aureus* cultures (Thorn, Reynolds and Greenman, 2011; Filipiak *et al*, 2012b), was measured at >1000 ppb for this strain, compared to between 40 and 110 ppb for the other two strains of *S. aureus*. Although the specific compounds produced by the three strains of *S. aureus* are similar, there appear to be differences in the levels of production between strains, which may be causing *S. aureus* NCIMB 6571 to be grouped separately to the other strains of *S. aureus* in the cluster analysis. This suggests strain to strain variation in the activity or production of the metabolic enzymes responsible for the production of these metabolites.

Of the 19 compounds quantified using SIFT-MS SIM scans, five are located in the region of the PCA loading plot (figure 6.4) associated with the positioning of *P. aeruginosa* on the associated plot of PCA score; ethanol, dimethyl sulphide, dimethyl disulphide, hydrogen cyanide and ammonia. One compound; acetone, appears to influence the position of *S. pyogenes* and the remaining 13 compounds; 1-butanol, Isobutyl alcohol, 2-methyl-2-propanol, 3-methyl-1-butanol, acetaldehyde, 2-methylpropanal, 2-methylbutanal, 3-methylbutanal, acetoin, butanone, 2,3-butanedione, 3-methylbutanoic acid and butane are most strongly associated with the position of *S. aureus* on the PCA plot.

MANOVA was used to identify which of the 19 compounds quantified occurred at significantly ($p < 0.01$) different concentrations between the three bacterial species analysed. This identified 8 compounds; 3-methyl-1-butanol, 2-methyl-2-propanol,

acetaldehyde, 2-methylbutanal, 3-methylbutanal, 2,3-butanedione, dimethyl sulphide and hydrogen cyanide, which were then selected for further analysis as potentially discriminant compounds. Hierarchical cluster analysis carried out using these 8 compounds gave rise to species specific clustering of all biofilm samples. However, it can still be seen in Figure 6.8 that the dissimilarity between strains of *S. aureus* NCIMB 6571 and the other *S. aureus* strains is larger than those within the other two species specific clusters. Analysis of the SIM scan data results in PCA plots that show less reliable species specific grouping than those produced from analysis of the full scan data. Figure 6.9 shows that *P. aeruginosa* biofilms occupy a discrete region on the two dimensional plot, but that one *S. pyogenes* biofilm appears to group closer to *S. aureus* than the other *S. pyogenes* biofilms. However, *S. aureus* and *S. pyogenes* do separate when plotted against the third principal component (Appendix II, Figure S2).

Figure 6.9 show that of the 8 compounds selected using MANOVA, hydrogen cyanide and dimethyl sulphide are driving the position of *P. aeruginosa* on the associated PCA plot. Both of these compounds have been identified and quantified in the headspace of *P. aeruginosa* culture in a previous study (Shestivska *et al.*, 2012) which used a similar approach, combining GC-MS and SIFT-MS for the analysis of *P. aeruginosa* cultured using liquid and solid media. In addition, hydrogen cyanide production by *P. aeruginosa* has been widely reported in the literature (Castric, Ebert and Castric, 1979; Askeland and Morrison, 1983; Gilchrist *et al.*, 2011, 2013; Smith *et al.*, 2013; Neerincx *et al.*, 2015), hence the inclusion of this compound in this study.

Six compounds; 2-methyl-2-propanol, 3-methyl-1-butanol, acetaldehyde, 2-methylbutanal, 3-methylbutanal, 2,3-butanedione, are driving the position of *S. aureus* on the PCA plot (Figure 6.9) suggesting high levels of production of these compounds from this species. Acetaldehyde and 2-methylbutanal were detected in the headspace of *S. aureus* liquid cultures in previous studies using SIFT-MS (Thorn, Reynolds and Greenman, 2011; Chippendale, Španěl and Smith, 2011), and 2-methyl-1-propanol, 3-methyl-1-butanol, acetaldehyde, 3-methylbutanal and 2,3-butanedione have been detected from *S. aureus* cultures by GC-MS (Filipiak *et al.*, 2012). Conversely, no compounds are strongly associated with the position of *S. pyogenes*, demonstrating that this species does not produce any of these compounds at high levels. Catabolism of pyruvate and leucine give rise to a number of the compounds responsible for the discrimination of *S. aureus* from the other two species; 3-methylbutanal and 3-methyl-1-butanol from leucine, and acetaldehyde and 2,3-butanedione from pyruvate. Suggesting that the enzymes required for these metabolic processes are produced by this species and not by the others.

There is considerable overlap between *S. pyogenes* and uninoculated controls in Figure 6.9, but unlike the FS data set, plotting the second and third principal components does not aid discrimination of *S. pyogenes* from uninoculated control samples. This suggests that using the specific volatile compounds identified within this work may not be suitable for successful discrimination of *S. pyogenes* from uninoculated controls. However, this may be possible if additional compounds that drive the discrimination of *S. pyogenes* can be identified. For example, in Figure 6.7,

there are seven product ions strongly associated with the positioning of *S. pyogenes* biofilms on the PCA plot (26, 30, 60, 144, 161, 175 and 196 m/z).

Cross referencing with the LabSyft library reveals possible compound identifications for three of these product ions, 60; trimethylamine, 161; 2-nonanone/decane and 175; decanal. However, a previous study of microbial volatiles that included trimethylamine did not detect this compound in the headspace of the strain of *S. pyogenes* analysed (Thorn, Reynolds and Greenman, 2011). Further investigation of volatile metabolites produced by *S. pyogenes* is warranted, as few studies have included this organism to date and only a limited number of volatile metabolites have been identified (Julák *et al.*, 2003; Thorn, Reynolds and Greenman, 2011).

In order to fully develop the use of quantification of volatile headspace compound concentrations for discrimination between these bacterial species and discrimination from control samples, it will be essential to identify the additional compounds that give rise to the product ions that drive the discrimination between *S. pyogenes* biofilms and uninoculated controls.

Comparison of the 22 'core' product ion peaks within the FS data set, with the SIFT-MS product ions used for quantification in the SIM scan analysis, shows that just 4 of the FS product ions are accounted for within the compounds quantified. These are 28; hydrogen cyanide, 63; dimethyl sulphide, 71; 3-methyl-1-butanol and 87; 2-methylbutanal/3-methylbutanal/2,3-Butanedione, suggesting the presence of further, as yet unidentified, discriminant compounds.

Analysis of multispecies biofilms complicates possible species discrimination. The data presented in Table 6.3 indicates that rather than a mixture of volatile compounds or product ion peaks associated with all species being detected, the volatile headspace is dominated by one of the species present within the biofilm. This is particularly evident with biofilms containing *P. aeruginosa* and *S. aureus* where the presence of *P. aeruginosa* appears to suppress the majority of the volatile compounds produced by *S. aureus* as a single species biofilm, resulting in a headspace analysis that closely mirrors that of *P. aeruginosa* alone.

However, a study using GC-MS to investigate volatile compound release and uptake by *S. aureus* and *P. aeruginosa* mono-cultures in liquid media found that a number of aldehydes were taken up from the media by *P. aeruginosa* (Filipiak *et al*, 2012a). The authors also found that a variety of these aldehydes were released by *S. aureus* cultures, several of which are included in this chapter; 2-methylpropanal, 3-methylbutanal, acetaldehyde, 2,3-butanedione. This suggests that the absence of these compounds from the headspace of *S. aureus* and *P. aeruginosa* multispecies biofilms may instead be a result of uptake by *P. aeruginosa* rather than suppression of release from *S. aureus*. This may explain the absence of *S. aureus* associated compounds from the biofilm headspace despite the enumeration data indicating that *S. aureus* is able to grow to 10^9 cfu slide⁻¹ in the presence of *P. aeruginosa*.

This finding requires further investigation if volatile analysis is to be used for the diagnosis of polymicrobial chronic wound infection. However, this would be less of an issue for diagnosis of infection of acute wounds, which generally results from invasion of a single pathogenic species and where early management of such

infections is essential to minimise the risk of sepsis (Edwards-Jones and Flanagan, 2013; Ma, Tian and Liang, 2016; Patil *et al.*, 2017). The findings reported in this chapter suggest that development of a diagnostic test, for identification of 3 important pathogens associated with causing clinically relevant wound infection, is feasible using volatile analysis.

Chapter 7: Discussion & Future Work

7.1 GENERAL DISCUSSION

For the first time, this research investigated volatile profiles of planktonic pathogenic bacteria cultured in a simulated wound fluid. This approach was then further progressed through the development and application of a collagen wound biofilm model continuously perfused with a simulated wound fluid to more closely simulate wound-like growth conditions. Comparison of detected volatile product ions (following background subtraction and a 10 cps threshold) highlights the presence of 30 product ions that are common to both the planktonic and biofilm models that were studied. The application of further thresholding of the detected product ions (a minimum of 10 cps in at least two strains of any species), resulted in a more selective profile of 26 product ions that were then used to discriminate species cultured within SWF. When these 26 volatile compounds are compared with product ions data derived from FS analysis of bacterial biofilms (discussed in Chapter 6), then 17 volatile compound product ions can be identified as being common to both the planktonic and biofilm volatiles data set. From this discrete set of 17 common product ion peaks (table 7.1), one product ion peak (28 m/z) influences the positioning of *P. aeruginosa* on both PCA plots that are shown in Figures 3.7 and 5.2 respectively. The product ion peak at 28 m/z may be indicative of hydrogen cyanide, a compound which has previously been reported as a potential biomarker of *P. aeruginosa* infection (Gilchrist *et al.*, 2011; Smith *et al.*, 2013a). Due to this, hydrogen cyanide was also included in the SIM scan analysis of biofilm headspace and was detected for all strains

of *P. aeruginosa* and subsequently selected by MANOVA as a potential discriminatory volatile compound. Hydrogen cyanide was not detected in the headspace of *S. aureus* or *S. pyogenes* bacterial biofilms. In total, 12 volatile compound product ion peaks influence the positioning of *S. aureus* on the PCA plots associated with planktonic and biofilm data sets (selected using t-tests and thresholding) have been identified. These are listed in Table 7.1 with suggested volatile compounds which these product ions may be derived from, based on cross referencing with the Syft Voice200 volatile compound library. Of the 17 compounds listed in Table 7.1, four do not show a clear association with the positioning of *S. aureus*, *S. pyogenes* or *P. aeruginosa* on the PCA plots from the planktonic culture data (Figure 3.2). The product ions 31 and 35 m/z drive the positioning of *E. coli*, whilst 49 and 50 m/z are closely associated with the positioning of *P. mirabilis* within this data set. Within the biofilm culture data (Figure 6.2) 35, 49 and 50 m/z, do not show a definitive association with any of the three species analysed, instead locating within the bottom right sector of the loading plot (Figure 6.2). Nine of the 17 product ions (listed in Table 7.1) common to planktonic and biofilm data sets (selected using t-tests and thresholding), were also included when the MANOVA statistical test was used to select discriminatory product ions within the biofilm data set. These product ions are 28, 50, 63, 64, 69, 87, 101, 105 and 106 m/z. Several of the compounds, which may be responsible for the product ions detected by SIFT-MS in full scan mode, were also detected by GC-MS and included in the subsequent SIM mode analysis, as detailed in chapter 6. The confirmation of the identity of these product ions from different analytical techniques gives increased confidence to the importance of these compounds for the discrimination of these

wound associated bacterial species. For example, 2,3-butanedione, 2-methylbutanal and 3-methylbutanal were detected from *S. aureus* biofilm headspace by GC-MS and also by SIFT-MS in SIM scan mode, and also correspond to product ion peaks associated with the identification of *S. aureus* within the FS headspace analysis. Furthermore, 2,3-butanedione, 2-methylbutanal and 3-methylbutanal have all previously been detected in the headspace of *S. aureus* cultures in other studies using SIFT-MS or GC-MS (Thorn, Reynolds and Greenman, 2011; Filipiak *et al.*, 2012). Acetoin was also identified from the headspace of *S. aureus* biofilms using GC-MS and detected using SIFT-MS in SIM scan mode in this study as well as in the headspace of *S. aureus* cultures in a previous study using GC-MS for quantification (Filipiak *et al.*, 2012b). However, in this present study, acetoin was detected at low levels in the headspace of *S. aureus* biofilms and was not selected as a potential discriminatory compound using MANOVA.

Table 7.1: Discriminatory volatile compound product ion peaks common to both the planktonic (Chapter 3) and biofilm (Chapter 6) headspace SIFT-MS analysis, with possible compound identifications based on the LabSyft compound library.

m/z ion	SWF planktonic culture			Collagen biofilm model			Compound
	SP	PA	SA	SP	PA	SA	
28		✓			✓		Hydrogen Cyanide
31						✓	Formaldehyde
35							Hydrogen sulphide
45			✓			✓	Acetaldehyde
46			✓			✓	Dimethyl amine
49							Methylmercaptan
50							-
51			✓			✓	Methanol
63			✓			✓	Acetaldehyde, Dimethylsulphide/ethanthiol
64			✓			✓	Hydrogen cyanide
69			✓			✓	2-methylbutanal/3-methylbutanal
87			✓			✓	2-methylbutanal/3-methylbutanal/2,3-butanedione
89			✓			✓	Acetoin/butanoic acid
101			✓			✓	3-methyl-2-pentanone/hexanal
105			✓			✓	3-methylbutanal/2,3-butanedione (secondary product)
106			✓			✓	-
113			✓			✓	2-octanol/2-heptenal

Acetaldehyde was detected using GC-MS, in the headspace of *S. pyogenes* biofilms cultured in the collagen wound biofilm model and from all three species, *S. pyogenes*, *S. aureus* and *P. aeruginosa*, using SIFT-MS in SIM scan mode. The 45 m/z product ion peak included in the FS analysis of biofilm headspace was detected at the greatest intensity from *S. aureus* biofilms, whereas acetaldehyde was detected at the lowest concentration from this species by SIFT-MS. This indicates that there may be other compounds, in addition to acetaldehyde, present in the headspace that result in the production of a product ion with a mass-to-charge ratio of 45 m/z. For example, lactic acid can give rise to a product ion peak at 45 m/z, which is known to be produced by *S. aureus* as an end point of glucose fermentation (Smith, 1991).

Conversely, there are 9 discriminatory product ions, obtained from the headspace analysis of planktonic cultures in SWF that were not included as discriminant product ions in the analysis of the FS data set of product ions derived from the headspace of biofilm cultures. Furthermore 29 product ions that were included for the analysis of biofilm data were not present in the planktonic data set. Of the 9 product ions in the planktonic culture data set, 4 were detected predominantly in the headspace of *E. coli* cultures and therefore the absence of these product ions is expected, since *E. coli* was not cultured in the collagen wound biofilm model. Of the remaining five product ions, three were detected predominantly from *S. aureus* planktonic cultures, whereby the product ion 81 m/z could potentially be a secondary product ion derived for acetaldehyde, 109 m/z from 4-methylphenol, or perhaps as a secondary product ion from 2-methylpropanal. The product ion at 123 m/z may be derived from ethylphenol, or could arise as a secondary product ion of 3-methylbutanal or 2,3-

butanedione, while the LabSyft library does not provide any likely compounds responsible for the 92 m/z product ion. The analysis of the headspace of biofilms of *P. aeruginosa*, *S. pyogenes* and *S. aureus* identified 29 potentially discriminant product ions using 10 cps as a threshold that were not selected in the planktonic culture data set. These include several product ions identified which could arise from compounds subsequently identified by GC-MS; ammonia (18 and 36 m/z), acetone (59 and 77 m/z), butanone (91 m/z) and butane (77 m/z). This also highlights the potential identification of additional compounds with further GC-MS analysis. The selection of a large number of discriminatory product ions using MANOVA for the analysis of the FS biofilm data, many of which are in addition to those derived from the 19 compounds included in the SIM mode analysis, provides further evidence of this. Identification of additional volatile compounds from which these product ions are derived, may facilitate improved groupings for identified bacterial species using SIM scan data, resulting in improved discrimination between bacterial species. In particular, it will be necessary to identify the compounds that give rise to the product ions that drive separation of *S. pyogenes* from uninoculated controls in Figure 6.7. This would facilitate the discrimination of *S. pyogenes* from uninoculated controls based on the quantification of known volatile compounds. This was not possible using SIM scan analysis with the compounds (19 in total) utilised within this study. This study determined that analysis of the headspace of multispecies biofilms containing two or more species of *S. aureus*, *S. pyogenes* and *P. aeruginosa*, resulted in a headspace profile dominated by the volatile compounds associated with one of the species present. When *P. aeruginosa* was present in the multispecies biofilm, the

profile of the biofilm headspace was most similar to that of *P. aeruginosa* single species biofilms. In the absence of *P. aeruginosa* (i.e. *S. aureus* and *S. pyogenes* multispecies biofilms), the volatile headspace profile was similar to that of single species *S. aureus* biofilms.

7.2 SUMMARY AND CONCLUSIONS

This research was carried out to investigate if volatile profiles derived from bacterial species associated with causing wound infection could be detected and utilised to enable discrimination. The rationale for this study was to inform the future development of rapid diagnostics that will aid diagnosis of wound infection and facilitate timely and appropriate treatment. Current clinical practice relies on clinical experience complimented by surface swab microbiology and blood tests for markers of inflammation. This approach often leads to empirical prescribing of broad spectrum antibiotics.

Point of care diagnostics have the potential to revolutionise treatment of wound infection. The ability to rule out infection would prevent over-use of antimicrobials when there is no clinical need. In addition, early identification of the causative organism of infection, combined with knowledge of local epidemiology, would expedite selection of the most appropriate drug, improving patient outcomes.

7.2.1 *Chapter 3*

This chapter addressed the first aim, “to investigate if planktonic cultures of wound associated bacteria produce species specific volatile profiles in vitro, enabling discrimination”.

This study demonstrates that using SIFT-MS and multivariate statistical analysis it is possible to discriminate wound-associated bacterial species based on the profile of selected SIFT-MS product ions and demonstrates that bacterial species associated

with causing wound infection produce species specific volatile profiles *in vitro*, when grown in planktonic culture in TSB and SWF. Volatile profiles vary between species and to a lesser extent, between strains of the same species under specific culture conditions. Culture conditions, including the composition of culture media and duration of incubation, influence the range of product ions and count rates of the resultant volatile compound mass spectra. It is evident from these results, as well as from other published studies, that culture conditions impact the production of microbial volatile metabolites. The ability to discriminate wound associated species when cultured in SWF, which provides a similar range of nutrients to wound exudate, lays the foundations for the development of this research in the subsequent chapters of this thesis.

7.2.2 Chapter 4

Chapter 4 addresses the second aim, “to investigate if the concept of species discrimination based on volatile compound detection could be applied to analysis of discarded wound dressings, as part of routine wound care”.

Following the successful discrimination of six species of bacteria in planktonic culture, a research study was carried out in collaboration with the Children’s burns research centre at Bristol Royal Hospital for Children and Southmead Hospital adult burns centre. The aim of this study was to investigate if the concept of species discrimination based on detected volatile profiles could easily be translated to a clinical setting, through the detection of volatile profiles emanating from discarded

dressings. The rationale for this approach was to try and establish a feasible methodology for the detection of bacterial volatiles directly associated with patients' wounds. This study demonstrated that it is possible to detect volatile profiles from discarded clinical wound dressings, and that the profile of volatiles differs between samples irrespective of dressing type. This suggests that the detected volatile profiles are derived from the patient and/or any bacteria present within the wound. However, these observed differences in the product ion profiles did not form groupings that correspond to the bacterial species detected on the wound surface by routine wound swabbing, when subjected to multivariate analysis (hierarchical cluster analysis). This study highlighted the potential difficulty of validating any new approach to the diagnosis of wound infection. As outlined above, diagnosis relies heavily on experienced clinicians recognising subtle signs and symptoms, and inevitably, the identification of infection will differ between clinicians. The routine use of wound surface swabbing does not represent an effective means of detecting the infecting organisms, particularly if these organisms lie deeper within the wound tissue. These factors will make testing the effectiveness of any new diagnostic methodologies very challenging. The findings of this chapter indicated that additional *in vitro* investigations of the volatile profiles of wound associated organisms grown under wound-like conditions was required before further development of the concept towards clinical applications. This led to the development of the biofilm model and subsequent study reported in Chapters 5 and 6.

7.2.3 Chapter 5

This Chapter addressed the third aim of the thesis “to develop and characterise a suitable biofilm model for culture and headspace analysis of wound associated bacterial biofilms, which provides wound-like culture conditions”.

Development of this model was necessary to better assess the feasibility of volatile analysis for the discrimination of bacterial species growing within a wound, where bacteria will either grow as aggregates on the surface or will be embedded within the semi-solid matrix of the wound bed. The specific culture conditions employed will likely affect the metabolic profile of the organisms under investigation, resulting in a change in the volatile metabolites produced, compared to those detected from the same bacteria grown as planktonic cultures in a simulated wound fluid. A collagen wound biofilm model that combines a continuous flow system with a collagen gel growth matrix has been successfully developed to enable the culture of wound associated microorganisms under controlled conditions that more closely simulate a real wound environment. Reproducible culture of steady-state biofilms of *S. aureus*, *P. aeruginosa* and *S. pyogenes* within the developed collagen wound biofilm model have been successfully characterised. The model can be utilised for real-time analysis of volatile metabolites throughout biofilm formation and growth, and for discrete sampling to allow comparison of headspace volatile profiles between species of bacterial biofilms at specific time points. The collagen wound biofilm model is also suitable for assessing antimicrobial efficacy against biofilms cultured under ‘wound-like’ conditions *in vitro*. Using the collagen wound biofilm model for the evaluation

of antimicrobial efficacy, a clinically relevant ceftazidime concentration was shown to fail in eradicating *P. aeruginosa*.

7.2.4 Chapter 6

Chapter 6 addressed the final two thesis aims, “to investigate if biofilm cultures of wound associated bacteria produce species specific volatile profile *in vitro* that can be used to discriminate between species” and “to investigate the effect of multispecies biofilms on bacterial volatile profiles *in vitro*”. The collagen wound biofilm model was applied to the study of volatile metabolites produced by wound associated bacterial species, allowing investigation of the volatile profiles detected from *S. aureus*, *P. aeruginosa* and *S. pyogenes* when these species are cultured as biofilms under wound-like growth conditions.

This study demonstrates that *S. aureus*, *P. aeruginosa* and *S. pyogenes* biofilms produce headspace gases that vary between species. These differences can be detected as volatile compound product ion profiles when employing SIFT-MS in full scan mode and through the quantification of specific volatile compounds in selected ion mode. Combined with the use of multivariate statistical analysis, these differences in volatile headspace profiles can be used to successfully discriminate between species. However, the discrimination between *S. pyogenes* and uninoculated controls was only possible using full scan product ion profiles and not by the data obtained from the quantification of 19 specific volatile compounds. The collagen wound biofilm model was also utilised to culture multispecies biofilms

containing *S. aureus*, *P. aeruginosa* and *S. pyogenes* either as dual species cultures or as biofilms containing all three bacterial species. Enumeration after 48 hours of total culture time demonstrated successful co-culture of these organisms in the collagen wound biofilm model. SIFT-MS was used to analyse and compare volatiles detected in the headspace of multispecies and single species biofilms. Identification of bacterial species using the detection of volatile metabolites is more complex when multiple species are present within the biofilm. In general, the multispecies biofilm headspace was dominated by volatiles strongly associated with one of the species present rather than exhibiting a range of volatiles characteristic of all species within the biofilm. The results of this study indicate that in a polymicrobial wound biofilm, the species investigated may be identified by the volatiles produced, but that this is also dependent upon the extent to which other bacterial species are present. Interestingly, the PCA plot comparing volatile profiles of single and multispecies biofilms suggests that *P. aeruginosa* may be identified regardless of the other species present, and that *S. aureus* may be identified if *P. aeruginosa* is absent. This study suggests that the application of volatile analysis to the diagnosis of clinically relevant wound infection may prove useful for identifying the causative organism where only a single organism is present, and for identifying *P. aeruginosa* and possibly *S. aureus* within an infection of polymicrobial aetiology.

Overall, this research has successfully demonstrated the use of volatile analysis for discrimination between three important pathogens associated with causing wound infections. The results presented within this thesis indicate that this approach to

wound diagnostics may be of particular use for the identification of the cause of infection within acute wounds, which are often caused by a single species. Application to the diagnosis of chronic wounds, which are more likely to be polymicrobial in aetiology, will be more complicated and will require further study.

The results of this research indicate that use of volatile analysis has excellent potential as a novel approach to the diagnosis of wound infection.

7.3 FUTURE WORK

7.3.1 *Volatile Analysis*

This research has successfully demonstrated the application of volatile analysis for the discrimination of wound associated bacterial species, primarily *P. aeruginosa*, *S. aureus* and *S. pyogenes*. Although these species are commonly isolated from wounds, a diverse range of other organisms are also capable of causing wound infection (Bessa *et al.*, 2015; Norbury *et al.*, 2016). Analysis of volatile profiles of a broad range of organisms that are implicated in wound infection, cultured in the collagen wound biofilm model must also be undertaken to further this research. This should include clinical isolates of all species of interest in addition to reference strains, and additional isolates of species already analysed. Analysis of additional strains and species under wound like conditions, in the collagen wound biofilm model, will help elucidate the potential of volatile profiling as a novel approach to the diagnosis of wound infection.

The GC-MS undertaken during this study identified 17 volatile compounds from the head space of three bacterial species, *P. aeruginosa*, *S. aureus* and *S. pyogenes*. To maximise the potential discrimination between a broad range of wound associated bacterial species, additional and extensive GC-MS analysis of all species of interest should be performed. As well as covering a broad range of wound associated bacterial species, this analysis should focus on optimising the GC-MS method, to maximise compound identification, and this may require the use of a variety of methods/materials to capture the volatile compounds. A number of pre-

concentration methods have been utilised for the identification of microbial volatiles from human breath samples, including thermal desorption tubes, SPME fibres and headspace sorptive extraction, all of which use a range of sorbent materials that exhibit affinities for a variety of compound types (Thalavitiya Acharige, Koshy and Koo, 2018). Application of multiple extraction methods could also be applied to the identification of volatile metabolites released from biofilm cultured bacteria, to maximise the range of compounds captured and ultimately identified by GC-MS analysis.

In addition, the collagen wound biofilm model combined with SIFT-MS could be used to monitor biofilm headspace volatile profiles during antimicrobial treatment. Not only to identify changes in volatile profiles which may occur during treatment, but also to determine if these profiles vary between susceptible and resistant isolates. A recent study using thermal desorption-gas chromatography-mass spectrometry (TD-GC-MS) found that the volatile profiles of bacterial species associated with causing urinary tract infections varied depending on antibiotic sensitivity (Smart *et al.*, 2019). The authors found that there were differences between sensitive and resistant isolates under normal culture conditions, but a greater number of compounds differed when the cephalosporin antibiotic cephalexin was added to the culture media. Further work is required in this area to explore this further.

7.3.2 *Collagen Wound Biofilm Model*

Within this research, the developed collagen wound biofilm model was utilised for the analysis of volatile headspace of wound associated biofilms and for the assessment of the efficacy of ceftazidime against *P. aeruginosa* biofilms (chapter 5). However, the use of this model could be applied to any number of *in vitro* studies focused on bacterial species associated with wound infection. Such studies could include assessing the efficacy of antimicrobial treatments on a range of pathogens associated with wound infection at various stages of biofilm development.

In addition, this model system could be utilised to investigate treatment strategies against multispecies biofilms, to investigate the effect of treatment on polymicrobial infections such as those commonly found in chronic wounds. In direct relation to the work described in this thesis, it would be of interest to utilise this model to further investigate the interactions between species when culturing multispecies biofilms. For example, confocal microscopy was used within this research to compare the structure of treated and untreated *P. aeruginosa* biofilms. This technique combined with species specific staining, such as fluorescent in situ hybridisation (FISH) could be utilised to visualise physical interactions between bacterial species within multispecies biofilms. Furthermore, it may also be possible to determine if the spatial arrangement of the included species changes as the biofilm matures. The use of FISH combined with confocal microscopy to visualise the orientation of five bacterial species and *Candida albicans* within multispecies biofilms has been previously demonstrated (Thurnheer, Gmür and Guggenheim, 2004).

In addition, further developments could be made to the collagen wound biofilm model to improve the provision of a 'wound like' environment by this model system. *In vivo*, organisms infecting the wound bed will be 'fed' from below by exudate seeping from the host tissue. Would biofilm models incorporating the supply of nutrients from below have been developed (Anderl, Franklin and Stewart, 2000; Duckworth *et al*, 2018). However, these model systems involve the development of biofilms on the surface of a permeable membrane (polycarbonate or cellulose).

Modification of the collagen wound biofilm model to supply SWF to the growing biofilm from below, while maintaining the continuous flow of fluid, would facilitate delivery of nutrients via a mechanism more akin to the real wound environment. Adaptation of the collagen wound biofilm model to facilitate delivery of simulated wound fluid in this manner is likely to be challenging due to the fragile nature of the collagen gel matrix, but casting the gels on to a permeable membrane instead of directly on to glass slides may facilitate this approach. Furthermore, delivery of SWF in this manner would allow the collagen wound biofilm model to be used for a wider range of antimicrobial studies, including assessment of topical treatments and antimicrobial dressing.

7.3.3 *Statistical Analysis*

The multivariate techniques used within this research, hierarchical cluster analysis and principal component analysis, are both unsupervised methods of analysis. Only the matrix of data is taken in to account during analysis and as such, these models

provide an unbiased summary of the data set without introducing bias from assigning groupings to the samples (Grace and Hudson, 2016). Of these two analyses, hierarchical cluster analysis gives a more precise description of the relationship between each individual sample within the data set. Although plotting only the first two or three principal components generated by PCA results in the loss of some of the information contained within the original data set, the majority of the variability will be accounted for. This method has the advantage that the plots of sample PCA scores and loading plots can be interpreted in combination. Thus allowing the influence of the original variables within the model and therefore on the separation of sample grouping to be determined.

The statistical approach used within this research could be developed further to employ the use of supervised statistical techniques such as partial least squared discriminant analysis (PLS-DA) where known group classification is included within the analysis. PLS-DA is often used to compliment PCA and aims to identify the differences between the known sample groupings and to identify the biologically relevant features within the model which account for such differences (Saccenti *et al.*, 2014; Grace and Hudson, 2016). A significant advantage of PLS-DA is that the model defines the relationship between the data set and the sample categories, so that the sample category can then be predicted based on the structure of an unknown data set (Szymańska *et al.*, 2012). Use of this statistical method to further analyse the data obtained during this research would allow testing of the model following the analysis of additional strains of each species by SIFT-MS as suggested in the previous section. The ability to predict sample groupings i.e. bacterial species,

based on the matrix of SIFT-MS data will be an essential step in the development of this research towards a diagnostic tool that can be implemented in a clinical setting. Interest in the use of machine learning for the analysis and implementation of multivariate data sets, including metabolomics data, has been increasing in recent years. Supervised machine learning is an application of artificial intelligence, where an algorithm is taught to map input data to specific outputs. Once trained, the algorithm can then classify unknown data based on what it has learned (Palma *et al*, 2018). Combining real-time detection of bacterial metabolites emanating from infected wounds with rapid analysis is a key requirement for useful implementation of this research for the development of point of care diagnostics.

7.3.4 *Diagnostic Applications*

The underlying motivation for the research described in this thesis was the need to transform the diagnosis of wound infection. Not only to improve patient outcomes, but also to facilitate appropriate prescribing of antibiotics only when an infection is genuinely present, an important strategy in the response to the AMR crisis. Development of the use of volatile analysis for clinical application could utilise SIFT-MS for direct or indirect assessment of patient wounds. Due to the size and high cost of a SIFT-MS instrument, this approach may only be feasible in a centralised hospital setting. A SIFT-MS study of volatile compounds from healthy human volunteers (Turner *et al*, 2008) successfully demonstrates the feasibility of collecting volatiles from human skin for direct analysis by SIFT-MS.

Secondly, development of a portable sensor device for point of care testing would enable widespread use. So called ‘electronic-nose’ technologies have been developed for application to disease diagnosis through detection of volatile compounds (Pavlou, Turner and Magan, 2002; Turner and Magan, 2004; Sethi, Nanda and Chakraborty, 2013). These systems consist of sensor arrays (e.g. conducting polymer sensors, metal oxide sensors, electrochemical sensors) for volatile characterisation generally based on pattern recognition, rather than detection of specific volatile compounds, and could be applied to the detection of volatile profiles of wound associated bacteria. Any new approach to wound diagnostics would require validation. However, the lack of a current gold standard for the diagnosis of wound infection may make this challenging; a large scale trial in parallel with current diagnostic protocols would be required.

References

- Agostinho, A.M., Hartman, A., Lipp, C., Parker, A.E., Stewart, P.S. and James, G.A. (2011) An in vitro model for the growth and analysis of chronic wound MRSA biofilms. *Journal of Applied Microbiology*. 111 (5), pp. 1275–1282. doi:10.1111/j.1365-2672.2011.05138.x.
- Allardyce, R.A., Hill, A.L. and Murdoch, D.R. (2006) The rapid evaluation of bacterial growth and antibiotic susceptibility in blood cultures by selected ion flow tube mass spectrometry. *Diagnostic Microbiology and Infectious Disease*. 55 (4), pp. 255–261. doi:10.1016/j.diagmicrobio.2006.01.031.
- Allardyce, R.A., Langford, V.S., Hill, A.L. and Murdoch, D.R. (2006) Detection of volatile metabolites produced by bacterial growth in blood culture media by selected ion flow tube mass spectrometry (SIFT-MS). *Journal of Microbiological Methods*. 65 (2), pp. 361–365. doi:10.1016/j.mimet.2005.09.003.
- Alou, L., Aguilar, L., Sevillano, D., Giménez, M.-J., Echeverría, O., Gómez-Lus, M.-L. and Prieto, J. (2005) Is there a pharmacodynamic need for the use of continuous versus intermittent infusion with ceftazidime against *Pseudomonas aeruginosa*? An in vitro pharmacodynamic model. *Journal of Antimicrobial Chemotherapy*. 55 (2), pp. 209–213. doi:10.1093/jac/dkh536.
- Alrawi, M., Crowley, T.P. and Pape, S.A. (2014) Bacterial colonisation of the burn wound: A UK experience. *Journal of Wound Care*. 23 (5), pp. 274–277. doi:10.12968/jowc.2014.23.5.274.
- Alvarez, C.S., Sierra-Sosa, D., Garcia-Zapirain, B., Yoder-Himes, D. and Elmaghraby, A. (2019) Detection of volatile compounds emitted by bacteria in wounds using gas sensors. *Sensors*. 19 (7), 1523. doi:10.3390/s19071523.
- Anderl, J.N., Franklin, M.J. and Stewart, P.S. (2000) Role of Antibiotic Penetration Limitation in *Klebsiella pneumoniae* Biofilm Resistance to Ampicillin and Ciprofloxacin. *Antimicrobial Agents and Chemotherapy*. 44 (7), pp. 1818–1824. doi:10.1128/AAC.44.7.1818-1824.2000.
- Archer, N.K., Mazaitis, M.J., Costerton, J.W., Leid, J.G., Powers, M.E. and Shirtliff, M.E. (2011) *Staphylococcus aureus* biofilms. *Virulence*. 2 (5), pp. 445–459. doi:10.4161/viru.2.5.17724.
- Ashrafi, M., Novak-Frazer, L., Bates, M., Baguneid, M., Alonso-Rasgado, T., Xia, G., Rautemaa-Richardson, R. and Bayat, A. (2018) Validation of biofilm formation on human skin wound models and demonstration of clinically translatable bacteria-specific volatile signatures. *Scientific Reports*. 8 (1), 9431. doi:10.1038/s41598-018-27504-z.

- Askeland, R.A. and Morrison, S.M. (1983) Cyanide production by *Pseudomonas fluorescens* and *Pseudomonas aeruginosa*. *Applied and environmental microbiology*. 45 (6), pp. 1802–1807.
- Aubert, G., Carricajo, A., Coudrot, M., Guyomarc'h, S., Auboyer, C. and Zeni, F. (2010) Prospective Determination of Serum Ceftazidime Concentrations in Intensive Care Units. *Therapeutic Drug Monitoring*. 32 (4), pp. 517–519. doi:10.1097/FTD.0b013e3181e60ca6.
- Audrain, B., Farag, M.A., Ryu, C.-M. and Ghigo, J.-M. (2015) Role of bacterial volatile compounds in bacterial biology. *FEMS Microbiology Reviews*. 39 (2), pp. 222–233. doi:10.1093/femsre/fuu013.
- Babic, M., Hujer, A. and Bonomo, R. (2006) What's new in antibiotic resistance? Focus on beta-lactamases. *Drug Resistance Updates*. 9 (3), pp. 142–156. doi:10.1016/j.drug.2006.05.005.
- Bagge, N., Hentzer, M., Andersen, J.B., Ciofu, O., Givskov, M. and Hoiby, N. (2004) Dynamics and Spatial Distribution of β -Lactamase Expression in *Pseudomonas aeruginosa* Biofilms. *Antimicrobial Agents and Chemotherapy*. 48 (4), pp. 1168–1174. doi:10.1128/AAC.48.4.1168-1174.2004.
- Barajas-Nava, L.A., López-Alcalde, J., Roqué i Figuls, M., Solà, I. and Bonfill Cosp, X. (2013) Antibiotic prophylaxis for preventing burn wound infection. In: Leticia A Barajas-Nava (ed.). *Cochrane Database of Systematic Reviews*. (6), CD008738. doi:10.1002/14651858.CD008738.pub2.
- Baroni, A., Buommino, E., De Gregorio, V., Ruocco, E., Ruocco, V. and Wolf, R. (2012) Structure and function of the epidermis related to barrier properties. *Clinics in Dermatology*. 30 (3), pp. 257–262. doi:10.1016/j.clindermatol.2011.08.007.
- Bay, L., Kragh, K.N., Eickhardt, S.R., Poulsen, S.S., Gjerdrum, L.M.R., Ghathian, K., Calum, H., Ågren, M.S. and Bjarnsholt, T. (2018) Bacterial Aggregates Establish at the Edges of Acute Epidermal Wounds. *Advances in Wound Care*. 7 (4), pp. 105–113. doi:10.1089/wound.2017.0770.
- Belkaid, Y. and Segre, J.A. (2014) Dialogue between skin microbiota and immunity. *Science*. 346 (6212), pp. 954–959. doi:10.1126/science.1260144.
- Berg, H.C. and Block, S.M. (1984) A Miniature Flow Cell Designed for Rapid Exchange of Media Under High-power Microscope Objectives. *Microbiology*. 130 (11), pp. 2915–2920. doi:10.1099/00221287-130-11-2915.
- Bertesteanu, S., Triaridis, S., Stankovic, M., Lazar, V., Chifiriuc, M.C., Vlad, M. and Grigore, R. (2014) Polymicrobial wound infections: Pathophysiology and current therapeutic approaches. *International Journal of Pharmaceutics*. 463 (2), pp. 119–126. doi:10.1016/j.ijpharm.2013.12.012.

Bessa, L.J., Fazii, P., Di Giulio, M. and Cellini, L. (2015) Bacterial isolates from infected wounds and their antibiotic susceptibility pattern: some remarks about wound infection. *International Wound Journal*. 12 (1), pp. 47–52. doi:10.1111/iwj.12049doi:10.1111/iwj.12049.

Blokhuis-Arkes, M.H.E., Haalboom, M., van der Palen, J., Heinzle, A., Sigl, E., Guebitz, G. and Beuk, R. (2015) Rapid enzyme analysis as a diagnostic tool for wound infection: Comparison between clinical judgment, microbiological analysis, and enzyme analysis. *Wound Repair and Regeneration*. 23 (3), pp. 345–352. doi:10.1111/wrr.12282.

Blumer, C. and Haas, D. (2000) Mechanism, regulation, and ecological role of bacterial cyanide biosynthesis. *Archives of Microbiology*. 173 (3), pp. 170–177. doi:10.1007/s002039900127.

Borlee, B.R., Goldman, A.D., Murakami, K., Samudrala, R., Wozniak, D.J. and Parsek, M.R. (2010) *Pseudomonas aeruginosa* uses a cyclic-di-GMP-regulated adhesin to reinforce the biofilm extracellular matrix. *Molecular Microbiology*. 75 (4), pp. 827–842. doi:10.1111/j.1365-2958.2009.06991.x.

Bowler, P.G. (2002) Wound pathophysiology, infection and therapeutic options. *Annals of Medicine*. 34 (6), pp. 419–427. doi:10.1080/078538902321012360.

Bowler, P.G., Duerden, B.I. and Armstrong, D.G. (2001) Wound Microbiology and Associated Approaches to Wound Management. *Clinical Microbiology Reviews*. 14 (2), pp. 244–269. doi:10.1128/CMR.14.2.244-269.2001.

Bowler, P.G., Jones, S.A., Walker, M. and Parsons, D. (2004) Microbicidal Properties of a Silver-Containing Hydrofiber?? Dressing Against a Variety of Burn Wound Pathogens. *Journal of Burn Care & Rehabilitation*. 25 (2), pp. 192–196. doi:10.1097/01.BCR.0000112331.72232.1B.

Brackman, G., Cos, P., Maes, L., Nelis, H.J. and Coenye, T. (2011) Quorum sensing inhibitors increase the susceptibility of bacterial biofilms to antibiotics in vitro and in vivo. *Antimicrobial Agents and Chemotherapy*. 55 (6), pp. 2655–2661. doi:10.1128/AAC.00045-11.

Branchet, M.C., Boisnic, S., Frances, C., Lesty, C. and Robert, L. (1991) Morphometric analysis of dermal collagen fibers in normal human skin as a function of age. *Archives of Gerontology and Geriatrics*. 13 (1), pp. 1–14. doi:10.1016/0167-4943(91)90011-E.

Branski, L.K., Al-Mousawi, A., Rivero, H., Jeschke, M.G., Sanford, A.P. and Herndon, D.N. (2009) Emerging Infections in Burns. *Surgical Infections*. 10 (5), pp. 389–397. doi:10.1089/sur.2009.024doi:10.1089/sur.2009.024.

Bridier, A., Briandet, R., Thomas, V. and Dubois-Brissonnet, F. (2011) Resistance of

bacterial biofilms to disinfectants: a review. *Biofouling*. 27 (9), pp. 1017–1032. doi:10.1080/08927014.2011.626899.

British Standards Institution (2006) BS EN ISO 20776-1: Clinical laboratory testing and in vitro diagnostic test systems - Susceptibility testing of infectious agents and evaluation of performance of antimicrobial susceptibility test devices. *British Standard Publication*. Available from: <https://www.standardsuk.com/products/BS-EN-ISO-20776-1-2006>.

Buijk, S.L.C.E., Gyssens, I.C., Mouton, J.W., Van Vliet, A., Verbrugh, H.A. and Bruining, H.A. (2002) Pharmacokinetics of ceftazidime in serum and peritoneal exudate during continuous versus intermittent administration to patients with severe intra-abdominal infections. *The Journal of antimicrobial chemotherapy*. 49 (1), pp. 121–128.

Burgeson, R.E. and Christiano, A.M. (1997) The dermal—epidermal junction. *Current Opinion in Cell Biology*. 9 (5), pp. 651–658. doi:10.1016/S0955-0674(97)80118-4.

Caldwell, D.E. and Lawrence, J.R. (1988) Study of attached cells in continuous-flow slide culture. In: *CRC handbook of laboratory model systems for microbial ecosystems*. Boca Raton: CRC Press. pp. 117–138.

Castric, P.A., Ebert, R.F. and Castric, K.F. (1979) The relationship between growth phase and cyanogenesis in *Pseudomonas aeruginosa*. *Current Microbiology*. 2 (5), pp. 287–292. doi:10.1007/BF02602861

Caylet, A., Escudié, R., Gévaudan, G., Hamelin, J., Brockmann, D. and Bernet, N. (2011) Impact of Hydraulic Retention Time (HRT) on biofilm development and microbial competition: molecular analysis and modelling. In: *IWA Biofilm Conference 2011 - Processes in Biofilms*, October 27-30, 2011.

Ceri, H., Olson, M.E., Stremick, C., Read, R.R., Morck, D. and Buret, A. (1999) The Calgary Biofilm Device: new technology for rapid determination of antibiotic susceptibilities of bacterial biofilms. *Journal of clinical microbiology*. 37 (6), pp. 1771–1776.

Chen, W., Zhang, Y.-M. and Davies, C. (2017) Penicillin-Binding Protein 3 Is Essential for Growth of *Pseudomonas aeruginosa*. *Antimicrobial Agents and Chemotherapy*. 61 (1), e01651-16. doi:10.1128/AAC.01651-16.

Chippendale, T.W.E., Gilchrist, F.J., Španěl, P., Alcock, A., Lenney, W. and Smith, D. (2014) Quantification by SIFT-MS of volatile compounds emitted by in vitro cultures of *S. aureus*, *S. pneumoniae* and *H. influenzae* isolated from patients with respiratory diseases. *Analytical Methods*. 6 (8), 2460. doi:10.1039/c4ay00209a.

Chippendale, T.W.E., Španěl, P. and Smith, D. (2011) Time-resolved selected ion

flow tube mass spectrometric quantification of the volatile compounds generated by *E. coli* JM109 cultured in two different media. *Rapid Communications in Mass Spectrometry*. 25 (15), pp. 2163–2172. doi:10.1002/rcm.5099.

Church, D., Elsayed, S., Reid, O., Winston, B. and Lindsay, R. (2006) Burn Wound Infections. *Clinical Microbiology Reviews*. 19 (2), pp. 403–434. doi:10.1128/CMR.19.2.403-434.2006.

Coenye, T. and Nelis, H.J. (2010) In vitro and in vivo model systems to study microbial biofilm formation. *Journal of Microbiological Methods*. 83 (2), pp. 89–105. doi:10.1016/j.mimet.2010.08.018.

Collier, P. and O’Neill, L.J. (2018) Two years on: an update on achievement towards the recommendations of the antimicrobial resistance report. *Journal of Applied Microbiology*. 125 (2), pp. 308–312. doi:10.1111/jam.13933.

Cooper, R., Bjarnsholt, T. and Alhede, M. (2014) Biofilms in wounds: a review of present knowledge. *Journal of Wound Care*. 23 (11), pp. 570–582. doi:10.12968/jowc.2014.23.11.570.

Cooper, R. and Lawrence, J.C. (1996) The isolation and identification of bacteria from wounds. *Journal of Wound Care*. 5 (7), pp. 335–340. doi:10.12968/jowc.1996.5.7.335.

Costello, E.K., Lauber, C.L., Hamady, M., Fierer, N., Gordon, J.I. and Knight, R. (2009) Bacterial Community Variation in Human Body Habitats Across Space and Time. *Science*. 326 (5960), pp. 1694–1697. doi:10.1126/science.1177486.

Costerton, J.W., Geesey, G.G. and Cheng, K.J. (1978) How bacteria stick. *Scientific American*. 238 (1), pp. 86–95.

Costerton, J.W., Lewandowski, Z., Caldwell, D.E., Korber, D.R. and Lappin-Scott, H.M. (1995) Microbial Biofilms. *Annual Review of Microbiology*. 49 (1), pp. 711–745. doi:10.1146/annurev.mi.49.100195.003431.

Costerton, J.W., Stewart, P.S. and Greenberg, E.P. (1999) Bacterial biofilms: A common cause of persistent infections. *Science*. 284 (5418), pp. 1318–1322. doi:10.1126/science.284.5418.1318.

Craciun, S. and Balskus, E.P. (2012) Microbial conversion of choline to trimethylamine requires a glycyl radical enzyme. *Proceedings of the National Academy of Sciences of the United States of America*. 109 (52), pp. 21307–21312. doi:10.1073/pnas.1215689109.

Crompton, R., Williams, H., Ansell, D., Campbell, L., Holden, K., Cruickshank, S. and Hardman, M.J. (2016) Oestrogen promotes healing in a bacterial LPS model of delayed cutaneous wound repair. *Laboratory Investigation*. 96 (4), pp. 439–449.

doi:10.1038/labinvest.2015.160.

Cutting, K.F. and White, R.J. (2002) Maceration of the skin and wound bed 1: its nature and causes. *Journal of Wound Care*. 11 (7), pp. 275–278.
doi:10.12968/jowc.2002.11.7.26414.

Daeschlein, G. (2013) Antimicrobial and antiseptic strategies in wound management. *International Wound Journal*. 10 (s1), pp. 9–14.
doi:10.1111/iwj.12175.

Dalton, T., Dowd, S.E., Wolcott, R.D., Sun, Y., Watters, C., Griswold, J.A. and Rumbaugh, K.P. (2011) An In Vivo Polymicrobial Biofilm Wound Infection Model to Study Interspecies Interactions. *PLoS ONE*. 6 (11), e27317.
doi:10.1371/journal.pone.0027317.

Demidova-Rice, T.N., Hamblin, M.R. and Herman, I.M. (2012) Acute and Impaired Wound Healing. *Advances in Skin & Wound Care*. 25 (7), pp. 304–314.
doi:10.1097/01.ASW.0000416006.55218.d0.

DiMuzio, E.E., Healy, D.P., Durkee, P., Neely, A.N. and Kagan, R.J. (2014) Trends in Bacterial Wound Isolates and Antimicrobial Susceptibility in a Pediatric Burn Hospital. *Journal of Burn Care & Research*. 35 (5), pp. e304–e311.
doi:10.1097/BCR.0000000000000058.

Dini, V., Salvo, P., Janowska, A., Di Francesco, F., Barbini, A. and Romanelli, M. (2015) Correlation Between Wound Temperature Obtained With an Infrared Camera and Clinical Wound Bed Score in Venous Leg Ulcers. *Wounds*. 27 (10), pp. 274–278.

Djordjevic, D., Wiedmann, M. and McLandsborough, L.A. (2002) Microtiter Plate Assay for Assessment of *Listeria monocytogenes* Biofilm Formation. *Applied and Environmental Microbiology*. 68 (6), pp. 2950–2958. doi:10.1128/AEM.68.6.2950-2958.2002.

Dolch, M.E., Hornuss, C., Klocke, C., Praun, S., Villinger, J., Denzer, W., Schelling, G. and Schubert, S. (2012a) Volatile compound profiling for the identification of Gram-negative bacteria by ion-molecule reaction-mass spectrometry. *Journal of Applied Microbiology*. 113 (5), pp. 1097–1105. doi:10.1111/j.1365-2672.2012.05414.x.

Dolch, M.E., Hornuss, C., Klocke, C., Praun, S., Villinger, J., Denzer, W., Schelling, G. and Schubert, S. (2012b) Volatile organic compound analysis by ion molecule reaction mass spectrometry for Gram-positive bacteria differentiation. *European Journal of Clinical Microbiology & Infectious Diseases*. 31 (11), pp. 3007–3013.
doi:10.1007/s10096-012-1654-2.

Dryahina, K., Sovová, K., Nemeč, A. and Španěl, P. (2016) Differentiation of pulmonary bacterial pathogens in cystic fibrosis by volatile metabolites emitted by

their in vitro cultures: *Pseudomonas aeruginosa*, *Staphylococcus aureus*, *Stenotrophomonas maltophilia* and the *Burkholderia cepacia* complex. *Journal of Breath Research*. 10 (3), 037102. doi:10.1088/1752-7155/10/3/037102.

Duckworth, P.F., Rowlands, R.S., Barbour, M.E. and Maddocks, S.E. (2018) A novel flow-system to establish experimental biofilms for modelling chronic wound infection and testing the efficacy of wound dressings. *Microbiological Research*. 215 pp. 141–147. doi:10.1016/j.micres.2018.07.009.

Duffy, E., Jacobs, M.R., Kirby, B. and Morrin, A. (2017) Probing skin physiology through the volatile footprint: Discriminating volatile emissions before and after acute barrier disruption. *Experimental Dermatology*. 26 (10), pp. 919–925. doi:10.1111/exd.13344.

Dufour, D., Leung, V. and Lévesque, C.M. (2010) Bacterial biofilm: structure, function, and antimicrobial resistance. *Endodontic Topics*. 22 (1), pp. 2–16. doi:10.1111/j.1601-1546.2012.00277.x.

Dummer, J., Storer, M., Sturney, S., Scott-Thomas, A., Chambers, S., Swanney, M. and Epton, M. (2013) Quantification of hydrogen cyanide (HCN) in breath using selected ion flow tube mass spectrometry—HCN is not a biomarker of *Pseudomonas* in chronic suppurative lung disease. *Journal of Breath Research*. 7 (1), 017105. doi:10.1088/1752-7155/7/1/017105.

Edwards-Jones, V. (2013) Chapter 6: Wound Infection. In: Madeleine Flanagan (ed.). *Wound Healing and Skin Integrity: Principles and Practice*. eBook. Wiley-Blackwell. pp. 133–149.

Edwards, R. and Harding, K.G. (2004) Bacteria and wound healing. *Current opinion in infectious diseases*. 17 (2), pp. 91–96.

Elliott, T.S.J. and Greenwood, D. (1984) The morphological response of *Pseudomonas aeruginosa* to azthreonam, cefoperazone, ceftazidime and N-formimidoyl thienamycin. *Journal of Medical Microbiology*. 17 (2), pp. 159–169. doi:10.1099/00222615-17-2-159.

Evans, C.A., Smith, W.M., Johnston, E.A. and Giblett, E.R. (1950) Bacterial Flora of the Normal Human Skin. *Journal of Investigative Dermatology*. 15 (4), pp. 305–324. doi:10.1038/jid.1950.105.

Fernández-Rivero, M., del Pozo, J., Valentín, A., de Diego, A., Pemán, J. and Cantón, E. (2017) Activity of Amphotericin B and Anidulafungin Combined with Rifampicin, Clarithromycin, Ethylenediaminetetraacetic Acid, N-Acetylcysteine, and Farnesol against *Candida tropicalis* Biofilms. *Journal of Fungi*. 3 (16), 3010016. doi:10.3390/jof3010016.

Filipiak, W., Sponring, A., Baur, M., Filipiak, A., Ager, C., Wiesenhofer, H., Nagl, M.,

Troppmair, J. and Amann, A. (2012) Molecular analysis of volatile metabolites released specifically by staphylococcus aureus and pseudomonas aeruginosa. *BMC Microbiology*. 12, 113. doi:10.1186/1471-2180-12-113.

Fisher, R.A., Gollan, B. and Helaine, S. (2017) Persistent bacterial infections and persister cells. *Nature Reviews Microbiology*. 15 (8), pp. 453–464. doi:10.1038/nrmicro.2017.42.

Fleming, D. and Rumbaugh, K. (2017) Approaches to Dispersing Medical Biofilms. *Microorganisms*. 5 (15), 5020015. doi:10.3390/microorganisms5020015.

Flemming, H.-C. and Wingender, J. (2010) The biofilm matrix. *Nature Reviews Microbiology*. 8 (9), pp. 623–633. doi:10.1038/nrmicro2415.

Fletcher, M. (1977) The effects of culture concentration and age, time, and temperature on bacterial attachment to polystyrene. *Canadian Journal of Microbiology*. 23 (1), pp. 1–6. doi:10.1139/m77-001.

Fowler, S.J., Basanta-Sanchez, M., Xu, Y., Goodacre, R. and Dark, P.M. (2015) Surveillance for lower airway pathogens in mechanically ventilated patients by metabolomic analysis of exhaled breath: a case-control study. *Thorax*. 70 (4), pp. 320–325. doi:10.1136/thoraxjnl-2014-206273.

Frederick, M.R., Kuttler, C., Hense, B.A. and Eberl, H.J. (2011) A mathematical model of quorum sensing regulated EPS production in biofilm communities. *Theoretical Biology and Medical Modelling*. 8. 8. doi:10.1186/1742-4682-8-8.

Fredricks, D.N. (2001) Microbial Ecology of Human Skin in Health and Disease. *Journal of Investigative Dermatology Symposium Proceedings*. 6 (3), pp. 167–169. doi:10.1046/j.0022-202x.2001.00039.x.

Furukawa, S., Kuchma, S.L. and O'Toole, G.A. (2006) Keeping Their Options Open: Acute versus Persistent Infections. *Journal of Bacteriology*. 188 (4), pp. 1211–1217. doi:10.1128/JB.188.4.1211-1217.2006.

Ghafoor, A., Hay, I.D. and Rehm, B.H.A. (2011) Role of Exopolysaccharides in Pseudomonas aeruginosa Biofilm Formation and Architecture. *Applied and Environmental Microbiology*. 77 (15), pp. 5238–5246. doi:10.1128/AEM.00637-11.

Gibbons, R.J., Berman, K.S., Knoettner, P. and Kapsimalis, B. (1966) Dental caries and alveolar bone loss in gnotobiotic rats infected with capsule forming streptococci of human origin. *Archives of Oral Biology*. 11 (6), pp. 549–563. doi:10.1016/0003-9969(66)90220-2.

Gilchrist, F.J., Alcock, A., Belcher, J., Brady, M., Jones, A., Smith, D., Spanel, P., Webb, K. and Lenney, W. (2011) Variation in hydrogen cyanide production between different strains of Pseudomonas aeruginosa. *European Respiratory Journal*. 38 (2),

pp. 409–414. doi:10.1183/09031936.00166510.

Gilchrist, F.J., Bright-Thomas, R.J., Jones, A.M., Smith, D., Španěl, P., Webb, A.K. and Lenney, W. (2013) Hydrogen cyanide concentrations in the breath of adult cystic fibrosis patients with and without *Pseudomonas aeruginosa* infection. *Journal of Breath Research*. 7 (2), 026010. doi:10.1088/1752-7155/7/2/026010.

Giwerzman, B., Lambert, P.A., Rosdahl, V.T., Shand, G.H. and Heiby, N. (1990) Rapid emergence of resistance in *Pseudomonas aeruginosa* in cystic fibrosis patients due to in-vivo selection of stable partially derepressed β -lactamase producing strains. *Journal of Antimicrobial Chemotherapy*. 26 (2), pp. 247–259. doi:10.1093/jac/26.2.247.

Goeres, D.M., Hamilton, M.A., Beck, N.A., Buckingham-Meyer, K., Hilyard, J.D., Loetterle, L.R., Lorenz, L.A., Walker, D.K. and Stewart, P.S. (2009) A method for growing a biofilm under low shear at the air–liquid interface using the drip flow biofilm reactor. *Nature Protocols*. 4 (5), pp. 783–788. doi:10.1038/nprot.2009.59.

Gosain, A. and DiPietro, L.A. (2004) Aging and Wound Healing. *World Journal of Surgery*. 28 (3), pp. 321–326. doi:10.1007/s00268-003-7397-6.

Grace, S.C. and Hudson, D.A. (2016) Processing and Visualization of Metabolomics Data Using R. In: *Metabolomics - Fundamentals and Applications*. InTech. pp. 116–124. doi:10.5772/65405.

Greenhalgh, D.G., Saffle, J.R., Holmes, J.H., Gamelli, R.L., Palmieri, T.L., Horton, J.W., Tompkins, R.G., Traber, D.L., Mazingo, D.W., Deitch, E. a, Goodwin, C.W., Herndon, D.N., Gallagher, J.J., Sanford, A.P., et al. (2007) American Burn Association Consensus Conference to Define Sepsis and Infection in Burns. *Journal of Burn Care & Research*. 28 (6), pp. 776–790. doi:10.1097/BCR.0b013e3181599bc9.

Greenman, J., Saad, S., Hewett, K., Thorn, R.M.S. and Reynolds, D.M. (2013) Review: In vitro biofilm models for studying oral malodour. *Flavour and Fragrance Journal*. 28 (4), pp. 212–222. doi:10.1002/ffj.3151.

Greenwood, D. (2008) *Antimicrobial drugs: chronicle of a twentieth century medical triumph*. Oxford: Oxford University Press.

Grice, E.A., Kong, H.H., Conlan, S., Deming, C.B., Davis, J., Young, A.C., Bouffard, G.G., Blakesley, R.W., Murray, P.R., Green, E.D., Turner, M.L. and Segre, J.A. (2009) Topographical and Temporal Diversity of the Human Skin Microbiome. *Science*. 324 (5931), pp. 1190–1192. doi:10.1126/science.1171700.

Grice, E.A., Kong, H.H., Renaud, G., Young, A.C., Bouffard, G.G., Blakesley, R.W., Wolfsberg, T.G., Turner, M.L. and Segre, J.A. (2008) A diversity profile of the human skin microbiota. *Genome Research*. 18 (7), pp. 1043–1050. doi:10.1101/gr.075549.107.

Guest, J.F., Ayoub, N., McIlwraith, T., Uchegbu, I., Gerrish, A., Weidlich, D., Vowden, K. and Vowden, P. (2015) Health economic burden that wounds impose on the National Health Service in the UK. *BMJ Open*. 5 (12), e009283. doi:10.1136/bmjopen-2015-009283.

Guest, J.F., Fuller, G.W. and Vowden, P. (2018) Costs and outcomes in evaluating management of unhealed surgical wounds in the community in clinical practice in the UK: a cohort study. *BMJ Open*. 8 (12), e022591. doi:10.1136/bmjopen-2018-022591.

Guo, S. and DiPietro, L.A. (2010) Factors Affecting Wound Healing. *Journal of Dental Research*. 89 (3), pp. 219–229. doi:10.1177/0022034509359125.

Gurjala, A.N., Geringer, M.R., Seth, A.K., Hong, S.J., Smeltzer, M.S., Galiano, R.D., Leung, K.P. and Mustoe, T.A. (2011) Development of a novel, highly quantitative in vivo model for the study of biofilm-impaired cutaneous wound healing. *Wound Repair and Regeneration*. 19 (3), pp. 400–410. doi:10.1111/j.1524-475X.2011.00690.x.

Ha, D.-G. and O'Toole, G.A. (2015) c-di-GMP and its Effects on Biofilm Formation and Dispersion: a *Pseudomonas aeruginosa* review. *Microbiology Spectrum*. 3 (2), MB-0003-2014. doi:10.1128/microbiolspec.MB-0003-2014.

Haalboom, M., Blokhuis-Arkes, M.H.E., Beuk, R.J., Meerwaldt, R., Klont, R., Schijffelen, M.J., Bowler, P.B., Burnet, M., Sigl, E. and van der Palen, J.A.M. (2019) Culture results from wound biopsy versus wound swab: does it matter for the assessment of wound infection? *Clinical Microbiology and Infection*. 25 (5), pp. 629.e7-629.e12. doi:10.1016/j.cmi.2018.08.012.

Haesler, E. and Ousey, K. (2018) Evolution of the wound infection continuum. *Wounds International*. 9 (4), pp. 6–10.

Haisma, E.M., Rietveld, M.H., de Breij, A., van Dissel, J.T., El Ghalbzouri, A. and Nibbering, P.H. (2013) Inflammatory and Antimicrobial Responses to Methicillin-Resistant *Staphylococcus aureus* in an In Vitro Wound Infection Model. *PLoS ONE*. 8 (12), e82800. doi:10.1371/journal.pone.0082800.

Hakonen, B., Lönnberg, L.K., Larkö, E. and Blom, K. (2014) A Novel Qualitative and Quantitative Biofilm Assay Based on 3D Soft Tissue. *International Journal of Biomaterials*. 2014, 768136. doi:10.1155/2014/768136.

Halász, A., Baráth, Á., Simon-Sarkadi, L. and Holzapfel, W. (1994) Biogenic amines and their production by microorganisms in food. *Trends in Food Science & Technology*. 5 (2), pp. 42–49. doi:10.1016/0924-2244(94)90070-1.

Hall, C.W. and Mah, T.-F. (2017) Molecular mechanisms of biofilm-based antibiotic resistance and tolerance in pathogenic bacteria. *FEMS Microbiology Reviews*. 41

(3), pp. 276–301. doi:10.1093/femsre/fux010.

Halstead, F.D., Lee, K.C., Kwei, J., Dretzke, J., Oppenheim, B.A. and Moiemmen, N.S. (2018) A systematic review of quantitative burn wound microbiology in the management of burns patients. *Burns*. 44 (1), pp. 39–56. doi:10.1016/j.burns.2017.06.008.

Høiby, N. (2009) Pseudomonas aeruginosa Infection In Cystic Fibrosis. Relationship between mucoid strains of Pseudomonas aeruginosa and the humoral immune response. *Acta Pathologica Microbiologica Scandinavica Section B Microbiology and Immunology*. 82B (4), pp. 551–558. doi:10.1111/j.1699-0463.1974.tb02365.x.

Høiby, N. and Axelsen, N.H. (2009) Identification and quantitation of precipitins against Pseudomonas aeruginosa in patients with Cystic Fibrosis by means of crossed immunoelectrophoresis with intermediate gel. *Acta Pathologica Microbiologica Scandinavica Section B Microbiology and Immunology*. 81B (3), pp. 298–308. doi:10.1111/j.1699-0463.1973.tb02207.x.

Høiby, N., Bjarnsholt, T., Givskov, M., Molin, S. and Ciofu, O. (2010) Antibiotic resistance of bacterial biofilms. *International Journal of Antimicrobial Agents*. 35 (4), pp. 322–332. doi:10.1016/j.ijantimicag.2009.12.011.

Høiby, N., Bjarnsholt, T., Moser, C., Bassi, G.L., Coenye, T., Donelli, G., Hall-Stoodley, L., Holá, V., Imbert, C., Kirketerp-Møller, K., Lebeaux, D., Oliver, A., Ullmann, A.J. and Williams, C. (2015) ESCMID guideline for the diagnosis and treatment of biofilm infections 2014. *Clinical Microbiology and Infection*. 21 (S1), pp. S1–S25. doi:10.1016/j.cmi.2014.10.024.

Hou, W., Sun, X., Wang, Z. and Zhang, Y. (2012) Biofilm-forming capacity of Staphylococcus epidermidis, Staphylococcus aureus, and Pseudomonas aeruginosa from ocular infections. *Investigative Ophthalmology and Visual Science*. 53 (9), pp. 5624–5631. doi:10.1167/jovs.11-9114.

Hughes, M.A. (2016) Wound infection: a knowledge deficit that needs addressing. *British Journal of Nursing*. 25 (6), TISSUE VIABILITY SUPPLEMENT.

Instrument Science (2006) Profile Series User Manual (1).

International Wound Infection Institute (2016) *Wound Infection in Clinical Practice*. Terry Swanson, Donna Angel, Geoff Sussman, Rose Cooper, Emily Haesler, Karen Ousey, Keryln Carville, Jacqui Fletcher, Lindsay Kalan, David Keast, David Leaper, Greg Schultz, Joyce Black, and Evan Call (eds.). Wounds International.

James, G.A., Swogger, E., Wolcott, R., Pulcini, E. deLancey, Secor, P., Sestrich, J., Costerton, J.W. and Stewart, P.S. (2008) Biofilms in chronic wounds. *Wound Repair and Regeneration*. 16 (1), pp. 37–44. doi:10.1111/j.1524-475X.2007.00321.x.

Jeschke, M.G. and Herndon, D.N. (2014) Burns in children: standard and new treatments. *The Lancet*. 383 (9923), pp. 1168–1178. doi:10.1016/S0140-6736(13)61093-4.

Jolivet-Gougeon, A. and Bonnaure-Mallet, M. (2014) Biofilms as a mechanism of bacterial resistance. *Drug Discovery Today: Technologies*. 11 pp. 49–56. doi:10.1016/j.ddtec.2014.02.003.

Julák, J., Procházková-Francisci, E., Stránská, E. and Rosová, V. (2003) Evaluation of exudates by solid phase microextraction–gas chromatography. *Journal of Microbiological Methods*. 52 (1), pp. 115–122. doi:10.1016/S0167-7012(02)00148-3.

Kaplan, J.B. (2010) Biofilm Dispersal: Mechanisms, Clinical Implications, and Potential Therapeutic Uses. *Journal of Dental Research*. 89 (3), pp. 205–218. doi:10.1177/0022034509359403.

Kassal, P., Kim, J., Kumar, R., de Araujo, W.R., Steinberg, I.M., Steinberg, M.D. and Wang, J. (2015) Smart bandage with wireless connectivity for uric acid biosensing as an indicator of wound status. *Electrochemistry Communications*. 56 pp. 6–10. doi:10.1016/j.elecom.2015.03.018.

Kathawala, M.H., Ng, W.L., Liu, D., Naing, M.W., Yeong, W.Y., Spiller, K.L., Van Dyke, M. and Ng, K.W. (2019) Healing of Chronic Wounds: An Update of Recent Developments and Future Possibilities. *Tissue Engineering Part B: Reviews*. 25 (5), pp. 429–444. doi:10.1089/ten.teb.2019.0019.

Kekonen, A., Bergelin, M., Johansson, M., Joon, N.K., Bobacka, J. and Viik, J. (2019) Bioimpedance sensor array for long-term monitoring of wound healing from beneath the primary dressings and controlled formation of h₂O₂ using low-intensity direct current. *Sensors*. 19 (11), . doi:10.3390/s19112505.

Kennedy, P., Brammah, S. and Wills, E. (2010) Burns, biofilm and a new appraisal of burn wound sepsis. *Burns*. 36 (1), pp. 49–56. doi:10.1016/j.burns.2009.02.017.

Kharazmi, A., Giwercman, B. and Høiby, N. (1999) Robbins device in biofilm research. In: *Methods in Enzymology*. pp. 207–215. doi:10.1016/S0076-6879(99)10018-1.

Klausen, M., Aaes-Jørgensen, A., Molin, S. and Tolker-Nielsen, T. (2003) Involvement of bacterial migration in the development of complex multicellular structures in *Pseudomonas aeruginosa* biofilms. *Molecular Microbiology*. 50 (1), pp. 61–68. doi:10.1046/j.1365-2958.2003.03677.x.

Kong, K.-F., Schneper, L. and Mathee, K. (2010) Beta-lactam antibiotics: from antibiosis to resistance and bacteriology. *APMIS*. 118 (1), pp. 1–36. doi:10.1111/j.1600-0463.2009.02563.x.

- Kucera, J., Sojka, M., Pavlik, V., Szuszkiewicz, K., Velebny, V. and Klein, P. (2014) Multispecies biofilm in an artificial wound bed—A novel model for in vitro assessment of solid antimicrobial dressings. *Journal of Microbiological Methods*. 103 pp. 18–24. doi:10.1016/j.mimet.2014.05.008.
- Kuchma, S.L., Connolly, J.P. and O’Toole, G.A. (2005) A Three-Component Regulatory System Regulates Biofilm Maturation and Type III Secretion in *Pseudomonas aeruginosa*. *Journal of Bacteriology*. 187 (4), pp. 1441–1454. doi:10.1128/JB.187.4.1441-1454.2005.
- Lachiewicz, A.M., Hauck, C.G., Weber, D.J., Cairns, B.A. and van Duin, D. (2017) Bacterial Infections After Burn Injuries: Impact of Multidrug Resistance. *Clinical Infectious Diseases*. 65 (12), pp. 2130–2136. doi:10.1093/cid/cix682.
- Ladygina, N., Dedyukhina, E.G. and Vainshtein, M.B. (2006) A review on microbial synthesis of hydrocarbons. *Process Biochemistry*. 41 (5), pp. 1001–1014. doi:10.1016/j.procbio.2005.12.007.
- Lajhar, S.A., Brownlie, J. and Barlow, R. (2018) Characterization of biofilm-forming capacity and resistance to sanitizers of a range of *E. coli* O26 pathotypes from clinical cases and cattle in Australia. *BMC Microbiology*. 18, 41. doi:10.1186/s12866-018-1182-z.
- Lam, J., Chan, R., Lam, K. and Costerton, J.W. (1980) Production of mucoid microcolonies by *Pseudomonas aeruginosa* within infected lungs in cystic fibrosis. *Infection and immunity*. 28 (2), pp. 546–556.
- Landis, S.J. (2008) Chronic Wound Infection and Antimicrobial Use. *Advances in Skin & Wound Care*. 21 (11), pp. 541–542. doi:10.1097/01.ASW.0000323584.35228.05.
- Levine, N.S., Lindberg, R.B., Mason, A.D. and Pruitt, B.A. (1976) The Quantitative Swab Culture and Smear: A quick, simple method for determining the number of viable aerobic bacteria on open wounds. *The Journal of Trauma: Injury, Infection, and Critical Care*. 16 (2), pp. 89–94. doi:10.1097/00005373-197602000-00002.
- Lewis, J.M., Savage, R.S., Beeching, N.J., Beadsworth, M.B.J., Feasey, N. and Covington, J.A. (2017) Identifying volatile metabolite signatures for the diagnosis of bacterial respiratory tract infection using electronic nose technology: A pilot study. *PloS ONE*. 12 (12), e0188879. doi:10.1371/journal.pone.0188879.
- Lewis, K. (2010) Persister Cells. *Annual Review of Microbiology*. 64 (1), pp. 357–372. doi:10.1146/annurev.micro.112408.134306.
- Li, G. and Young, K.D. (2013) Indole production by the tryptophanase TnaA in *Escherichia coli* is determined by the amount of exogenous tryptophan. *Microbiology*. 159, pp. 402–410. doi:10.1099/mic.0.064139-0.

Li, S., Mohamedi, A.H., Senkowsky, J., Nair, A. and Tang, L. (2020) Imaging in Chronic Wound Diagnostics. *Advances in Wound Care* 9 (5), pp. 245–463. doi:10.1089/wound.2019.0967.

Lipp, C., Kirker, K., Agostinho, A., James, G. and Stewart, P. (2010) Testing wound dressings using an in vitro wound model. *Journal of wound care*. 19 (6), pp. 220–226. doi:10.12968/jowc.2010.19.6.48468.

Losquadro, W.D. (2017) Anatomy of the Skin and the Pathogenesis of Nonmelanoma Skin Cancer. *Facial Plastic Surgery Clinics of North America*. 25 (3), pp. 283–289. doi:10.1016/j.fsc.2017.03.001.

Luján, A.M., Maciá, M.D., Yang, L., Molin, S., Oliver, A. and Smania, A.M. (2011) Evolution and Adaptation in *Pseudomonas aeruginosa* Biofilms Driven by Mismatch Repair System-Deficient Mutators Christophe Herman (ed.). *PLoS ONE*. 6 (11), e27842. doi:10.1371/journal.pone.0027842.

Ma, X.-Y., Tian, L.-X. and Liang, H.-P. (2016) Early prevention of trauma-related infection/sepsis. *Military Medical Research*. 3, 33. doi:10.1186/s40779-016-0104-3.

Macgregor, L., Calne, S., Day, K., Jones, J., Pugh, A. and Walker, J. (2008) Wound Infection in Clinical Practice. *International Wound Journal*. 5 (s3), pp. 1–11. doi:10.1111/j.1742-481X.2008.00488.x.

Malone, M., Bjarnsholt, T., McBain, A.J., James, G.A., Stoodley, P., Leaper, D., Tachi, M., Schultz, G., Swanson, T. and Wolcott, R.D. (2017) The prevalence of biofilms in chronic wounds: a systematic review and meta-analysis of published data. *Journal of Wound Care*. 26 (1), pp. 20–25. doi:10.12968/jowc.2017.26.1.20.

Marrie, T.J. and Costerton, J.W. (1984) Scanning and Transmission Electron Microscopy of In Situ Bacterial Colonization of Intravenous and Intraarterial Catheters. *Journal of Clinical Microbiology* 19 (5), pp 687–693.

McDougald, D., Rice, S.A., Barraud, N., Steinberg, P.D. and Kjelleberg, S. (2012) Should we stay or should we go: mechanisms and ecological consequences for biofilm dispersal. *Nature Reviews Microbiology*. 10, pp. 39–50. doi:10.1038/nrmicro2695.

Di Meglio, P., Perera, G.K. and Nestle, F.O. (2011) The Multitasking Organ: Recent Insights into Skin Immune Function. *Immunity*. 35 (6), pp. 857–869. doi:10.1016/j.immuni.2011.12.003.

Mehmood, N., Hariz, A., Templeton, S. and Voelcker, N.H. (2015) A flexible and low power telemetric sensing and monitoring system for chronic wound diagnostics. *BioMedical Engineering OnLine*. 14, 17. doi:10.1186/s12938-015-0011-y.

Meigel, W.N., Gay, S. and Weber, L. (1977) Dermal architecture and collagen type

distribution. *Archives for Dermatological Research*. 259, pp. 1–10.
doi:10.1007/BF00562732.

Mellott, A., Zamierowski, D. and Andrews, B. (2016) Negative Pressure Wound Therapy in Maxillofacial Applications. *Dentistry Journal*. 4, 30.
doi:10.3390/dj4030030.

Metcalf, D.G., Bowler, P.G. and Hurlow, J. (2014) A clinical algorithm for wound biofilm identification. *Journal of Wound Care*. 23 (3), pp. 137–142.
doi:10.12968/jowc.2014.23.3.137.

Mir, M.A., Khurram, M.F. and Khan, A.H. (2017) What should be the antibiotic prescription protocol for burn patients admitted in the department of burns, plastic and reconstructive surgery. *International Wound Journal*. 14, pp. 194–197.
doi:10.1111/iwj.12588.

Mittelman, M.W., Kohring, L.L. and White, D.C. (1992) Multipurpose laminar-flow adhesion cells for the study of bacterial colonization and biofilm formation. *Biofouling*. 6 (1), pp. 39–51. doi:10.1080/08927019209386208.

Monroe, D. (2007) Looking for Chinks in the Armor of Bacterial Biofilms. *PLoS Biology*. 5 (11), pp. 2458–2461 doi:10.1371/journal.pbio.0050307.

Morton, L.M. and Phillips, T.J. (2016) Wound healing and treating wounds. *Journal of the American Academy of Dermatology*. 74 (4), pp. 589–605.
doi:10.1016/j.jaad.2015.08.068.

Munita, J.M. and Arias, C.A. (2016) Mechanisms of Antibiotic Resistance. *Microbiology Spectrum*. 4 (2), pp. 481–511. doi:10.1128/microbiolspec.VMBF-0016-2015.

Murray, R.A. (2001) Limitations to the Use of Solid-Phase Microextraction for Quantitation of Mixtures of Volatile Organic Sulfur Compounds. *Analytical Chemistry*. 73 (7), pp. 1646–1649. doi:10.1021/ac001176m.

Mustoe, T.A., O’Shaughnessy, K. and Kloeters, O. (2006) Chronic Wound Pathogenesis and Current Treatment Strategies: A Unifying Hypothesis. *Plastic and Reconstructive Surgery*. 117 (SUPPLEMENT), pp. 35S–41S.
doi:10.1097/01.prs.0000225431.63010.1b.

Nawaz, M.S., Davis, J.W., Wolfram, J.H. and Chapatwala, K.D. (1991) Degradation of organic cyanides by *Pseudomonas aeruginosa*. *Applied biochemistry and biotechnology*. 28–29 pp. 865–875.

Neerincx, A.H., Geurts, B.P., Van Loon, J., Tiemes, V., Jansen, J.J., Harren, F.J.M., Kluijtmans, L.A.J., Merkus, P.J.F.M., Cristescu, S.M., Buydens, L.M.C. and Wevers, R.A. (2016) Detection of *Staphylococcus aureus* in cystic fibrosis patients using

breath VOC profiles. *Journal of Breath Research*. 10, 046014. doi:10.1088/1752-7155/10/4/046014.

Neerinx, A.H., Mandon, J., van Ingen, J., Arslanov, D.D., Mouton, J.W., Harren, F.J.M., Merkus, P.J.F.M. and Cristescu, S.M. (2015) Real-time monitoring of hydrogen cyanide (HCN) and ammonia (NH₃) emitted by *Pseudomonas aeruginosa*. *Journal of Breath Research*. 9, 027102. doi:10.1088/1752-7155/9/2/027102.

Nestle, F.O., Di Meglio, P., Qin, J.-Z. and Nickoloff, B.J. (2009) Skin immune sentinels in health and disease. *Nature Reviews Immunology*. 9 (10), pp. 679–691. doi:10.1038/nri2622.

Nguyen, K.T., Seth, A.K., Hong, S.J., Geringer, M.R., Xie, P., Leung, K.P., Mustoe, T.A. and Galiano, R.D. (2013) Deficient cytokine expression and neutrophil oxidative burst contribute to impaired cutaneous wound healing in diabetic, biofilm-containing chronic wounds. *Wound Repair and Regeneration*. 21 (6), pp. 833–841. doi:10.1111/wrr.12109.

Nickel, J.C., Wright, J.B., Ruseska, I., Marrie, T.J., Whitfield, C. and Costerton, J.W. (1985) Antibiotic resistance of *Pseudomonas aeruginosa* colonizing a urinary catheter in vitro. *European Journal of Clinical Microbiology*. 4 (2), pp. 213–218. doi:10.1007/BF02013600.

Nicks, B.A., Ayello, E.A., Woo, K., Nitzki-George, D. and Sibbald, R.G. (2010) Acute wound management: revisiting the approach to assessment, irrigation, and closure considerations. *International Journal of Emergency Medicine*. 3 (4), pp. 399–407. doi:10.1007/s12245-010-0217-5.

Nizio, K.D., Perrault, K.A., Troobnikoff, A.N., Ueland, M., Shoma, S., Iredell, J.R., Middleton, P.G. and Forbes, S.L. (2016) In vitro volatile organic compound profiling using GC×GC-TOFMS to differentiate bacteria associated with lung infections: a proof-of-concept study. *Journal of Breath Research*. 10, 026008. doi:10.1088/1752-7155/10/2/026008.

Norbury, W., Herndon, D.N., Tanksley, J., Jeschke, M.G. and Finnerty, C.C. (2016) Infection in Burns. *Surgical Infections*. 17 (2), pp. 250–255. doi:10.1089/sur.2013.134.

Nyström, A. and Bruckner-Tuderman, L. (2019) Matrix molecules and skin biology. *Seminars in Cell & Developmental Biology*. 89 pp. 136–146. doi:10.1016/j.semcdb.2018.07.025.

O'Hara, M. and Mayhew, C.A. (2009) A preliminary comparison of volatile organic compounds in the headspace of cultures of *Staphylococcus aureus* grown in nutrient, dextrose and brain heart bovine broths measured using a proton transfer reaction mass spectrometer. *Journal of Breath Research*. 3, 027001.

doi:10.1088/1752-7155/3/2/027001.

O'Neill, J. (2014) Antimicrobial Resistance: Tackling a crisis for the health and wealth of nations. *The Review on Antimicrobial Resistance*.

O'Neill, J. (2016) Tackling Drug-Resistant Infections Globally: Final Report and Recommendations the Review on Antimicrobial Resistance. *The Review on Antimicrobial Resistance*.

O'Toole, G. and Kolter, R. (1998a) Initiation of biofilm formation in *Pseudomonas fluorescens* WCS365. *Molecular microbiology*. 28 (3), pp. 449–461.

O'Toole, G. and Kolter, R. (1998b) Flagellar and twitching motility are necessary for *Pseudomonas aeruginosa* biofilm development. *Molecular Microbiology*. 30 (2), pp. 295–304. doi:10.1046/j.1365-2958.1998.01062.x.

O'Toole, G.A. and Wong, G.C. (2016) Sensational biofilms: surface sensing in bacteria. *Current Opinion in Microbiology*. 30, pp. 139–146. doi:10.1016/j.mib.2016.02.004.

Oh, J., Byrd, A.L., Deming, C., Conlan, S., Kong, H.H. and Segre, J.A. (2014) Biogeography and individuality shape function in the human skin metagenome. *Nature*. 514 (7520), pp. 59–64. doi:10.1038/nature13786.

Olsen, I. (2015) Biofilm-specific antibiotic tolerance and resistance. *European Journal of Clinical Microbiology & Infectious Diseases*. 34 (5), pp. 877–886. doi:10.1007/s10096-015-2323-z.

Olson, M.E., Ceri, H., Morck, D.W., Buret, A.G. and Read, R.R. (2002) Biofilm bacteria: formation and comparative susceptibility to antibiotics. *Canadian Journal of Veterinary Research*. 66, pp. 86–92.

Palma, S.I.C.J., Tragedo, P., Porteira, A.R., Frias, M.J., Gmboa, H. and Roque, A.C.A. (2018) Machine learning for the meta-analyses of microbial pathogens' volatile signatures. *Scientific Reports* 8, 3360. doi:10.1038/s41598-018-21544-1.

Passos da Silva, D., Schofield, M., Parsek, M. and Tseng, B. (2017) An Update on the Sociomicrobiology of Quorum Sensing in Gram-Negative Biofilm Development. *Pathogens*. 6, 51. doi:10.3390/pathogens6040051.

Patil, N.K., Bohannon, J.K., Luan, L., Guo, Y., Fensterheim, B., Hernandez, A., Wang, J. and Sherwood, E.R. (2017) Flt3 Ligand Treatment Attenuates T Cell Dysfunction and Improves Survival in a Murine Model of Burn Wound Sepsis. *SHOCK*. 47 (1), pp. 40–51. doi:10.1097/SHK.0000000000000688.

Pavlou, A., Turner, A.P.F. and Magan, N. (2002) Recognition of anaerobic bacterial isolates in vitro using electronic nose technology. *Letters in Applied Microbiology*. 35 (5), pp. 366–369. doi:10.1046/j.1472-765X.2002.01197.x.

Percival, S.L. (2017) Importance of biofilm formation in surgical infection. *British Journal of Surgery*. 104 (2), pp. e85–e94. doi:10.1002/bjs.10433.

Peterson, E. and Kaur, P. (2018) Antibiotic Resistance Mechanisms in Bacteria: Relationships Between Resistance Determinants of Antibiotic Producers, Environmental Bacteria, and Clinical Pathogens. *Frontiers in Microbiology*. 9, 2928. doi:10.3389/fmicb.2018.02928.

Petrova, O.E. and Sauer, K. (2016) Escaping the biofilm in more than one way: desorption, detachment or dispersion. *Current Opinion in Microbiology*. 30 pp. 67–78. doi:10.1016/j.mib.2016.01.004.

Phair, J., Joshi, M., Benson, J., McDonald, D. and Davis, J. (2014) Laser patterned carbon–polyethylene mesh electrodes for wound diagnostics. *Materials Chemistry and Physics*. 143 (3), pp. 991–995. doi:10.1016/j.matchemphys.2013.10.035.

Pompilio, A., Galardi, G., Verginelli, F., Muzzi, M., Di Giulio, A. and Di Bonaventura, G. (2017) Myroides odoratimimus Forms Structurally Complex and Inherently Antibiotic-Resistant Biofilm in a Wound-Like in vitro Model. *Frontiers in Microbiology*. 8, 2591. doi:10.3389/fmicb.2017.02591.

Del Pozo, J.L. (2018) Biofilm-related disease. *Expert Review of Anti-infective Therapy*. 16, pp. 51–65. doi:10.1080/14787210.2018.1417036.

Price, B.L., Lovering, A.M., Bowling, F.L. and Dobson, C.B. (2016) Development of a Novel Collagen Wound Model To Simulate the Activity and Distribution of Antimicrobials in Soft Tissue during Diabetic Foot Infection. *Antimicrobial Agents and Chemotherapy*. 60 (11), pp. 6880–6889. doi:10.1128/AAC.01064-16.

Purcaro, G., Rees, C.A., Melvin, J.A., Bomberger, J.M. and Hill, J.E. (2018) Volatile fingerprinting of Pseudomonas aeruginosa and respiratory syncytial virus infection in an in vitro cystic fibrosis co-infection model. *Journal of Breath Research*. 12, 046001. doi:10.1088/1752-7163/aac2f1.

Rahimi, R., Ochoa, M., Parupudi, T., Zhao, X., Yazdi, I.K., Dokmeci, M.R., Tamayol, A., Khademhosseini, A. and Ziaie, B. (2016) A low-cost flexible pH sensor array for wound assessment. *Sensors and Actuators, B: Chemical*. 229 pp. 609–617. doi:10.1016/j.snb.2015.12.082.

Rajpaul, K. (2015) Biofilm in wound care. *British Journal of Community Nursing*. 20 (Sup3), pp. S6–S11. doi:10.12968/bjcn.2015.20.Sup3.S6.

Ren, S., Hinzman, A.A., Kang, E.L., Szczesniak, R.D. and Lu, L.J. (2015) Computational and statistical analysis of metabolomics data. *Metabolomics*. 11 (6), pp. 1492–1513. doi:10.1007/s11306-015-0823-6.

Rhoads, D.D., Wolcott, R.D. and Percival, S.L. (2008) Biofilms in wounds:

management strategies. *Journal of Wound Care*. 17 (11), pp. 502–508. doi:10.12968/jowc.2008.17.11.31479.

Robins, S.P., Milne, G., Duncan, A., Davies, C., Butt, R., Greiling, D. and James, I.T. (2003) Increased Skin Collagen Extractability and Proportions of Collagen Type III Are Not Normalized after 6 Months Healing of Human Excisional Wounds. *Journal of Investigative Dermatology*. 121 (2), pp. 267–272. doi:10.1046/j.1523-1747.2003.12373.x.

Roth, R.R. and James, W.D. (1989) Microbiology of the skin: Resident flora, ecology, infection. *Journal of the American Academy of Dermatology*. 20 (3), pp. 367–390. doi:10.1016/S0190-9622(89)70048-7.

Roy, R., Tiwari, M., Donelli, G. and Tiwari, V. (2018) Strategies for combating bacterial biofilms: A focus on anti-biofilm agents and their mechanisms of action. *Virulence*. 9 (1), pp. 522–554. doi:10.1080/21505594.2017.1313372.

Saccenti, E., Hoefsloot, H.C.J., Smilde, A.K., Westerhuis, J.A. and Hendriks, M.M.W.B. (2014) Reflections on univariate and multivariate analysis of metabolomics data. *Metabolomics*. 10 (3), pp. 361–374. doi:10.1007/s11306-013-0598-6.

Said, J., Dodoo, C.C., Walker, M., Parsons, D., Stapleton, P., Beezer, A.E. and Gaisford, S. (2014) An in vitro test of the efficacy of silver-containing wound dressings against *Staphylococcus aureus* and *Pseudomonas aeruginosa* in simulated wound fluid. *International Journal of Pharmaceutics*. 462 (1–2), pp. 123–128. doi:10.1016/j.ijpharm.2013.12.037.

Sauer, K., Camper, A.K., Ehrlich, G.D., Costerton, J.W. and Davies, D.G. (2002) *Pseudomonas aeruginosa* Displays Multiple Phenotypes during Development as a Biofilm. *Journal of Bacteriology*. 184 (4), pp. 1140–1154. doi:10.1128/jb.184.4.1140-1154.2002.

Savage, J.M. and Jeffery, S.L.A. (2013) Use of 3D photography in complex-wound assessment. *Journal of Wound Care*. 22 (3), pp. 156–160. doi:10.12968/jowc.2013.22.3.156.

Saxena, P., Joshi, Y., Rawat, K. and Bisht, R. (2019) Biofilms: Architecture, Resistance, Quorum Sensing and Control Mechanisms. *Indian Journal of Microbiology*. 59 (1), pp. 3–12. doi:10.1007/s12088-018-0757-6.

Schaber, J.A., Triffo, W.J., Suh, S.J., Oliver, J.W., Hastert, M.C., Griswold, J.A., Auer, M., Hamood, A.N. and Rumbaugh, K.P. (2007) *Pseudomonas aeruginosa* Forms Biofilms in Acute Infection Independent of Cell-to-Cell Signaling. *Infection and Immunity*. 75 (8), pp. 3715–3721. doi:10.1128/IAI.00586-07.

Schindelin, J., Arganda-Carreras, I., Frise, E., Kaynig, V., Longair, M., Pietzsch, T.,

- Preibisch, S., Rueden, C., Saalfeld, S., Schmid, B., Tinevez, J.-Y., White, D.J., Hartenstein, V., Eliceiri, K., et al. (2012) Fiji: an open-source platform for biological-image analysis. *Nature Methods*. 9 (7), pp. 676–682. doi:10.1038/nmeth.2019.
- Schulz, S. and Dickschat, J.S. (2007) Bacterial volatiles: the smell of small organisms. *Natural Product Reports*. 24 (4), pp. 814–842. doi:10.1039/b507392h.
- Scotter, J.M., Allardyce, R.A., Langford, V.S., Hill, A. and Murdoch, D.R. (2006) The rapid evaluation of bacterial growth in blood cultures by selected ion flow tube–mass spectrometry (SIFT-MS) and comparison with the BacT/ALERT automated blood culture system. *Journal of Microbiological Methods*. 65 (3), pp. 628–631. doi:10.1016/j.mimet.2005.09.016.
- Sethi, S., Nanda, R. and Chakraborty, T. (2013) Clinical application of volatile organic compound analysis for detecting infectious diseases. *Clinical Microbiology Reviews*. 26 (3), pp. 462–475. doi:10.1128/CMR.00020-13.
- Sharp, D. and Davis, J. (2008) Integrated urate sensors for detecting wound infection. *Electrochemistry Communications*. 10 (5), pp. 709–713. doi:10.1016/j.elecom.2008.02.025.
- Shestivska, V., Antonowicz, S.S., Dryahina, K., Kubišta, J., Smith, D. and Španěl, P. (2015) Direct detection and quantification of malondialdehyde vapour in humid air using selected ion flow tube mass spectrometry supported by gas chromatography/mass spectrometry. *Rapid Communications in Mass Spectrometry*. 29 (11), pp. 1069–1079. doi:10.1002/rcm.7198.
- Shestivska, V., Španěl, P., Dryahina, K., Sovová, K., Smith, D., Musílek, M. and Nemeč, A. (2012) Variability in the concentrations of volatile metabolites emitted by genotypically different strains of *Pseudomonas aeruginosa*. *Journal of Applied Microbiology*. 113 (3), pp. 701–713. doi:10.1111/j.1365-2672.2012.05370.x.
- Sheybani, R. and Shukla, A. (2017) Highly sensitive label-free dual sensor array for rapid detection of wound bacteria. *Biosensors and Bioelectronics*. 92, pp. 425–433. doi:10.1016/j.bios.2016.10.084.
- Shortt, R. and Thoma, A. (2008) Empirical Antibiotics Use in Soft Tissue Infections. *Canadian Journal of Plastic Surgery*. 16 (4), pp. 201–204. doi:10.1177/229255030801600402.
- Sibbald, G., Orsted, H., Schultz, G., Coutts, P. and Keast, D. (2003) Preparing the Wound Bed 2003: Focus on Infection and Inflammation. *Wound Management & Prevention*. 49 (11), pp. 24–51.
- Siddiqui, A.R. and Bernstein, J.M. (2010) Chronic wound infection: Facts and controversies. *Clinics in Dermatology*. 28 (5), pp. 519–526. doi:10.1016/j.clindermatol.2010.03.009.

- Singer, A.J. and Clark, R.A.F. (1999) Cutaneous Wound Healing. Franklin H. Epstein (ed.). *New England Journal of Medicine*. 341 (10), pp. 738–746. doi:10.1056/NEJM199909023411006.
- Singh, S., Young, A. and McNaught, C.-E. (2017) The physiology of wound healing. *Surgery*. 35 (9), pp. 473–477. doi:10.1016/j.mpsur.2017.06.004.
- Sjöberg, T., Mzezewa, S., Jönsson, K., Robertson, V. and Salemark, L. (2003) Comparison of Surface Swab Cultures and Quantitative Tissue Biopsy Cultures to Predict Sepsis in Burn Patients: A Prospective Study. *Journal of Burn Care & Rehabilitation*. 24 (6), pp. 365–370. doi:10.1097/01.BCR.0000095507.45481.76.
- Slade, E.A., Thorn, R.M.S., Lovering, A.M., Young, A. and Reynolds, D.M. (2017) In vitro discrimination of wound-associated bacteria by volatile compound profiling using selected ion flow tube-mass spectrometry. *Journal of Applied Microbiology*. 123 (1), pp. 233–245. doi:10.1111/jam.13473.
- Slade, E.A., Thorn, R.M.S., Young, A. and Reynolds, D.M. (2019) An in vitro collagen perfusion wound biofilm model; with applications for antimicrobial studies and microbial metabolomics. *BMC Microbiology*. 19, 310. doi:10.1186/s12866-019-1682-5.
- Smart, A., de Lacy Costello, B., White, P., Avison, M., Batty, C., Turner, C., Persad, R. and Ratcliffe, N. (2019) Sniffing out resistance – Rapid identification of urinary tract infection-causing bacteria and their antibiotic susceptibility using volatile metabolite profiles. *Journal of Pharmaceutical and Biomedical Analysis*. 167 pp. 59–65. doi:10.1016/j.jpba.2019.01.044.
- Smith, D. and Španěl, P. (2011) Ambient analysis of trace compounds in gaseous media by SIFT-MS. *The Analyst*. 136, 2009–2032. doi:10.1039/c1an15082k.
- Smith, D., Španěl, P., Gilchrist, F.J. and Lenney, W. (2013) Hydrogen cyanide, a volatile biomarker of *Pseudomonas aeruginosa* infection. *Journal of Breath Research*. 7, 044001. doi:10.1088/1752-7155/7/4/044001.
- Smith, S.M. (1991) D-lactic acid production as a monitor of the effectiveness of antimicrobial agents. *Antimicrobial Agents and Chemotherapy*. 35 (2), pp. 237–241. doi:10.1128/AAC.35.2.237.
- Španěl, P., Wang, T. and Smith, D. (2004) Quantification of hydrogen cyanide in humid air by selected ion flow tube mass spectrometry. *Rapid Communications in Mass Spectrometry*. 18 (16), pp. 1869–1873. doi:10.1002/rcm.1566.
- Spear, M. (2012) Wound exudate - the good, the bad, and the ugly. *Plastic Surgical Nursing*. 32 (2), pp. 77–79.
- Spooner, A.D., Bessant, C., Turner, C., Knobloch, H. and Chambers, M. (2009)

Evaluation of a combination of SIFT-MS and multivariate data analysis for the diagnosis of *Mycobacterium bovis* in wild badgers. *The Analyst*. 134 (9), pp. 1922–1927. doi:10.1039/b905627k.

Stewart, P.S. (2015) Antimicrobial Tolerance in Biofilms. *Microbiology Spectrum*. 3 (3), MB-0010-2014. doi:10.1128/microbiolspec.MB-0010-2014.

Stoodley, P., Sauer, K., Davies, D.G. and Costerton, J.W. (2002) Biofilms as Complex Differentiated Communities. *Annual Review of Microbiology*. 56 (1), pp. 187–209. doi:10.1146/annurev.micro.56.012302.160705.

Storer, M.K., Hibbard-Melles, K., Davis, B. and Scotter, J. (2011) Detection of volatile compounds produced by microbial growth in urine by selected ion flow tube mass spectrometry (SIFT-MS). *Journal of Microbiological Methods*. 87 (1), pp. 111–113. doi:10.1016/j.mimet.2011.06.012.

Sun, H., Tian, F., Liang, Z., Sun, T., Yu, B., Yang, S.X., He, Q., Zhang, L. and Liu, X. (2017) Sensor Array Optimization of Electronic Nose for Detection of Bacteria in Wound Infection. *IEEE Transactions on Industrial Electronics*. 64 (9), pp. 7350–7358. doi:10.1109/TIE.2017.2694353.

Sun, T., Tian, F.C., Bi, Y.T., Zhong, X.Z., He, J., Yang, T.C., Guo, Q.S., Lei, Y., Lu, Y., Zeng, L. and He, Q.H. (2019) Local warning integrated with global feature based on dynamic spectra for FAIMS data analysis in detection of clinical wound infection. *Sensors and Actuators, B: Chemical*. 298 (June), 126926. doi:10.1016/j.snb.2019.126926.

Sun, Y., Dowd, S.E., Smith, E., Rhoads, D.D. and Wolcott, R.D. (2008) In vitro multispecies Lubbock chronic wound biofilm model. *Wound Repair and Regeneration*. 16 (6), pp. 805–813. doi:10.1111/j.1524-475X.2008.00434.x.

Syft Technologies Ltd (2012) *Voice200® Advanced User's Guide*.

Szymańska, E., Saccenti, E., Smilde, A.K. and Westerhuis, J.A. (2012) Double-check: Validation of diagnostic statistics for PLS-DA models in metabolomics studies. *Metabolomics*. 8 pp. 3–16. doi:10.1007/s11306-011-0330-3.

Taverna, D., Pollins, A.C., Sindona, G., Caprioli, R.M. and Nanney, L.B. (2015) Imaging mass spectrometry for assessing cutaneous wound healing: Analysis of pressure ulcers. *Journal of Proteome Research*. 14 (2), pp. 986–996. doi:10.1021/pr5010218.

Thalavitiya Acharige, M.J., Koshy, S.S. and Koo, S. (2018) The Use of Microbial Metabolites for the Diagnosis of Infectious Diseases. *Advanced Techniques in Diagnostic Microbiology*. pp. 261–272. doi:10.1007/978-3-319-33900-9_12.

The European Committee on Antimicrobial Susceptibility Testing (2018) *Breakpoint*

tables for interpretation of MICs and zone diameters. Version 8.1. Available from: <http://www.eucast.org>.

Thet, N.T., Alves, D.R., Bean, J.E., Booth, S., Nzakizwanayo, J., Young, A.E.R., Jones, B. V. and Jenkins, A.T.A. (2016) Prototype Development of the Intelligent Hydrogel Wound Dressing and Its Efficacy in the Detection of Model Pathogenic Wound Biofilms. *ACS Applied Materials & Interfaces*. 8 (24), pp. 14909–14919. doi:10.1021/acsami.5b07372.

Thomas, S., Fear, M., Humphreys, J., Disley, L. and Waring, M. (1996) The effect of dressings on the production of exudate from venous leg ulcers. *Wounds*. 8 (5), pp. 145–150.

Thorn, R.M.S. and Greenman, J. (2009) A novel in vitro flat-bed perfusion biofilm model for determining the potential antimicrobial efficacy of topical wound treatments. *Journal of Applied Microbiology*. 107 (6), pp. 2070–2079. doi:10.1111/j.1365-2672.2009.04398.x.

Thorn, R.M.S. and Greenman, J. (2012) Microbial volatile compounds in health and disease conditions. *Journal of Breath Research*. 6, 024001. doi:10.1088/1752-7155/6/2/024001.

Thorn, R.M.S., Reynolds, D.M. and Greenman, J. (2011) Multivariate analysis of bacterial volatile compound profiles for discrimination between selected species and strains in vitro. *Journal of Microbiological Methods*. 84 (2), pp. 258–264. doi:10.1016/j.mimet.2010.12.001.

Thurnheer, T., Gmür, R. and Guggenheim, B. (2004) Multiplex FISH analysis of a six-species bacterial biofilm. *Journal of Microbiological Methods*. 56 (1), pp. 37–47. doi:10.1016/j.mimet.2003.09.003.

Tolker-nielsen, T. and Sternberg, C. (2014) *Pseudomonas Methods and Protocols. Methods in Molecular Biology*. Alain Filloux and Juan-Luis Ramos (eds.). New York, NY: Springer New York.

Trengove, N.J., Langton, S.R. and Stacey, M.C. (1996) Biochemical analysis of wound fluid from nonhealing and healing chronic leg ulcers. *Wound Repair and Regeneration*. 4 (2), pp. 234–239. doi:10.1046/j.1524-475X.1996.40211.x.

Turner, A.P.F. and Magan, N. (2004) Electronic noses and disease diagnostics. *Nature Reviews Microbiology*. 2 (2), pp. 161–166. doi:10.1038/nrmicro823.

Turner, C., Parekh, B., Walton, C., Španěl, P., Smith, D. and Evans, M. (2008) An exploratory comparative study of volatile compounds in exhaled breath and emitted by skin using selected ion flow tube mass spectrometry. *Rapid Communications in Mass Spectrometry*. 22 (4), pp. 526–532. doi:10.1002/rcm.3402.

- Turner, C., Španěl, P. and Smith, D. (2006) A longitudinal study of methanol in the exhaled breath of 30 healthy volunteers using selected ion flow tube mass spectrometry, SIFT-MS. *Physiological Measurement*. 27 (7), pp. 637–648. doi:10.1088/0967-3334/27/7/007.
- Uppal, S.K., Ram, S., Kwatra, B., Garg, S. and Gupta, R. (2007) Comparative evaluation of surface swab and quantitative full thickness wound biopsy culture in burn patients. *Burns*. 33 (4), pp. 460–463. doi:10.1016/J.BURNS.2006.08.015.
- Valentini, M. and Filloux, A. (2016) Biofilms and Cyclic di-GMP (c-di-GMP) Signaling: Lessons from *Pseudomonas aeruginosa* and Other Bacteria. *Journal of Biological Chemistry*. 291 (24), pp. 12547–12555. doi:10.1074/jbc.R115.711507.
- Vinogradov, A.M., Winston, M., Rupp, C.J. and Stoodley, P. (2004) Rheology of biofilms formed from the dental plaque pathogen *Streptococcus mutans*. *Biofilms*. 1 (1), pp. 49–56. doi:10.1017/S1479050503001078.
- Vuolo, J. (2004) Current options for managing the problem of excess wound exudate. *The Professional nurse*. 19 (9), pp. 487–491.
- Vyas, K.S. and Wong, L.K. (2016) Detection of Biofilm in Wounds as an Early Indicator for Risk for Tissue Infection and Wound Chronicity. *Annals of Plastic Surgery*. 76 (1), pp. 127–131. doi:10.1097/SAP.0000000000000440.
- Wang, T., Španěl, P. and Smith, D. (2004) A selected ion flow tube study of the reactions of H₃O⁺, NO⁺ and O₂⁺ with some phenols, phenyl alcohols and cyclic carbonyl compounds in support of SIFT-MS and PTR-MS. *International Journal of Mass Spectrometry*. 239 (2–3), pp. 139–146. doi:10.1016/j.ijms.2004.07.022.
- Wang, Y., Xu, R., He, W., Yao, Z., Li, H., Zhou, J., Tan, J., Yang, S., Zhan, R., Luo, G. and Wu, J. (2015) Three-Dimensional Histological Structures of the Human Dermis. *Tissue Engineering Part C: Methods*. 21 (9), pp. 932–944. doi:10.1089/ten.tec.2014.0578.
- Werthén, M., Henriksson, L., Jensen, P.Ø., Sternberg, C., Givskov, M. and Bjarnsholt, T. (2010) An in vitro model of bacterial infections in wounds and other soft tissues. *APMIS*. 118 (2), pp. 156–164. doi:10.1111/j.1600-0463.2009.02580.x.
- White, R., Jeffery, S., Elstone, A. and Cutting, K. (2015) Sepsis and chronic wounds: The extent of the issue and what we should we be aware of. *Wounds UK*. 11 (4), pp. 16–22.
- Whitney, J.D. (2005) Overview: Acute and chronic wounds. *Nursing Clinics of North America*. 40 (2), pp. 191–205. doi:10.1016/j.cnur.2004.09.002.
- Wijetunge, C.D., Li, Z., Saeed, I., Bowne, J., Hsu, A.L., Roessner, U., Bacic, A. and Halgamuge, S.K. (2013) Exploratory analysis of high-throughput metabolomic data.

Metabolomics. 9 (6), pp. 1311–1320. doi:10.1007/s11306-013-0545-6.

Wilke, M.S., Lovering, A.L. and Strynadka, N.C. (2005) β -Lactam antibiotic resistance: a current structural perspective. *Current Opinion in Microbiology*. 8 (5), pp. 525–533. doi:10.1016/j.mib.2005.08.016.

Windey, K., De Preter, V. and Verbeke, K. (2012) Relevance of protein fermentation to gut health. *Molecular Nutrition & Food Research*. 56 (1), pp. 184–196. doi:10.1002/mnfr.201100542.

Woods, J., Boegli, L., Kirker, K.R., Agostinho, A.M., Durch, A.M., deLancey Pulcini, E., Stewart, P.S. and James, G.A. (2012) Development and application of a polymicrobial, in vitro, wound biofilm model. *Journal of Applied Microbiology*. 112 (5), pp. 998–1006. doi:10.1111/j.1365-2672.2012.05264.x.

World Health Organization (2016) WHO | Global action plan on AMR. Available from: <https://www.who.int/antimicrobial-resistance/global-action-plan/en/>.

Worley, B. and Powers, R. (2013) Multivariate Analysis in Metabolomics. *Current Metabolomics*. 1 (1), pp. 92–107. doi:10.2174/2213235x11301010092.

Yao, Z., Kahne, D. and Kishony, R. (2012) Distinct Single-Cell Morphological Dynamics under Beta-Lactam Antibiotics. *Molecular Cell*. 48 (5), pp. 705–712. doi:10.1016/j.molcel.2012.09.016.

Zobell, C.E. and Anderson, D.Q. (1936) Observations on the Multiplication of Bacteria in Different Volumes of Stored Sea Water and the Influence of Oxygen Tension and Solid Surfaces. *The Biological Bulletin*. 71 (2), pp. 324–342. doi:10.2307/1537438.

Zscheppank, C., Wiegand, H.L., Lenzen, C., Wingender, J. and Telgheder, U. (2014) Investigation of volatile metabolites during growth of *Escherichia coli* and *Pseudomonas aeruginosa* by needle trap-GC-MS. *Analytical and Bioanalytical Chemistry*. 406 (26), pp. 6617–6628. doi:10.1007/s00216-014-8111-2.

Appendix I: Published Material

ORIGINAL ARTICLE

***In vitro* discrimination of wound-associated bacteria by volatile compound profiling using selected ion flow tube-mass spectrometry**

E.A. Slade¹, R.M.S. Thorn¹, A.M. Lovering², A. Young³ and D.M. Reynolds¹

¹ Faculty of Health and Applied Sciences, University of the West of England Centre for Research in Biosciences, University of the West of England, Bristol, UK

² Antimicrobial Reference Laboratory Southmead Hospital, Westbury-on-Trym, Bristol, UK

³ The Scar Free Foundation Centre for Children's Burns Research, Bristol Royal Hospital for Children, Bristol, UK

Keywords

bacterial metabolism, selected ion flow tube-mass spectrometry, species discrimination, volatile compound, wound.

Correspondence

Robin Michael Statham Thorn, Centre for Research in Biosciences, Faculty of Health and Applied Sciences, Frenchay Campus, Coldharbour Lane, Bristol BS16 1QY, UK.
E-mail: robin2.thorn@uwe.ac.uk

2017/0302: received 13 February 2016, revised 31 March 2017 and accepted 12 April 2017

doi:10.1111/jam.13473

Abstract

Aims: To determine if bacterial species responsible for clinically relevant wound infection produce specific volatile profiles that would allow their speciation.

Methods and Results: Selected ion flow tube-mass spectrometry (SIFT-MS) in full mass scan mode was used to analyse headspace gases produced by wound-associated bacteria grown *in vitro*, so as to enable identification of bacterial volatile product ion profiles in the resulting mass spectra. Applying multivariate statistical analysis (hierarchical clustering and principal component analysis) to the resultant mass spectra enabled clear speciation. Moreover, bacterial volatile product ions could be detected from artificially contaminated wound dressing material, although the pattern of product ions detected was influenced by culture conditions.

Conclusions: Using selected product ions from the SIFT-MS mass spectra it is possible to discriminate wound-associated bacterial species grown under specific *in vitro* culture conditions.

Significance and Impact of the Study: The results of this study have shown that wound-associated bacteria can be discriminated using volatile analysis *in vitro* and that bacterial volatiles can be detected from wound dressing material. This indicates that volatile analysis of wounds or dressing material to identify infecting microbes has potential and warrants further study.

Introduction

Infection of the wound bed is detrimental to healing, resulting in a failure of the wound to move through the phases of healing in a timely manner (Bowler *et al.* 2001; Werthén *et al.* 2010). This has been demonstrated experimentally in animal models (Gurjala *et al.* 2011; Pastar *et al.* 2013). Colonization and infection of the wound bed develops and changes over time and is dependent on body location; early colonizers are likely to originate from the patient's own skin flora and include coagulase-negative staphylococci and *Staphylococcus aureus*. Subsequently, Gram-negative rods derived from the

gastrointestinal, oral and genitourinary mucosa, and from the local environment may begin to invade (Bowler *et al.* 2001). As wounds mature it is known that anaerobes will play a greater role, as the wound microenvironment is changed by autogenic succession (Bowler *et al.* 2001; Daeschlein 2013). Early diagnosis and management of clinically relevant wound infection is essential to avoid complications. Clinicians currently rely on clinical symptoms, signs and nonspecific laboratory tests for indicators of infection for early diagnosis. Wound and blood cultures are often utilized, but can take several days to be reported and interpretation in the context of wound infection can be difficult (Macgregor *et al.* 2008;

Barajas-Nava *et al.* 2013; Blokhuis-Arkes *et al.* 2015). Burn wounds present additional challenges; the release of high levels of inflammatory mediators result from an altered baseline metabolic profile and a systemic response to injury seen in the burns patient (Greenhalgh *et al.* 2007; Jeschke and Herndon 2014). Standard indicators of infection are therefore difficult to apply and experienced burns specialists are required to attempt to identify subtle signs of infection without definitive point of care testing available (Greenhalgh *et al.* 2007). The World Health Organization (2014) estimates that 265 000 deaths worldwide occur annually as a direct result of burn wound injuries. Sepsis and other complications resulting from infection are the number one cause of mortality in patients with severe burns (Bowler *et al.* 2001; Church *et al.* 2006; Schultz *et al.* 2013; World Health Organization 2014; Saaq *et al.* 2015). Loss of the protective skin barrier, often over a large area of the skin surface, results in a high risk of infection, complicated by an induced state of immunosuppression (Church *et al.* 2006; Schultz *et al.* 2013; Saaq *et al.* 2015). A recent study based in a major UK regional burn centre identified *Staph. aureus* as the most common organism cultured from burn wound swabs, although several other organisms were also identified including β -haemolytic streptococcus, *Pseudomonas aeruginosa*, *Escherichia coli* and coagulase-negative staphylococci (Alrawi *et al.* 2014). Similarly, these organisms were also among the most commonly isolated from burn wounds in a study carried out in an American hospital, with the exception of β -haemolytic streptococcus (DiMuzio *et al.* 2014). A fast, noninvasive method for diagnosing wound infection would benefit patients by allowing clinicians to detect infection at an early stage, enabling appropriate treatment to be promptly administered, reducing the risk of further complications. Furthermore, a UK government-commissioned review (O'Neill 2015) highlights the need for rapid diagnostic tests as a key strategy in the battle against the rise of antimicrobial resistance. In particular, to facilitate a reduction in the use of empiric therapy by allowing treatment to be optimized quickly and to promote a transition from the use of broad-spectrum agents to targeted antibiotics. Introduction of a rapid test for infection, carried out in the clinic, would also aid the reduction of overuse by allowing the implementation of a strategy, whereby antibiotic therapy is not administered to patients without a positive bedside test to prove it is required. This may be of particular importance in the burns clinic where symptoms of inflammation are common, but not necessarily associated with the presence of infection.

Production of volatile compounds (VCs) occurs as a result of normal bacterial metabolism; a diverse and complex array of bacterial VCs have been identified, with up

to 80 different compounds reportedly produced by a single bacterial species (Schulz and Dickschat 2007; Thorn and Greenman 2012). Characteristic VCs of certain micro-organisms have long been recognized by microbiologists, for example, the distinctive odour of indole from *E. coli*. Previous work has shown that using selected ion flow tube-mass spectrometry (SIFT-MS) analysis, it is possible to detect and quantify the different types and concentrations of VCs produced by a range of bacterial species *in vitro* (Thorn *et al.* 2011) and that by employing appropriate statistical techniques the characteristic VC profiles can be used to discriminate between bacterial species. In addition, SIFT-MS analysis has been used to investigate bacterial volatiles emanating from a variety of sample types including; blood culture samples (Allardyce *et al.* 2006a,b; Scotter *et al.* 2006), serum (Spooner *et al.* 2009), urine (Storer *et al.* 2011) and breath (Dummer *et al.* 2013; Gilchrist *et al.* 2013), as well as micro-organisms prepared in liquid culture medium (Thorn *et al.* 2011; Shestivska *et al.* 2015).

SIFT-MS technology was originally developed to study the production of molecules that occur in cold interstellar clouds and is described extensively in the literature (Wang *et al.* 2004; Španěl *et al.* 2006; Smith and Španěl 2011, 2015). Reagent ions (H_3O^+ , NO^+ , O_2^+) generated in a gas ion discharge source are selected by a quadrupole mass filter and injected into a fast flowing carrier gas (usually helium) in the reaction flow tube. Here, the sample gas is introduced via a heated sample inlet and chemical ionization occurs resulting in the production of characteristic product ions. Downstream reagent and product ions are separated and counted by a further quadrupole mass spectrometer and electron multiplier detector system. Absolute concentrations of trace gases can be quantified based on the ratios of ion count rates and the reaction rate constants determined by detailed studies of the reaction of VCs with the three precursor ions.

The main aim of this study is to detect and discriminate wound-associated bacteria, grown *in vitro*, using SIFT-MS coupled with multivariate data analysis. Bacterial species were cultured in complex media; (tryptone soya broth (TSB)) and in simulated wound fluid (SWF) to simulate wound similar conditions (Werthén *et al.* 2010). This approach was developed to determine whether the main bacterial species associated with wound infection produce characteristic volatile profiles, which could be used to develop a diagnostic tool for speciation. Wound dressing removal is associated with increased pain which can cause considerable patient distress, this in itself can contribute to delayed wound healing (Price *et al.* 2008; Upton *et al.* 2012). The ability to assess a wound for infection without removing the dressing, or by

direct assessment of discarded dressing material to minimize additional interference with the wound, would be an advantage. With this in mind, the final aim of this study was to investigate the detection of species-specific profiles from sterile dressing material inoculated with wound-associated bacteria. This will help determine if future volatile analysis of real patient-discarded dressing material has the potential to be used to diagnose bacterial species present in the wound bed.

Materials and methods

Preparation and maintenance of bacterial cultures

Bacterial cultures were maintained on beads (Microbank; Pro Lab Diagnostics, Canada) at -80°C , resuscitated as required on tryptone soya agar (Oxoid, UK) and incubated aerobically at 37°C , with the exception of *Streptococcus pyogenes* cultures, which were resuscitated on blood agar (Oxoid). All working cultures were stored on sealed plates at 4°C . The following bacterial strains were used during this study; *E. coli* NCTC 10418 (EC1), *E. coli* ATCC 10536 (EC2), *E. coli* NCTC 12900 (EC3), *E. coli* SMD 6099 (clinical isolate) (EC4), *Ps. aeruginosa* NCIMB 10548 (PA1), *Ps. aeruginosa* ATCC 15442 (PA2), *Ps. aeruginosa* NCIMB 8295 (PA3), *Ps. aeruginosa* CC197 (clinical isolate) (PA4), *Proteus mirabilis* NCIMB 701880 (PM1), *Pr. mirabilis* NP1 (clinical isolate) (PM2), *Pr. mirabilis* NP4 (clinical isolate) (PM3), *Pr. mirabilis* NP6 (clinical isolate) (PM4), *Staph. aureus* CC174 (SA1), *Staph. aureus* NCIMB 6571 (SA2), *Staph. aureus* NTCC 6538 (SA3), methicillin resistant *Staph. aureus* (Llewelyn; clinical strain) (SA4), *Staphylococcus epidermidis* NCTC 11536 (SE1), *Staphylococcus epidermidis* NCIMB 12721 (SE2), *Strep. pyogenes* NCTC 10871 (SP1) and *Strep. pyogenes* NCTC 10874 (SP2).

Liquid broth cultures for headspace analysis

Overnight plate cultures were used to prepare a test suspension of each micro-organism in 10 ml TSB (Oxoid, UK) adjusted to an $\text{OD}_{620\text{ nm}}$ of 0.20. One millilitre of the test suspension was used to inoculate 9 ml of sterile TSB, aseptically dispensed into sterile 40-ml glass vials with a PTFE screw cap containing a silicone septum (Supelco, UK), resulting in a final starting $\text{OD}_{620\text{ nm}}$ of 0.02 in each vial. For each bacterial strain used, three separate vials were inoculated, and on each day the experiment was performed, three vials containing 10 ml sterile TSB were incubated as controls. Test and control vials were incubated aerobically at 37°C and 200 rev min^{-1} (Stuart S150 Orbital Incubator; Bibby Scientific, UK) for 5 h.

Liquid cultures (simulated wound fluid) for headspace analysis

Overnight plate cultures were used to prepare a test suspension of each micro-organism in 10 ml diluent containing 0.85% NaCl with 0.1% peptone (Oxoid) adjusted to an $\text{OD}_{620\text{ nm}}$ of 0.20. One millilitre of the test suspension was used to inoculate 40-ml glass vials (as specified previously), containing 5 ml fetal bovine serum (FBS) (Sigma Aldrich) and 4 ml sterile diluent, resulting in a SWF containing FBS and 0.85% NaCl with 0.1% peptone at a ratio of 1 : 1 by volume (Werthén *et al.* 2010) inoculated with the organism of interest at a final starting $\text{OD}_{620\text{ nm}}$ of 0.02 in each test vial. Test vials were prepared in triplicate and incubated for 5 h prior to analysis as described above.

Wound dressing cultures; simulated wound fluid

Overnight plate cultures were used to prepare test suspensions in 10 ml diluent containing 0.85% NaCl with 0.1% peptone (Oxoid) adjusted to an $\text{OD}_{620\text{ nm}}$ of 0.20. Ten millilitres of SWF was used to moisten a $10 \times 10\text{ cm}$ nonadherent sterile wound dressing, composed of a cellulose pad laminated with a film of polyethylene, housed on a wire support in a sterile incubation chamber. One millilitre of bacterial test suspension was used to inoculate the dressing. Inoculated dressings were incubated in the sealed incubation chambers for 5 h at 37°C . Throughout the incubation period the dressing samples were slowly perfused with sterile SWF at a rate of approximately 2 ml h^{-1} via a sterile needle, to simulate the conditions of a moderately exuding dressed wound (50 ml in 24 h; Thomas *et al.* 1996). Following the incubation period, dressing samples were aseptically removed from the incubation chambers and transferred to individual 1-l gas sampling bags (Tedlar[®]; Supelco) which were sealed and filled with synthetic air (20% oxygen, 80% nitrogen). The gas sampling bags were incubated for a further 1 h at 37°C to allow the equilibration of the headspace gases.

SIFT-MS analysis

Following incubation, samples were analysed by SIFT-MS (Profile 3; Instrument Science Limited, UK) in 'Full Mass Scan' mode using the H_3O^+ precursor ion; each sample was analysed three times using repeat scans of 100 s, over a spectrum range of 10–200 m/z , to generate a total of nine scans per bacterial strain from three independent replicate samples. Samples were introduced to the instrument by piercing the silicone septum of the sample vial with a sterile needle attached to the SIFT-MS direct

sampling inlet, samples were vented with a second sterile needle attached to a $0.2 \mu\text{mol l}^{-1}$ syringe filter (Ministat; Sartorius Stedim Biotech, Germany) to allow the free flow of headspace gases. Similarly, dressing samples were analysed by piercing the silicone septum of the gas sampling bag with a sterile needle attached to the direct sampling inlet of the SIFT-MS instrument.

Data analysis

Mean count rates were calculated for each detected mass-to-charge ratio (m/z) product ion across the mass spectrum for each bacterial strain included in the analysis ($n = 3$). Where a product ion was detected in both the headspace of a bacterial culture and the uninoculated control, t -tests were performed to compare the count rate detected. Only product ions detected at significant levels ($P < 0.05$) from the bacterial cultures compared to background control levels were included for further analysis. The mean product ion count rate of background volatiles from the uninoculated culture media were then subtracted from those detected in bacterial culture headspace, to determine the total count rate attributed to production of VCs in the bacterial culture. Any corrected negative values were disregarded (indicating a reduction significantly below the background levels), as were reagent ion peaks. A threshold detection signal of 10 counts per second (cps) was applied to identify discriminant VC product ion data. Further selection was required to identify discriminate product ions for the SWF data. To achieve this product ions were disregarded if the 10 cps threshold was met by only a single strain of any species included in the study.

Ward's method of Hierarchical clustering was applied to the resultant data set. This is a data mining technique, whereby an algorithm is used to score the dissimilarity between cases in the data set and a matrix constructed. The dissimilarity matrix is visualized through the production of a dendrogram, in which the branching of the clusters groups the cases with the least dissimilarity, and the distance between the nodes indicates the relationship between the clusters. The data were subsequently transformed using principal component analysis (PCA), visualized by constructing plots of the principal components scores for each data set. All data were analysed using Microsoft Excel 2013 (Microsoft Corporation, Redmond, WA) and IBM SPSS Statistics ver. 20.0 (IBM Corporation, Armonk, NY). A correction for multiple comparisons was not performed. Using the SIFT-MS kinetics library database, which has been compiled by the instrument manufacturers through detailed studies of the reactions between neutral analyte compounds and the three reagent ions, it is possible to make preliminary

identifications of the VCs based on the detected SIFT-MS product ions.

Results

Headspace analysis of wound-associated bacteria cultured in complex growth medium

Multivariate analysis of the headspace count rates (\log_{10}) of selected mass spectra product ions using Ward's method of Hierarchical clustering analysis is visualized by the dendrogram in Fig. 1. This shows successful discrimination between *Pr. mirabilis*, *E. coli*, *Staph. aureus* and *Staph. epidermidis* based on the profile of selected VC product ions detected. The data were transformed using PCA to reduce the selected variables to principal components. The first two principal components account for 36.3 and 21.7% of the variability within the data respectively (Fig. 2a). Plotting the scores generated by PCA enables the complex data set to be represented in two-dimensional space and clearly visualizes the association of each bacterial strain with the derived principal components and shows that the strains of *Pr. mirabilis* and *E. coli*, occupy discrete regions of the two-dimensional plot. *Staphylococcus aureus* and *Staph. epidermidis* appear to occupy overlapping regions on this plot, however, when the third component is employed (accounting for 10.1% of the total variance) to construct a three-dimensional plot, these two species separate along the z-axis (not shown). Figure 2(b) shows the loading of the eigenvectors representing 51 selected product ions based on the selection criteria described in the materials and methods. It should be noted that when the initial t -tests were performed, negative product ion count rate values were disregarded since these represent the consumption of substrates in the growth medium by the bacterial species, which was not the focus of this study. The 51 selected product ions constitute the original variables for the PCA shown in Fig. 2a. This eigenvector plot (Fig. 2b) shows the contribution of each of the original variables; product ion count rates, to the derived first two principal components and indicates the influence of these variables in determining the position of each test strain. It is important to note that both the absence and presence of product ions dictates the spatial location of the given bacterial strain within the principal component plot. For example, when considering *Ps. aeruginosa* and *Strep. pyogenes* within the principal component, plot the absence of the majority of detected product ions and the presence of product ions m/z 18 and 28 are responsible for the plotted location of these species. This data set shows no significant differentiation between *Ps. aeruginosa* and *Strep. pyogenes* based on the profile of selected VC product ions

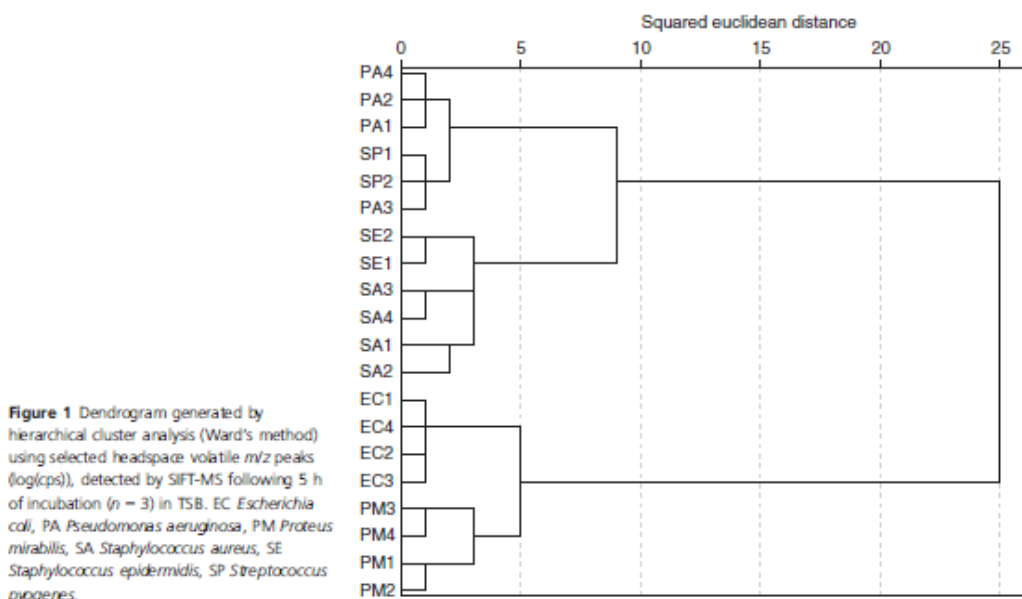


Figure 1 Dendrogram generated by hierarchical cluster analysis (Ward's method) using selected headspace volatile m/z peaks ($\log(\text{cps})$), detected by SIFT-MS following 5 h of incubation ($n = 3$) in TSB. EC, *Escherichia coli*, PA, *Pseudomonas aeruginosa*, PM *Proteus mirabilis*, SA *Staphylococcus aureus*, SE *Staphylococcus epidermidis*, SP *Streptococcus pyogenes*.

detected following 5 h of incubation in TSB. This was predominantly due to the absence of product ions detected in the culture headspace, rather than the presence of numerous similar volatile product ions. Although a total of 51 product ions were selected for the analysis of all bacterial species, many of the 51 product ions were absent from the headspace of both *Ps. aeruginosa* and *Strep. pyogenes* strains and this is likely to be the reason for the inability to discriminate between these species. To further assess whether these species could be differentiated based on volatile analysis when cultured in TSB, independent samples were cultured for 24 h and the headspace gases were analysed by SIFT-MS and multivariate analysis performed on the data as previously described. Following product ion selection, hierarchical cluster analysis implementing Ward's method resulted in the production of a dendrogram showing the two species separated into discrete clusters, indicating differences between headspace VC product ions of *Ps. aeruginosa* and *Strep. pyogenes* detected following 24 h of incubation (Fig. 3).

Headspace analysis of wound-associated bacteria cultured in a simulated wound fluid

Hierarchical clustering analysis of selected product ions implementing Ward's method and using squared Euclidean distance as a measure of resemblance enabled

discrimination of *Pr. mirabilis*, *E. coli*, *Strep. pyogenes* and *Ps. aeruginosa* at the species level and staphylococci at the genus level as visualized by the dendrogram shown in Fig. 4. Principal component analysis was utilized to transform this data set, the first two principal components account for 34.3 and 19.7% of the total variance (Fig. 5a). It can be seen by plotting the PCA scores that strains of *E. coli* and staphylococci each occupy specific discrete regions of the two-dimensional plot. Figure 5(b) shows the loading plot of 26 original variables (product ions) detected by SIFT-MS headspace analysis on the first two principal components, generated by the PCA represented in Fig. 5a. In Fig. 5a, strains of *Pr. mirabilis*, *Ps. aeruginosa* and *Strep. pyogenes* appear to occupy overlapping regions, however, when plotted in three dimensions employing the third principal component (accounting for 9.5% of the total variance), strains of these species are separated along the z-axis (data not shown).

Wound dressing cultures; simulated wound fluid

Figure 6 shows the SIFT-MS product ions detected following analysis of the headspace of wound dressing material inoculated with *Ps. aeruginosa* (PA2), *E. coli* (EC2) and *Staph. aureus* (SA3). The plot includes only the VCs detected at levels significantly higher than the uninoculated controls, following background subtraction. High background count rates across the mass spectral range

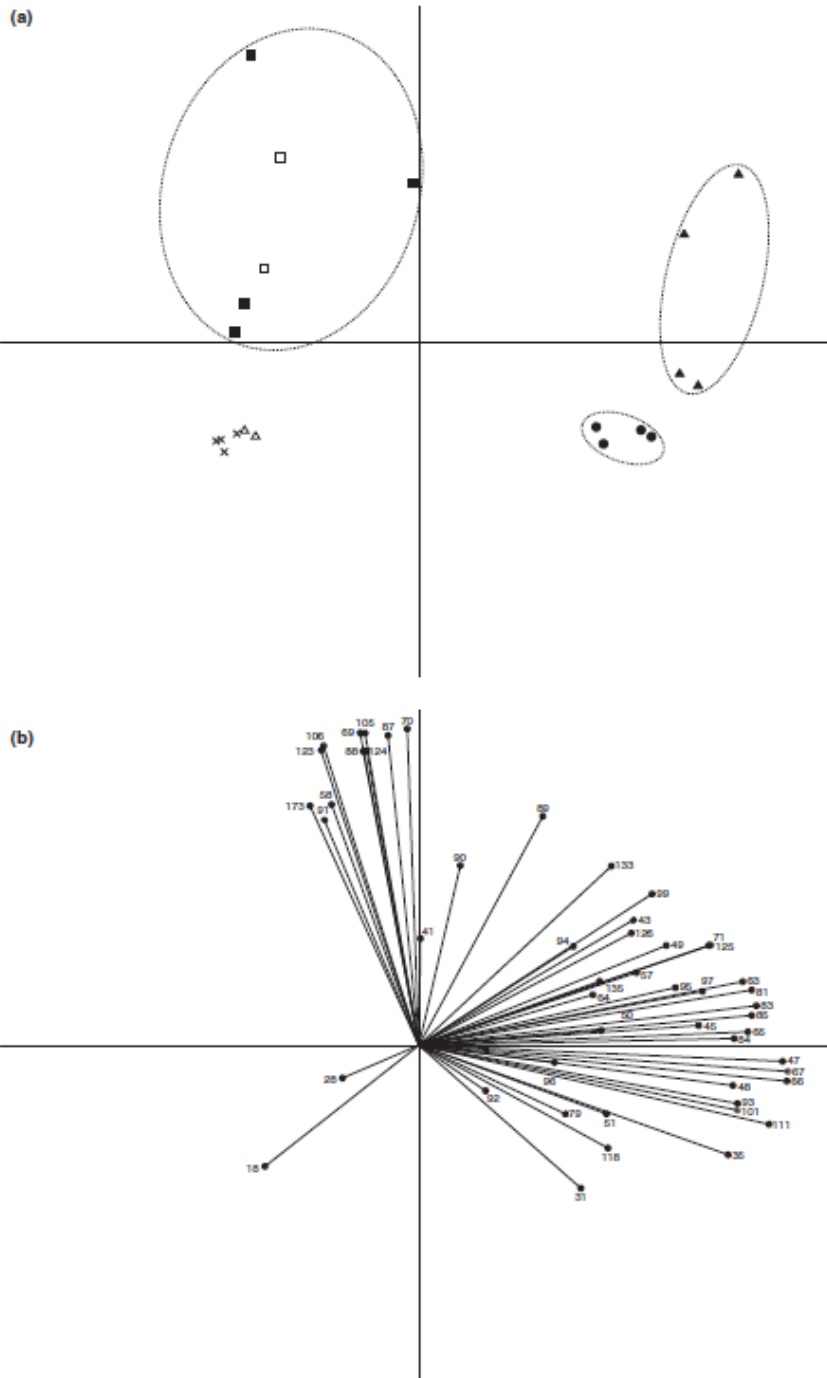


Figure 2 (a) Plot of the scores of the first two principal components generated by principle component analysis of SIFT-MS concentration data of selected headspace volatiles of bacterial cultures ($n = 3$) incubated for 5 h in TSB. Principal component 1 (horizontal axis) accounts for 36.3% of the total variation in the original data set and principal component 2 (vertical axis) accounts for 21.7%. Filled circle—*Escherichia coli*, cross—*Pseudomonas aeruginosa*, filled triangle—*Proteus mirabilis*, open square—*Staphylococcus epidermidis*, filled square—*Staphylococcus aureus*, open triangle—*Streptococcus pyogenes*. (b) Principal component analysis loading plot—selected m/z peaks detected by SIFT-MS analysis of cultures incubated for 5 h in TSB. Data points indicate the loading of each m/z peak (variable) on the first two principal components generated from the principal component analysis.

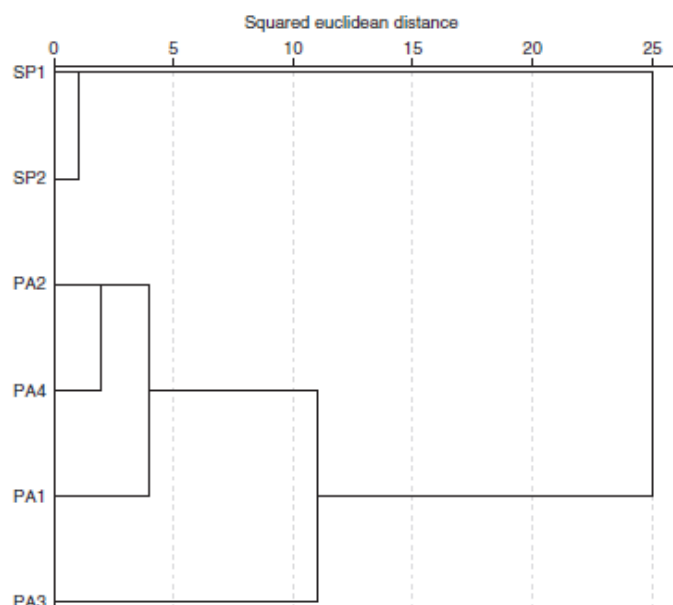


Figure 3 Dendrogram generated by hierarchical cluster analysis (Ward's method) using selected headspace volatile m/z peaks ($\log(\text{cps})$), detected by SIFT-MS following 24 h of incubation ($n = 3$) in TSB. PA—*Pseudomonas aeruginosa*, SP—*Streptococcus pyogenes*.

were detected from the uninoculated dressing material. However, a range of VC product ions were detected above the background count rates from the inoculated dressing samples. Interestingly, these differed from those detected in the headspace of the same species cultured in liquid medium, in both the number and the mass-to-charge ratio of product ions detected. Only 12 product ions were detected in the headspace of the wound dressing material and of these only six were common to the product ions detected in the headspace of bacteria cultured in SWF.

Discussion

The main study aim was to identify wound-associated bacterial species specific volatile profiles *in vitro*. The mass spectral profile of VC product ions derived from the wound-associated bacterial species included in this study varies between species. This also extends to some strains from a single species, as reported in previous

studies (Thorn *et al.* 2011; Shestivska *et al.* 2015). This study has demonstrated that the culture conditions namely composition of culture media and duration of incubation, influence the range of product ions and count rates of the resultant VC mass spectra. The range and relative concentrations of bacterial VCs under varying physicochemical conditions has been previously observed in other research studies (O'Hara and Mayhew 2009; Chippendale *et al.* 2011; Dolch *et al.* 2012a; Dolch *et al.* 2012b). The range and count rates of product ions detected are greater in TSB, a complex nutrient-rich commercially available culture media, compared to a SWF containing peptone, NaCl and FBS. A comparison of the discriminant product ions produced when bacteria were grown in either TSB (Fig. 2) or SWF (Fig. 5), shows that there are clear differences as well as similarities. For example, m/z 28 is clearly important for the discrimination of *Ps. aeruginosa*. The differing nutrient sources in the culture media almost certainly results in the upregulation of altered bacterial metabolic pathways, resulting in

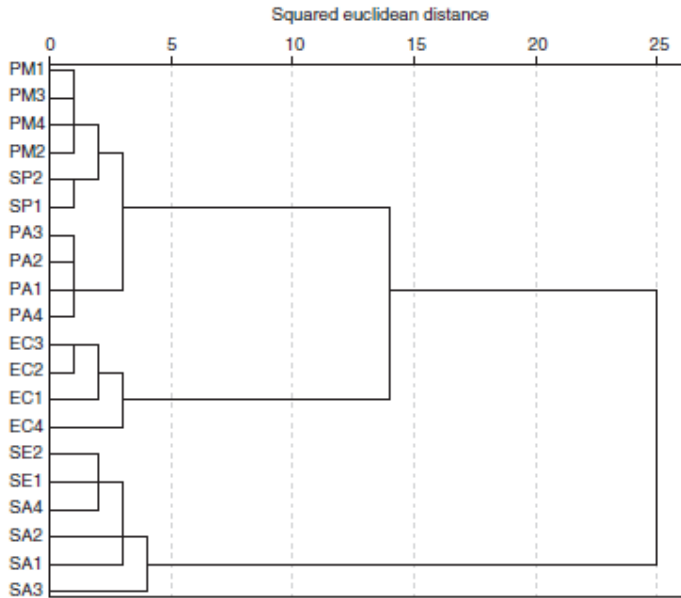


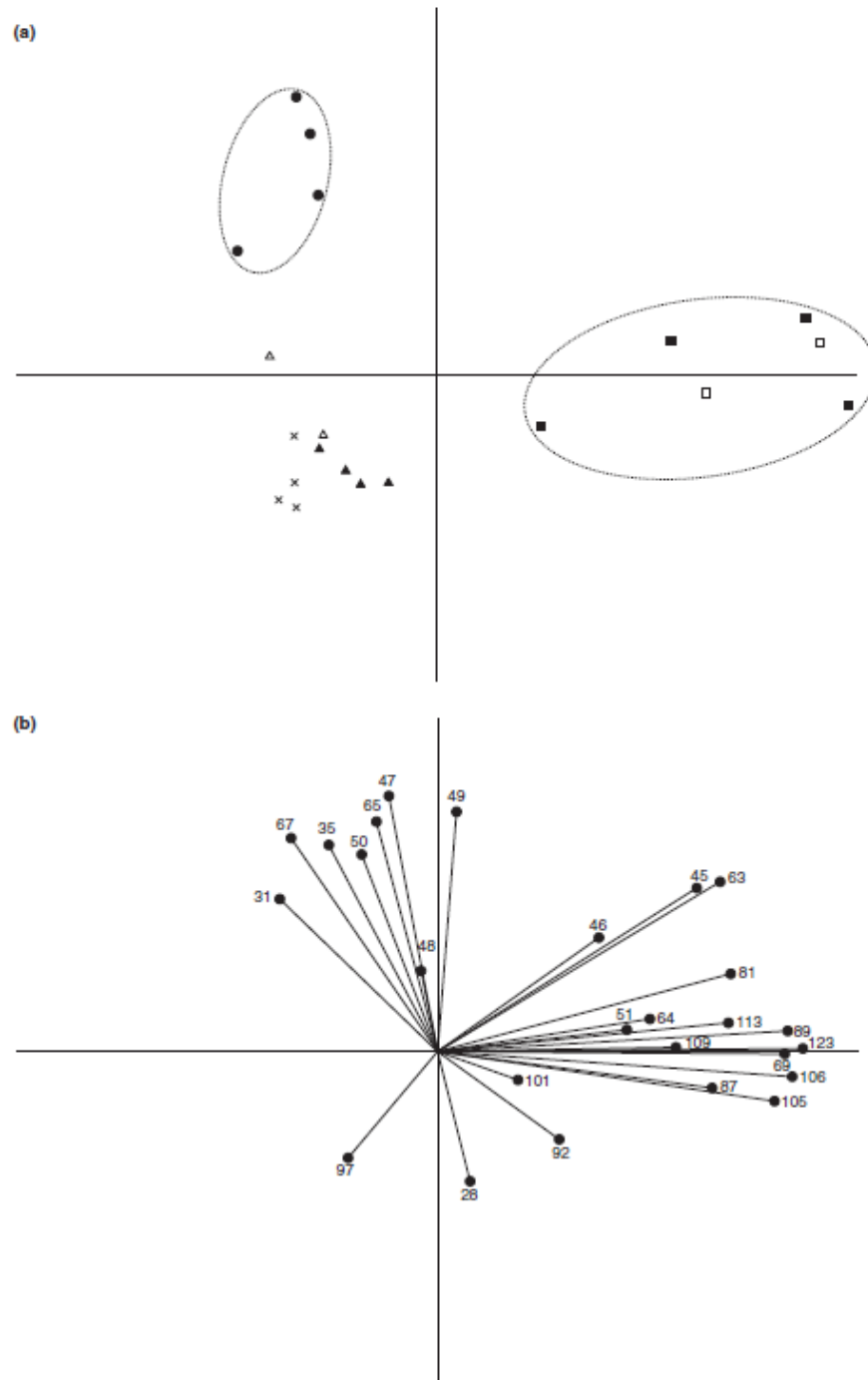
Figure 4 Dendrogram generated by hierarchical cluster analysis (Ward's method) using 26 selected headspace volatile m/z peaks ($\log(\text{cps})$), detected by SIFT-MS following 5 h of incubation ($n = 3$) in SWF. EC *Escherichia coli*, PA *Pseudomonas aeruginosa*, PM *Proteus mirabilis*, SA *Staphylococcus aureus*, SE *Staph. epidermidis*, SP *Streptococcus pyogenes*.

the production of different volatile metabolites (Audrain *et al.* 2015).

The results from this study demonstrate that, it is possible to discriminate wound-associated bacterial species based on the detected VC product ion profiles, whether cultures are grown within complex medium (TSB) or under wound similar conditions (in SWF). After 5 h of incubation it was possible to discriminate several species based on the profiles using Ward's method of hierarchical clustering analysis; however, it was not possible to discriminate between strains of *Ps. aeruginosa* and *Strep. pyogenes*. Similarly, when the transformed data set was plotted as principal components, *Ps. aeruginosa* and *Strep. pyogenes* occupy closely adjacent regions on the two-dimensional plot. This is the result of the absence of product ions detected in the headspace of either species under these conditions, visualized by comparing the two plots in Fig. 2. Increasing the incubation period to 24 h resulted in an increase in the number and count rates of

SIFT-MS product ions detected from *Ps. aeruginosa*. This included high count rates for the m/z 18 product ion in all strains and the m/z 28 product ion in two of the four strains analysed. Hierarchical clustering analysis of the data obtained after 24 h of incubation resulted in successful discrimination between the stains of these two species, based on the clustering shown in the resulting dendrogram. It is possible to make a preliminary identification of the VCs which correspond with the detected SIFT-MS product ions, using predetermined reaction rate constants. When using the H_3O^+ reagent ion, m/z 18 and 28 product ions indicate the presence of protonated ammonia and hydrogen cyanide respectively (Španěl *et al.* 2004; Turner *et al.* 2006). It has been reported elsewhere that both ammonia and hydrogen cyanide production are characteristic of *Ps. aeruginosa* (Nawaz *et al.* 1991; Gilchrist *et al.* 2011). A recent study (Neerinx *et al.* 2015) which investigated the production of these volatiles over time in a number of *Ps. aeruginosa* strains determined

Figure 5 (a) Plot of the scores of the first two principal components generated by principle component analysis of SIFT-MS concentration data of selected headspace volatiles of bacterial cultures ($n = 3$) incubated for 5 h in SWF. Principal component 1 (horizontal axis) accounts for 34.3% of the total variation in the original data set and principal component 2 (vertical axis) accounts for 19.7%. Filled circle—*Escherichia coli*, cross—*Pseudomonas aeruginosa*, filled triangle—*Proteus mirabilis*, open square—*Staphylococcus epidermidis*, filled square—*Staphylococcus aureus*, open triangle—*Streptococcus pyogenes*. (b) Principal component analysis loading plot—selected m/z peaks detected by SIFT-MS analysis of cultures incubated for 5 h in SWF. Data points indicate the loading of each m/z peak (variable) on the first two principal components generated from the principal component analysis.



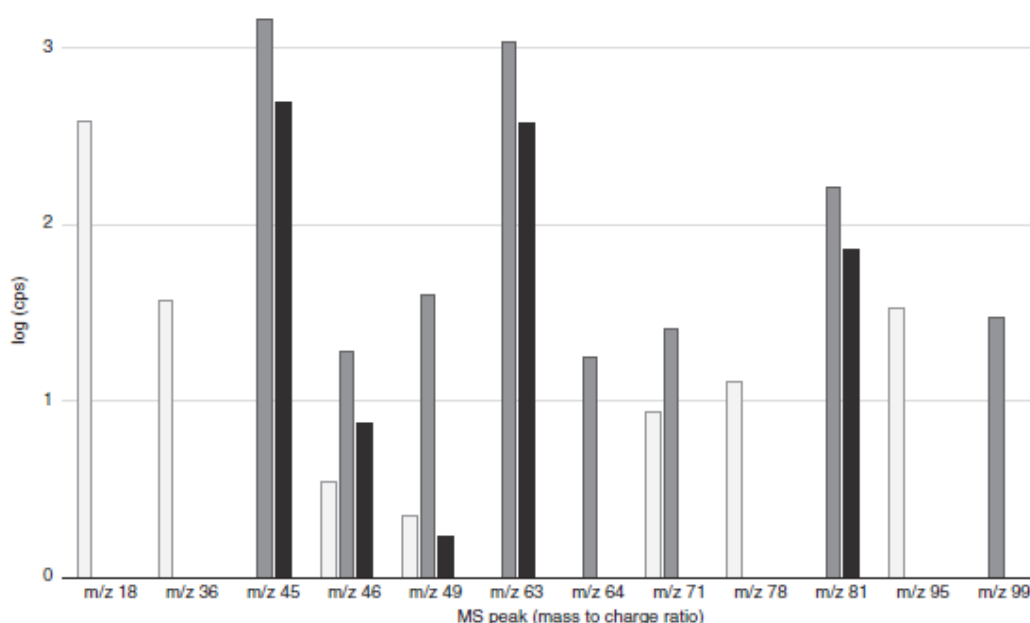


Figure 6 Mass charge peaks detected at levels significantly greater ($P < 0.05$) than control levels (SWF only) from dressing material inoculated with *Pseudomonas aeruginosa* PA2 (pale grey), *Escheichia coli* EC2 (dark grey) or *Staphylococcus aureus* SA3 (black), incubated for 5 h at 37°C while continuously perfused with sterile SWF.

that both compounds began to rise above detectable levels only in older cultures, as they began to enter stationary phase. This would explain the presumptive detection of these important volatiles only after 24 h of culture within this study. It is highly likely that production of these particular volatiles will be important for identification of *Ps. aeruginosa* *in vivo*, where growth conditions result in a slow growing biofilm state. Indeed, elevated hydrogen cyanide concentrations in nose-exhaled breath have been identified using SIFT-MS as a potential biomarker of *Ps. aeruginosa* infection in adult cystic fibrosis patients (Gilchrist *et al.* 2013).

The results of this study successfully demonstrated that it is possible to discriminate wound-associated bacterial species based on a profile of selected SIFT-MS product ions when cultured under wound similar conditions. Using Ward's method of hierarchical clustering analysis to determine strain relatedness, four of the six bacterial species were successfully discriminated, based on the clustering shown in the resulting dendrogram. Using PCA and constructing a plot of the first three principal component scores resulted in similar discrimination of the bacterial species investigated to the hierarchical clustering analysis, indicating that either of these techniques maybe suitable for modelling this data set. However, the two

species of staphylococci could not be discriminated from each other. Further analysis of the headspace of both species of staphylococci following 24 h of incubation in SWF, also failed to successfully discriminate these species, in contrast to staphylococci cultured in complex culture media (TSB). Future work will assess whether it is possible to discriminate between species of staphylococci based on volatile headspace analysis when these species are grown as biofilm rather than in liquid culture. A biofilm model will simulate more closely the real wound environment (James *et al.* 2008). The altered growth conditions will likely affect the metabolic profile of the organism and result in a change in the volatile metabolites produced.

This study also investigated the detection of species-specific profiles from sterile dressing material inoculated with wound-associated bacteria; continuously perfused with a SWF. A range of SIFT-MS product ions with count rates significantly greater than background control levels were detected from the bacterial species analysed. In addition, the different species resulted in the detection of different mass spectra profiles (Fig. 6). This indicates that volatile analysis of wound dressing material to identify infecting microbes may be possible. Further research is required to validate this approach, and a pilot study is

now being undertaken to identify volatile product ion spectra from the gaseous headspace of patient's discarded wound dressings. Ultimately, it will be essential to identify clinically relevant infection as well as the causative organism. However, the ability to identify microbial VC product ions among the background derived from the dressing, demonstrates that assessment of a dressed wound or discarded dressing may be a valid approach.

As previously discussed, the profile of the product ions of the species grown in wound dressing material was different to those detected from the same species grown using the same medium (SWF) in liquid culture. This suggests that the growth conditions as well as the medium have an influence over the metabolic state of the organism and therefore the array of volatiles produced. The bacterial cultures were exposed to the same total volume of SWF over the 5-h incubation period for both culture conditions. The differing traits of bacterial biofilms compared to their planktonic counterparts are now well documented (Cooper *et al* 2014) and the development of biofilm within the wound dressing material is likely to be a contributing factor to the differing profiles identified. Biofilms occurring in the wound bed *in vivo* are not adhered to a solid surface, such as the fibres of dressing material, but the semi-solid structures that make up the tissue (Cooper *et al* 2014). Development of a wound biofilm model based on a continuously perfused semi-solid matrix would be an advantage for future research. This would allow volatile profiles of the wound-associated organisms to be investigated under conditions that closely simulate wound infection and would further facilitate the development of this approach to wound diagnostics. It is highly likely that unique product ion profiles are produced when these bacterial species cause infection in real wounds, not only as a result of the specific growth conditions but also due to interactions between the bacterial species and the host immune response.

Using the predetermined reaction rate constants, presumptive identification of the neutral analyte compounds which correspond to the detected SIFT-MS product ions is possible. However, it is important to be aware that the reaction of a single selected precursor ion with similar VCs or compound fragments can result in the production of the same product ions. For example, utilizing the H_3O^+ precursor ion as used within this study, the production of 89 *m/z* product ion can result from the protonation of a number of different analytes with a molecular weight of 88 Da, including pentanol ($C_5H_{12}O$), butyric acid (C_3H_7COOH) and putrescine ($C_4H_{12}N_2$). Furthermore, if a mixture known to contain more than one of these compounds were analysed using the H_3O^+ precursor ion in a multi-ion monitoring (MIM) mode (not used within this study) it would only be possible to

determine the total partial pressure of all compounds resulting in the common product ion (Wang *et al* 2004). In some cases it may be possible to rule out the presence of certain compounds based on the nature of the sample being analysed. However, pentanol ($C_5H_{12}O$), butyric acid (C_3H_7COOH) and putrescine ($C_4H_{12}N_2$) could all be produced as a result of bacterial metabolism, as products of fermentation and decarboxylation reactions (Schulz and Dickschat 2007; Thorn and Greenman 2012; Audrain *et al* 2015). Ambiguity in the identification of neutral analyte compounds can potentially be overcome by the analysis of the sample using multiple precursor ions, usually H_3O^+ and NO^+ , as the reaction of compounds with different precursor ions can result in the production of different product ions. The compounds may then be identified and quantified using the appropriate precursor ion reaction (Wang *et al* 2004). This study has demonstrated that using SIFT-MS and multivariate statistical analysis it is possible to discriminate wound-associated bacterial species based on the profile of selected SIFT-MS product ions when these species are grown in complex culture media, both in TSB and SWF. Furthermore, our proof-of-principle experiment has confirmed that it is possible to detect VC product ions derived from bacteria when cultured within wound dressing material using a SWF. Future investigations must focus on identifying the compounds present in the headspace of bacterial culture by utilizing GC/MS for preliminary exploratory analysis and multiple precursor ions for SIFT-MS studies using MIM mode to accurately quantify the volatiles of interest identified.

Acknowledgements

This work was supported by the University of the West of England, Bristol via an internal QR research grant (2014/15).

Conflict of Interest

No conflict of interest declared.

References

- Allardyce, R.A., Hill, A.L. and Murdoch, D.R. (2006a) The rapid evaluation of bacterial growth and antibiotic susceptibility in blood cultures by selected ion flow tube mass spectrometry. *Diagn Microbiol Infect Dis* 55, 255–261.
- Allardyce, R.A., Langford, V.S., Hill, A.L. and Murdoch, D.R. (2006b) Detection of volatile metabolites produced by bacterial growth in blood culture media by selected ion flow tube mass spectrometry (SIFT-MS). *J Microbiol Methods* 65, 361–365.

- Alrawi, M., Crowley, T.P. and Pape, S.A. (2014) Bacterial colonisation of the bum wound: a UK experience. *J Wound Care* **23**, 274–277.
- Audrain, B., Farag, M.A., Ryu, C.M. and Ghigo, J.M. (2015) Role of bacterial volatile compounds in bacterial biology. *FEMS Microbiol Rev* **39**, 222–233.
- Barajas-Nava, L.A., López-Alcalde, J., Roqué i Figuls, M., Solà, I. and Bonfill Cosp, X. (2013) Antibiotic prophylaxis for preventing burn wound infection. *Cochrane Database Syst Rev* **6**, CD008738.
- Blokhuys-Arkes, M.H.E., Haalboom, M., van der Palen, J., Heinzle, A., Sigl, E., Guebitz, G. and Beuk, R. (2015) Rapid enzyme analysis as a diagnostic tool for wound infection: comparison between clinical judgment, microbiological analysis, and enzyme analysis. *Wound Repair Regen* **23**, 345–352.
- Bowler, P.G., Duerden, B.I. and Armstrong, D.G. (2001) Wound microbiology and associated approaches to wound management. *Clin Microbiol Rev* **14**, 244–269.
- Chippendale, T.W.E., Španěl, P. and Smith, D. (2011) Time-resolved selected ion flow tube mass spectrometric quantification of the volatile compounds generated by *E. coli* JM109 cultured in two different media. *Rapid Commun Mass Spectrom* **25**, 2163–2172.
- Church, D., Elsayed, S., Reid, O., Winston, B. and Lindsay, R. (2006) Burn wound infections. *Clin Microbiol Rev* **19**, 403–434.
- Cooper, R., Bjamsholt, T. and Alhede, M. (2014) Biofilms in wounds: a review of present knowledge. *J Wound Care* **23**, 570–582.
- Daeschlein, G. (2013) Antimicrobial and antiseptic strategies in wound management. *Int Wound J* **10**, 9–14.
- DiMuzio, E.E., Healy, D.P., Durkee, P., Neely, A.N. and Kagan, R.J. (2014) Trends in bacterial wound isolates and antimicrobial susceptibility in a pediatric bum hospital. *J Burn Care Res* **35**, e304–e311.
- Dolch, M.E., Hornuss, C., Klocke, C., Praun, S., Villinger, J., Denzer, W., Schelling, G. and Schubert, S. (2012a) Volatile compound profiling for the identification of Gram-negative bacteria by ion-molecule reaction-mass spectrometry. *J Appl Microbiol* **113**, 1097–1105.
- Dolch, M.E., Hornuss, C., Klocke, C., Praun, S., Villinger, J., Denzer, W., Schelling, G. and Schubert, S. (2012b) Volatile organic compound analysis by ion molecule reaction mass spectrometry for Gram-positive bacteria differentiation. *Eur J Clin Microbiol Infect Dis* **31**, 3007–3013.
- Dummer, J., Storer, M., Stumey, S., Scott-Thomas, A., Chambers, S., Swanney, M. and Epton, M. (2013) Quantification of hydrogen cyanide (HCN) in breath using selected ion flow tube mass spectrometry—HCN is not a biomarker of *Pseudomonas* in chronic suppurative lung disease. *J Breath Res* **7**, 17105.
- Gilchrist, F.J., Alcock, A., Belcher, J., Brady, M., Jones, A., Smith, D., Španěl, P., Webb, K. et al. (2011) Variation in hydrogen cyanide production between different strains of *Pseudomonas aeruginosa*. *Eur Respir J* **38**, 409–414.
- Gilchrist, F.J., Bright-Thomas, R.J., Jones, A.M., Smith, D., Španěl, P., Webb, A.K. and Lenney, W. (2013) Hydrogen cyanide concentrations in the breath of adult cystic fibrosis patients with and without *Pseudomonas aeruginosa* infection. *J Breath Res* **7**, 26010.
- Greenhalgh, D.G., Saffle, J.R., Holmes, J.H., Gamelli, R.L., Palmieri, T.L., Horton, J.W., Tompkins, R.G., Traber, D.L. et al. (2007) American burn association consensus conference to define sepsis and infection in burns. *J Burn Care Res* **28**, 776–790.
- Gurjala, A.N., Geringer, M.R., Seth, A.K., Hong, S.J., Smeltzer, M.S., Galiano, R.D., Leung, K.P. and Mustoe, T.A. (2011) Development of a novel, highly quantitative in vivo model for the study of biofilm-impaired cutaneous wound healing. *Wound Repair Regen* **19**, 400–410.
- James, G.A., Swogger, E., Wolcott, R., Pulcini, Ed., Secor, P., Sestrich, J., Costerton, J.W. and Stewart, P.S. (2008) Biofilms in chronic wounds. *Wound Repair Regen* **16**, 37–44.
- Jeschke, M.G. and Herndon, D.N. (2014) Burns in children: standard and new treatments. *Lancet* **383**, 1168–1178.
- Macgregor, L., Calne, S., Day, K., Jones, J., Pugh, A. and Walker, J. (2008) Wound infection in clinical practice. *Int Wound J* **5**, iii–11.
- Nawaz, M.S., Davis, J.W., Wolfram, J.H. and Chapatwala, K.D. (1991) Degradation of organic cyanides by *Pseudomonas aeruginosa*. *Appl Biochem Biotechnol* **28–29**, 865–875.
- Neerinx, A.H., Mandon, J., van Ingen, J., Arslanov, D.D., Mouton, J.W., Harren, F.J.M., Merkus, P.J.F.M. and Cristescu, S.M. (2015) Real-time monitoring of hydrogen cyanide (HCN) and ammonia (NH₃) emitted by *Pseudomonas aeruginosa*. *J Breath Res* **9**, 27102.
- O'Hara, M. and Mayhew, C.A. (2009) A preliminary comparison of volatile organic compounds in the headspace of cultures of *Staphylococcus aureus* grown in nutrient, dextrose and brain heart bovine broths measured using a proton transfer reaction mass spectrometer. *J Breath Res* **3**, 27001.
- O'Neill, J. (2015) Rapid diagnostics: stopping unnecessary use of antibiotics. *Indep Rev AMR*.
- Pastar, I., Nusbaum, A.G., Gil, J., Patel, S.B., Chen, J., Valdes, J., Stojadinovic, O., Plano, L.R. et al. (2013) Interactions of methicillin resistant *Staphylococcus aureus* USA300 and *Pseudomonas aeruginosa* in polymicrobial wound infection. *PLoS ONE* **8**, e56846.
- Price, P.E., Fagervik-Morton, H., Mudge, E.J., Beele, H., Ruiz, J.C., Nyström, T.H., Lindholm, C., Maume, S. et al. (2008) Dressing-related pain in patients with chronic wounds: an international patient perspective. *Int Wound J* **5**, 159–171.
- Saaq, M., Ahmad, S. and Zaib, M.S. (2015) Burn wound infections and antibiotic susceptibility patterns at Pakistan

- institute of medical sciences, Islamabad, Pakistan. *World J Plast Surg* **4**, 9–15.
- Schultz, L., Walker, S.A.N., Elligsen, M., Walker, S.E., Simor, A., Mubareka, S. and Daneman, N. (2013) Identification of predictors of early infection in acute burn patients. *Burns* **39**, 1355–1366.
- Schulz, S. and Dickschat, J.S. (2007) Bacterial volatiles: the smell of small organisms. *Nat Prod Rep* **24**, 814–842.
- Scotter, J.M., Allardyce, R.A., Langford, V.S., Hill, A. and Murdoch, D.R. (2006) The rapid evaluation of bacterial growth in blood cultures by selected ion flow tube-mass spectrometry (SIFT-MS) and comparison with the BacT/ALERT automated blood culture system. *J Microbiol Methods* **65**, 628–631.
- Shestivska, V., Antonowicz, S.S., Dryahina, K., Kubišta, J., Smith, D. and Španěl, P. (2015) Direct detection and quantification of malondialdehyde vapour in humid air using selected ion flow tube mass spectrometry supported by gas chromatography/mass spectrometry. *Rapid Commun Mass Spectrom* **29**, 1069–1079.
- Smith, D. and Španěl, P. (2011) Ambient analysis of trace compounds in gaseous media by SIFT-MS. *Analyst* **136**, 2009.
- Smith, D. and Španěl, P. (2015) Pitfalls in the analysis of volatile breath biomarkers: suggested solutions and SIFT-MS quantification of single metabolites. *J Breath Res* **9**, 22001.
- Španěl, P., Wang, T. and Smith, D. (2004) Quantification of hydrogen cyanide in humid air by selected ion flow tube mass spectrometry. *Rapid Commun Mass Spectrom* **18**, 1869–1873.
- Španěl, P., Dryahina, K. and Smith, D. (2006) A general method for the calculation of absolute trace gas concentrations in air and breath from selected ion flow tube mass spectrometry data. *Int J Mass Spectrom* **249–250**, 230–239.
- Spooner, A.D., Bessant, C., Turner, C., Knobloch, H. and Chambers, M. (2009) Evaluation of a combination of SIFT-MS and multivariate data analysis for the diagnosis of *Mycobacterium bovis* in wild badgers. *Analyst* **134**, 1922.
- Storer, M.K., Hibbard-Melles, K., Davis, B. and Scotter, J. (2011) Detection of volatile compounds produced by microbial growth in urine by selected ion flow tube mass spectrometry (SIFT-MS). *J Microbiol Methods* **87**, 111–113.
- Thomas, S., Fear, M., Humphreys, J., Disley, L. and Waring, M. (1996) The effect of dressings on the production of exudate from venous leg ulcers. *Wounds* **8**, 145–149.
- Thorn, R.M.S. and Greenman, J. (2012) Microbial volatile compounds in health and disease conditions. *J Breath Res* **6**, 24001.
- Thorn, R.M.S., Reynolds, D.M. and Greenman, J. (2011) Multivariate analysis of bacterial volatile compound profiles for discrimination between selected species and strains in vitro. *J Microbiol Methods* **84**, 258–264.
- Turner, C., Španěl, P. and Smith, D. (2006) A longitudinal study of ammonia, acetone and propanol in the exhaled breath of 30 subjects using selected ion flow tube mass spectrometry, SIFT-MS. *Physiol Meas* **27**, 637–648.
- Upton, D., Solowiej, K., Hender, C. and Woo, K.Y. (2012) Stress and pain associated with dressing change in patient with chronic wounds. *J Wound Care* **21**, 53–58.
- Wang, T., Španěl, P. and Smith, D. (2004) A selected ion flow tube study of the reactions of H₃O⁺, NO⁺ and O₂⁺ with some phenols, phenyl alcohols and cyclic carbonyl compounds in support of SIFT-MS and PTR-MS. *Int J Mass Spectrom* **239**, 139–146.
- Werthén, M., Henriksson, L., Jensen, P.Ø., Stenberg, C., Givskov, M. and Bjarnsholt, T. (2010) An in vitro model of bacterial infections in wounds and other soft tissues. *APMIS* **118**, 156–164.
- World Health Organization (2014) Burns. Available at: <http://www.who.int/mediacentre/factsheets/fs365/en/>

METHODOLOGY ARTICLE

Open Access

An in vitro collagen perfusion wound biofilm model; with applications for antimicrobial studies and microbial metabolomics



Elisabeth A. Slade¹, Robin M. S. Thom¹, Amber Young² and Darren M. Reynolds^{1,3*}

Abstract

Background: The majority of in vitro studies of medically relevant biofilms involve the development of biofilm on an inanimate solid surface. However, infection in vivo consists of biofilm growth on, or suspended within, the semi-solid matrix of the tissue, whereby current models do not effectively simulate the nature of the in vivo environment. This paper describes development of an in vitro method for culturing wound associated microorganisms in a system that combines a semi-solid collagen gel matrix with continuous flow of simulated wound fluid. This enables culture of wound associated reproducible steady state biofilms under conditions that more closely simulate the dynamic wound environment. To demonstrate the use of this model the antimicrobial kinetics of ceftazidime, against both mature and developing *Pseudomonas aeruginosa* biofilms, was assessed. In addition, we have shown the potential application of this model system for investigating microbial metabolomics by employing selected ion flow tube mass spectrometry (SIFT-MS) to monitor ammonia and hydrogen cyanide production by *Pseudomonas aeruginosa* biofilms in real-time.

Results: The collagen wound biofilm model facilitates growth of steady-state reproducible *Pseudomonas aeruginosa* biofilms under wound like conditions. A maximum biofilm density of 10^{10} cfu slide⁻¹ was achieved by 30 h of continuous culture and maintained throughout the remainder of the experiment. Treatment with ceftazidime at a clinically relevant dose resulted in a 1.2–1.6 log reduction in biofilm density at 72 h compared to untreated controls. Treatment resulted in loss of complex biofilm architecture and morphological changes to bacterial cells, visualised using confocal microscopy. When monitoring the biofilms using SIFT-MS, ammonia and hydrogen cyanide levels peaked at 12 h at 2273 ppb (± 826.4) and 138 ppb (± 49.1) respectively and were detectable throughout experimentation.

Conclusions: The collagen wound biofilm model has been developed to facilitate growth of reproducible biofilms under wound-like conditions. We have successfully used this method to: (1) evaluate antimicrobial efficacy and kinetics, clearly demonstrating the development of antimicrobial tolerance in biofilm cultures; (2) characterise volatile metabolite production by *P. aeruginosa* biofilms, demonstrating the potential use of this method in metabolomics studies.

Keywords: Biofilm, Collagen, Wound, In vitro model, Volatile metabolite, *Pseudomonas aeruginosa*

* Correspondence: Darren.Reynolds@uwe.ac.uk

¹Centre for Research in Biosciences, University of the West of England, Bristol, UK

³University of the West of England, Frenchay Campus, Goldharbour Lane, Bristol BS16 1QY, England

Full list of author information is available at the end of the article



© The Author(s). 2019 **Open Access** This article is distributed under the terms of the Creative Commons Attribution 4.0 International License (<http://creativecommons.org/licenses/by/4.0/>), which permits unrestricted use, distribution, and reproduction in any medium, provided you give appropriate credit to the original author(s) and the source, provide a link to the Creative Commons license, and indicate if changes were made. The Creative Commons Public Domain Dedication waiver (<http://creativecommons.org/publicdomain/zero/1.0/>) applies to the data made available in this article, unless otherwise stated.

Background

It is widely accepted that bacteria commonly exist in sessile communities known as biofilms, rather than as individual free swimming cells [1]. Biofilms are implicated in a range of clinically relevant infections including lung infection in cystic fibrosis, endocarditis, osteomyelitis, acute burn infection and chronic wound infection [2, 3]. Established biofilms are typically highly tolerant to antimicrobials and the host immune response [4]. The extracellular polymeric substance (EPS) protects bacterial cells within the biofilm by providing a physical barrier which decreases penetration of antimicrobials and agents of the host immune system [5, 6]. Furthermore, this biofilm phenotype is often coupled with a reduced metabolic activity and growth rate, typically seen within the interior of biofilm communities, which reduces the susceptibility to those antimicrobials which target such processes [7, 8]. A recent review of clinical studies conducted between 2008 and 2015, concluded that biofilms were present in 78.2% of chronic wounds [9], indicating the important role that biofilms play in the development of a chronic wound state. Detailed investigation of the distribution of infecting organisms within chronically infected wounds has demonstrated differences in the depth of microbial biofilm aggregates embedded within the wound bed [10–13]. For example, one study demonstrated the presence of *Pseudomonas aeruginosa* micro colonies embedded deeper within the wound bed than those of *Staphylococcus aureus* which were found closer to the wound surface [12]. The role of biofilms in the infection of acute wounds has been less well characterized, however biofilm formation has been observed in animal models of acute burn wound and surgical site infection [11, 14, 15].

In vitro studies of biofilms employ one of two approaches; a closed multi-well plate based model, or an open flow system with the continuous perfusion of nutrient into the model and waste products continuously exiting the system [16]. Both of these approaches often involve the development of biofilms on solid surfaces, usually plastic or glass. Microbial infection in vivo consists of biofilm growth on the surface of, or suspended within, the semi-solid matrix of the tissue, unless adhered to an implanted medical device or catheter [17]. Collagen based gel matrices have been used as a substratum for culturing biofilms in vitro, in an attempt to closely simulate the semi-solid nature of the wound [18–22]. However, a limitation of these closed systems, is that they do not simulate the replacement of nutrients and moisture that occur within the wound bed due to the production of exudate, which provides the continuous flux of nutrients available to the biofilm during formation and growth [23, 24].

To further our understanding and knowledge of wound infection processes, a wound biofilm model is required that better simulates the wound environment. This could be achieved by the combination of a continuous flow biofilm model system with a semi-solid 'wound-like' growth substrate and a more representative growth media. We describe an in vitro method for culturing wound associated microorganisms within a collagen wound biofilm model, combining a drip flow reactor system (Biosurface technologies, MZ, USA) with a three-dimensional type I collagen gel growth matrix and continuous perfusion of a previously developed simulated wound fluid (SWF) [18, 21, 25, 26]. To demonstrate the application of this method, it has been utilized to study the antimicrobial kinetics of ceftazidime, when used to treat *P. aeruginosa* biofilms during early or late stage development. *P. aeruginosa* is among the most commonly isolated pathogens from both chronic and acute burn wound infections [27, 28] and biofilms have been shown to rapidly result in systemic infection in a mouse model of acute burn infection [14]. Ceftazidime is considered a first choice antipseudomonal antibiotic [29, 30] for treatment when there is a high risk of systemic infection developing from an infected wound. To further demonstrate the potential of this novel model, a preliminary investigation of microbial metabolomics in relation to microbial biofilm development was undertaken using selected ion flow tube mass spectrometry (SIFT-MS). Ammonia and hydrogen cyanide have previously been reported as important potential diagnostic metabolites detected in the headspace of *P. aeruginosa* liquid cultures in vitro [31], and in *P. aeruginosa* infections in vivo [32, 33], through analysis of the exhaled breath of cystic fibrosis patients. Hydrogen cyanide is generated through decarboxylation of the amino acid glycine by the membrane bound hydrogen cyanide synthase enzyme [34], ammonia is produced by the metabolism of nitrogen containing compounds including hydrogen cyanide [31]. Real-time monitoring of bacterial volatile metabolites, has gained momentum in recent years as a potential rapid diagnostic tool [32, 35–41]. The novel collagen wound biofilm model reported here, allows the development of this diagnostic approach in the context of wound infection. For example by the detection of volatile metabolite profiles emitted by biofilm cultures, produced under conditions which closely simulate the wound environment.

Results

Characterization of the in vitro collagen perfusion wound biofilm model

The un-inoculated collagen growth matrix, which polymerizes at 37 °C to form a hydrated three-dimensional semi-solid gel layer on the surface of the microscope

slide coupons, was imaged using scanning electron microscopy (SEM). The fixation and dehydration process required for preparation of samples for SEM results in collapse of the three-dimensional structure, although the mesh-like network of long collagen fibers remains clearly visible (Fig. 1a). SEM imaging of a *P. aeruginosa* biofilm cultured on the collagen gel growth matrix shows a dense layer of microbial cells masking the collagen fibers below. Multiple layers of *P. aeruginosa* are visible, as is the dehydrated biofilm extracellular polymeric substances (EPS) which can be seen connecting adjacent bacterial cells (Fig. 1b).

The developed novel collagen wound biofilm model system supports growth of reproducible *P. aeruginosa* biofilms during both early and late stage development. A maximum biofilm density of 10^{10} cfu slide⁻¹ (dictated by the experimental conditions) was achieved by 30 h of continuous culture.

Figure 2 shows growth of *P. aeruginosa* NCIMB 10548 biofilms over 72 h at 33°C in the collagen wound biofilm model. The maximum density was maintained at an approximately steady-state of 6.0×10^{10} – 8.0×10^{10} cfu slide⁻¹, from 30 h until the end of experimentation (72

h) and equates to a microbial burden per gram of collagen of 4×10^{10} – 5.3×10^{10} cfu g⁻¹. In addition to sampling for enumeration, biofilms were sampled after 6, 12, 24 and 48 h of continuous culture for confocal microscopy, to determine the structural arrangement of bacterial cells and biofilm architecture during growth and development (Fig. 3). The biofilm sampled at 6 h consisted of sparsely arranged *P. aeruginosa* cells with some small aggregates (Fig. 3a), whereas at 12 h the cell density had increased and some larger aggregates were visible (Fig. 3b). At 24 h the density of the bacterial cells had again increased, in line with the enumeration data (Fig. 2), whereby more complex structural formations and the development of surface protrusions and channels can be seen (Fig. 3c). At 48 h, the biofilm architecture within the maturing biofilm shows evidence of increased variability in surface topography, as described within other biofilm studies [42–44].

Application of the collagen wound biofilm model for studying antimicrobial kinetics

To demonstrate the application of this novel method the collagen wound biofilm model was used to investigate the antimicrobial activity of antibiotic therapy against biofilms at a clinically relevant dose. To confirm susceptibility of *P. aeruginosa* NCIMB 10548 to ceftazidime, planktonic minimum inhibitory concentration (MIC) values were determined ($n = 3$) using a standard microdilution multi-well plate assay [45]; the MIC was determined to be 2.0 mg L^{-1} . The clinical breakpoint for ceftazidime against *P. aeruginosa* according to the European Committee on Antimicrobial Susceptibility testing is 8 mg L^{-1} [46]. Hence, the MIC of 2.0 mg L^{-1} , indicates that this strain is considered sensitive to ceftazidime. Once susceptibility of the strain was confirmed the efficacy of ceftazidime against *P. aeruginosa* biofilms was investigated using the collagen wound biofilm model. A target serum concentration of 40 mg L^{-1} for continuous infusion of ceftazidime is recommended for effective treatment of *P. aeruginosa* infections in vivo [29, 30, 47], hence this drug concentration was selected to challenge the *P. aeruginosa* biofilms in the collagen wound biofilm model. Figure 4 shows the change in biofilm density resulting from ceftazidime treatment at 40 mg L^{-1} , compared to normal growth conditions. Treatment was started after either 6 h or 30 h of continuous culture, to enable comparison of treatment efficacy on the early stage of biofilm formation and on established steady state maturing *P. aeruginosa* biofilms. When treatment was initiated at the early stage of biofilm formation, the total biofilm density decreased for the first 12 h of treatment to approximately 5×10^8 cfu slide⁻¹ (1.63 log reduction compared to untreated controls; $p < 0.01$). The biofilm density remained

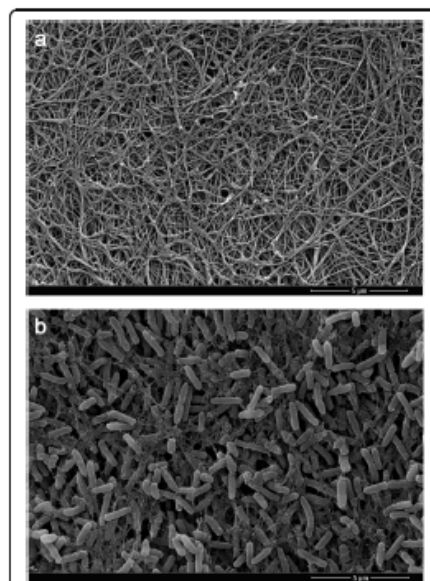
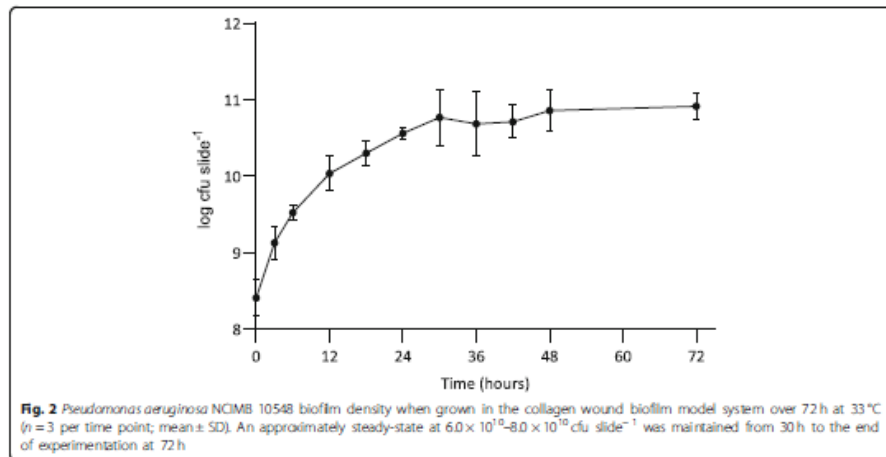


Fig. 1 Scanning electron micrographs of **a** collagen gel and **b** *Pseudomonas aeruginosa* NCIMB 10548 biofilm cultured on a collagen gel matrix



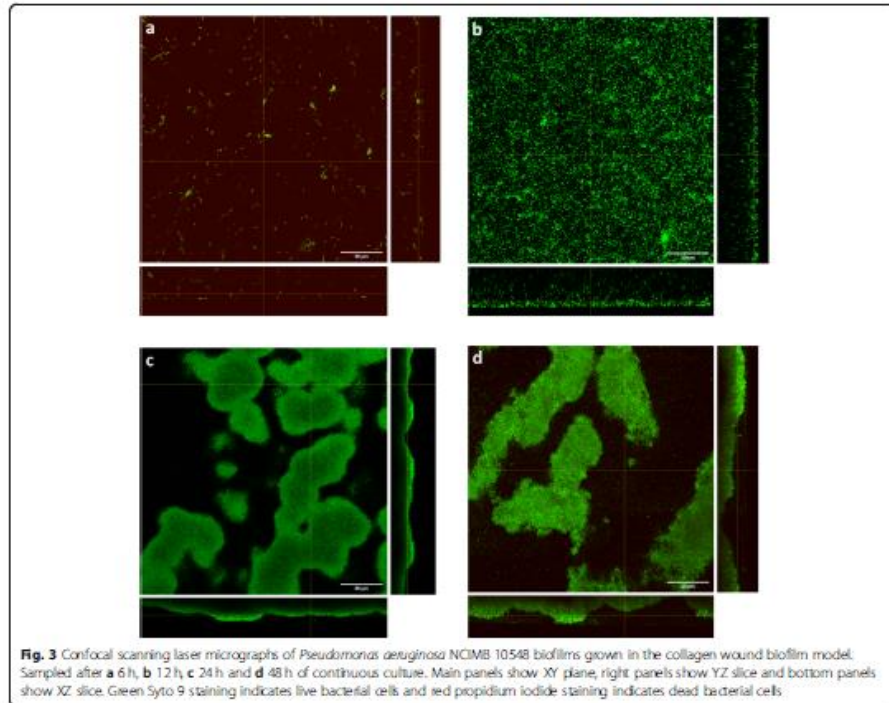
stable at the subsequent sampling time, but increased over the following 24 h to reach a density of 2×10^9 cfu slide⁻¹. This density was maintained until the final sampling time (72 h of continuous culture) resulting in a significant 1.6 log reduction compared to untreated controls ($p < 0.05$) at the end of experimentation. During treatment of established maturing biofilms, the biofilm density gradually decreased ultimately resulting in a mean biofilm density of 5.5×10^9 cfu slide⁻¹ at 72 h (a significant 1.2 log reduction compared to the untreated control; $p < 0.05$). When comparing treatment initiated at the early stage of biofilm development or on established maturing biofilms, although both treatment regimens exhibited a significant antimicrobial effect, there was no significant difference in biofilm density between these treatment groups after 72 h of continuous culture.

Figure 5 shows confocal scanning laser micrographs of *P. aeruginosa* biofilms treated with 40 mg L^{-1} ceftazidime. Samples for both treatment regimens were imaged after both 18 h and 42 h of exposure to the ceftazidime; this corresponds to a total culture time of 24 h and 48 h for the samples where antibiotic treatment was started at the early stage of biofilm formation, and 48 h and 72 h total culture time for the samples where treatment was started on established biofilms. Samples imaged following 18 h of exposure to ceftazidime at 40 mg L^{-1} (Fig. 5; a1 & b1) both show some elongation of *P. aeruginosa* cells. Within the confocal z-stack, it was observed that this was most pronounced in the bacterial cells nearest to the surface of the biofilms, whereas cells deeper within the biofilm were morphologically more similar to

the untreated sample (Fig. 3). After 42 h of antibiotic exposure, it was observed that there was a high proportion of elongated bacterial cells (Fig. 5; a2 & b2). The biofilm appears less densely packed with clear spaces between the tangles of filamentous cells, compared to untreated biofilms shown in Fig. 3. By comparing untreated (Fig. 3c) and treatment of early stage biofilms (Fig. 5; a1 and a2) it is clear that the ceftazidime treatment prevents the development of complex biofilm architecture. In addition, when comparing untreated (Fig. 3d) and the treatment of established biofilms (Fig. 5; b1), it is evident that ceftazidime treatment has resulted in the collapse of the characteristic three-dimensional biofilm structure. Demonstrating the effect of ceftazidime on the complex biofilm structure, as well as the morphology of individual bacterial cells.

Application of the collagen wound biofilm model for studying biofilm metabolomics

Selected ion flow tube mass spectrometry was used to monitor headspace concentrations of volatile metabolites in real-time. Detection of ammonia and hydrogen cyanide was chosen to demonstrate the capability of analyzing volatile metabolites produced by developing *P. aeruginosa* biofilms in the collagen wound biofilm model. Biofilm headspace was sampled and analyzed repeatedly using the SIFT-MS instrument throughout the 72 h duration of biofilm growth and development. Figure 6 shows the concentration of ammonia and hydrogen cyanide respectively, detected in the headspace of *P. aeruginosa* biofilm cultures. The concentration of both compounds (ppb) had an initial peak at 12 h, with a

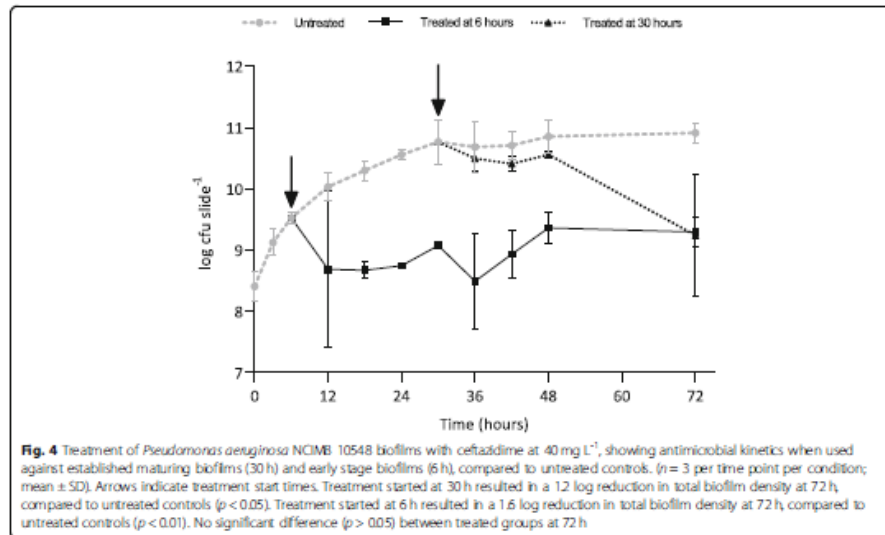


mean concentration of 2273 ppb for ammonia and 138 ppb for hydrogen cyanide. The hydrogen cyanide concentration then dropped to a mean concentration of 81 ppb at 18 h before again increasing gradually to a peak of 191 ppb. The concentration of ammonia also dropped, with a mean concentration of 797 ppb recorded at 21 h and then continued to fluctuate between approximately 600 and 1200 ppb for the remaining duration of analysis. The concentration of both ammonia and hydrogen cyanide remained at levels detectable using SIFT-MS throughout the duration of growth and development of *P. aeruginosa* biofilms within the collagen wound biofilm model.

Discussion

The dermis of human skin is primarily composed of the protein collagen [48]. Type I collagen is the most abundant type found in human skin and is distributed throughout all layers of the dermis [49]. We have successfully developed a dynamic collagen wound biofilm model utilising a three-dimensional collagen gel growth

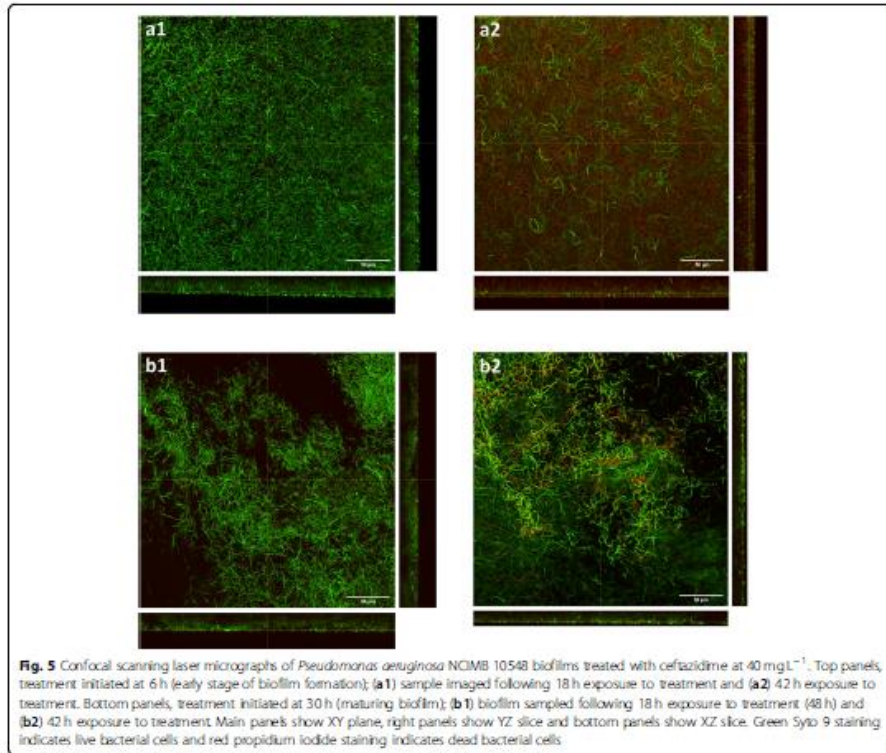
matrix comprised of a mesh of polymerized type I collagen fibres (Fig. 1), to simulate the semi-solid wound environment found *in vivo*. Continuous perfusion with SWF provides replacement of moisture and nutrients, and removal of waste products, that would be provided by the flow of exudate within infected wounds [50]. The simulated wound fluid provides a similar range of nutrients as exudate, a high protein fluid that leaks from the blood vessels in response to inflammation associated with wound healing processes [51]. Biochemical analysis of wound fluid has shown that a similar range of constituents are present when compared to serum, with concentrations in wound fluid at lower levels than in serum for the majority of components [52]. This suggests use of a simulated wound fluid comprised of 50% serum will provide a suitable range of nutrients, many of which will be at biologically relevant concentrations. We have validated the growth of *P. aeruginosa* with this method and demonstrated that it enables culture of reproducible steady state biofilms at a density greater than that considered to be the critical threshold of clinically relevant



wound infection. A density of 10^5 cfu g⁻¹ tissue is considered the critical threshold indicative of clinically relevant wound infection [53–55], with a bioburden of between 10^9 and 10^{11} cfu g⁻¹ tissue identified from infected wounds with the heaviest bacterial loads [54, 56]. Hence, the density achieved within the collagen wound biofilm model represents an appropriate bacterial load, reflective of a challenging clinical situation for assessing antimicrobial efficacy. Characterisation of the collagen wound biofilm model has focused on cultivation of *P. aeruginosa* NCIMB 10548, a commercially available strain originally isolated from an infected wound. However, future studies could apply the collagen wound biofilm model to investigate the growth rate and susceptibility of clinical isolates of *P. aeruginosa* and other wound associated species.

MIC assays are routinely used clinically to determine the susceptibility of bacterial isolates to the antibiotic treatments available. However, as demonstrated within this study, this is unlikely to predict the effectiveness of antimicrobials against biofilms and hence their therapeutic effectiveness against biofilm infections. To demonstrate the application of this model system for evaluating the efficacy and kill kinetics of antimicrobial agents, both developing and established *P. aeruginosa* biofilms were challenged with the cephalosporin antibiotic ceftazidime. There was no significant difference (p > 0.05) in the final biofilm density after 72 h of

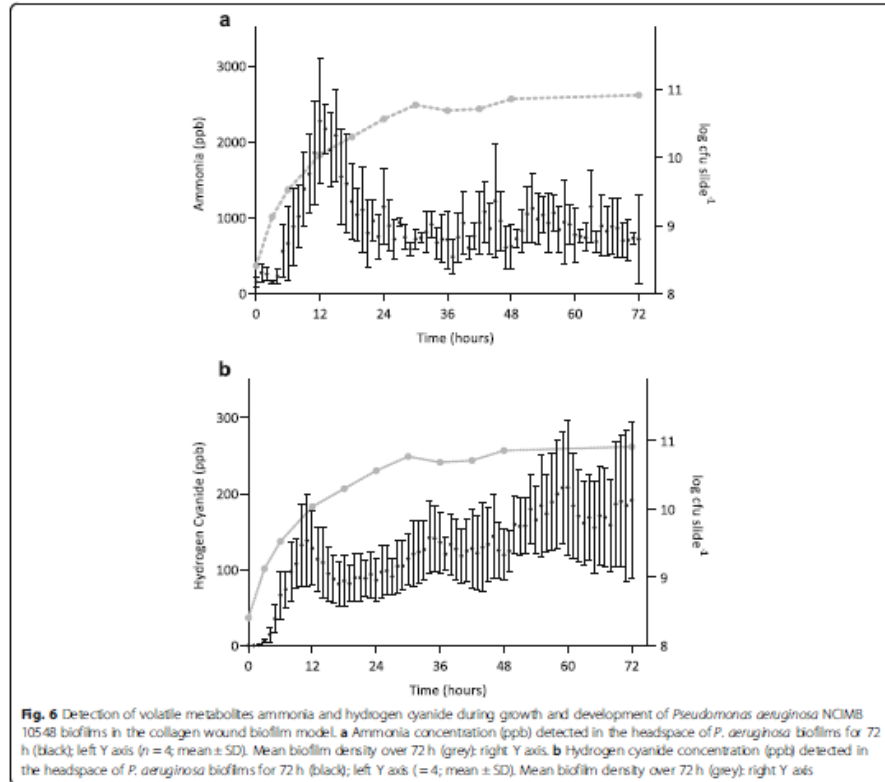
continuous culture, when comparing the two treatment start times. Both treatment strategies resulted in a significant reduction of total biofilm density at 72 h compared to the untreated biofilm. Although a statistically significant reduction in viable *P. aeruginosa* biofilm density was demonstrated, the remaining mean biofilm density of 2.2×10^9 and 5.5×10^9 cfu slide⁻¹ for the two treatment regimens equates to 1.5×10^9 and 3.6×10^9 cfu g⁻¹ of collagen 'tissue' respectively. This density remains vastly in excess of the 10^5 cfu g⁻¹ of 'tissue', used as the critical threshold indicative of invasive infection and risk of sepsis in studies of quantitative microbiological analysis of wound biopsy samples [54, 55]. It has previously been reported that there are differences between the planktonic MIC and the concentration of ceftazidime (and a range of other antimicrobials) required to eradicate biofilms, with concentrations 1000-fold greater than the MIC unable to eradicate *P. aeruginosa* biofilms within a static model [57]. Using the collagen wound biofilm model, we have shown the time course of the development of such tolerance for the first time under wound like conditions in vitro, and visualized the effect of drug treatment on the biofilm structure. Ceftazidime treatment resulted in distinct morphological changes in the general biofilm architecture as well as the discrete bacterial cells. This elongation response by *P. aeruginosa* to β -lactam antibiotics, including ceftazidime, has been described previously and was observed to result



in cell lysis and a reduction in viable cells in planktonic culture [58]. It has been determined that inhibition of penicillin binding protein 3 (PBP3) by β -lactam antibiotics is responsible for causing filamentation in *P. aeruginosa*. This has been demonstrated by deletion of the gene required for PBP3 expression and comparison of the resulting morphological changes to those seen when *P. aeruginosa* was exposed to sub-lethal concentrations of β -lactam antibiotics [59]. This phenomena has also been observed in response to β -lactam exposure in *Escherichia coli* [60], where cell elongation is reported to be the first of a four step process leading to eventual cell lysis.

The developed method facilitates investigation of microbial metabolomics, including volatile metabolites produced by bacterial species associated with causing clinically relevant wound infection [38]. Selected ion flow tube mass spectrometry was used for real-time detection of the volatile compounds ammonia and

hydrogen cyanide in the collagen wound biofilm model. Monitoring of volatile compounds during biofilm growth and development from a perfusion biofilm model has not been reported previously. In the collagen wound biofilm model, the concentration of both compounds increased for approximately the first 12 h, corresponding to the most rapid increase in biofilm density. Subsequently, the concentration of both compounds decreased from 12 to 24 h. Investigations of real-time production of hydrogen cyanide and ammonia from reference strains and clinical isolates of *P. aeruginosa* in liquid culture indicated a peak in hydrogen cyanide concentration at the transition to stationary phase only [31]. Interestingly, the drop in concentration of both volatile compounds between 12 and 24 h, corresponds with distinct changes in the arrangement of bacterial cells and development of the biofilm structures observed by confocal microscopy (Fig. 3), as well as a decrease in the rate at which the biofilm density was increasing. When the



biofilm density had stabilized within the collagen wound biofilm model (≥ 30 h), the concentration of ammonia also stabilized. In contrast, the concentration of hydrogen cyanide continued to gradually increase throughout the remaining analysis time. Again, this is in contrast to that reportedly seen in planktonic culture [31], whereby production of hydrogen cyanide was maintained for only 1 to 4 h after the initial peak. These differences may result from changes in the metabolic activity associated with the biofilm mode of growth, coupled with the continuous supply of substrates for metabolism and removal of waste products within our model, which is more representative of the *in vivo* environment. The concentration of both hydrogen cyanide and ammonia remained at levels detectable by SIFT-MS throughout the 72 h sampling time, confirming the potential application of detection of these compounds as markers of *P.*

aeruginosa presence that could usefully be exploited through development of rapid point of care diagnostic devices.

Conclusions

The collagen wound biofilm model has been successfully developed and evaluated for the growth of steady-state biofilms under wound like conditions. We have demonstrated the potential of the collagen wound biofilm model for use in metabolomics studies, by characterising volatile metabolite production from *P. aeruginosa*, a clinically relevant pathogen associated with wound infection. Furthermore, the collagen wound biofilm model not only demonstrates the failure of biofilm eradication using a clinically relevant ceftazidime concentration, but also allows the evaluation of antimicrobial kinetics, clearly demonstrating the development of tolerance in

the biofilm cultures during treatment of biofilms at both early and late stage development.

Methods

Preparation and maintenance of bacterial cultures

P. aeruginosa (NCIMB 10548) was maintained on beads (Pro-Lab Diagnostics, Birkenhead, UK) at -80°C , resuscitated as required on Tryptone Soya Agar (TSA) (Oxoid Ltd. Basingstoke, UK) and incubated aerobically at 37°C . Working cultures were stored on sealed plates at 4°C .

Collagen coating of glass slide coupons

The collagen gel matrix was prepared based on the method described by Werthén et al. (2010) by preparing a collagen solution (2.0 mg mL^{-1}) in simulated wound fluid (SWF) [18, 21, 25, 26]. The SWF comprised of equal volumes of fetal bovine serum (Life Technologies Limited, Paisley, UK) and a solution of 0.1% bacteriological peptone (Oxoid Ltd. Basingstoke, UK) and 0.85% sodium chloride (Fisher Scientific Limited, Loughborough, UK). High concentration collagen (type I) from rat tail in 0.02 M Acetic Acid (Corning Incorporated, Wiesbaden, Germany) was neutralized to pH7 with 1 M sodium hydroxide according to manufacturer instructions and diluted to the desired concentration with SWF. For example, to prepare 10 mL of 2.0 mg mL^{-1} collagen solution in SWF from a collagen stock solution of 9.59 mg mL^{-1} ; $48\text{ }\mu\text{L}$ of ice cold sodium hydroxide was added to 7.866 mL of ice cold SWF and mixed. On ice, 2.086 mL of ice cold collagen stock solution was then added and the solution mixed gently. Sterile glass microscope slides measuring $76\text{ mm} \times 26\text{ mm}$ were coated with 1.5 mL of neutralized collagen solution (2.0 mg mL^{-1}), resulting in a depth of $760\text{ }\mu\text{m}$. Collagen coated slides were incubated at 37°C for 1 h to allow polymerization of the three-dimensional collagen matrix.

Preparation of bacterial cultures

Overnight plate cultures (18–24 h) were used to prepare a suspension of *P. aeruginosa* in 10 mL SWF, adjusted to an $\text{OD}_{620\text{nm}}$ of 0.20, equivalent to $2 \times 10^8\text{ cfu mL}^{-1}$. One milliliter of the test suspension was used to inoculate each collagen coated microscope slide (individually housed in sterile petri dishes) and incubated at 33°C for 2 h to allow initial adherence of bacterial cells.

Growth of bacterial biofilms within the collagen wound biofilm model

Following incubation, the inoculated slides were rinsed gently three times with 1 mL of sterile SWF to remove planktonic cells, and carefully transferred to individual channels within the drip flow reactor (Biosurface Technologies Corporation, Bozeman, MT, USA). Sterile silicone tubing (3 mm ID) was used to connect a 500 mL

Duran bottle containing the sterile SWF medium to the miniert valve lid inlets via a 23 Gauge 1.25 in sterile needle. Waste was collected in 250 mL Duran bottles connected to the waste outlet ports using lengths of sterile silicone tubing (8 mm ID). The reactor was incubated at 33°C to simulate average wound bed temperature [61] for 48–72 h at an angle of 10° to allow SWF to flow through the individual chambers of the model system (Fig. 7). The collagen wound biofilm model was continuously perfused with SWF at a flow rate of 2 mL hr^{-1} for the duration of incubation to simulate the flow of a moderately exuding wound (50 mL over 24 h) [62].

Imaging of bacterial biofilms and collagen matrix

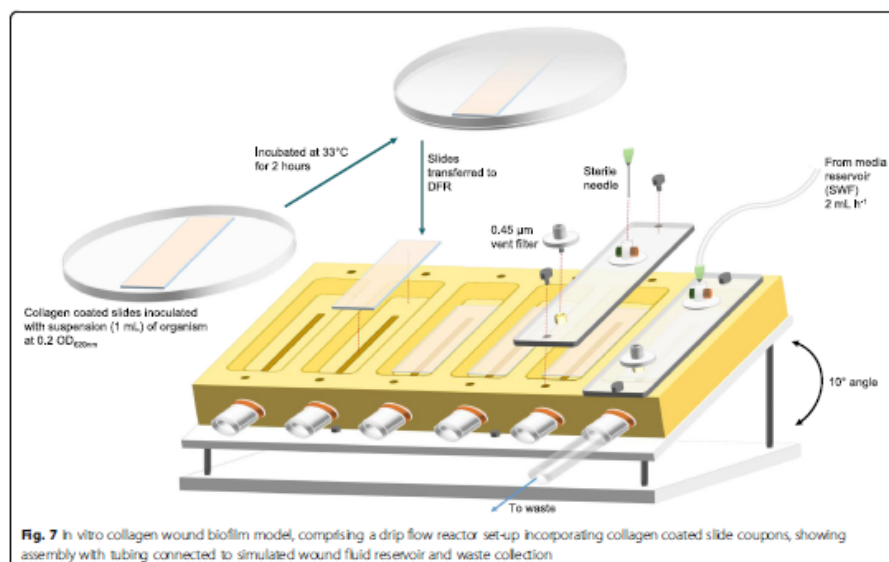
During preparation of collagen gel matrices for imaging experiments, a #1 glass cover slip measuring $18\text{ mm} \times 18\text{ mm}$ was included between the microscope slide and collagen gel layer. The inclusion of a coverslip facilitated the sampling of a suitable sized section of the biofilm for microscopy. This was removed by cutting the collagen around the cover slip with a bespoke square stainless steel cutter and lifting away the coverslip supporting the biofilm sample with the aid of a scalpel blade.

Scanning Electron microscopy (SEM)

Biofilm samples and an un-inoculated collagen gel control were fixed in 4% Glutaraldehyde (Sigma-Aldrich Company Limited, Gillingham, UK) in a 0.1 M phosphate buffer for 1 h at room temperature. This was rinsed in phosphate buffered saline (PBS) and dehydrated with increasing concentrations of ethanol and hexamethyldisilazane (Acros Organics, Geel, Belgium), air dried in a fume hood, mounted and gold sputter coated. A FEI Quanta 650 FEG scanning electron microscope operating at 10 kV was used to examine the samples.

Confocal scanning laser microscopy

Biofilm samples were stained using the FilmTracer LIVE/DEAD Biofilm Viability Kit (Fisher Scientific UK Limited, Loughborough, UK) according to manufacturer's instructions: $3\text{ }\mu\text{L}$ each of Component A (SYTO 9 green fluorescent nucleic acid stain 3.34 mM in DMSO) and Component B (Propidium iodide 20 mM in DMSO) were added to 1 mL of sterile filtered deionized water to prepare a working solution. Three hundred microliters of the prepared staining solution was gently added to the biofilm surface. Samples were incubated at room temperature for 30 min in the dark. Following incubation samples were rinsed gently with sterile filtered deionized water to remove excess stain and imaged using the $\times 40$ oil objective of the Leica DMi8 Inverted microscope with confocal



scanner (Leica Microsystems (UK) Ltd., Milton Keynes, UK). Confocal Z-stack scans were exported to Fiji [63] for image processing.

Enumeration of bacterial biofilms

Bacterial biofilms were sampled at 0, 3 and 6 h, then every 6 h until 48 h and finally at 72 h. At each time point a coated slide was aseptically removed from the reactor and the entire collagen layer containing the bacterial biofilm scraped into a 50 mL falcon tube using a sterile L-shaped scraper, while rinsing with 3×1 mL PBS. Two milliliters of $500 \mu\text{g mL}^{-1}$ collagenase solution (Life Technologies Limited, Paisley, UK) was added to the tube, mixed and incubated at 37°C for 20 min and then mixed by vortexing and incubated for a further 20 min. The resulting suspension was disrupted by sonication in a water bath (Fisherbrand FB11078, Fisher Scientific Limited, Loughborough, UK) at 35 kHz for 5 min. Collagenase solution was washed from the bacterial cells; whereby the suspension was centrifuged at $4000 \times g$, the supernatant discarded and pellet re-suspended in 10 mL PBS a total of two times. Bacterial density (cfu slide^{-1}) was determined by serially diluting in PBS and spiral plating (Whitley Automated Spiral Plater, Don Whitley Scientific Limited, Bingley, UK) on to TSA. Colonies were counted after 24 h incubation at 37°C .

Antimicrobial susceptibility - broth microdilution

The antimicrobial susceptibility of *P. aeruginosa* NCIMB 10548 to ceftazidime was tested based on the broth microdilution method described by BS EN ISO 20776-1:2006 [45]. Ceftazidime was prepared at concentrations ranging from 256 mg L^{-1} to 0.25 mg L^{-1} . Fifty microliters of each antibiotic concentration and a control of 0 mg L^{-1} of ceftazidime were dispensed in triplicate into wells of a 96 well multi-well plate. Overnight plate cultures were used to prepare a standardized suspension ($1 \times 10^6 \text{ cfu mL}^{-1}$) of *P. aeruginosa* NCIMB 10548 in 10 mL Muller-Hinton Broth (MHB) (Oxoid Ltd. Basingstoke, UK). Fifty microliters of the inoculum suspension were added to each of the wells of the multi-well plate containing 50 μL of MHB or MHB with ceftazidime. The resulting final inoculum was approximately $5 \times 10^5 \text{ cfu mL}^{-1}$ and final ceftazidime concentrations ranged from 128 mg L^{-1} to 0.125 mg L^{-1} , plus antibiotic free controls. Additionally, three wells were prepared containing 100 μL of MHB only as un-inoculated negative controls. The multi-well plate was then incubated at 37°C for 18 h. The inoculum suspension was serially diluted and 100 μL spread plated on to TSA and incubated at 37°C overnight to confirm appropriate inoculum preparation. Following incubation each well of the plate was visually inspected to identify turbidity to

indicate growth of the test organism by comparison to the controls. Agar plates were counted after 18–24 h to confirm inoculum density was within the required range.

Antimicrobial susceptibility – biofilms

Biofilm cultures were grown on collagen coated slides in the drip flow reactor system as described above. Ceftazidime treatment was started after either 6 h, when cultures are at an early stage of biofilm development, or 30 h of continuous culture, when biofilms are established and maturing. Residual SWF was drained via the tubing and the media reservoir refilled with fresh SWF containing ceftazidime at 40 mg L⁻¹. Biofilms were sampled periodically as described above to determine the effect of ceftazidime treatment on biofilm density over time.

SIFT-MS analysis of bacterial biofilms

Volatile compounds were sampled from the headspace of collagen wound biofilm cultures by connecting the heated sample inlet of the selected ion flow tube mass spectrometry (SIFT-MS) instrument (Voice200Ultra, Syft Technologies, Christchurch, NZ) to the reactor channel via a length of PEEK tubing. To connect the PEEK tubing, bespoke modified biofilm reactor lids with an additional valve port were used. The SIFT-MS instrument was operated in selected ion mode (SIM) using the H₃O⁺, NO⁺ and O₂⁺ reagent ions to quantify hydrogen cyanide and ammonia concentrations in the biofilm headspace throughout the 72 h growth and development period.

Data analysis

Biofilm enumeration data were analyzed by performing t-tests comparing specific time points of interest using Graphpad Prism 7 (GraphPad Software Inc, California, USA). SIFT-MS data for each independent *P. aeruginosa* biofilm were extracted using MATLAB R2018a (The MathWorks, Inc., Natick, Massachusetts, United States). In order to remove signal noise from the data the mean concentration of each compound was calculated for each hour of analysis.

Abbreviations

CFU: Colony Forming Units; EPS: Extracellular Polymeric Substances; MHB: Mueller-Hinton Broth; MIC: Minimum Inhibitory Concentration; NCIMB: National Collection of Industrial Food and Marine Bacteria; OD: Optical Density; PBP3: Penicillin Binding Protein 3; PBS: Phosphate Buffered Saline; ppb: Parts Per Billion; SEM: Scanning Electron Microscopy; SIFT-MS: Selected Ion Flow Tube Mass Spectrometry; SIM: Selected Ion Mode; SWF: Simulated Wound Fluid; TSA: Tryptone Soya Agar

Acknowledgements

The authors would like to thank Professor Andrew Lovering at North Bristol NHS trust for his scientific support throughout this research.

Authors' contributions

E.A.S., R.M.S.T., A.Y. and D.M.R. conceptualised the project. E.A.S. carried out all experimental work and processed the data. E.A.S., R.M.S.T., A.Y. and D.M.R. all

contributed to the analysis of the data that is presented. D.M.R., R.M.S.T. and A.Y. supervised the research. E.A.S., R.M.S.T., A.Y. and D.M.R. co-created the manuscript and contributed to towards the final iteration. All authors read and approved the final manuscript.

Funding

The authors would like to thank the University of the West of England, Bristol, North Bristol NHS trust and the Children's Burns Research Centre, University Hospitals Bristol NHS Foundation Trust for co-funding the research. The funding organisations were not involved in the design of the study, the collection, analysis, or interpretation of data, or in writing the manuscript.

Availability of data and materials

The datasets used and/or analysed during the current study are available from the corresponding author on reasonable request.

Ethics approval and consent to participate

Not applicable.

Consent for publication

Not applicable.

Competing interests

The authors declare that they have no competing interests.

Author details

¹Centre for Research in Biosciences, University of the West of England, Bristol, UK. ²Scar Free Foundation Centre for Children's Burns Research, Bristol Royal Hospital for Children, Bristol, UK. ³University of the West of England, Frenchay Campus, Coldharbour Lane, Bristol BS16 1QY, England.

Received: 20 June 2019 Accepted: 11 December 2019

Published online: 30 December 2019

References

- Gupta P, Sarkar S, Das B, Bhattacharjee S, Tribedi P. Biofilm, pathogenesis and prevention—a journey to break the wall: a review. *Arch Microbiol*. 2016;198:1–15. <https://doi.org/10.1007/s00203-015-1148-6>.
- Harby N, Bjarnsholt T, Moser C, Bassi G, Coenye T, Donelli G et al. ESCMID guideline for the diagnosis and treatment of biofilm infections 2014. *Clin Microbiol Infect*. 2015;21:S1–25. <https://doi.org/10.1016/j.cmi.2014.10.024>.
- Furukawa S, Kuchma SL, O'Toole GA. Keeping their options open: acute versus persistent infections. *J Bacteriol*. 2006;188:1211–7. <https://doi.org/10.1128/JB.188.4.1211-1217.2006>.
- Cooper R, Bjarnsholt T, Alhede M. Biofilms in wounds: a review of present knowledge. *J Wound Care*. 2014;23:570–82. <https://doi.org/10.12968/jowc.2014.23.11.570>.
- Jessitts AJ, Franklin MJ, Benglund D, Sasaki M, Lord C, Bleasdale JB, et al. Compromised host defense on *Pseudomonas aeruginosa* biofilms: characterization of neutrophil and biofilm interactions. *J Immunol*. 2003;171:4329–39. <https://doi.org/10.4049/JIMMUNOL.171.8.4329>.
- Hall CW, Mah T-F. Molecular mechanisms of biofilm-based antibiotic resistance and tolerance in pathogenic bacteria. *FEMS Microbiol Rev*. 2017;41:276–301. <https://doi.org/10.1093/femrev/fux010>.
- Davies D. Understanding biofilm resistance to antibacterial agents. *Nat Rev Drug Discov*. 2003;2:114–22. <https://doi.org/10.1038/nrd1008>.
- Alhede M, Kragh KN, Quortrup K, Allesen-Holm M, van Genrip M, Christensen LD, et al. Phenotypes of non-attached *Pseudomonas aeruginosa* aggregates resemble surface-attached biofilm. *PLoS One*. 2011;6:e27943. <https://doi.org/10.1371/journal.pone.0027943>.
- Malone M, Bjarnsholt T, McBain AJ, James GA, Stoodley P, Lesper D, et al. The prevalence of biofilms in chronic wounds: a systematic review and meta-analysis of published data. *J Wound Care*. 2017;26:20–5. <https://doi.org/10.12968/jowc.2017.26.1.20>.
- Kirketepp-Møller K, Jensen PO, Fazli M, Madsen KG, Pedersen J, Moser C, et al. Distribution, organization, and ecology of bacteria in chronic wounds. *J Clin Microbiol*. 2008;46:2717–22. <https://doi.org/10.1128/JCM.00501-08>.
- Davis SC, Ricotti C, Guzzariga A, Welsh E, Eaglstein WH, Metz PM. Microscopic and physiologic evidence for biofilm-associated wound colonization in vivo. *Wound Repair Regen*. 2008;16:23–9. <https://doi.org/10.1111/j.1524-475X.2007.00803.x>.

12. Fadl M, Bjarnholt T, Kriestep-Møller K, Jørgensen B, Andersen AS, Kroghelt KA, et al. Nonrandom distribution of *Pseudomonas aeruginosa* and *Staphylococcus aureus* in chronic wounds. *J Clin Microbiol*. 2009;47:4084–9. <https://doi.org/10.1128/JCM.01395-09>.
13. Johani K, Malone M, Jensen S, Gasbell I, Dickson H, Hu H, et al. Microscopy visualisation confirms multi-species biofilms are ubiquitous in diabetic foot ulcers. *Int Wound J*. 2017;16:1160–9. <https://doi.org/10.1111/iwj.12777>.
14. Schaber JA, Triffo WJ, Suh SJ, Oliver JW, Hassett MC, Griswold JA, et al. *Pseudomonas aeruginosa* forms biofilms in acute infection independent of cell-to-cell signaling. *Infect Immun*. 2007;75:3715–21. <https://doi.org/10.1128/AID00586-07>.
15. Thompson MG, Black CC, Pavlicek RL, Honnold CL, Wise MC, Alameh YA, et al. Validation of a novel marine wound model of *Acinetobacter baumannii* infection. *Antimicrob Agents Chemother*. 2014;58:1332–42. <https://doi.org/10.1128/AAC.01946-13>.
16. Coenye T, Nelis HJ. In vitro and in vivo model systems to study microbial biofilm formation. *J Microbiol Methods*. 2010;83:89–105. <https://doi.org/10.1016/j.mimet.2010.08.018>.
17. James GA, Swigger E, Wolcott R, Pulcini E, deLancey, Secor P, Setrich J, et al. Biofilms in chronic wounds. *Wound Repair Regen*. 2008;16:37–44. <https://doi.org/10.1111/j.1524-475X.2007.00321.x>.
18. Werthén M, Henriksson L, Jensen PO, Stenberg C, Givskov M, Bjarnholt T. An in vitro model of bacterial infections in wounds and other soft tissues. *APMS*. 2010;118:156–64. <https://doi.org/10.1111/j.1600-0463.2009.02580.x>.
19. Backman G, Cas P, Maes L, Nelis HJ, Coenye T. Quorum sensing inhibitors increase the susceptibility of bacterial biofilms to antibiotics in vitro and in vivo. *Antimicrob Agents Chemother*. 2011;55:2655–61.
20. Hakonen B, Lönnberg UK, Larkö E, Blom K. A novel qualitative and quantitative biofilm assay based on 3D soft tissue. *Int J Biomater*. 2014;2014:1–5. <https://doi.org/10.1155/2014/768136>.
21. Price BL, Lovering AM, Bowling R, Dobson CB. Development of a novel collagen wound model to simulate the activity and distribution of antimicrobials in soft tissue during diabetic foot infection. *Antimicrob Agents Chemother*. 2016;60:6880–9.
22. Pompilio A, Galardi G, Verginelli F, Muzzi M, Di Giulio A, Di Bonaventura G. Microbial odourant forms structurally complex and inherently antibiotic-resistant biofilm in a wound-like in vitro model. *Front Microbiol*. 2017;8:1–14. <https://doi.org/10.3389/fmicb.2017.02591>.
23. Thom RMS, Greenman J. A novel in vitro flat-bed perfusion biofilm model for determining the potential antimicrobial efficacy of topical wound treatments. *J Appl Microbiol*. 2009;107:2070–9. <https://doi.org/10.1111/j.1365-2672.2009.04988.x>.
24. Rhoads DD, Wolcott RD, Percival SL. Biofilms in wounds: management strategies. *J Wound Care*. 2008;17:502–8. <https://doi.org/10.12968/jowc.2008.17.11.31479>.
25. Bowler PG, Jones SA, Walker M, Parsons D. Microbicidal properties of a silver-containing hydrofiber dressing against a variety of burn wound pathogens. *J Burn Care Rehabil*. 2004;25:192–6. <https://doi.org/10.1097/01.BCR.0000112311.72232.18>.
26. Said J, Dadoo CC, Walker M, Parsons D, Stapleton P, Beezer AE, et al. An in vitro test of the efficacy of silver-containing wound dressings against *Staphylococcus aureus* and *Pseudomonas aeruginosa* in simulated wound fluid. *Int J Pharm*. 2014;462:123–8. <https://doi.org/10.1016/j.jpharm.2013.12.037>.
27. Ahawi M, Crowley TP, Pape SA. Bacterial colonisation of the burn wound: a UK experience. *J Wound Care*. 2014;23:274–7. <https://doi.org/10.12968/jowc.2014.23.5.274>.
28. Banski LK, Al-Mousawi A, Rivero H, Jeschke MG, Sanfird AP, Herndon DN. Emerging infections in burns. *Surg Infect*. 2009;10:389–97. <https://doi.org/10.1089/sur.2009.024>.
29. Abu L, Aguilar L, Sevillaño D, Gmélner M-, Echeverría O, Gómez-Lus MH, et al. Is there a pharmacodynamic need for the use of continuous versus intermittent infusion with ceftazidime against *Pseudomonas aeruginosa*? An in vitro pharmacodynamic model. *J Antimicrob Chemother*. 2005;55:209–13. <https://doi.org/10.1093/jac/dk536>.
30. Aubert G, García A, Coudrot M, Guyomarch S, Auboyer C, Zeni F. Prospective determination of serum ceftazidime concentrations in intensive care units. *Ther Drug Monit*. 2010;32:517–9. <https://doi.org/10.1097/FTD.0b013e3181e60ca6>.
31. Neefen AH, Mandon J, van Igen J, Anáñon DD, Mouton RW, Hamen FM, et al. Real-time monitoring of hydrogen cyanide (HCN) and ammonia (NH₃) emitted by *Pseudomonas aeruginosa*. *J Breath Res*. 2015;9:027102. doi: <https://doi.org/10.1088/1752-7155/9/2/027102>.
32. Gilchrist FJ, Bright-Thomas RJ, Jones AM, Smith D, Španěl P, Webb AK, et al. Hydrogen cyanide concentrations in the breath of adult cystic fibrosis patients with and without *Pseudomonas aeruginosa* infection. *J Breath Res*. 2013;7:026010. <https://doi.org/10.1088/1752-7155/7/2/026010>.
33. Smith D, Španěl P, Gilchrist FJ, Lenney W. Hydrogen cyanide, a volatile biomarker of *Pseudomonas aeruginosa* infection. *J Breath Res*. 2013;7:044001. <https://doi.org/10.1088/1752-7155/7/4/044001>.
34. Blumer C, Haas D. Mechanism, regulation, and ecological role of bacterial cyanide biosynthesis. *Arch Microbiol*. 2000;173:170–7. <https://doi.org/10.1007/s002039900127>.
35. Spooner AD, Bessant C, Turner C, Knobloch H, Chambers M. Evaluation of a combination of SFT-MS and multivariate data analysis for the diagnosis of *Mycobacterium bovis* in wild badgers. *Analyst*. 2009;134:1922. <https://doi.org/10.1039/b905062k>.
36. Storer MK, Hibbard-Melles K, Davis B, Scotter J. Detection of volatile compounds produced by microbial growth in urine by selected ion flow tube mass spectrometry (SIFT-MS). *J Microbiol Methods*. 2011;87:111–3. <https://doi.org/10.1016/j.mimet.2011.06.012>.
37. Dummer J, Storer M, Stuney S, Scott-Thomas A, Chambers S, Swanney M, et al. Quantification of hydrogen cyanide (HCN) in breath using selected ion flow tube mass spectrometry—HCN is not a biomarker of *Pseudomonas* in chronic suppurative lung disease. *J Breath Res*. 2013;7:017105. <https://doi.org/10.1088/1752-7155/7/1/017105>.
38. Slade EA, Thom RMS, Lovering AM, Young A, Reynolds DM. In vitro discrimination of wound-associated bacteria by volatile compound profiling using selected ion flow tube-mass spectrometry. *J Appl Microbiol*. 2017;123:233–45. <https://doi.org/10.1111/jam.13473>.
39. Lewis JM, Savage RS, Beeching NJ, Beadsworth MBI, Feasey N, Covington JA. Identifying volatile metabolite signatures for the diagnosis of bacterial respiratory tract infection using electronic nose technology: a pilot study. *PLoS One*. 2017;12:e0188879. <https://doi.org/10.1371/journal.pone.0188879>.
40. Greenman J, Saad S, Hewett K, Thom RMS, Reynolds DM. Review: in vitro biofilm models for studying oral malodour. *Flavour Fragr J*. 2013;28:212–22. <https://doi.org/10.1002/ffj.3151>.
41. Ashrafi M, Novak-Frazer L, Bates M, Baguneid M, Alonso-Rasgado T, Xia G, et al. Validation of biofilm formation on human skin wound models and demonstration of clinically translatable bacteria-specific volatile signatures. *Sci Rep*. 2018;8:9431. <https://doi.org/10.1038/s41598-018-27504-z>.
42. Luján AM, Maciá MD, Yang L, Molin S, Oliver A, Smania AM. Evolution and adaptation in *Pseudomonas aeruginosa* biofilms driven by mismatch repair system-deficient mutants. *PLoS One*. 2011;6:e27842. <https://doi.org/10.1371/journal.pone.0027842>.
43. Klausen M, Aaes-Jørgensen A, Molin S, Tolker-Nielsen T. Involvement of bacterial migration in the development of complex multicellular structures in *Pseudomonas aeruginosa* biofilms. *Mol Microbiol*. 2003;50:61–8. <https://doi.org/10.1046/j.1365-2958.2003.03677.x>.
44. Ghafoor A, Hay ID, Rehm BHA. Role of exopolysaccharides in *Pseudomonas aeruginosa* biofilm formation and architecture. *Appl Environ Microbiol*. 2011;77:238–46. <https://doi.org/10.1128/AEM.00637-11>.
45. British Standards Institution. BS EN ISO 20776-1: Clinical laboratory testing and in vitro diagnostic test systems - Susceptibility testing of infectious agents and evaluation of performance of antimicrobial susceptibility test devices. 2006. <https://www.bsi.com/standards/products/BS-EN-ISO-20776-1-2006>.
46. The European Committee on Antimicrobial Susceptibility Testing. Breakpoint tables for interpretation of MICs and zone diameters. Version 8.1. 2018. <http://www.eucast.org>.
47. Bujk S, Gysens IC, Mouton RW, Van Vliet A, Verbrugh HA, Bruining HA. Pharmacokinetics of ceftazidime in serum and peritoneal exudate during continuous versus intermittent administration to patients with severe intra-abdominal infections. *J Antimicrob Chemother*. 2002;49:121–8. <http://www.ncbi.nlm.nih.gov/pubmed/11751775>.
48. Church D, Elsayed S, Reid O, Winston B, Lindsay R. Burn wound infections. *Clin Microbiol Rev*. 2006;19:403–34. <https://doi.org/10.1128/CMR.19.2.403-434.2006>.
49. Meigel WN, Gay S, Weber L. Dermal architecture and collagen type distribution. *Arch Dermatological Res*. 1977;259:1–10. <https://doi.org/10.1007/BF00562732>.
50. Vuolo J. Current options for managing the problem of excess wound exudate. *Prof Nurse*. 2004;19:487–91.

51. Cutting KF, White RJ. Maceration of the skin and wound bed 1: its nature and causes. *J Wound Care*. 2002;11:275–8. <https://doi.org/10.12968/jowc.2002.11.7.26414>.
52. Trengove NJ, Langton SR, Stacey MC. Biochemical analysis of wound fluid from nonhealing and healing chronic leg ulcers. *Wound Repair Regen*. 1996;4:204–9. <https://doi.org/10.1006/j.1524-475X.1996.40211.x>.
53. Bowler PG, Duerden BJ, Armstrong DG. Wound microbiology and associated approaches to wound management. *Clin Microbiol Rev*. 2001;14:244–69. <https://doi.org/10.1128/CMR.14.2.244-269.2001>.
54. Spjberg T, Mazzewa S, Jönsson K, Robertson V, Salemark L. Comparison of surface swab cultures and quantitative tissue biopsy cultures to predict Sepsis in burn patients: a prospective study. *J Burn Care Rehabil*. 2003;24:365–70. <https://doi.org/10.1097/01.BCR.0000095507.45481.76>.
55. Uppal SK, Ram S, Kwatra B, Garg S, Gupta R. Comparative evaluation of surface swab and quantitative full thickness wound biopsy culture in burn patients. *Burns*. 2007;33:460–3. <https://doi.org/10.1016/j.burns.2006.08.015>.
56. Levine NS, Lindberg RB, Mason AD, Pruitt BA. The quantitative swab culture and smear: a quick, simple method for determining the number of viable aerobic bacteria on open wounds. *J Trauma Inj Infect Crit Care*. 1976;16:89–94. <https://doi.org/10.1097/00005373-197602000-00002>.
57. Ceri H, Olson ME, Stremick C, Read RR, Morck D, Buret A. The Calgary biofilm device: new technology for rapid determination of antibiotic susceptibilities of bacterial biofilms. *J Clin Microbiol*. 1999;37:1771–6. <https://jcm.asm.org/content/37/9/1771.abstract>.
58. Elliott TSJ, Greenwood D. The morphological response of *Pseudomonas aeruginosa* to aztreonam, cefepime, ceftazidime and N-hormimidoyl thienamycin. *J Med Microbiol*. 1984;17:159–69. <https://doi.org/10.1099/00222615-17-2-159>.
59. Chen W, Zhang Y-M, Davies C. Penicillin-binding protein 3 is essential for growth of *Pseudomonas aeruginosa*. *Antimicrob Agents Chemother*. 2017; 61:e01651–16. <https://doi.org/10.1128/AAC.01651-16>.
60. Yao Z, Kahne D, Kishony R. Distinct single-cell morphological dynamics under beta-lactam antibiotics. *Mol Cell*. 2012;48:705–12. <https://doi.org/10.1016/j.molcel.2012.09.016>.
61. Dini V, Salvo P, Janowska A, Di Francesco F, Barbini A, Romanelli M. Correlation between wound temperature obtained with an infrared camera and clinical wound bed score in venous leg ulcers. *Wounds*. 2015;27:274–8. <https://www.woundresearch.com/article/correlation-between-wound-temperature-obtained-infrared-camera-and-clinical-wound-bed-score>.
62. Thomas S, Fear M, Humphreys J, Disley I, Waring M. The effect of dressings on the production of exudate from venous leg ulcers. *Wounds*. 1996;8:145–50.
63. Schindelin J, Arganda-Carreras I, Frise E, Kaynig V, Longair M, Pietzsch T, et al. Fiji: an open-source platform for biological-image analysis. *Nat Methods*. 2012;9:676–82. <https://doi.org/10.1038/nmeth.2019>.

Publisher's Note

Springer Nature remains neutral with regard to jurisdictional claims in published maps and institutional affiliations.

Ready to submit your research? Choose BMC and benefit from:

- fast, convenient online submission
- thorough peer review by experienced researchers in your field
- rapid publication on acceptance
- support for research data, including large and complex data types
- gold Open Access which fosters wider collaboration and increased citations
- maximum visibility for your research: over 100M website views per year

At BMC, research is always in progress.

Learn more biomedcentral.com/submissions



Appendix II: Supplementary Material

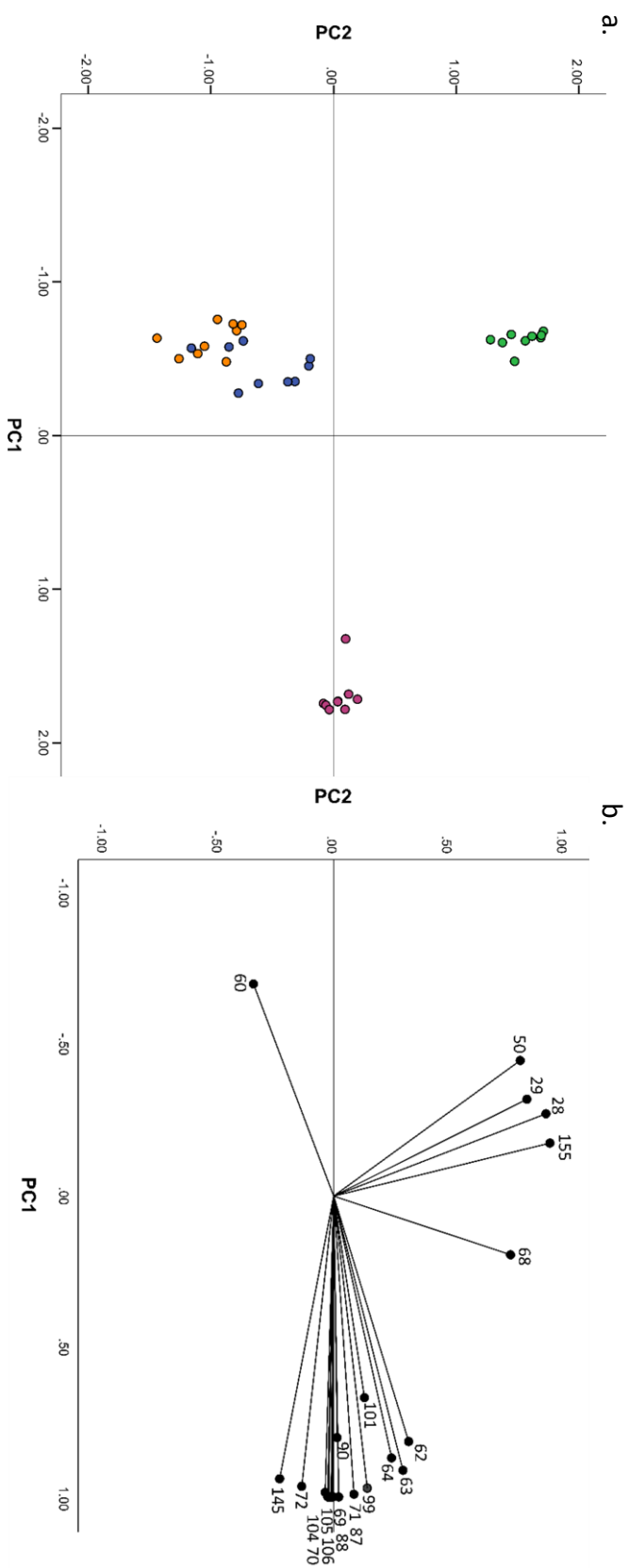


Figure S1: (a) Plot of the scores of the first two principal components generated by principle component analysis of SIFT-MS full scan data of 22 'core' headspace volatile product ion peaks of bacterial biofilms and uninoculated controls (n = 3 scans per sample). Principal component 1 (horizontal axis) accounts for 67.4% of the total variation in the original data set and principal component 2 (vertical axis) accounts for 19.1% of the total variation. *Pseudomonas aeruginosa* (Green), *Staphylococcus aureus* (Pink), *Streptococcus pyogenes* (Orange), control (Blue). (b) Principal component analysis loading plot of selected m/z peaks. Data points indicate the loading of each m/z peak (variable) on the first two principal components generated from the principal component analysis.

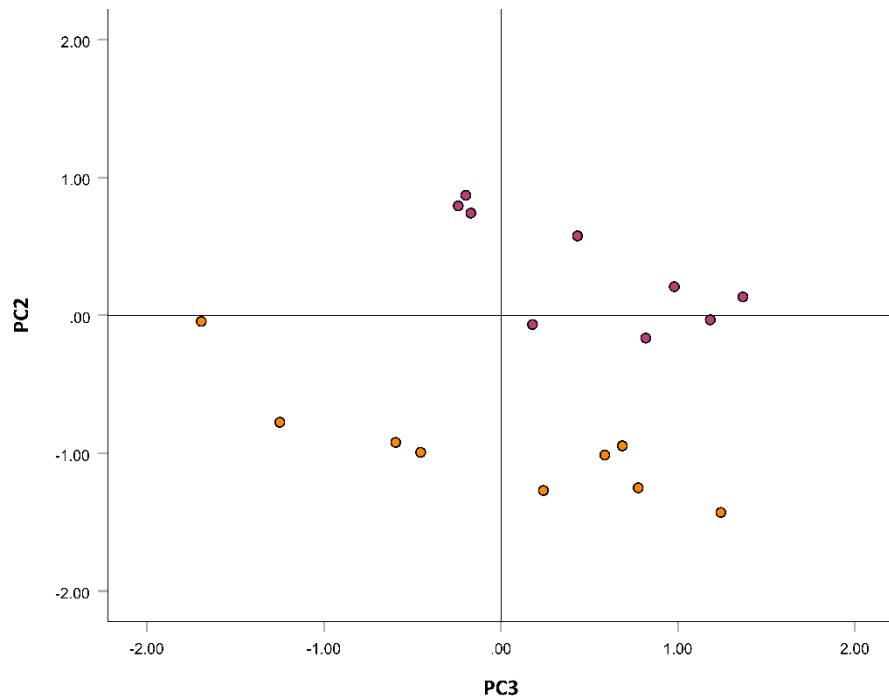


Figure S2: Plot of the scores of the second and third principal components generated by principle component analysis of SIFT-MS SIM data of selected headspace volatile compound concentrations (ppb) of bacterial biofilms and uninoculated controls, showing *Streptococcus pyogenes* (Orange) and *Staphylococcus aureus* (Pink) only. Principal component 2 accounts for 26.1 % of the variation within the original data set, while the third components accounts for 5.45 % of the variation.